Plasmas hors équilibre thermodynamique et applications : développement de sources UV-X, dépollution (DéNOx, DéCOV), et production de gaz de synthèse

Ahmed Khacef

UNIVERSITE D'ORLEANS

CENTRE NATIONAL DE LA RECHERCHE SCIENTIFIQUE

GREMI

HABILITATION A DIRIGER DES RECHERCHES

Discipline : Physique des Plasmas

Plasmas hors équilibre thermodynamique et applications : développement de sources UV-X, dépollution (DéNOx, DéCOV), et production de gaz de synthèse

---

Par

AHMED KHACEF

Soutenue le 21 février 2007 devant le jury :

Rapporteurs :

Khaled Hassouni	Professeur Université Paris-Nord (Paris XIII)
Stéphane Pasquiers	Directeur de Recherche CNRS - LPGP (Orsay)
Pierre Vervisch	Directeur de Recherche CNRS - CORIA (Rouen)

Examinateurs :

Gérald Djega-Mariadassou	Professeur Université Pierre et Marie Curie (Paris VI)
Iskender Gökalp	Directeur de Recherche CNRS - ICARE (Orléans)
Claude Fleurier	Directeur de Recherche CNRS - DRRT Centre
Jean-Michel Pouvesle	Directeur de Recherche CNRS - GREMI (Orléans)
Jean-Marie Cormier	Professeur Université d'Orléans

à Farida
Wissem
Leïla
Imène

REMERCIEMENTS

Les études rapportées dans ce mémoire ont été réalisées au GREMI unité mixte de recherche CNRS-Université d'Orléans. J'exprime toute ma reconnaissance aux Directeurs successifs du laboratoire, Messieurs André Bouchoule, Claude Fleurier et Jean Michel Pouvesle, pour l'accueil qu'ils m'ont réservé au GREMI.

Ces remerciements s'adressent tout particulièrement à Monsieur Jean Michel Pouvesle avec lequel j'ai débuté dans les sous sols du GREMI et qui a assuré le suivi d'une majeure partie de ces travaux en me faisant profiter pleinement de toutes ses compétences scientifiques. Sa disponibilité, ses encouragements constants, ses conseils ainsi que son soutien toujours enthousiaste m'ont été très précieux.

J'associe également à ces remerciements Monsieur Jean Marie Cormier qui a dirigé la partie Plasma-Chimie de ce travail pour son soutien, sa disponibilité et sa grande expérience.

J'exprime mes vifs remerciements aux membres du jury Messieurs Gerald Djega-Mariadassou, Iskender Gökalp, Jean Marie Cormier et Jean Michel Pouvesle, et en particulier aux rapporteurs de ces travaux Messieurs Khaled Hassouni, Stéphane Pasquiers et Pierre Vervisch qui ont bien voulu consacrer une part de leur temps à l'étude et à la critique de ce mémoire.

J'adresse des remerciements particuliers à l'ensemble des membres de l'équipe "Sources de rayonnement" (Eric Robert, Christophe Cachoncinlle, Raymond Viladrosa, Jean Michel Pouvesle), et de l'équipe "Chimie Plasma" (Elise El Ahmar, Fakhreddine Ouni, Jean Marie Cormier, Olivier Aubry) avec une mention spéciale à nos deux thésards de service Elise et Fakhri.

Je remercie vivement Messieurs Gérald Djega-Mariadassou, Cyril Thomas, et François Baudin du LRS (Université Pierre et Marie Curie, Paris VI) pour les échanges fructueux que nous avons eu ensemble et aussi pour m'avoir fait bénéficier de leur compétences dans le domaine de la catalyse.

Mes remerciements vont aussi à Jörgen Stevefelt, Mehrdad Nikravech, Olivier Motret, Iulan Rusu, ainsi qu'à tous les collègues des milieux académique et industriel avec lesquels j'ai collaboré durant ces dernières années.

Ce travail n'aurait pu aboutir sans l'aide technique de Messieurs André Bonnet, Jean Claude Pellicer et Guy Coudrat pour la mécanique, Bernard Dumax et Sébastien Dozias pour l'électronique et l'informatique, Jacky Mathias pour l'optique et Philippe Lefaucheux pour "tout le reste". Qu'ils trouvent ici mes plus chaleureux remerciements tant pour leur disponibilité que pour leur patience et leur gentillesse.

Je voudrais aussi remercier Mesdames Sylvie Jauffrion et Evelyne Coudert pour leur gentillesse et leur grande efficacité à faciliter les procédures administratives.

Finalement, Je voudrais exprimer ma grande joie de travailler au GREMI. Je remercie sincèrement tout ses personnels (permanents et non permanents) pour l'ambiance très agréable et fructueuse qu'ils ont contribué à créer et pour la qualité des relations humaines que j'ai tissées avec eux.

TABLE DE MATIERES

INTRODUCTION

Mes premières activités de recherche ont été initiées en 1978 à l'Université des Sciences et de Technologie et au Centre d'Etudes Nucléaires d'Alger en collaboration avec l'Institut de Physique Lebedev de l'Académie des Sciences de l'Union Soviétique (Russie actuellement). Ces travaux concernaient le rayonnement X (Bremsstrahlung) émis lors de l'interaction laser de puissance-matière. Dès septembre 1985 a commencé ma grande aventure orléanaise au GREMI (Groupe de Recherche sur l'Energétique des Milieux Ionisés) avec dans un premier temps la préparation d'une thèse de Magister (équivalent thèse de troisième cycle) sur les transferts d'excitation et de charge dans les plasmas d'hélium à haute pression et dans un deuxième temps une thèse de Doctorat d'Etat sur les plasmas à base de gaz rares à haute pression crées par décharge électrique rapide ou rayons X. Ces deux thèses ont été réalisées sous la direction scientifique de J.M. Pouvesle Directeur de Recherche au CNRS et soutenues à l'Université d'Alger.

Ce présent document est présenté en vue de l'obtention de l'Habilitation à Diriger les Recherches décrit une synthèse des activités de recherche que j'ai menées après la fin de ma thèse de doctorat d'Etat. Ces travaux ont été réalisés en partie au sein de l'équipe "*Décharges impulsionnelles haute tension, Sources de rayonnement*" dirigée par J.M. Pouvesle et en partie dans l'équipe "*Plasmas hors équilibre, Chimie Plasma*" sous la direction de J.M. Cormier (Professeur à l'Université d'Orléans). Ces recherches bien que très différentes dans leurs applications, se placent dans le domaine assez large de la physique des plasmas non thermiques avec une composante plasma-chimie réactive. L'intérêt a été porté sur les décharges haute tension impulsionnelles ou alternatives sinusoïdales. Ces décharges pouvant être de différents types : décharge haute pression pré-ionisées, décharge basse pression, décharge à barrière diélectrique (DBD), et décharge luminescente à pression atmosphérique (DLPA).

Mes principales contributions à ces domaines de recherche concernent d'une part le développement et l'utilisation de nouvelles sources de rayonnement dans le domaine UV-X et d'autre part, le traitement des effluents gazeux et la valorisation des alcanes et des alcools pour la production d'hydrogène.

Nos travaux expérimentaux sur les sources de rayonnement UV-X incohérent ont été motivés par les besoins d'un grand nombre de laboratoires à travers le monde de nouvelles sources de photons d'énergie supérieure à 3 eV pour des applications tant dans les domaines des hautes technologies que dans celui des recherches plus fondamentales (micro-électronique, traitement de matériaux, médecine et biologie, diagnostics, radiographie éclair, ...). Ces besoins avaient relancé l'intérêt pour l'étude de l'excitation des gaz rares à des pressions atmosphériques, ou dans leurs phases condensées. Ces gaz étant connus pour émettre de larges continua de rayonnement dans le domaine UV-VUV. Dans le cas de l'argon par exemple, ces continus permettent de couvrir la quasi-totalité du domaine spectral 80-400 nm. Habituellement, l'excitation de ces milieux faisait appel à l'utilisation d'équipements tels que synchrotrons, faisceaux d'ions ou gros canons à électrons. De tels systèmes présentent le désavantage d'être technologiquement très lourds, très onéreux et très peu disponibles. Le challenge était alors de pouvoir concevoir de nouveaux moyens d'excitation, à l'échelle d'un

laboratoire de recherche, conduisant à des niveaux de fluorescence suffisants pour l'utilisation des techniques de diagnostics spectroscopiques conventionnelles. Ces différentes motivations nous ont conduit à développer des décharges électriques impulsionnelles et de très courtes durées, d'une part pour être utilisées comme moyen d'excitation de plasmas de mercure et de néon-xénon intéressant directement le laser exciplexe XeCl et d'autre part, comme moyen de production d'impulsions de rayonnement X de grande puissance qui à leur tour pourront être utilisés pour la photo-ionisation de gaz rares à très haute pression (jusqu'à 30 bars). La génération des impulsions de rayonnement X a fait appel à une technologie comparable à celle mise au point au Center for Quantum Electronics de l'Université du Texas à Dallas, laboratoire du Pr C.B. Collins, avec qui nous travaillons en collaboration depuis plusieurs années. L'optimisation à des puissances élevées de ces sources "flash X" impulsionnelles, très compactes et pouvant fonctionner à des taux de répétition relativement élevés, initialement développées pour l'excitation d'échantillons gazeux à très haute pression pour la génération de la fluorescence UV-VUV, a ouvert la voie à d'autres applications très attractives.

Le deuxième thème abordé concerne l'utilisation des plasmas froids produits par DBD ou DLPA pour le traitement des effluents gazeux et la valorisation des alcanes et des alcools pour la production d'hydrogène. Ces types de décharges présentent l'avantage de générer des plasmas fortement hors-équilibre favorisant la production massive d'espèces chimiquement actives (radicaux, atomes et molécules excitées, ...) à partir d'électrons primaires particulièrement énergétiques. Le coût énergétique de transformation d'espèces reste relativement faible en raison d'un faible échauffement des espèces neutres. De nombreuses applications potentielles ont été explorées avec succès. Elles concernent principalement la dépollution et la valorisation des hydrocarbures.

Les recherches sur la dépollution que nous avons initiées avec les industriels de l'automobile ont été recentrées sur le couplage plasma-catalyseur. L'utilisation d'une DBD impulsionnelle associée à un catalyseur composite a ouvert une voie très intéressante pour la réduction des oxydes d'azote de gaz d'échappement de moteur fonctionnant en mélange pauvre (lean burn). Mis à part un dépôt de brevet, ces travaux n'ont pas été publiés essentiellement pour des raisons de confidentialité.

Les plasmas non thermiques de type DLPA (décharge glissante, décharge tournante, décharge stationnaire) ont montrées des possibilités intéressantes pour la production d'hydrogène à partir du méthane et plus récemment à partir du propane et d'éthanol. Les réacteurs classiques à décharges glissantes permettent d'obtenir des coûts énergétiques de transformation intéressants, mais les conversions obtenues sont faibles. Ceci est principalement dû au fait qu'une grande partie du gaz à traiter ne "*voit*" pas la décharge et s'écoule à une distance trop grande du fil de plasma. Ce comportement est amélioré en resserrant les décharges autour de l'écoulement et en favorisant le contact gaz-plasma par des techniques auxiliaires. L'une de ces techniques consiste à utiliser un soufflage magnétique qui introduit une rotation de la décharge améliorant ainsi l'effet de balayage du plasma.

Les plasmas non thermiques sont aussi susceptibles de favoriser le fonctionnement des moteurs thermiques. Un traitement des gaz à l'admission pour produire de l'hydrogène et/ou des espèces radicalaires permettrait d'améliorer la combustion et de réduire la pollution. Les résultats préliminaires obtenus à l'aide d'un réacteur à décharge tournante monté sur banc moteur ont confirmés ces effets. Le système est en phase d'optimisation pour une nouvelle campagne d'expériences.

Les qualités spécifiques des générateurs électriques mis en œuvre pour créer des plasmas froids et chimiquement actifs sont essentielles. Pour de meilleures performances il est nécessaire d'optimiser le couplage énergétique entre la source et le plasma afin de réduire les pertes dans le système. Deux types de générateurs de fonctionnement complètement différents sont utilisés : un générateur impulsionnel (nanoseconde) THT (kV) à taux de répétition variable (du mono-coup à 1 kHz) et un générateur alternatif sinusoïdal fonctionnant à 50 Hz ou à 20 kHz.

Ces sources électriques ont été conçues et réalisées au laboratoire. Les schémas adoptés et les techniques de réalisation correspondantes constituent un savoir faire qui est un atout important pour l'évolution de nos recherches.

Le présent mémoire résume les résultats expérimentaux obtenus dans ces différents domaines de recherche. Les études ont été effectuées dans le cadre de programmes, d'actions, et de groupements de recherche (AC, ACI, GDR, GDRE) impliquant d'une part plusieurs laboratoires nationaux et étrangers et d'autre part, différents partenaires industriels.

Ce mémoire est structuré en cinq sections distinctes. Après une présentation brève de mon curriculum vitæ, je présente mes activités de recherche dans la première partie. Ces activités sont organisées selon trois chapitres présentés suivant une progression chronologique décroissante. Le premier chapitre traite des plasmas réactifs à la pression atmosphérique, appliquées à la dépollution, à la production de gaz de synthèse et d'hydrogène, et à l'aide à la combustion de moteur thermique. Le deuxième chapitre est consacré au développement de sources flash X et à leur utilisation dans différents domaines d'application, par exemple l'excitation de gaz rares à haute pression pour la production de rayonnement dans le domaine UV-VUV. Le troisième chapitre présente les études sur la caractérisation de plasmas proches des milieux actifs des lasers de puissance (XeCl par exemple). Cette partie se termine par les références bibliographiques (chapitre 4) et les perspectives que je souhaite suivre pour mes recherches futures (chapitre 5).

La deuxième section présente les actions conduites en marge de mes travaux de recherche afin de mener à bien les différents projets : encadrement d'étudiants, diffusion de l'information scientifique, suivi de collaborations nationales et internationales, organisation d'événements scientifiques, ...

La section 3 récapitule mes activités d'enseignement dans les établissements d'enseignement supérieur (Université des Sciences d'Alger, Institut des Sciences biomédicales d'aller, et Université d'Orléans).

La section 4 liste l'ensemble de ma production scientifique (publications, communications, ...). Enfin, un certain nombre d'articles que j'ai publié sur les thèmes abordés ont été sélectionnés pour être inclus dans la cinquième et dernière section de ce document.

CURRICULUM VITÆ

Ahmed KHACEF

Ingénieur de Recherche au CNRS

GREMI, Orléans

I. 1. Parcours Professionnel

- Depuis déc. 2003 : Ingénieur de Recherche, Equipe "*Plasma-Chimie*", GREMI Orléans.
  Enseignant vacataire, Faculté des Sciences et IUT Département GEA (Gestion des Entreprises et des Administrations), Université d'Orléans.
- Déc. 2000-nov. 2003 : Ingénieur d'Etudes, Equipe "*Plasma-Chimie*", GREMI
  Enseignant vacataire, Faculté des Sciences, Antenne de Bourges, et IUT GEA, Université d'Orléans.
- Oct. 1998-oct. 2000 : Chercheur contractuel au CNRS, Equipe "*Plasma-Chimie*", GREMI
- Sept. 1995-août 1998 : ATER (Attaché Temporaire d'Enseignement et de Recherche) en 30e puis en 63e section du CNU, Faculté des Sciences, Université d'Orléans et Equipe "*Sources impulsionnelles haute tension*", GREMI.
- Oct. 1993-mai 1995 : Chercheur contractuel, Equipe "Sources impulsionnelles haute tension", GREMI.
- Nov. 1990-janv. 1991 : Professeur Invité, Faculté des Sciences, Université d'Orléans.
- Sept. 1977-sept. 1993 : Enseignant-Chercheur, Equipe "*Interaction Plasma laser*", CEN (Centre d'Etudes Nucléaires), USTHB (Université des Sciences et de la Technologie Houari Boumediène), INSB (Institut National des Sciences Biomédicales), Alger.

I. 2. Séjours invités

- Nov. 1990–Janv. 1991 : Professeur invité à l'UFR Sciences, Université d'Orléans.
- Juil. 1982 : Séjour de recherche au laboratoire de fusion inertielle de l'Institut de Physique Lebedev, (Moscou)

I. 3. Formation

- Décembre 1997 : Doctorat d'Etat en Physique, Option Electronique Quantique-Physique des plasmas. "*Plasmas à base de gaz rares à haute pression crées par décharge électrique rapide ou rayons X présentant un intérêt pour le développement de nouvelles sources UV-X ou lasers excimères*", Direction J.M. Pouvesle, Directeur de Recherche au CNRS.

- Juin 1988 : Thèse de Magister (équivalent thèse de troisième cycle) en Physique, Option Electronique Quantique-Physique des plasmas. "*Transferts d'excitation et de charge dans les plasmas d'hélium à haute pression : Effets des collisions multiples*", direction J.M. Pouvesle et M. Benaïssa Professeur USTHB Alger.
- Juin 1977 : DES (Diplôme d'études supérieures DES) en Physique, Option Physique du Solide, Faculté des Sciences, Université d'Alger.
- Juin 1973 : Baccalauréat de l'Enseignement Secondaire, Série Mathématiques, Académie d'Alger.

I. 4. Résumé des publications

- 22 articles dans des journaux Internationaux
- 01 chapitre de livre
- 04 présentations invitées
- 44 publications dans les actes de conférence internationales avec comité de lecture
- 11 publications dans les actes de conférence nationales avec comité de lecture
- 01 brevet
- 02 publications universitaires
- 19 livrables de contrats ou de projets

I. ACTIVITES DE RECHERCHE

CHAPITRE 1 : PLASMAS REACTIFS A LA PRESSION ATMOSPHERIQUE

Les procédés faisant appel à des plasmas atmosphériques non-thermiques (appelés aussi "plasmas froids" ou plasmas hors-équilibre thermodynamique) sont en fort développement, particulièrement dans les domaines liés à l'environnement et à l'énergétique. Ces plasmas présentent une très grande efficacité énergétique, notamment en raison du faible chauffage du gaz.

En effet dans de tels plasmas, les électrons atteignent des énergies (températures) élevées (10-12 eV soit ~ 10^5 K) et les particules lourdes restent à la température proche de l'ambiante. Les électrons par impact direct sur les molécules ou atomes du gaz, vont engendrer des ions, des espèces excitées mais surtout des radicaux hautement réactifs (exemple O, OH, N dans l'air). Ces radicaux sont responsables des mécanismes d'oxydation donc d'élimination des polluants dans la phase gazeuse. Ainsi les électrons servent de relais pour transférer l'énergie électrique (ou électromagnétique) directement sous forme de réactivité chimique, sans avoir à chauffer le gaz.

Différents types de plasmas à pression atmosphérique sont utilisés selon les applications recherchées. Ces plasmas peuvent être produits par des décharges électriques (Corona impulsionnelle, décharge à barrière diélectrique (DBD) ou décharge silencieuse, décharge pré-ionisée, décharge continue, décharge luminescente à pression atmosphérique (DLPA)) [1-10] ou par des faisceaux d'électrons [11]. Parmi ces techniques, les décharges couronnes, les DBD et les décharges luminescentes sont les plus utilisées dans les domaines liés à la dépollution et au développement de nouveaux vecteurs énergétique (hydrogène).

Bien que l'efficacité des décharges électriques soit prouvée pour la conversion de certaines molécules, il est maintenant admis que la décharge utilisée seule n'est pas en mesure d'éliminer complètement les polluants et leurs mélanges, sans parler des espèces secondaires, éventuellement indésirables, qui sont inévitablement produites du fait même de la création du plasma dans les effluents à traiter [12]. Il devient alors nécessaire de coupler la décharge électrique à une autre technique d'élimination des molécules. L'utilisation conjointe du plasma et de la catalyse semble à l'heure actuelle une voie très prometteuse pour la réduction des oxydes

d'azote issus des échappements automobiles ainsi que pour la purification de l'air (odeurs, traces de composés aromatiques, ...)

Nous avons mis en œuvre un certain nombre de décharges électriques à la pression atmosphérique répondant à des besoins spécifiques. Un résumé des résultats obtenus avec des plasmas non thermiques réalisés au moyen de décharges à barrière diélectriques impulsionnelles (pour les études des procédés de destruction de polluants en phase gaz) et de décharges luminescentes à pression atmosphérique pour la valorisation des alcanes (production de gaz de synthèse et d'hydrogène) et pour l'amélioration de la combustion dans les moteurs thermiques est présenté. Les détails de nos résultats les plus significatifs sont donnés en références [12-21].

La partie dépollution de ce travail a été réalisée le cadre de plusieurs programmes de recherche :

- ARC (ACTION DE RECHERCHE CONCERTEE) "*Application des plasmas froids au traitement des gaz d'échappement*" du GIE PSA- PEUGEOT - CITROËN-RENAULT / CNRS(ECODEV) / PREDIT impliquant les laboratoires GREMI, LCSR (Orleans), ENSCP (Paris), LPGP (Orsay), LRS (Paris), LMR (Paris), et CORIA (Rouen).
- AC (ACTION CONCERTEE) NON POLLUTION-DEPOLLUTION (NDP), NOUVEAUX PROCEDES/NOUVELLES METHODES : "*DéCOV par Plasmas*" CNRS-MINISTERE DE LA RECHERCHE impliquant les laboratoires GREMI, LPGP, et CORIA
- Convention de Recherche avec la société SAINT GOBAIN "*Application des plasmas froids au traitement des effluents gazeux issus des fours Verriers (DéSOx) "*
- Convention d'étude avec la société FEDERAL MOGUL "*Conversion par plasma froid du chlorure de méthylène"*
- GDR CATAPLASME *"Mécanismes de destruction des* COV, *à basse température, par association plasma froid-catalyseur*" regroupant les laboratoires GREMI, LPGP, LIMHP, CORIA, et LACCO.

La partie hydrogène et applications de ce travail a été réalisée le cadre de :

- PROGRAMME EUROPÉEN SYNFUELS (Corpernicus ICAS2-2000-10004) "*Feasibility study of a novel technology for natural gas liquefaction based on plasma catalysis and Fischer-Tropsch synthesis*" avec INSTITUT FÜR NIEDERTEMPERATUR-PLASMAPHYSIK GREIFSWALD (INP) (ALLEMAGNE), RUSSIAN RESEARCH CENTER KURTCHATOV INSTITUTE, MOSCOW, (RUSSIE), BORESKOV INSTITUTE OF CATALYSIS, NOVOSIBIRSK, (RUSSIE).
- AC (ACTION CONCERTEE) ENERGIE "*PLASMHYRAD : Combustion assistée par hydrogène et radicaux générés par un plasma non thermique*" avec les laboratoires GREMI, LME, LCSR, et LPGP.
- GDR EUROPEEN (FRANCO-ITALIEN) *"Energetics and safety of hydrogen*" regroupant les laboratoires IRC-CNR (Naples), DIC-UNINA (Naples), DIC-UNIPI (PISE), DMA (Rome), IN-CNAR (Naples), IENI-CNR (Padoue), POLIMI (Milan), ENEL (Pise) du coté italien et GREMI, CORIA, LCSR, LEES (Bourges), PC2A (Lille), LCD (Poitiers), CETHIL (Lyon) pour le côté français.

A. Application à la Dépollution

Les principaux polluants liés aux activités industrielles sont de différents types : dioxyde de soufre (SO_2), oxydes d'azote ($NOx=NO+NO_2$), ozone (O_3), composés organiques volatils (COV), monoxyde de carbone (CO), poussières, ... Les émissions de ces polluants sont maintenant réglementées et les normes européennes et internationales sur les taux admissibles sont de plus en plus contraignantes pour les industriels. Afin de répondre à la réglementation, plusieurs technologies classiques de dépollution des effluents gazeux ont montrés une grande efficacité de traitement dépendante du débit de l'effluent ainsi que de la nature et de la concentration des molécules qu'il faut éliminer.

Parmi les techniques les plus couramment utilisées, selon le domaine industriel concerné (chimie, automobile, ...), on peut citer l'oxydation thermique ou catalytique [21], la réduction catalytique sélective avec l'ammoniac (SCR-NH_3) [22], ou les hydrocarbures (HC) imbrûlés ou ajoutés (SCR-HC) [23]. Ces techniques donnent d'excellents résultats lorsque les effluents gazeux sont fortement pollués. Par contre, l'utilisation de ces techniques pour traiter de faibles concentrations de polluants (<1000 ppm) nécessite un chauffage additionnel du système conduisant une dépense énergétique prohibitive surtout pour les installations requérant un flux de gaz important, jusqu'à plusieurs centaines voire milliers de m^3/h.

Dans le domaine automobile, le respect des normes anti-pollution a conduit les constructeurs d'automobiles à développer de nouveaux moteurs, pour lesquels les rejets contiennent une quantité importante d'oxygène, et ne peuvent plus être traités par les méthodes catalytiques conventionnelles.

La réduction des oxydes d'azote (déNOx) en post-combustion essence est réalisée par des catalyseurs, dit *trois-voies* ou TWC[1], dont l'activité est optimale en mélange stœchiométrique (richesse[2] autour de 1) à l'admission du moteur. Les TWC sont constitués d'un support alumine permettant de stabiliser des oxydes de terres rares CeO_2-ZrO_2 (environ 20% en masse) sur lesquels sont dispersés des métaux nobles (Pt, Pd, et Rh) (0.01 à 0.04% en masse). Le platine et le palladium sont particulièrement actifs en oxydation de CO et des HC imbrûlés en CO_2 et H_2O, alors que le rhodium est reconnu comme le plus efficace pour réduire sélectivement NO en N_2 [23].

Comme le montre la figure 1, l'utilisation de la TWC sur véhicules Diesel ou essence *Lean Burn* (mélange pauvre : richesse < 1) est inadaptée pour la réduction des NOx à cause de l'excès d'O_2 nécessaire au fonctionnement de ces moteurs. D'un autre coté, de nombreuses études [24-25] ont montré l'efficacité de la SCR-HC. Toutefois, cette technique seule ne permet pas d'obtenir une activité déNOx permettant de répondre aux normes actuelles et futures.

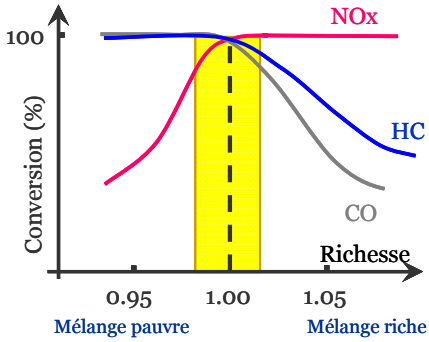

Figure 1: *Conversion de CO, des HC (hydrocarbures imbrulés) et des NOx en fonction de la richesse pour un catalyseur trois voies à T>250°C.*

Actuellement, aucun catalyseur n'est suffisamment efficace et stable pour permettre une activité déNOx répondant aux normes établies sur véhicules Diesel ou essence en mélange pauvre dans une gamme de température allant de l'ambiante jusqu'à 400°C. La technologie plasma non thermique seule ou couplée à un catalyseur judicieusement choisi apparaît comme une alternative à la voie purement thermique ou catalytique. Les processus plasma-catalyse pouvant être décrits suivant deux étapes bien distinctes. D'une part l'oxydation par plasma de NO en NO_2 et d'autre part, la réduction sélective catalytique des NOx en N_2 par

[1] *TWC: Three way catalysis*

[2] *La richesse R est définie par la valeur réelle du dosage air-carburant par rapport au dosage stœchiométrique à l'admission du moteur :*

$$R = \frac{(\text{Débit air}/\text{Débit carburant})_{\text{Réel}}}{(\text{Débit air}/\text{Débit carburant})_{\text{Stoechiométrie}}}$$

consommation des HC même dans des conditions de richesse en oxygène. La perspective d'activer le catalyseur par un plasma dès la température ambiante est donc particulièrement intéressante, car cela permettrait d'abaisser fortement le coût énergétique du procédé, notamment lorsqu'il s'agit de traiter un flux de gaz important contenant une faible concentration de polluants.

A. 1. Décharge à Barrière Diélectrique

Contrairement aux décharges directes classiques où le plasma est crée à travers le gaz entre deux électrodes, les réacteurs DBD présentent la particularité d'avoir au moins une électrode recouverte d'un matériau diélectrique (figure 2). Cette configuration permet de limiter le courant et de répartir le plasma dans tout le volume interélectrodes. Les plasmas générés se composent d'une multitude de micro-décharges filamentaires (ou "*streamers*") de durée de vie très brèves (qq. 10 ns), de diamètre apparent de l'ordre de 100 µm, répartis aléatoirement et perpendiculairement à l'axe du réacteur. Les caractéristiques du plasma dépendent fortement de la nature du gaz, de la pression, de la distance interélectrodes, des propriétés du diélectrique, ...

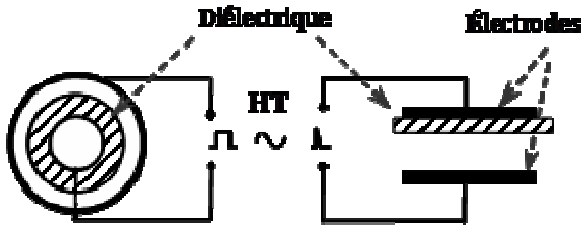

Figure 2 : *Réacteur DBD cylindrique et plan*

A la pression atmosphérique, la densité électronique dans le *streamer* est de l'ordre de 10^{14} à 10^{15} cm^{-3}. Au cours de l'établissement de la micro-décharge le diélectrique se polarise progressivement, la charge de surface réduit le champ moyen et le courant à l'intérieur de la micro-décharge diminue puis s'annule, la micro-décharge s'éteint. Si une haute tension est maintenue aux bornes des électrodes d'autres micro-décharges peuvent se développer. Elles se formeront préférentiellement sur d'autres sites en raison de la présence d'une charge de surface résiduelle au pied de la micro-décharge précédente. Le diélectrique joue deux rôles complémentaires. D'une part, il distribue les micro-décharges sur toute sa surface et d'autre part, il limite la quantité de charges pour chaque micro-décharge évitant ainsi le passage à un régime d'arc.

Les principales réactions chimiques caractéristiques de la DBD interviennent dans la phase "*Streamer*" : ce sont des réactions produites par des collisions électroniques. Après l'extinction du streamer et la recombinaison des charges, les différentes espèces neutres créées (molécules et radicaux) réagissent dans un milieu dont la température est voisine de la température ambiante. Les caractéristiques du plasma dépendent fortement de la nature du gaz, de la pression, de la distance interélectrodes, des propriétés du diélectrique, ...

Le grand intérêt des DBD pour les applications chimiques est directement lié à la nature même des "*streamers*" qui permettent d'obtenir des électrons très énergétiques sans transfert thermique significatif. Il est possible, d'autre part, de traiter une grande partie des espèces contenues dans le réacteur même si le volume propre de chaque "*streamer*" reste très faible par rapport au volume du réacteur.

Le réacteur DBD utilisé pour la réduction des NOx (et par la suite la conversion de SO_2 et la dégradation des COV) est du type fil – cylindre de 16 cm^3 de volume et de distance interélectrodes de 5.5 mm [12]. Le réacteur est couplé à un générateur impulsionnel dont la fréquence peut être ajustable entre 0 et 1 kHz. L'impulsion HT aux bornes des électrodes a une amplitude de 20 kV avec un front de montée de 20 ns et une largeur à mi-hauteur (FWHM) de 80 ns. La puissance électrique maximale mesurée à la prise et consommée par le système est de l'ordre de 100 W. Le tableau 1 fixe les conditions expérimentales.

Energie par impulsion	35 mJ et 195 mJ
Fréquence	Jusqu'à 1 kHz
Tension de décharge	20 kV
VVH	60 000 h^{-1}
Débit gazeux	16 L mn^{-1}
Température du mélange	Jusqu'à 400°C
Pression	1 Atm

Tableau 1 : *Conditions de l'étude*

Le dispositif expérimental dédié à ces études est montré sur la figure 3. Il se compose essentiellement d'un dispositif de distribution et de conditionnement des gaz (adapté pour réaliser des mélanges vapeur d'eau - gaz en proportions contrôlées, des réacteurs (différents types ont été testés), d'un four et des éléments annexes (alimentations H.T. et de leurs électroniques de commande, moyens de diagnostic).

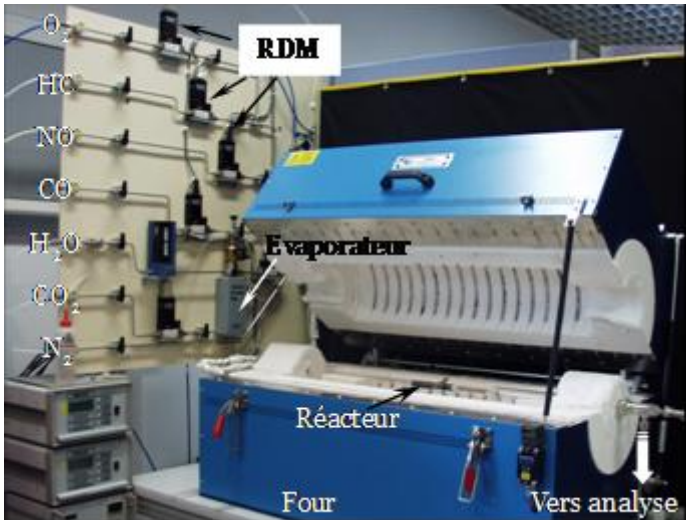

Figure 3 : *Vue d'ensemble du dispositif expérimental*

L'approche expérimentale adoptée consiste à étudier des mélanges de composition de complexité croissante (O_2-C_3H_6, N_2-C_3H_6, N_2-NO-C_3H_6, O_2-N_2-NO-C_3H_6, CO-O_2-N_2, CO-NO-N_2, CO-NO-O_2-N_2, CO-NO-O_2-C_3H_6-N_2). L'objectif final étant d'arriver à des mélanges représentatifs des gaz d'échappement de véhicules diesel et essence en mélange pauvre dont les compositions sont données dans le tableau 2. Les expériences ont été menées dans une large gamme de température (entre 20 et 400°C).

Espèces	Standard	Diesel	Essence LB
O_2	10%	12%	6%
H_2O	10%	10%	10%
NO	500 ppm	300 ppm	1000 ppm
C_3H_6	1500 ppmC	900 ppmC	3000 ppmC
CO	-	500 ppm	3000 ppm
CO_2	-	10%	10%

Tableau 2 :*Composition des mélanges étudiés*

Les diagnostics physico-chimiques en ligne des effluents en sortie de réacteur s'appuient essentiellement sur un détecteur d'oxydes (CO, NO, NO_2) par méthode électrochimique, un spectromètre infra rouge à transformée de Fourier-FTIR (NO,

NO_2, CO, CO_2, C_3H_6, CH_2O, CH_2O_2, CH_3ONO_2, ...), et un chromatographe en phase gazeuse-CG couplé à un spectromètre de masse-SM (analyse des phases liquide et gazeuse).

A. 2. Destruction des oxydes d'azote : Résultats marquants

A. 2. 1. Plasma seul

La figure 4 montrant les spectres d'absorption infrarouge des systèmes C_3H_6-N_2, NO-C_3H_6-N_2 et O_2-NO-C_3H_6-N_2 illustre la complexité de la cinétique des mélanges ternaires ou supérieurs [13].

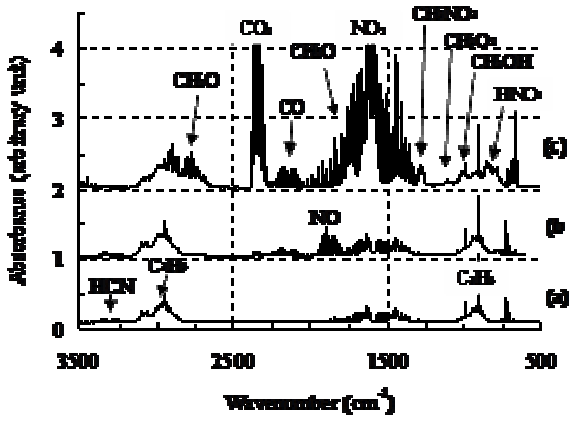

Figure 4: *Spectres FTIR caractéristiques à 4 cm^{-1} de résolution (T=22°C et E_d=27 J/L) :*
(a) C_3H_6 (500 ppm) - N_2,
(b) NO (500 ppm)-C_3H_6 (500 ppm)-N_2,
(c) O_2 (10%)-NO (500 ppm)-C_3H_6 (500 ppm)-N_2

Pour le premier mélange, la conversion du propène (50% à 27 J/L) mène à la production de l'acide cyanhydrique (HCN). L'ajout de 500 ppm de NO à ce mélange favorise l'oxydation partielle de NO en NO_2 et de C_3H_6 en CO, CO_2, et CH_2O (formaldéhyde). Dans ce cas l'oxydation de NO en NO_2 est très faible (<5%) et NO peut être chimiquement réduit en azote. L'oxydation de NO en NO_2 domine très rapidement sur les réactions de réduction et de dissociation lorsque O_2 est ajouté au mélange (cas c).

Quelques dixièmes de % sont suffisants pour provoquer l'oxydation à faible énergie électrique déposée pendant la décharge. Dans ces conditions de richesse en oxygène (10%), une fraction significative de l'énergie injectée dans le plasma est dissipée dans la dissociation de l'oxygène [12, 26-27]. Dans ce cas les principaux produits de décharges sont le NO_2 en proportion très majoritaire par rapport aux HC partiellement oxydés ou azotés tels que les aldéhydes (formaldéhyde CH_2O, acétaldéhyde CH_3CHO), et les molécules de type R-NOx (nitrate de méthyle CH_3ONO_2, nitrométhane CH_3NO_2) [12].

Un exemple typique de résultats expérimentaux obtenus dans un mélange standard sans H_2O est donné sur la figure 5.

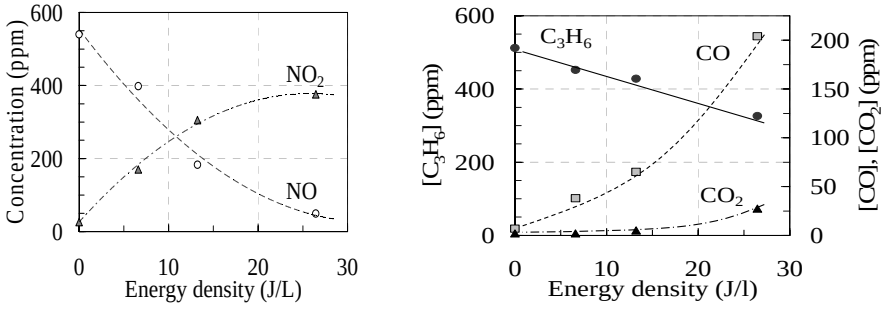

Figure 5 : *NO, NO_2, CO, CO_2 et C_3H_6 en fonction de la densité d'énergie pour un mélange standard sans H2O (T=22°C).*

A. 2. 1. a. Effet de l'hydrocarbure sur la conversion de NO

L'addition de l'hydrocarbure (ici le propène) provoque une modification sensible de la cinétique en cause dans l'oxydation de NO en NO_2. Cette oxydation est couplée à la chimie d'oxydation de l'hydrocarbure. Les données expérimentales (figure 6a) ont montré qu'un rapport C_1/NOx égal à 3 était nécessaire pour une oxydation optimum de NO en NO_2 dans le plasma. L'augmentation de la concentration d'hydrocarbure au delà de 500 ppm n'a aucune influence sur la conversion de NO [3, 12, 27-29]. C'est pour cette raison que pour toutes ces études la concentration de NO a été fixée à 500 ppm.

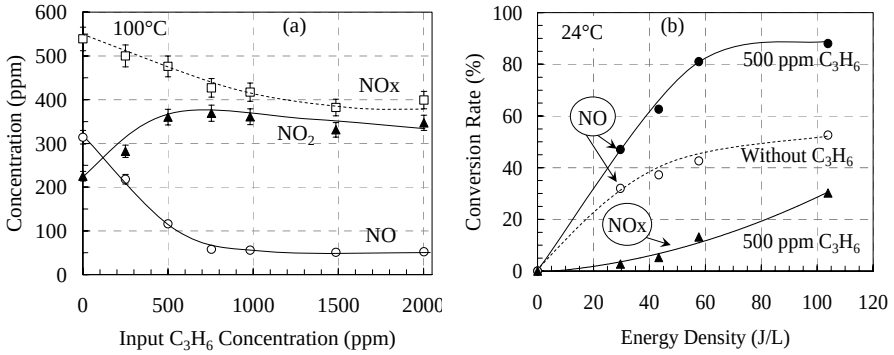

Figure 6 : *Effet de C_3H_6 sur l'oxydation de NO en NO_2 : (a) 500 ppm NO dans 94% d'air à E_d=44 J/L, (b) 500 ppm NO dans 19.6% d'air N_2 complément*

En absence d'hydrocarbure, les radicaux oxygène sont les responsables de l'oxydation de NO en NO_2 et la concentration des NOx ($NO+NO_2$) demeure constante même pour des densités d'énergie les plus élevées (jusqu'à 103 J/L).

L'ajout de C_3H_6 dans le mélange a pour effet d'augmenter le taux d'oxydation de NO et d'abaisser le coût énergétique de cette conversion (figure 6b). Le coût énergétique pour la conversion de NO (calculé à l'aide de la formule de Puchkarev et al [30]) est environ 2 fois plus faible que celui obtenu dans le cas d'un mélange sans C_3H_6 (25 eV/molécule contre 42 eV/molécule). Ces coûts énergétiques semblent élevés au regard des conversions obtenues. L'introduction de vapeur d'eau dans le mélange ainsi que l'optimisation des paramètres électriques peuvent conduire à une réduction significative des coûts énergétiques compatibles avec une application industrielle.

A. 2. 1. b. Effet de la vapeur d'eau sur la conversion de NO

Dans un gaz "humide" sans propène, la formation de radicaux hydroxyl OH par dissociation électronique de H_2O et par les réactions de H_2O avec les métastable de l'oxygène devient importante et conduit à la production d'acide (HNO_2 et HNO_3) par des réactions avec NO et NO_2. Cette cinétique change complètement quand le propène est présent dans le milieu. En effet, des analyses cinétiques détaillées [26, 31-32] ont montrées qu'en présence de propène, l'oxydation de NO en NO_2 n'est plus assurée par les radicaux oxygène mais par les radicaux peroxydes HO_2, formés à partir des espèces intermédiaires issues de l'oxydation de C_3H_6. Dans ce cas, les radicaux OH réagissent préférentiellement avec l'hydrocarbure minimisant ainsi la formation d'acide indésirable dans certaines applications (automobile par exemple).

Comme le montre la figure 7, l'introduction de H_2O (10% dans notre cas) dans le milieu plasma a pour conséquence directe une diminution de la concentration des oxydes d'azote [12]. Plus de 92% de NO est oxydé en NO_2 à seulement 7 J/L alors que ce taux ne dépasse pas 60% dans le mélange sans eau. L'ajout d'eau dans le mélange a pour effet de réduire considérablement le coût énergétique de la

transformation (facteur 2.2 en comparaison avec les données obtenues sans eau dans des conditions expérimentales similaires). A titre d'exemple et pour les conditions de la figure 7, l'énergie nécessaire pour l'oxydation d'une molécule de NO passe de 15 eV à une densité d'énergie de 27 J/L à seulement 4 eV à 7 J/L. Ces résultats ont servi de base de comparaison à deux modèles cinétiques, l'un développé par l'équipe de S. Pasquiers du LPGP à Orsay et l'autre développé par l'équipe de M. J. Kushner [33] de l'Université de l'Illinois (USA). Les résultats sont montrés dans les articles cités en référence. Dans tous les cas l'accord modèle-expérience est très satisfaisant [12,33].

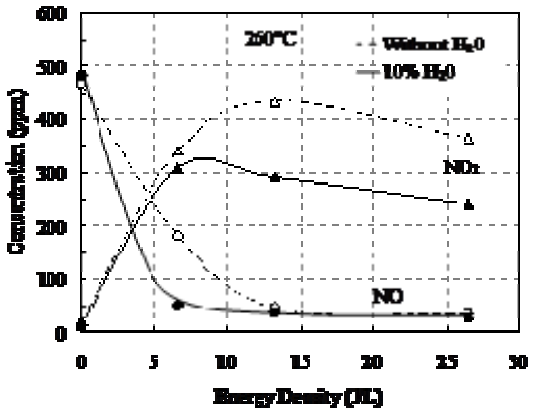

Figure 7 : *Effet de H_2O sur l'oxydation de NO en NO_2 en fonction de la densité d'énergie pour un mélange standard à 260°C*

Dans ces conditions de richesse en O_2 et en H_2O, l'analyse des phases liquide et gazeuse issue de la décharge par chromatographie montre la présence de sous produits tels que: l'acétaldéhyde (CH_3CHO), l'oxyde de propylène (C_3H_6O), l'acide formique (CH_2O_2), le méthanol (CH_3OH), le nitrate de méthyle (CH_3ONO_2), le nitrométhane (CH_3NO_2), et l'éthyle acétate ($CH_3COOC_2H_5$).

A. 2. 1. c. Effet du dépôt d'énergie

L'efficacité d'un procédé de dépollution dépend essentiellement du dépôt d'énergie dans le milieu. Contrairement à ce qui a été publié dans la littérature jusqu'à maintenant, le paramètre principal qui conditionne l'efficacité du traitement plasma n'est pas la densité d'énergie (exprimée en J/L) mais la manière dont cette énergie est injectée dans le milieu [15]. De plus, la nature des produits formés après traitement plasma diffère d'un réacteur à un autre. Pour un réacteur donné, la nature, la forme, et l'intensité de l'excitation électrique apparaissent comme étant les facteurs à maîtriser.

Dans le cas de la DBD impulsionnelle et à densité d'énergie équivalente, une meilleure conversion des oxydes d'azote et de l'hydrocarbure est obtenue dans des conditions de faible énergie déposée par impulsion et haute cadence de traitement. Il apparaît aussi que ce régime de fonctionnement conduit à la réduction du coût énergétique de traitement. La figure 8 montre un exemple de résultats obtenus pour deux régimes de fonctionnement du réacteur :

- Régime 1 : énergie par impulsion élevée (195 mJ) et faible fréquence (jusqu'à 40 Hz)
- Régime 2 : énergie par impulsion faible (35 mJ) fréquence élevée (jusqu'à 200 Hz).

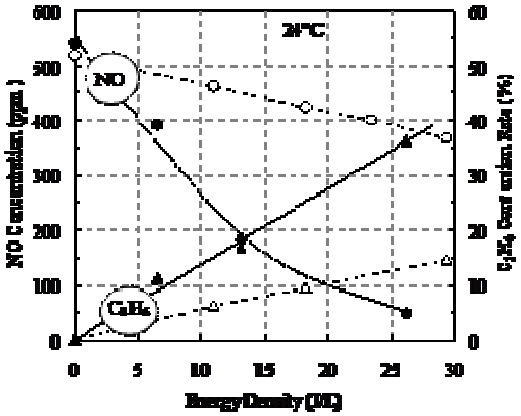

Figure 8 : *Concentration de NO et taux de conversion de C_3H_6 en fonction de la densité d'énergie : Régime 1 (pointillés) et Régime 2 (traits pleins) : Mélange 10%O_2, 500 ppm NO, 500 ppm C_3H_8 et N_2 en complément*

Dans le domaine d'énergie 0-30 J/L, il apparaît que l'efficacité du réacteur pour la conversion des NOx et de l'hydrocarbure est d'autant plus élevée que la fréquence de la décharge est élevée et que l'énergie déposée par impulsion est faible. Dans ce cas (régime 1), les taux de conversion de NO et de C_3H_6 sont respectivement de 91% et de 40% à une densité d'énergie de 27 J/L. Ces valeurs sont à comparer à 29% et 15% obtenues pour un fonctionnement dans le régime 2.

Dans le cas du réacteur DBD excité par un générateur sinusoïdal, seulement 30% de NO sont convertis à une densité d'énergie équivalente de 30 J/L. De plus, l'analyse en sortie de réacteur a montré que seul le formaldéhyde à été observé dans les mêmes conditions expérimentales. Les produits tels que $C_2H_5ONO_2$, CH_3ONO_2, HONO, et CH_2O_2 n'ont pas été détectés pour ce type d'excitation.

En conclusion, nous pouvons dire que pour un réacteur donné, la nature, la forme, et l'intensité de l'excitation électrique apparaissent comme étant les facteurs à maitriser pour une efficacité de traitement des effluents gazeux optimum. De plus, la nature des produits formés après traitement plasma diffère d'un réacteur à un autre. Ceci montre que la comparaison des résultats issus d'expériences mettant en œuvre des réacteurs et des excitations différentes est à prendre avec beaucoup de précautions.

A. 2. 1. d. Mélanges synthétiques diesel et essence LB

Les expériences avec les mélanges synthétiques Diesel et essence LB ont été réalisées en fonction de la température (jusqu'à 400°C) et de la densité d'énergie couvrant le domaine 0-27 J/L. Un exemple de résultats obtenus est montré figure 9. Pour les deux mélanges, l'efficacité de conversion des NOx croît avec la densité d'énergie pour atteindre environ 60% à 27 J/L quelque soit la température du mélange gazeux (150°C ou 300°C). A plus faible densité d'énergie le traitement semble plus efficace à plus forte température. Dans le cas du mélange Essence LB (contenant 3000 ppmC de C_3H_6) à 150°C le coût énergétique moyen est d'environ 11 eV/molécule de NO_x transformée. Ce qui revient à dire que pour convertir 60% des NOx présents dans un échappement de véhicule (débit de 100 L/s), il faudrait dépenser environ 2.6% de la puissance totale disponible dans un moteur de 100 kW. Ce pourcentage est compatible avec les exigences des constructeurs (< 5%).

La conversion du NO, par l'action du plasma, est due en grande partie à son oxydation en NO_2. A basse énergie déposée et en présence de concentrations modérées d'hydrocarbures, NO ne peut pas être complètement converti. Il serait nécessaire, pour poursuivre le traitement du polluant, de coupler le réacteur plasma à un procédé catalytique. On attend du plasma la formation d'espèces chimiques susceptibles d'activer le catalyseur.

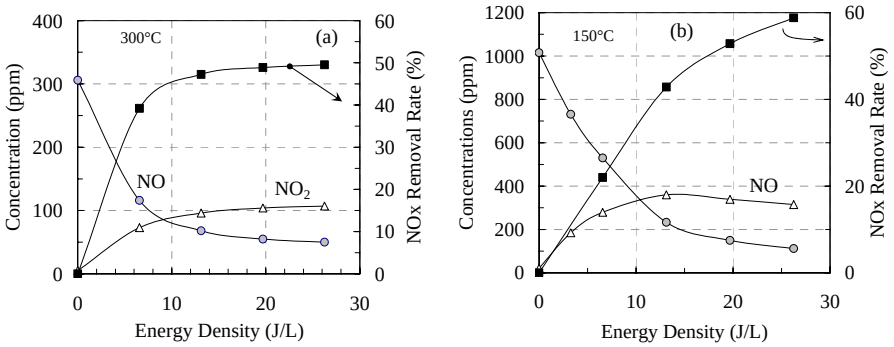

Figure 9 : *Concentration de NO et NO_2 et taux de conversion des NOx en fonction de la densité d'énergie pour des mélanges synthétiques : (a) Diesel à 300°C et (b) Essence Lean burn à 150°C.*

A. 2. 1. e. Réacteur prototype et essais sur banc moteur

Les travaux réalisés dans le cadre de ce programme ont permis d'aboutir à la construction d'un réacteur plasma prototype à l'échelle ½ (figure 10) pour valider les résultats laboratoires. Seuls les NOx ($NO+NO_2$) ont pu être mesurés dans le cadre des essais sur banc moteur (moteur PSA DW 10) au CERTAM en collaboration avec le CORIA (Rouen), la quantification des espèces hydrocarbonées étant très complexe à réaliser à partir d'un échappement moteur. Nous nous sommes focalisés sur les produits de décharges en fonction de plusieurs paramètres clés, tels que le rapport HC/NOx, la température et la vitesse volumique horaire (VVH).

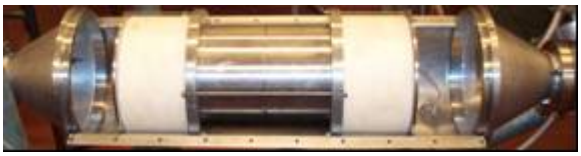

Figure 10 : *Réacteur déNOx prototype dans sa coque*

Les essais concernant l'influence du rapport HC/NOx ont montré l'importance capitale de l'action des HC sur les taux de conversion de NO en NO_2. Les points définis par des rapports HC/NOx les plus élevés (1.45) de ces essais conduisent à un taux de conversion très intéressant (70%) s'accompagnement d'une consommation électrique faible (8 J/L). Les points moteurs utilisés pour ces essais sont caractérisés par des concentrations en hydrocarbures imbrûlés très faibles, au maximum 164 ppm dans cette étude. Il serait intéressant par le biais de contrôle moteur adapté, de pouvoir explorer des domaines où la concentration des HC est plus importante (jusqu'à 3000 ppm), afin de confirmer leur action positive sur la conversion de NO en NO_2 comme il a été montré pour les gaz d'échappement synthétiques.

A. 2. 2. Couplage plasma-catalyseur

Les résultats obtenus sur l'aspect transformation chimique ont été dans l'ensemble prometteurs, ce qui a poussé les constructeurs à approfondir l'étude de cette technologie plasma avec certains des partenaires de l'ARC : le GREMI, le LPGP, et le LRS. La suite des travaux s'est donc orientée vers le couplage d'un réacteur plasma et d'un catalyseur disposé en aval.

Les travaux antérieurs du LRS sur la réduction des NOx en N_2 (avec le méthane) [34] ont montré que trois fonctions catalytiques semblaient nécessaires pour cette réaction :

(i) oxydation de NO en NO_2,

(ii) activation de l'hydrocarbure par oxydation ménagée par NO_2 avec formation d'aldéhyde et d'alcool,

(iii) chimisorption associative de NO sur un cation métallique stabilisé par le

support du catalyseur.

Si le plasma permet l'oxydation partielle des HC ($C_xH_yO_z$), alors un catalyseur caractérisé uniquement par une fonction de réduction des NOx par ces espèces réductrices activées, devrait être au moins aussi efficace qu'un catalyseur complet, en présence d'un réacteur plasma en amont. Les différents matériaux catalytiques utilisés dans cette étude ont été un support oxyde (CeO_2-ZrO_2), un catalyseur complet (Rh-Pd/CeO_2-ZrO_2) comprenant les trois fonctions requises pour le déNOx et un catalyseur simplifié où deux des fonctions, assurées par le plasma (formation de NO_2 et des espèces $C_xH_yO_z$), ont été supprimées.

Les résultats ont montré que le plasma permet de modifier favorablement les propriétés du mélange gazeux sur une plage étendue de température (20-400°C), de telle sorte que la fonction oxydante du catalyseur n'est plus indispensable (figure 11) [16].

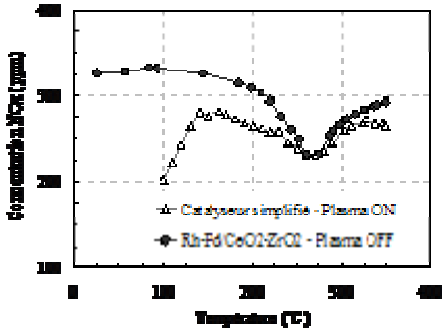

Figure 11 : *Concentration des NOx en fonction de la température en présence de plasma (36 J/L) pour le catalyseur simplifié et sans plasma pour catalyseur complet (8% O_2, 1.7% H_2O, 340 ppm NO, 1900 ppm C_3H_6, N_2).*

Il est aussi montré qu'il est possible d'atteindre des taux de réduction de NO en N_2 (déNOx) significatifs à l'échelle laboratoire, dépassant 40% dans ces conditions de mélange (8% O_2, 1.7% H_2O, 340 ppm NO, 1900 ppm C_3H_6, N_2). De plus le maximum de conversion apparaît à une température inférieure de l'ordre de 40°C par rapport aux expériences réalisées sans plasma suggérant la disponibilité à plus basse température pour le déNOx des espèces partiellement oxydées de l'hydrocarbure formées par le plasma [16].

Cette étude a permis de vérifier que l'hypothèse des mécanismes proposée par le LRS était pertinente. Elle s'est poursuivi à travers une thèse (F. Baudin) de catalyse déNOx assistée par plasma non-thermique dont l'objectif était de mettre au point un prototype plasma-catalyse en excès d'oxygène permettant d'obtenir une activité déNOx maximale dans une fenêtre de température la plus large possible. Plusieurs formulations catalytiques ont été testées. Afin de respecter les engagements avec nos partenaires industriels les détails des résultats obtenus au cours de cette thèse ne peuvent pas être présentés ici. Néanmoins, nous pouvons dire, que pour des conditions expérimentales précises et une formulation catalytique donnée, l'effet du plasma est très significatif puisqu'il a permis de diminuer la température de fonctionnement du catalyseur d'environ 200°C avec une activité déNOx multipliée par un facteur quatre. Un exemple d'une analyse GCMS réalisées en sortie de réacteur plasma en absence et en présence d'un catalyseur composite est montré sur la figure 12. Sans aller dans les détails, Tous les composés CxHyOz non aromatiques ainsi que les R-NOx ont été entièrement consommés. D'un autre coté, le catalyseur seul est très sensible à la présence d'eau dans le mélange qui se traduit par une désactivation du catalyseur. En présence de plasma cette sensibilité est plus limitée.

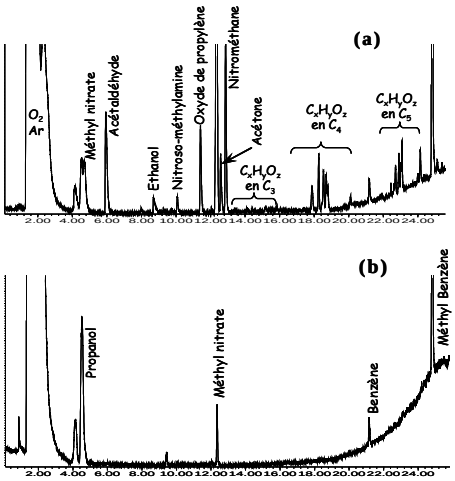

Figure 12 : Chromatogrammes de la phase gaz :
(a) Plasma seul (sans catalyseur)
(b) Catalyseur avec plasma en amont

Ces études ont conduit à la publication d'un brevet d'invention concernant un système de traitement des NOx de gaz d'échappement d'un moteur thermique de véhicule automobile, comprenant, dans une ligne d'échappement un plasma non-thermique suivi d'un catalyseur de réduction des oxydes d'azote. L'élément catalyseur comprend des éléments catalytiques de types différents présentant des fenêtres thermiques d'activité catalytique différentes disposés, suivant le sens d'écoulement des gaz, par ordre décroissant des fenêtres thermiques d'activité catalytique. Mis à part ce dépôt de brevet, les travaux issus de ces études n'ont pour l'instant pas été publiés essentiellement pour des raisons de confidentialité.

A. 3. Conversion de SO_2

Les études sur la conversion du SO_2 ont été menées sur la même plateforme expérimentale que pour le déNOx dans des mélanges intéressant l'industrie verrière (tableau 3) à des températures allant jusqu'à 500°C.

Le but du traitement de SO_2 et des NOx ($NO+NO_2$), dans ces mélanges contenant une concentration en eau élevée, est leur conversion en acides (H_2SO_4, HNO_2, HNO_3) qui dans une installation industrielle peuvent être neutralisées chimiquement en présence de NH_3 pour former des sels (sulfate d'ammoniac $(NH_4)_2SO_4$ et sulfate nitrate d'ammoniac $(NH_4)_2SO_4$-$2NH_4NO_3$) utilisés fréquemment en agriculture comme fertilisants.

	Composition (N_2 en complément)					
	O_2 (%)	H_2O (%)	CO_2 (%)	NO (ppm)	NO_2 (ppm)	SO_2 (ppm)
#1	8	16	14	523	49	163
#2	8	11.5	16.5	373	39	630

Tableau 3 : *Composition des mélanges étudiés*

Le résultat le plus significatif obtenu est la conversion élevée SO_2 (100% et 60% pour les mélanges #1 et #2, respectivement) à faible dépôt d'énergie (< 30 J/L) quelque soit la température du milieu comprise entre l'ambiante et 500°C [14]. Ces résultats extrapolés à des débits industriels (1000 m^3/h) donnent une consommation énergétique trois fois inférieure à celle consommée lors de l'utilisation des techniques traditionnelles (SCR, SNCR, Reburning) pour le traitement de tels gaz.

L'efficacité de conversion des NOx dans ces mélanges très oxydants est limitée (30% à 30 J/L). Ce résultat, nullement surprenant, est dû principalement aux

réactions de réduction de NO_2 en NO qui deviennent d'une importance comparable aux processus d'oxydation de NO en NO_2. Ce phénomène est d'autant plus important que la température du milieu est élevée. Afin d'améliorer la conversion des NOx il est nécessaire d'ajouter un agent réducteur dans le mélange comme il a été montré dans les études précédentes, [12-13].

A. 4. Dégradation des COV

Le moyen le plus efficace d'éliminer les COV est de les décomposer par oxydation totale, soit par procédé purement thermique à une température supérieure à 700 °C, soit par l'utilisation d'un catalyseur d'oxydation qui permet d'augmenter considérablement la vitesse de pyrolyse mais qui nécessite néanmoins de chauffer les effluents gazeux et le catalyseur à des températures comprises entre 200 et 400 °C. Ceci pose un sérieux problème de consommation d'énergie lorsqu'il s'agit de traiter un flux de gaz important, jusqu'à plusieurs centaines de m^3/h. Par ailleurs, il est maintenant admis que le plasma utilisé seul n'est pas en mesure d'éliminer complètement les polluants et leurs mélanges sans créer des espèces secondaires, éventuellement indésirables, qui sont inévitablement produites du fait même de la création du plasma dans les effluents. Bien que l'efficacité des décharges électriques soit prouvée pour l'élimination de certaines molécules, les phénomènes mis en jeu sont encore trop mal connus. Cette connaissance est pourtant essentielle pour une bonne maîtrise du procédé, pour son optimisation en termes de rendement et de coût énergétique.

Nos recherches se situent dans cet axe et ont essentiellement pour objectif les aspects de cinétique chimique de transformation de molécules tests, hydrocarbures légers tels que l'éthylène (C_2H_4) et le propane (C_3H_8) en faibles concentrations (typiquement inférieures à 1 000 ppm), par une décharge filamentaire de type Décharge à Barrière Diélectrique impulsionnelle dans une atmosphère "sèche" et une autre saturée en vapeur d'eau. L'influence de l'énergie injectée dans le plasma a été étudiée pour différentes conditions de mélanges et de débits. Un bilan des espèces dans la phase gaz en sortie de réacteur a été effectué. Ces études rentrent dans le cadre de l'AC NPD et ont été élargies au GDR CATAPLASME.

Le traitement plasma de C_2H_4 (460 ppm) et C_3H_8 (1 000 ppm) dans de l'air sec ou saturé en eau a montré que les taux de conversion et les concentrations des principaux produits issus de la décomposition de ces molécules, c'est-à-dire CO et CO_2, augmentaient avec l'énergie injectée dans le plasma [35]. De plus, l'importance du dépôt d'énergie sur l'efficacité du traitement et sur la nature et la quantité des sous produits formés est encore une fois démontrée. Des espèces observées à faible énergie déposée (formaldéhyde CH_2O et acide formique CH_2O_2 par exemple) disparaissent au profit de molécules de type R-NOx (méthyle nitrate CH_3ONO_2) avec une production importante de NOx (NO et NO_2) quand l'énergie est augmentée. D'une manière générale, les études paramétriques menées pour des mélanges saturés en vapeur d'eau ont montrés une augmentation des taux de conversion des polluants et une diminution de la concentration en CO pour toutes les tensions étudiées (voir l'exemple de la figure 13). Aucun effet significatif n'est cependant observé pour le CO_2. Ce comportement, en milieu humide, est traduit par une production favorisée d'espèces du type $C_xH_yO_z$ telles que les aldéhydes - (CH_2O) et acétaldéhyde (CH_3HCO) - et de type R-NOx tel que CH_3ONO_2.

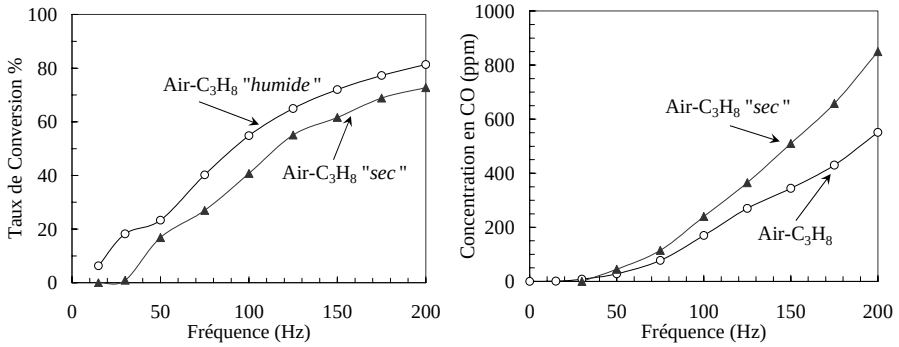

Figure 13: *Influence de l'énergie injectée et de H_2O sur la conversion de C_3H_8 et sur la formation de CO.*

Une troisième molécule, très stable à température ambiante, le chlorure de méthylène (CH_2Cl_2), a été étudiée sur site industriel (société FEDERAL MOGUL) dans un réacteur prototype multi-DBD alimenté par un générateur de tension alternative sinusoïdale de fréquence 50 Hz. Les résultats préliminaires, que nous ne pouvons décrire ici en détails afin de respecter les engagements avec nos partenaires industriels, sont très encourageants puisqu'ils nous ont permis de mesurer des taux de conversion du chlorure de méthylène supérieurs à 50% (figure 14) avec un coût énergétique acceptable pour les industriels.

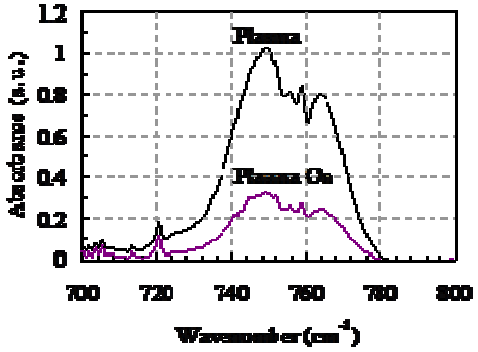

Figure 14: *Spectre FTIR d'un échantillon avec et sans traitement plasma prélevé en sortie de réacteur (Débit de gaz : 169 m^3/h).*

B. Application à la production de gaz de synthèse et H_2

La production d'hydrogène, son transport et son stockage constituent un enjeu fondamental compte tenu de l'évolution des réserves de combustibles fossiles et de la nécessité de disposer de nouveaux vecteurs énergétiques non polluants. Ces différents aspects sont bien connus des scientifiques et d'un public de plus en plus large sensibilisé aux problèmes énergétiques.

Les technologies dominantes aujourd'hui pour la production de gaz de synthèse ($CO+H_2$) à partir des hydrocarbures sont le vapo-reformage (reformage à la vapeur), l'oxydation partielle et le reformage autothermique, combinaison des deux précédentes, surtout utilisé pour la production de carburant liquide de synthèse [36]. Les procédés de vapo-reformage utilisent généralement un catalyseur au nickel à haute température (850-950°C) et à pression élevée (20-30 bars). La maximisation de la production de H_2 s'effectuant par conversion de CO en H_2 (réaction WGS[3]) par adjonction d'eau puis par purification (tamis moléculaire, membranes).

Récemment, de nouvelles voies de production d'hydrogène sont apparues. Il s'agit de méthodes basées sur des énergies renouvelables (décomposition de l'eau par micro-algues et micro-organismes biologiques, énergie solaire) et des procédés plasmas non thermiques [18-19, 37-39]. Dans ce cadre, deux actions importantes utilisant des plasmas non thermiques pour produire H_2 ont été menée dans le cadre du contrat européen "*Synfuels*" et de l'action de recherche concertée ENERGIE du CNRS "*Plasmhyrad*". La première action a été élargie au cas des alcanes (méthane, propane) dans le cadre de la thèse de F. Ouni et ouvre une autre perspective à partir de la biomasse (bio-éthanol, par exemple). La deuxième action est orientée vers le traitement des gaz à l'admission d'un moteur thermique produisant de l'hydrogène et/ou des espèces radicalaires afin de permettre l'amélioration de la combustion et la réduction de la pollution. Cette étude fait l'objet de la thèse d'E. El Ahmar. L'intérêt de la technologie plasma froids réside

[3] *WGS: Water Gas Shift, réaction de conversion de CO en H_2 par adjonction d'eau.*

dans ses performances élevées (efficacité de conversion, faibles coûts énergétiques), la compacité des équipements et le faible coût de mise en œuvre.

B. 1. Décharges Luminescentes à la Pression Atmosphérique (DLPA)

Les réacteurs à plasma non thermique sont de type décharges luminescentes à la pression atmosphérique (DLPA) alimentées par des alimentations oscillantes basées sur un transformateur à fuites magnétiques élévateur de tension (220 V/15 kV) et délivrant un faible courant (< 200 mA) à une fréquence de 50 Hz. Ces réacteurs se présentent sous diverses variantes technologiques : réacteur à décharge glissante tri-anode et Glidarc, réacteur à décharge tournante, et réacteur à décharge stationnaire. La technologie du réacteur tri-anodes est originale et fait appel à une technique de soufflage magnétique, par l'utilisation d'aimants permanents placés judicieusement dans la structure du réacteur, et qui permet de créer la décharge dans un volume de gaz plus important qu'en absence d'aimant. L'allongement de la décharge, due à la force de Laplace (proportionnelle au produit du courant et du champ magnétique), a pour effet d'augmenter sa résistance ce qui induit une auto-limitation du courant et un fonctionnement électrique relativement stable de ce type de réacteur. La figure 15 montre des photographies de ces différentes décharges réalisées dans des conditions expérimentales très différentes les unes des autres.

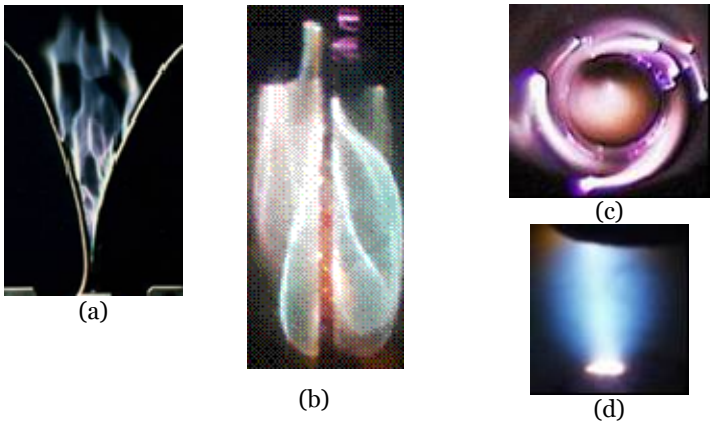

Figure 15 : *Aspect des décharges : (a) décharge glissante type Glidarc, (b) décharge tri-anodes, (c) décharge tournante, et (c) décharge stationnaire.*

Parmi ces systèmes DLPA, le réacteur *Glidarc* constitue une référence phénoménologique permettant de mieux appréhender le fonctionnement des autres réacteurs. La décharge glissante de type *Glidarc* apparaît entre deux électrodes profilées : elle s'amorce là où la distance inter-électrodes est le plus faible, puis se déplace le long des électrodes en s'allongeant sous l'effet d'un flux de gaz transversal. La décharge peut être décrite comme un fin cordon de plasma (diamètre≈2 mm, longueur variant avec le débit de gaz) relativement chaud (≈ 3000 K au centre), entrainé par le courant de gaz et dont les extrémités se déplacent le long des électrodes (sauts à la cathode, glissement à l'anode). La décharge suit alors un cycle périodique amorçage-élongation-extinction. L'élongation de la colonne de plasma s'effectue à champ électrique constant. La tension aux bornes de la décharge augmente progressivement jusqu'à atteindre la tension disruptive au col des électrodes ; un nouvel arc se forme alors, court-circuitant le premier qui s'éteint au sommet du réacteur. Ces décharges présentent les caractéristiques suivantes [40-42]

- Courant < 1A
- $T_e \approx 1$ eV
- $T_{Filament\ plasma} \approx 3000$ K (au centre)
- $T_{gaz} \approx 400$ K
- Puissance électrique déposée : qq. 100 W

Dans la configuration *Glidarc* le volume de gaz réellement balayé par la décharge par unité de temps reste bien inférieur au débit volumique du gaz, ce qui

limite l'efficacité de ce type de réacteur pour certaines applications. Le passage spontané du régime de décharge au régime d'arc peut être évité d'une part en limitant le courant de fonctionnement (alimentation électrique) et d'autre part, en augmentant le débit de gaz permettant ainsi d'accroitre la vitesse de déplacement des pieds d'arc sur les électrodes et réduire ainsi l'émission thermoélectronique.

Les réactions chimiques caractéristiques du procédé à étudier s'effectuent dans le fil de plasma ionisé et à sa périphérie illustrant ainsi l'intérêt des décharges électriques qui permettent de traiter un volume de gaz important alors que les apports d'énergie restent très localisés. Aussi, l'augmentation sensible de la température du gaz rend la description des mécanismes physico-chimiques plus complexe car les mécanismes collisionnels purement électroniques interviennent simultanément avec les mécanismes chimiques classiques.

B. 2. Valorisation des alcanes et alcools

Les travaux décrits ici concernent principalement la production d'hydrogène par décharge glissante tri-anodes à partir du méthane et du propane et par décharge stationnaire à partir de l'éthanol [18-19, 43-47]. L'étude expérimentale permet de quantifier la production d'hydrogène et les sous produits ainsi que le coût énergétique (exprimé en Wh/L de H_2 produit). Ces expériences ont montrés que les principales réactions en compétition sont les réactions de vapo-reformage et de craquage décrites par les équations (1) et (2) :

$$C_nH_m + nH_2O \rightarrow (n+\frac{m}{2})H_2 + nCO \quad (1)$$

$$C_nH_m \rightarrow \frac{m}{2}H_2 + nC \quad (2)$$

La sélectivité vapo-reformage/craquage dépend essentiellement du rapport molaire eau/alcane. Si pour le méthane la réaction de vapo-reformage domine quelque soit ce rapport (entre 1 et 9), la situation est différente dans le cas du propane pour lequel une diminution du rapport molaire (inférieur à 15) favoriserait la production de H_2 "propre" via la réaction de craquage. Dans ce cas, le dépôt de carbone sur les électrodes et les parois du réacteur génère des instabilités qui influent négativement sur le fonctionnement de celui-ci.

En plus du gaz de synthèse (H_2+CO) et l'alcane non transformés, les sous produits de la réaction sont essentiellement le CO_2 et les hydrocarbures en C_2 comme le montre l'exemple donné par la figure 16.

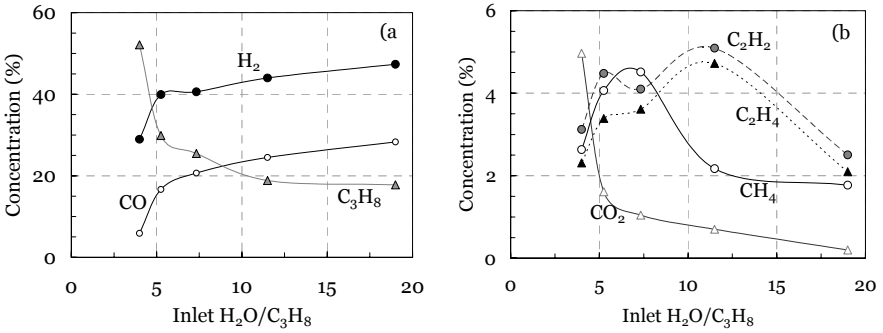

Figure 16 : *Concentrations des principales espèces (a) et des sous produits (b) en sortie de réacteur plasma pour le système C_3H_8-H_2O (Q=100 L min^{-1}, P=1 kW).*

Le tableau 4 synthétise les principaux indicateurs que sont le taux de conversion, les proportions de gaz produits, ainsi que le coût énergétique de production de H_2. Bien que les taux de conversion obtenus sur le réacteur tri-anodes soient environ deux fois supérieurs à ceux obtenus avec la décharge tournante, tous les systèmes testés se caractérisent par de faibles taux de conversion qui restent dans tous les cas inférieurs à 40%. Si les taux de conversion peuvent être facilement améliorés par l'utilisation d'une nouvelle configuration de réacteur, la proportion de CO en sortie de réacteur restera à des niveaux rédhibitoires puisque, compte tenu des résultats actuels, il semble difficile

d'atteindre des niveaux inférieurs à 1% pour une application pile à combustible par exemple.

Valeurs maximales	CH_4	C_3H_8	C_2H_5OH
Taux de conversion	35%	30%	39%
Proportion de H_2	50%	50%	72%
Proportion de CO	15%	30%	28%
Proportion de CO_2	0.4%	5%	12%
Proportion en C_2H_2, C_2H_4, C_2H_6	1%	6%	2%
Coût énergétique (Wh/L (H_2)	0.5	1	-

Tableau 4: *Performances des réacteurs DLPA pour le traitement du méthane, du propane, et de l'éthanol.*

Dans une étude complémentaire, nous avons montré que le niveau de CO pouvait être réduit par la réaction WGS initié par DBD impulsionnelle [48]. Ce résultat est remarquable car il était admis jusqu'a maintenant que la réaction WGS ne pouvait pas être réalisée par décharge à barrière diélectrique. Bien que les conversions obtenues lors des premiers essais soient de l'ordre de 35%, l'utilisation de ce type de réacteur mérite d'être approfondie car ses potentialités pour cette application n'ont pas encore été cernées, en particulier l'effet de son association avec un catalyseur. L'utilisation d'un réacteur DBD couplé au réacteur DLPA pourrait permettre d'obtenir des taux de conversion de CO acceptables. D'autre part, Il est à noter que le passage du combustible dans une DBD aura un effet complémentaire de "nettoyage" puisque d'autres molécules polluantes, telles les molécules soufrées peuvent être converties.

Les coûts énergétiques varient entre 0,2 et 1 W h par litre de H_2 produit. Ces coûts sont du même ordre de grandeur que les valeurs publiées pour des systèmes similaires. Dans ce cas la puissance nécessaire pour obtenir des effets significatifs pour une production d'hydrogène embarquée sur automobile serait inférieure à 1 kW [49]. La technologie plasma permet donc de s'approcher de conditions économiques viables si on considère uniquement les coûts de production ; elle n'est cependant pas encore directement applicable car les conversions obtenues sont insuffisantes.

B. 3. Aide à la combustion

Les plasmas non thermiques sont aussi susceptibles de favoriser le fonctionnement des moteurs thermiques et de réduire la pollution. L'objectif de l'étude est d'évaluer l'intérêt d'un traitement des gaz d'admission par plasma pour les moteurs thermiques en étudiant d'une part les effets induits par un apport d'hydrogène et d'autre part, l'influence des espèces radicalaires produites par le plasma. Dans ce qui suit seul l'effet de l'hydrogène est présenté, l'effet des radicaux est en court d'étude.

Les travaux ont été réalisés dans un premier temps avec un réacteur de type *Glidarc* et poursuivi par la suite avec un réacteur à décharge tournante beaucoup plus efficace [20, 50-51]. L'étude est limitée à des mélanges comprenant 16 à 30 % de méthane dans l'air. En effet, les mélanges les plus pauvres sont explosifs (la limite supérieure d'explosivité est de 15%) et les plus riches provoquent un dépôt de carbone sur les électrodes et les parois du réacteur. Dans ces conditions, l'oxydation partielle de CH_4 se trouve favorisé comme le montre la figure 17 et les proportions H_2, CO, et CO_2 obtenues par traitement plasma atteignent respectivement 20, 10 et 2% pour un taux de conversion de CH_4 d'environ 80%.

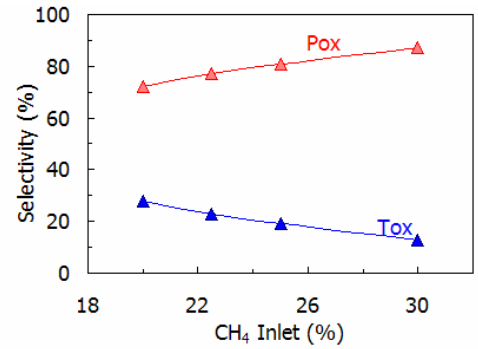

Figure 17 : *Sélectivité oxydation partielle/oxydation totale pour une puissance électrique de 200 W et un débit total de 20 L/min.*

La figure 18 montre l'implantation du réacteur plasma sur le moteur monocylindre (Renault J4S) à allumage commandé fonctionnant au gaz naturel. L'air d'admission est séparé en air primaire et air secondaire, seul le mélange méthane - air secondaire est soumis à la décharge plasma, ceci dans le but de conserver une richesse nettement supérieure à la stœchiométrie et d'éviter ainsi l'inflammation du mélange hors moteur.

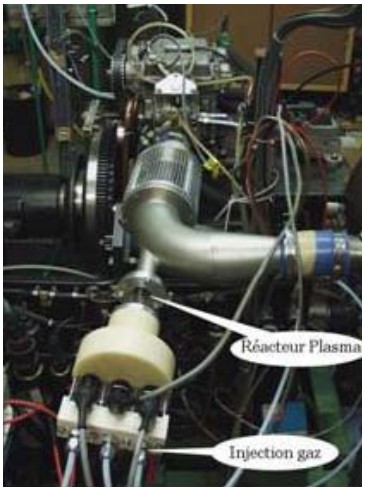

Figure 18 : *Dispositif plasma sur le banc moteur du LME*

Les essais sur banc moteur n'ont pas montré des changements importants du régime moteur lors de la mise en fonctionnement du plasma. Les effets constatés bien que de faible amplitude sont cependant reproductibles et intéressants. Ils concernent principalement l'évolution des NOx, du CO, des HC imbrûlés, et du paramètre αP_{max} (α représente l'angle vilebrequin pour lequel la pression dans le cylindre du moteur est maximale). Les figures 19 et 20 donnent un exemple de ces résultats.

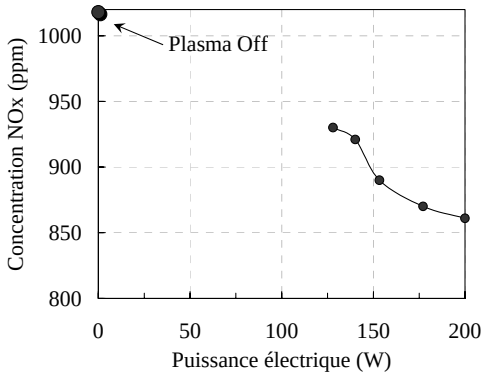

Figure 19 : *Concentration des NOx en sortie moteur. Plasma : 30% CH_4, 16 L/min ; Moteur : Débits gaz naturel (16 L/min), air (190 L/min), 470°C*

Les effets positifs concernent l'évolution de la concentration des NOx et des hydrocarbures imbrulés [51]. Pour une puissance électrique injectée de 200 W la réduction des NOx et des HC imbrulés se situent autour de 15 et 12% respectivement. L'évolution du monoxyde de carbone est défavorable puisque nous mesurons une augmentation de la concentration d'environ 30% par rapport aux résultats sans plasma. La combustion est donc favorisée (Pression maximale supérieure) et le délai d'inflammation diminue en présence de l'hydrogène bien que l'oxydation totale ne soit pas réalisée puisque la quantité de monoxyde de carbone augmente. Ce résultat est corroboré par l'évolution du paramètre αP_{max} qui diminue lorsque la quantité d'hydrogène injecté augmente.

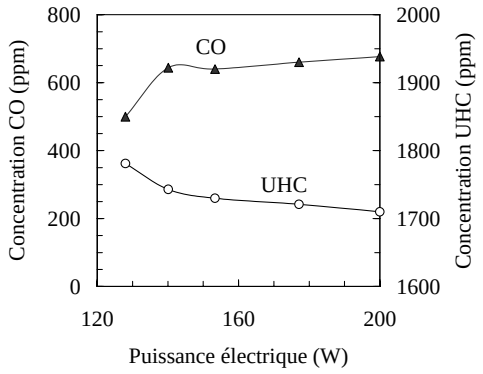

Figure 20 : *Concentration de CO et des hydrocarbures imbrulés en sortie moteur. Même conditions expérimentales que celles de la figure 20*

C. Conclusion

Les technologies plasma non thermiques faisant appel aux Décharges à Barrière Electrique ou aux Décharges Luminescentes à Pression Atmosphérique ont montrées leurs efficacités dans des domaines aussi variés que la dépollution, le traitement de surface, la stérilisation ou la production d'hydrogène. Ces technologies peuvent apporter des solutions simples et robustes pour la mise en œuvre de procédés novateurs.

Dans le domaine de la dépollution, les voies tout plasma ont été explorées et nous orientons nos recherches actuelles vers l'utilisation de systèmes hybrides associant un plasma froids à un catalyseur. Nos études ont montrées que la réduction des oxydes d'azote issus des échappements automobiles peut être assurée efficacement par l'utilisation d'une décharge à barrière diélectrique fonctionnant en régime impulsionnel couplée à un catalyseur composite en post-décharge sans fonction oxydante (plusieurs formulations catalytiques avec des fenêtres de température d'activité différentes). En effet, nous avons montrés que le plasma permet de former les espèces partiellement oxydées de l'hydrocarbure, très utiles pour la réaction de déNOx, dès la température ambiante. Les taux de déNOx obtenus dans nos conditions expérimentales atteignent 60% avec une dépense énergétique compatible avec la consommation d'un véhicule (< 3% de l'énergie totale disponible dans le moteur).

Les résultats concernant la valorisation des alcanes et alcools par traitement DLPA sont tout à fait encourageants et nous pensons continuer ce thème de recherche avec une orientation vers le traitement de la biomasse par plasma non thermique associé ou pas à un réacteur de pyrolyse haute température.

CHAPITRE 2. SOURCES FLASH DE RAYONNEMENT X : DEVELOPPEMENT ET APPLICATIONS

Le rayonnement X[4] a été, depuis sa découverte il y a plus d'un siècle, un des outils les plus puissants pour explorer les propriétés de la matière dans des domaines intéressants une très large communauté scientifique. Pour continuer à délivrer des faisceaux de rayonnement X aux propriétés de plus en plus compétitives plusieurs générations de Synchrotron ou de sources plasma-laser ont été développées. Malgré des progrès remarquables (impulsion ultra brève, faible divergence, flux de photons élevés) réalisés, ces sources restent des équipements très coûteux et de dimensions ne se prêtant pas à une utilisation aisée en laboratoire ou sur une chaîne de production. Aussi, il existe un réel besoin pour le développement de sources compactes, transportables et accessibles aux laboratoires ou à l'industrie. Ces sources pouvant avoir des performances comparables sinon élevées à celles des gros équipements disponibles.

Bien que plus conventionnelles, les décharges rapides haute tension, dans le vide ou dans un gaz basse pression, semblent pour l'instant offrir une alternative très attrayante pour la réalisation de telles sources [52-61]. Ces développements bénéficient des progrès réalisés dans le domaine de l'électronique rapide, des alimentations HT, du stockage d'énergie, et des systèmes de commutation rapide. L'objectif est de produire des sources de rayonnement X durs (jusqu'à 450 keV) à foyer unique délivrant des flux de photons X élevés (>10^{10} photons par tir) dans des impulsions courtes (domaine nanoseconde) et fonctionnant à des fréquences de répétition élevées (jusqu'au kHz). Ces sources peuvent trouver application dans des domaines traditionnels comme l'observation et l'étude de phénomènes ultra rapides, la radiographie éclair à haute cadence (médecine, biologie, matériaux), la pré-ionisation de lasers à gaz, la photoexcitation et la photo-ionisation (atomes, molécules, agrégats), ou dans les domaines apparus récemment concernant les diagnostics des milieux fluides denses, des milieux polyphasiques ou des milieux turbulents.

Dans ce qui suit, nous présenterons les trois différentes sources impulsionnelles de rayonnement X polychromatique que nous avons développées et optimisées pour fonctionner à haute cadence. La première est la source 50 keV, basée sur la technologie des lignes Blumlein, et conçue initialement pour la photo-ionisation d'échantillons gazeux à très haute pression pour la génération de la fluorescence

[4] *X désigne le rayonnement électromagnétique dans le domaine spectral de l'ordre du keV jusqu'à quelques centaines de keV.*

dans le domaine UV[5]-VUV[6]. Les deux autres sources utilisent la technologie des générateurs HT multi-lignes pour produire des photons X plus durs (100 keV pour la seconde et 450 keV pour la troisième) dans des impulsions très courtes (quelques nanosecondes) et pouvant fonctionner selon deux modes distincts : le mode "quasi-continu" (quelque centaines de Hz) ou le mode "rafale" (jusqu'à 5 impulsions au kHz). Ces systèmes ont été utilisés pour la radiographie éclair ainsi que dans le domaine biologique (stérilisation, décontamination). Ces sources très énergétiques (débit de dose supérieur à 6 $kRmin^{-1}$) et de taille très réduite (volume <0.2 m^3) peuvent être très attractives pour d'autres applications. Ces travaux ont fait l'objet de plusieurs publications [61-80].

Ces travaux de recherche ont été réalisés le cadre de :

- Contrat d'Aide à l'Innovation ANVAR "*Développement d'un générateur impulsionnel de rayons X*" en collaboration avec la Société INEL
- Convention de recherche ETBS-DGA "*Étude d'un générateur impulsionnel de rayons X durs à très haute cadence en mode rafale*"
- Convention d'étude INRA–CRITT–HYGINOV "*Effet de l'irradiation X sur les bactéries*"

A. Développement et performances de sources flash X

Les décharges rapides HT dans des milieux à basse ou très basse pression sont connues depuis longtemps pour produire efficacement du rayonnement dans le domaine des X "durs" (jusqu'à quelques centaines de keV). Le principe de base de l'émission des rayons X repose sur le bombardement électronique d'une anode métallique. Cependant les électrons ne sont pas fournis par un filament chauffé comme pour le cas de tubes continus, mais issus d'une décharge électrique haute tension rapide entre deux électrodes. Le résultat est la production d'impulsion nanoseconde de rayons X. Ce type de source impulsionnelle est couramment désigné flash X. Ces sources X s'articulent autour de trois sous-ensembles essentiels : une alimentation électrique dont le dimensionnement est compatible avec la charge rapide des éléments de stockage, un dispositif de mise en forme d'impulsions électrique rapides (domaine ns) couplé à un dispositif multiplicateur de tension (configuration Blumlein ou faisceaux de lignes, selon le cas), et une diode X conventionnelle de faible impédance dont la pression résiduelle est contrôlée [61-62].

La génération des impulsions électriques à front de montée très rapide ($dV/dt > 10^{13}$ $V\,s^{-1}$) et de durée de quelques dizaines de nanosecondes nécessite le développement de circuit de faible inductance associant deux bancs de condensateur disposés en géométrie Blumlein et un élément de commutation HT rapide. Les éléments de stockage et de transfert de l'énergie peuvent être soit des capacités discrètes HT, soit des lignes de décharge de faible impédance. Le choix de lignes de décharge de faible impédance a été motivé par d'une part, le fait de pouvoir fabriquer des lignes de self propre très faible et d'autre part, de pouvoir travailler à des tensions de charge peu élevées dans la mesure où des surtensions très significatives aux bornes des électrodes lors des décharges peuvent être obtenues avec ces systèmes. Les performances de la source X sont étroitement liées aux caractéristiques du système de génération d'impulsion incluant l'élément de commutation (thyratron, pseudo-spark, éclateurs : mono-spark ou roto-spark

[5]*UV (Ultra Violet) : Région du spectre électromagnétique correspondant à un rayonnement dont la longueur d'onde (λ) est comprise entre 200 nm et 400 nm.*

[6]*VUV (Vacuum Ultra Violet) ou Ultra Violet du Vide : Région spectrale entre la limité inférieure du domaine UV et quelques nm. Cette dénomination est due à la forte absorption de l'oxygène et de l'azote dans ce domaine (jusqu'à environ 60 nm), qui implique d'éviter tout contact avec l'air de l'ensemble des éléments de la chaîne de mesure spectroscopique*

simples ou déclenchés par DBD). Un important travail sur la génération d'impulsion très haute tension, cœur de ces dispositifs, nous a permis de mettre au point des sources flash compactes capables de produire à partir d'un seul foyer des impulsions de photons X d'énergie élevée (jusqu'à quelques centaines de keV), à très haute fréquence (jusqu'à 400 Hz en fonctionnement continu et 1 kHz en mode rafale).

Selon le système, la HT appliquée à l'étage primaire du générateur se situe dans la gamme 5-40 kV correspondant à des énergies électriques stockées pouvant atteindre quelques dizaines de joules. La libération de cette énergie sous un courant transitoire de plusieurs kA et des tensions de plusieurs dizaines de kV conduit à l'émission d'impulsions de rayonnement X de largeur se situant entre quelques ns à quelques dizaines de ns. Ce rayonnement est principalement constitué des raies caractéristiques du matériau utilisé pour l'anode, c'est-à-dire des photons autour de 8 keV pour Cu et W et de 17 keV pour Mo, au-dessus d'un large continu de bremsstrahlung qui se termine à une énergie caractéristique de la tension maximale appliquée à la diode X (jusqu'à 450 keV pour la troisième source). Le choix de la tension de fonctionnement et des matériaux constitutifs des électrodes permet de modifier les énergies des raies émises ainsi que la proportion de rayonnement issue de ces raies et de celle du bremsstrahlung. Le caractère polychromatique de l'émission X et la non disponibilité de spectromètre adapté à ces sources qui émettent des flux de photons élevé (> 10^{10} photons/tir) rend difficile une mesure précise de la distribution spectrale. Toutefois, une estimation assez complète du spectre X a été abordée expérimentalement par la méthode des absorbants et par modélisation. Les résultats ont montré que environ 90% des photons sont émis dans les raies caractéristiques du matériau de l'anode et environ 10% dans le continu de bremsstrahlung s'étendant jusqu'à des domaines d'énergie permise par les tensions d'alimentation employées. Les mesures de l'énergie maximale du spectre ont été confirmées à l'aide du détecteur SILENA couplé à un analyseur multicanal et calibré à l'aide d'une source étalon de ^{132}Cs d'activité égale à 1µCi qui émet des raies à 32 et 662 keV.

Trois sources émettant des photons X durs ont été développées [55, 61-62]. La première que nous appellerons "***source 50 keV***" est basée sur la technologie des lignes Blumlein [55]. Les deux autres sources appelées respectivement SPHINX (**S**ource de **PH**otons **I**mpulsionnelle **N**anoseconde **X**) et "***source 450 keV***" utilisent la technologie des faisceaux de lignes [61]. Le développement et l'optimisation de ces sources a nécessité plusieurs années de travail car les problèmes à résoudre se situaient à tous les étages du dispositif : stockage de l'énergie, système de mise en forme de l'impulsion, commutation rapide, multiplication de tension, et diode X.

Les impulsions X, très reproductibles, présentent une largeur à mi-hauteur (FWHM) comprise entre 5 et 40 ns dépendant de la configuration des électrodes et de la pression résiduelle régnant dans la diode. Un exemple typique de l'évolution temporelle de l'impulsion X obtenue avec ces systèmes est montré sur la figure 21.

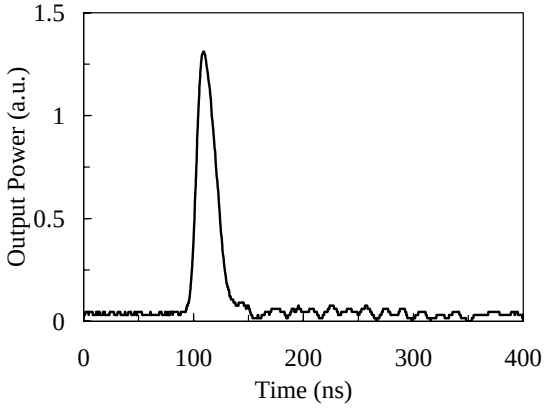

Figure 21 : *Evolution temporelle typique de l'impulsion X [61].*

Ces impulsions peuvent être produites à des fréquences maximale de 400 Hz pour la source 450 keV en mode continu durant quelques dizaines de seconde (figure 22) ou jusqu'à 1 kHz en mode rafale de 2 à 5 impulsions (figure 23). Ce taux de répétition de 400 Hz n'est absolument pas une limite du système lui même mais, il est dû aux performances de l'alimentation HT disponible au moment de cette étude. Dans ces conditions, il n'y a pas de capacité réservoir, et le maintien de la charge aux bornes du système de transfert capacitif n'est pas assuré en utilisation à très haute fréquence.

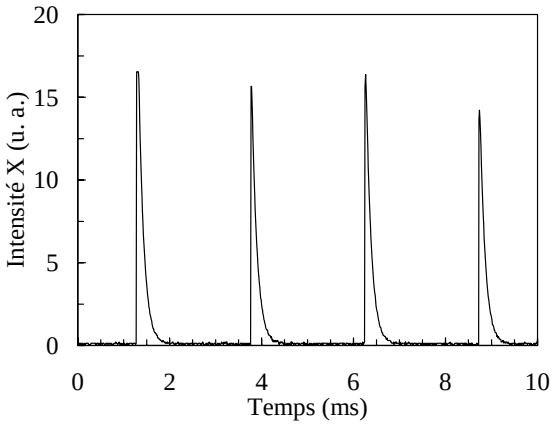

Figure 22 : Série d'impulsions X à 400 Hz obtenue avec la source 450 keV. (La largeur des impulsions apparente mesurée est due à l'adaptation d'impédance : largeur réelle : 22 ns)

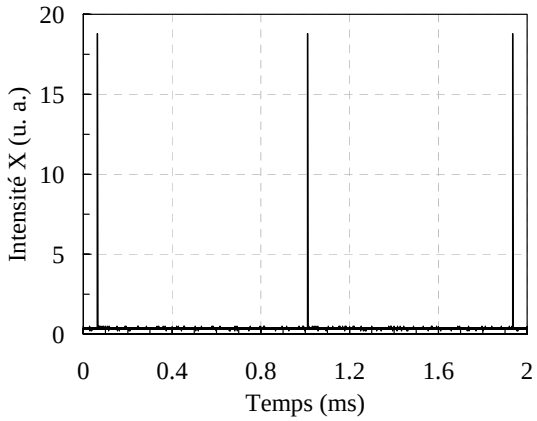

Figure 23 : Rafale de trois impulsions X (1 mR à 1 m) à 1 kHz (source 450 keV)

La durée de fonctionnement du système, sans réduction sensible de la dose, est limitée par les dégradations que subit l'anode. Ce phénomène d'érosion est beaucoup plus rapide dans le cas d'une cathode pointe. Pour la source 50 keV une anode tournante et un système externe de réglage de l'espace interélectrodes a considérablement augmenté la fiabilité du système permettant un fonctionnement en routine à (10-20) Hz pendant plusieurs jours sans modification importante de la dose émise (fluctuations autour de la dose moyenne < 15% sur plusieurs heures). Pour les deux autres sources (diode de configuration anode pointe-cathode creuse) le fonctionnement en routine à quelque dizaines de Hz est cependant limité à quelques minutes comme le montre le graphique de la figure 24.

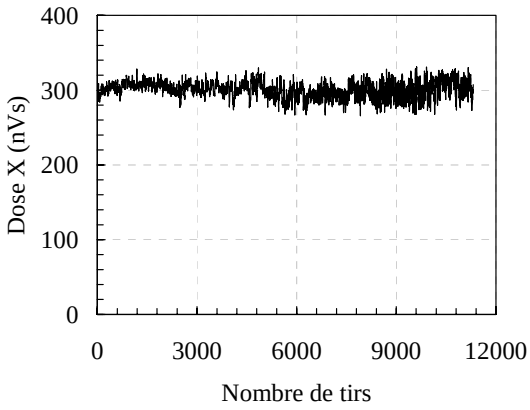

Figure 24 : *Variation de la dose de rayonnement X en fonction du nombre de tirs (source 450 keV) pour une tension de choc de 300 kV et un taux de répétition de 10 Hz.*

Des résultats intéressants ont été obtenus en changeant la nature du gaz dans la diode X. Ces résultats sont montrés sur la figure 25 (les résultats avec l'air doivent comparés à ceux obtenus avec N_2). Dans le cas de gaz rares légers la pression de fonctionnement peut-être largement étendue sans diminution de la dose émise. Ceci est intéressant pour des applications spécifiques ne nécessitant pas l'utilisation de fenêtres spéciales ou de système de pompage complexe.

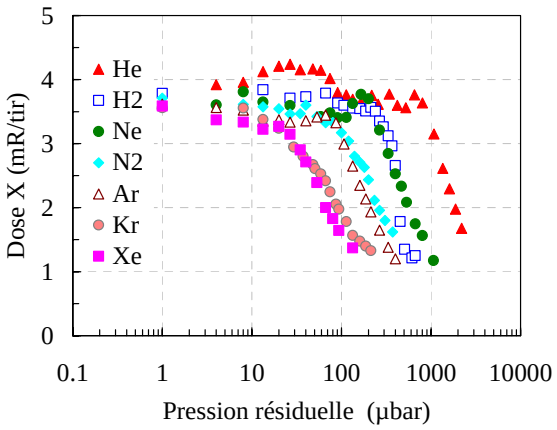

Figure 25 : *Dose émise en fonction de la pression résiduelle dans la diode X pour différents gaz de remplissage [62].*

La géométrie et la dimension de la source de rayonnement X est un paramètre essentiel pour les applications de radiographie éclair ou de diagnostics par exemple. Différentes géométries d'électrodes (pointe, rondin, lame, couronne, etc.) ont été testées afin de trouver un compromis entre des sources X de foyers réduits et des flux de rayons X suffisants.

Dans ce qui suit nous donnons les principales performances des différentes sources développées. Le choix de la source peut être fixé selon l'application envisagée pour un fonctionnement en mode mono-coup, en mode pulsé en continu, ou alors en mode rafale.

A. 1. La source 50 keV

Energie max. stockée	6 J à 37.5 kV
Energie des photons X	5 - 50 keV
Géométrie de la source	Filament long. 10 cm ou Ponctuelle Φ<300 µm
Durée de l'impulsion	3 - 22 ns
Dose[7] à fenêtre de sortie	Jusqu'à 2 R/tir
Taux de répétition	Mono-coup - 50 Hz
Flux de photons X (E>5 keV)	Quelques 10^{12}/tir
Dimension du système (hors pompage et alimentation HT)	1.4 x 0.3 x 0.3 m^3

Tableau 5 : *Performances de la source SPHINX*

A. 2. La source sphinx

Energie des photons X	5 - 100 keV
Géométrie de la source	Ponctuelle Φ< 300 µm
Durée de l'impulsion	3 - 30 ns
Dose à la fenêtre de sortie	1 R/tir
Taux de répétition	Mono-coup - 60 Hz
Dimension du système (tout compris)	< 0.2 m^3

Tableau 6 : *Performances de la source 100 keV*

A. 3. La source 450 keV

Energie des photons X	5 - 450 keV
Géométrie de la source	Ponctuelle Φ < 300 µm
Durée de l'impulsion	3 - 40 ns
Dose à 1 m du foyer	> 3 mR/tir
Taux de répétition Fonctionnement prolongé Mode rafale	Jusqu'à 400 Hz Jusqu'à 3 tirs au kHz
Dimension du système (tout compris)	< 0.4 m^3

Tableau 7 : *Performances de la source 450 keV*

B. Applications des sources flash X

Les résultats obtenus avec les sources X que nous avons développées au GREMI montrent que ce type d'appareils est bien adapté à une utilisation en laboratoire, dans l'industrie ou sur le terrain. La durée très brève des impulsions permet d'étudier des phénomènes ultra rapides et la cadence de tir élevée d'envisager des développements intéressants contrôle non destructif et en cinéradiographie par exemple. La production de flux de photons très énergétiques rend ces sources particulièrement bien adaptées à l'excitation de systèmes physiques même relaxants sur des temps très courts. Ces systèmes peuvent aussi être utilisés en

[7] *L'exposition aux rayons X est souvent exprimée en röntgens (R). Le röntgen (R) est une unité associée au degré d'ionisation produit dans l'air. Une exposition aux rayons X d'un röntgen produit une dose tissulaire d'environ 1 rad: 1 R = 1 rad= 2.58.10^{-4} C kg^{-1}.*

biologie et dans l'agroalimentaire pour la stérilisation et la décontamination. Dans ce qui suit, nous présenterons quelques exemples de ces applications.

B. 1. Radiographie éclair

La figure 26 montre un exemple de radiographies (sans filtre) d'une main et d'une bougie d'allumage automobile obtenu en mode mono-coup avec une impulsion d'une durée de 20 ns. Le contraste élevé de ces radiographies montre clairement l'efficacité du système pour deux matériaux absorbants très différents utilisés dans des secteurs d'activité très éloignés l'un de l'autre (médecine et industrie).

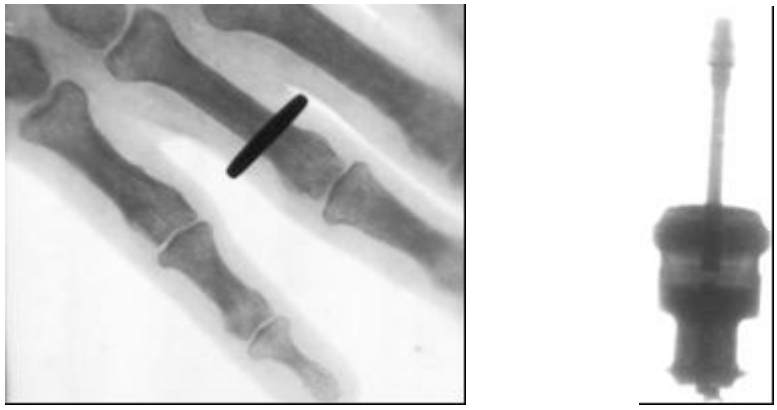

Figure 26 : *Radiographies de la main de l'auteur et d'une bougie d'allumage automobile par flash X : Impulsion unique de 20 ns sur film Polaroid ISO 3000.*

La radiographie éclair en mode mono-coup sur des objets en mouvement a aussi été explorée avec satisfaction comme l'a montré une série de radiographies effectuées sur des projectiles en vol à très grande vitesse au centre d'essais de la DGA à bourges. La figure 27 en donne un exemple et permet d'apprécier la netteté de l'image malgré une vitesse élevée de l'ordre de 700 m s^{-1}.

Figure 27 : *Radiographie d'un projectile en vol à 700 m s^{-1} obtenue avec une impulsion de 20 ns (source SPHINX, autorisation reproduction DGA-ETBS)*

B. 2. Stérilisation et décontamination

Des études sur l'inactivation des bactéries *Escherichia coli* et *Yersinia enterocolitica* en milieu liquide par irradiation X ont été menées en collaboration avec l'INRA. Les effets du rayonnement X sur ces bactéries ont été mesurés en termes de taux d'abattement bactérien et de la D_{10}-value qui représente la dose (ou l'énergie) nécessaire pour réduire de 90% la population initiale de bactéries. A titre d'exemple, l'irradiation d'une population d'*Escherichia coli* à un débit de dose de 7.2 10^4 kRs^{-1} pendant 15 mn conduit à un taux d'abattement bactérien de 99.8% avec une D_{10}-*value* de 28 Gy[8] soit un ordre de grandeur plus faible que les valeurs obtenues avec les faisceaux d'électrons ou les rayons γ [81].

La figure 28 illustre l'effet des photons X sur 2 tapis bactériens (B : *E. coli* ; C : *Y. enterocolitica*). Le tapis A *(E. coli)* est donné pour référence (sans irradiation). Dans le cas B, nous observons que l'irradiation X (source de géométrie conique) a

[8]*La quantité d'énergie absorbée par unité de poids d'un organe ou tissu est appelée la dose absorbée. Elle s'exprime en grays (Gy) : 1 Gy = 100 rads=1 J* Kg^{-1}.

irrémédiablement inactivé les bactéries *E. coli* puisque 4 jours après le traitement aucune population ne s'est développée. Dans le cas C, le traitement a été moins efficace (conditions expérimentales différentes) et les quelques bactéries qui ont survécues se développent de nouveau.

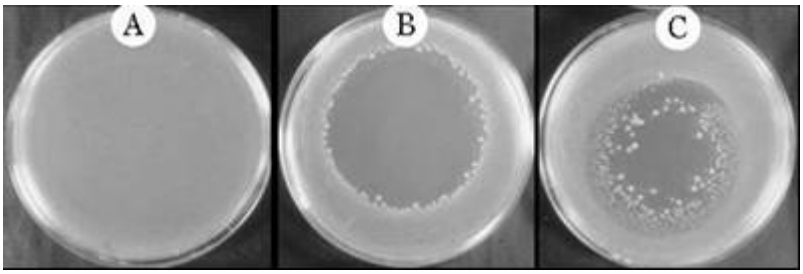

Figure 28: *Boite de pétris contenant les bactéries 4 jours après l'irradiation*
A : Colonie de référence (sans irradiation X)
B : Escherichia coli : Dose absorbée: 79.2 Gy
C : Yersinia enterocolitica : Dose absorbée: 79.2 Gy

Ces résultats confortent l'hypothèse de l'efficacité des sources flash X pour ces applications. Cette technologie appliquée dans le domaine agroalimentaire doit être complétée par des études sur d'éventuelles modifications des propriétés organoleptiques (saveur, goût, teneur en vitamines,...) du produit traité.

B. 3. Excitation de gaz rares à haute pression

Les plasmas de gaz rares à haute pression (jusqu'à 60 Atm) sont connus pour émettre de larges et intenses continus dans le domaine dans le domaine UV-VUV [82-89]. La génération de cette fluorescence était jusqu'alors uniquement accessible aux grands instruments (synchrotrons, faisceaux d'ions lourds ou légers). Les recherches s'étaient focalisées, non pas sur les "*premiers continus*"[9] ou "*second continus*"[10], bien connus et parfaitement identifiés mais sur les dits "*troisièmes continus*" situés à des longueurs d'onde un peu plus élevées et mis en évidence depuis plusieurs décennies [90]. Ces continus intenses présentent une largeur spectrale tout à fait exceptionnelle, jusqu'à 100 nm. L'analyse spectrale de ces fluorescences observées dans des conditions expérimentales très différentes montre une structure particulièrement complexe qui varie avec le temps et la pression du gaz. Même si l'origine moléculaire ionique de ces continus était établie, ce comportement rendait difficile l'attribution de ces fluorescences à tel ou tel système moléculaire bien défini.

La fluorescence des plasmas de gaz rares (He, Ne, Ar, Kr, Xe) à des pressions comprises entre 0.1 et 30 bars excités par la source flash 50 keV spécialement développée pour cette étude est étudiée sur un domaine de longueur d'onde compris entre la coupure des hublots en MgF_2 (110 nm) et le proche infrarouge (800 nm). Les impulsions de rayonnement sont envoyées dans une cellule de gaz à haute pression de 10 cm^3 à travers une fenêtre en kapton (coupure à 5 keV). La fluorescence produite est suffisamment intense pour être analysée par des moyens de diagnostic tout à fait conventionnels (spectromètre, photomultiplicateur, chaîne d'acquisition rapide).

La distribution spectrale du rayonnement X autour de 10 keV permet de déposer efficacement dans le gaz la quasi-totalité de l'énergie rayonnée disponible, de 80 % dans Ne à 30 Atm jusqu'à presque 100 % dans Xe à qq. Atm (figure 29). Le dépôt d'énergie se fait par photo-excitation des couches internes des atomes. Les

[9] *Transitions entre les deux premiers états excités dans des niveaux vibrationnels élevés et le fondamental répulsif de la molécule Rg_2, à grandes distances internucléaires (Rg= gaz rare).*

[10] *Transitions entre ces mêmes premiers états excités, mais dans les niveaux vibrationnels les plus bas, sur le fondamental répulsif de la molécule Rg_2. A haute pression, compte tenu de la relaxation vibrationnelle très rapide, seul le second continu est produit efficacement.*

électrons très rapides produits perdent rapidement leur énergie par collisions avec les atomes du gaz produisant à leur tour des ions et des atomes excités. La densité électronique du milieu a pu être estimée de l'ordre de 10^{12} cm^{-3}. Pour tous les gaz étudiés, le spectre est complètement dominé par les continus UV-VUV, la fluorescence dans les domaines visible et proche infrarouge restant tout à fait négligeable, pour ainsi dire inexistante.

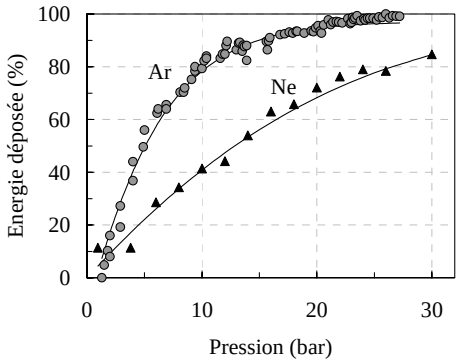

Figure 29 : *Energie déposée au travers d'une lame d'Ar et de Ne en fonction de la pression. Comparaison entre les résultats expérimentaux (points) et la simulation (traits).*

La fluorescence correspondant au "*troisième continu*" a été observée pour tous les gaz rares excepté pour les plus légers tels que l'hélium et le néon pour lesquelles les expériences n'ont montré aucune fluorescence significative dans le large domaine de longueur d'onde exploré (110-800 nm) même pour les pressions les plus élevées supportées par la cellule [63-69]. L'absence de fluorescence était prévisible dans le cas de He mais pas dans le cas de Ne. En effet, si He reste complètement transparent aux photons X émis par le flash (énergie d'une dizaine de keV), la situation est tout autre pour Ne puisque environ 80% de l'énergie incidente est déposée dans ce gaz à la pression de 30 bars (figure 29). La restitution de cette énergie se fait probablement à des longueurs d'onde inférieures à la limite de détection de notre système (110 nm). A titre d'exemple, les spectres obtenus dans les cas de l'argon, du krypton, et du xénon sont donnés dans la figure 30. Les spectres produits sont exclusivement constitués de l'émission des seconds et *troisièmes continus* de gaz rares dans le domaine UV-VUV. Il est important de souligner que l'émission du "*troisième continu*" du krypton et du xénon constitue une première mise en évidence en excitation par flash de rayonnement X.

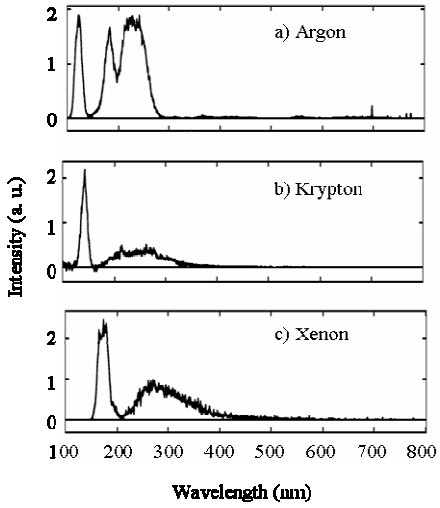

Figure 30 : *Spectres d'émission intégrés de la fluorescence de gaz rares en excitation par flash X : (a) Ar à 3 bar, (b) Kr à 2 bar, et (c) Xe à 1 bar. L'aile rouge des 2nd continus de Ar, Kr, et Xe (centrés à 126, 148, et 173 nm respectivement) est observée.*

Une des particularités des spectres d'émission obtenus en excitation par flash X est l'absence de fluorescence significative à des longueurs d'onde plus grandes que celle du "*troisième continu*" et ce jusqu'au proche infrarouge. L'observation des spectres d'émission de l'argon à des pressions de quelques bars révèle la présence de quatre raies atomiques de faible intensité. Ces raies situées aux longueurs d'onde λ = 772.4, 763.5, 751.4, et 696.5 nm correspondent aux transitions issues d'un même groupe d'états excités Ar(4p) peuplés principalement par recombinaison dissociative de l'ion moléculaire Ar_2^+ dans son état fondamental. Il apparaît donc que les états excités Ar^* peuplés lors de l'excitation par flash X le sont par recombinaison des ions moléculaires et non pas à l'issue de processus collisionnels impliquant des électrons énergétiques et des atomes neutres dans leur état fondamental. En d'autres termes, l'excitation de gaz rares par flash de rayonnement X permet de déposer l'énergie exclusivement dans les états ioniques. Cette dernière remarque singularise l'excitation par flash X par rapport aux autres techniques d'excitation plus conventionnelles (canons à électrons, décharge électrique rapide). Enfin, on peut justifier l'absence de fluorescence de Ne dans le domaine spectral visible par le très faible peuplement des états excités de l'atome neutre dans ce type d'excitation par flash X.

Alors que les *"seconds continus"* ont une forme régulière avec un maximum relativement bien déterminé, les "*troisièmes continus*" présentent une structure assez complexe qui dépend de nombreux paramètres, entre autres de la pression mais aussi du moyen d'excitation, suggérant par la même que la forme spectrale des "*troisièmes continus*" dépend fortement du mode de peuplement des états excitées à l'origine des transitions. Un exemple de spectres d'émission intégrés (sur la durée de l'émission du "*troisième continu*") de la fluorescence de Ar entre 150 et 300 nm à des pressions de 0.5, 1.3, 8, et 17 bars est montré figure 31.

Il apparaît clairement que la pression du gaz joue un rôle fondamental dans la forme spectrale de la fluorescence des "*troisièmes continus*" des gaz rares [63]. A basse pression, le "*troisième continu*" de Ar apparaît sous la forme d'une composante spectrale unique centrée vers 200 nm. Avec l'augmentation de la pression la forme du spectre d'émission se modifie considérablement en une structure plus complexe qui fait apparaître différentes composantes spectrales. On passe donc d'une seule composante spectrale centrée vers 200 nm à 0.5 bar à plusieurs composantes présentant des maxima d'intensité vers 185, 220 et 245 nm et des minima vers 200 et 240 nm à 17 bars. Comme dans le cas de Ar, les spectres d'émission intégrés du Kr et de Xe évoluent assez fortement avec la pression du gaz [63]. Des mesures d'absorption de rayonnement ont permis d'écarter la possibilité d'une auto-absorption transitoire au sein de ces plasmas. Ces expériences d'absorption ont nécessité le développement d'une source plasma créée par interaction laser exciplexe XeCl - cible solide (laiton). Le rayonnement résultant a été enregistré avant et après traversée du volume de gaz rare photo-excité par le flash X. Nous n'avons mesuré aucune absorption significative du rayonnement dans les plasmas à l'origine de l'émission du "*troisième continu*" de l'argon.

Par ailleurs, à une pression donnée, l'analyse résolue dans le temps de la fluorescence révèle également une variation très marquée de la forme des spectres en fonction du temps au cours de la relaxation des plasmas. Ces études confirment ainsi la nature complexe de cette émission et permettent de comprendre la situation quelque peu confuse quant à l'attribution des fluorescences observées à une espèce moléculaire ionique. En effet, la plupart des auteurs se sont intéressés au "*troisième continu*" sur un domaine de pression peu étendu et pour certains sans la disponibilité d'une spectroscopie résolue en temps. La très grande variété des conditions expérimentales dans lesquelles nous avons produit les troisièmes continus nous a permis, à partir d'un dispositif unique, d'obtenir une vision beaucoup plus générale de la fluorescence des gaz rares.

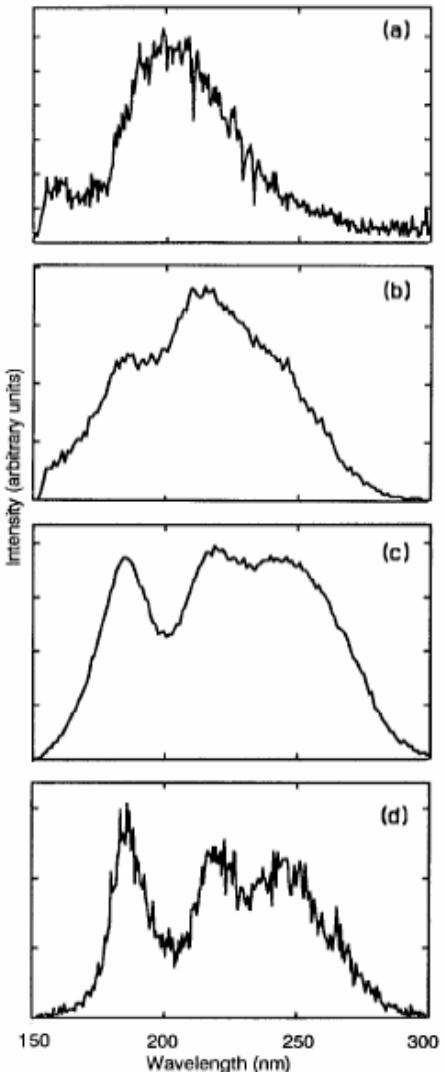

Figure 31 : *Spectres d'émission intégrés de la fluorescence correspondant au "troisième continu" de Ar à : (a) 0.5, (b) 1, (c) 8, et 17 bars*

A la suite de l'ensemble des mesures expérimentales effectuées en excitation par flash X, il nous était apparu nécessaire de reconsidérer l'appellation "*troisième continu*". Ainsi les dénommés "*troisièmes continus*" des gaz rares étaient en fait constitués de multiples composantes spectrales, au moins cinq dans le cas de Ar et de Kr (voir tableau 8). Cela a permis d'introduire les notions de troisième, quatrième, cinquième, sixième et septième continus de gaz rares que nous avons proposé d'identifier sous la dénomination plus générales de "*Continus des ions moléculaires de gaz rares*". Nous avons par ailleurs démontré que leur production ne peut pas s'expliquer par l'intervention d'une seule espèce origine comme cela était habituellement tenté. En plus des dimères, ces continus font intervenir les trimères ioniques.

Gaz rare	Domaine λ (nm) littérature	λ (nm) des maxima : composantes mises en évidence au GREMI
He	55-600	67*, 350
Ne	85-110 et 160-400	99*, 240
Ar	150-300	160, 185, 220, 220, 245
Kr	170-500	170, 225, 230, 245, 300
Xe	190-500	290

Tableau 8 : *Domaine de longueur d'onde des "Continus des ions moléculaires" de gaz rares.*

D'autre part, ces travaux ont permis de mettre en évidence la fluorescence des ions hétéronucléaires de gaz rares à des pressions très élevées. La figure 32 montre l'historique sur 60 ns, après la fin de l'excitation, du spectre d'émission intégré sur 10 ns de la fluorescence du plasma de Ar avec 0.7% de Ne à une pression totale de 1.3 bars.

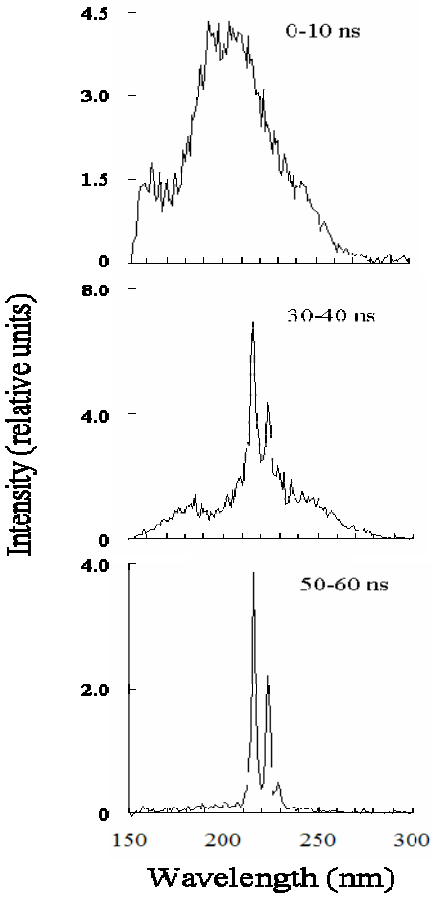

Figure 32 : *Spectres intégrés sur des fenêtres temporelles de 10 ns de la fluorescence d'un plasma d'Ar-Ne (100:0.7) à une pression de 1.3 bars.*

L'observation de ce spectre montre encore une fois tout l'intérêt de la spectroscopie résolue en temps dans ce genre d'étude. Dans les premiers instants de la relaxation, l'émission du plasma est essentiellement dominée par le "*troisième continu*" de Ar. Après cela, nous observons une disparition progressive de ce continu avec l'apparition simultanée des nouvelles émissions des exciplexes ioniques $(ArNe)^+$ aux longueurs d'ondes 216 et 224 nm. Finalement, après 60 ns de la fin de l'excitation, le spectre ne se compose plus que de la fluorescence de $(ArNe)^+$. Dans ces conditions expérimentales, cette fluorescence dure encore quelques centaines de nanosecondes et met en lumière des processus de peuplement des états Ne^+ sur des temps relativement très longs. Ce phénomène n'a pas été étudié dans le cadre de nos recherches.

Les fluorescences des exciplexes ioniques $(ArNe)^+$ à λ=216 nm et λ=224 nm mises en évidence pour la première fois par Tanaka et al [91] dans des expériences de décharges constitue un résultat inédit en excitation par rayonnement X.

La figure 33 donne un exemple typique de spectre de la fluorescence issue d'un plasma de Ar - Xe obtenu pour une pression de 3 bars et une concentration partielle de Xe égale à 0.7 %. Le spectre d'émission observé est constitué du second continu de Xe centré à 176 nm, des émissions très intenses des exciplexes ioniques $(ArXe)^+$ à λ=328 nm et moins intenses à λ=508 nm, et des raies atomiques de ArI (4p - 4s) à 697, 750, 763, 772 nm. Une des particularités de ces spectres est

l'absence totale de la fluorescence du "*troisième continu*" du xénon entre 180 et 500 nm pour tout le domaine de pressions partielles de Xe exploré. Dans ce cas, la formation de l'exciplexe ionique $(ArXe)^+$ résulte probablement de collisions entre l'ion du gaz majoritaire Ar^+ et les atomes du gaz minoritaire Xe comme il a été suggéré par Tanaka et al [91] et Millet et al [92].

Il est important de souligner que, comme dans le cas des émissions de $(ArNe)^+$, celles des exciplexes ioniques $(ArXe)^+$ excitées par flash X à des pressions multi-atmosphériques a constitué un résultat inédit [65].

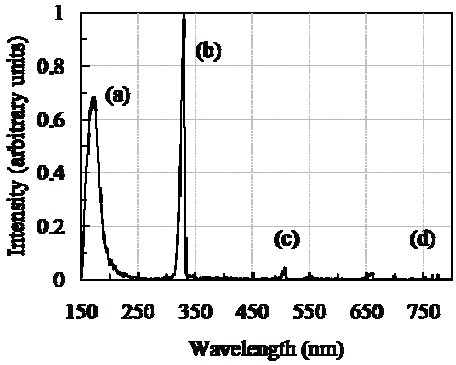

Figure 33 : Spectre résolu en temps (0-50 ns) de la fluorescence d'un plasma d'Ar-Xe (100:0.7) à 3 bars.
(a) Second continu de Xe centré à 176 nm
(b) Emission de l'exciplexe $(ArXe)^+$ à 328 nm
(c) Emission de l'exciplexe $(ArXe)^+$ à 508 nm
(d) Emission des raies de ArI à 697, 750, 763, et 772 nm

C. Conclusion

Ce chapitre a regroupé un ensemble de travaux réalisés dans le cadre très vaste des recherches que j'ai menées sur les nouvelles sources impulsionnelles de rayonnement couvrant le domaine spectral UV – X et leurs applications. Les résultats obtenus, dont certains sont originaux, ont ouverts la voie à plusieurs programmes de recherche et ont permis la réalisation de trois thèses de doctorat. Ces études, qui se poursuivent encore au laboratoire, sont essentiellement axées sur l'optimisation de ces systèmes flash de rayonnement X pour de nouvelles applications telles que la radiographie pulmonaire chez le petit animal, l'imagerie de fluorescence induite par rayonnement X, les diagnostics de milieux poly-phasiques (jets cryogéniques), et la cinéradiographie de pièces métalliques dans un disjoncteur industriel. De plus, un transfert de technologie a été réalisé sur l'une des sources et un développement industriel est en cours.

CHAPITRE 3. CINETIQUE REACTIONNELLE : MILIEUX ACTIFS DES LASERS EXCIMERES

Les lasers impulsionnels à halogénures de gaz rares de grande énergie ont fait l'objet de recherches intensives à l'échelle mondiale. De nombreuses molécules ont été exploitées pour la génération de rayonnements cohérents, parmi lesquelles ArF (193 nm), KrF (249 nm), XeCl (308 nm), XeF (351 nm). La cinétique des milieux actifs de ces lasers fonctionnant à des pressions de plusieurs bars, constitués d'un gaz rare léger (Ne) servant de gaz tampon, d'un gaz rare lourd (Ar, Kr ou Xe) et d'un donneur d'halogène (HCl ou F_2), est très complexe. Des études [93-95], principalement théoriques, ont permis d'élaborer une grande diversité de modèles cinétiques faisant intervenir un nombre important d'espèces et de réactions. Ces modèles différent largement aussi bien sur la nature des mécanismes retenus que sur la valeur de certains taux de réaction. Aussi, il s'est avéré nécessaire de réaliser des expériences spécifiques avec pour objectif d'une part, la détermination expérimentale de certaines constantes réactionnelles et d'autre part, l'établissement des canaux réactionnels prédominants conduisant à l'émission laser de l'exciplexe XeCl. Un accent particulier a été mis sur l'analyse de la réactivité des ions moléculaires Ne_2^+ avec Xe produisant ainsi l'ion Xe^+ nécessaire à la formation ultérieure de XeCl en présence de porteur de chlore. Cette réaction, qui constitue une importante source d'ions Xe^+, était tantôt considérée comme un processus très important tantôt complètement ignorée. Il paraissait donc intéressant de clarifier cette situation.

Pour mener à bien ces études nous avons utilisé entre autres méthodes, la notion "traceur". Un "traceur" est une espèce excitée ou ionisé, produit d'une réaction, permettant de mesurer l'évolution temporelle d'une autre espèce du plasma non accessible directement. Cette méthode, utilisable dans des conditions précises, a permis notamment de déterminer une valeur du taux termoléculaire de transfert de charge de Ne_2^+sur le xénon. Nous reportant aussi les résultats de l'étude du rayonnement émis par les états excités du xénon atomique (états 7 p) sur des temps extrêmement longs dans la post-décharge (≈20 μs comparés aux temps caractéristiques des espèces produites par le plasma ≈500 ns). Ce phénomène est attribué à une boucle de peuplement des ions atomiques Xe^+, composé entre autres de processus d'ionisation Penning de deux métastables atomiques du xénon (Xe^*),

suivi par la recombinaison électronique. La décroissance de la fluorescence des niveaux 7p indique clairement que le principal canal de destruction de ces états est un processus à trois corps.

Une partie de ces recherches ont été réalisées dans le cadre d'une convention du groupement *EUREKA-Lasers Excimères* (EUROLASERS EU 205) regroupant pour la partie française le *GDR* 919 (LPGP-Orsay, CPAT-Toulouse, IMFM-Marseille, GREMI-Orléans) et les sociétés ONERA, CGE, et SOPRA.

Ce chapitre commente une partie des études publiées en [96-104].

I. Expérience

Dans les lasers excimères pompés par décharge électrique, les énergies de l'ordre de quelques dizaines de J/L sont injectées dans le milieu en des temps se situant entre 20 ns et 1 µs. De telles énergies sont généralement stockées par effet capacitif dans des lignes de formation d'impulsion sous une tension donnée. Afin de se rapprocher le plus des conditions réelles de fonctionnement de ce type de lasers (décharges ultra-brèves, haute pression, mélange de gaz corrosifs), un dispositif expérimental combinant une décharge principale dans une configuration de type Blumlein à une pré-ionisation a été développé (figure 34). L'homogénéité du plasma a été assuré par l'utilisation d'une pré-ionisation de type corona.

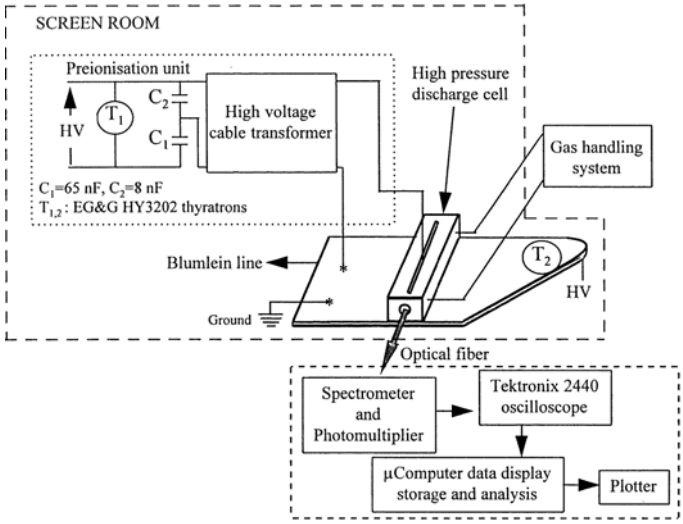

Figure 34 : *Dispositif expérimental : Cinétique de post-décharge aux pressions atmosphériques*

Ce dispositif nous a permis d'obtenir des impulsions de tension (12 kV pour la décharge principale et 60 kV pour la pré-ionisation) de 10 ns de durée (FWHM) à des taux de répétition relativement bas (1 - 16 Hz) pour éviter tout échauffement du mélange gazeux. Les plasmas ainsi obtenus sont homogènes jusqu'à des pressions de 5 atmosphères pour cette étude. Le plasma est observé longitudinalement à travers des hublots de quartz et la lumière émise est analysé par les outils de diagnostics spectroscopiques conventionnels (fibre optique, spectromètre, tubes photomultiplicateurs).

II. Cinétique des plasmas atmosphériques de Ne-Xe

L'évolution temporelle d'un plasma de Ne-Xe non entretenu est caractérisé par une phase d'excitation qui correspond au dépôt d'énergie dans le milieu sous forme d'ionisation et d'excitation du gaz et, une phase de relaxation (post-décharge) correspondant à la désexcitation collisionnelle ou radiative et, à la recombinaison des ions et des électrons. Les mécanismes réactionnels pendant la première phase

sont fortement dépendant de la technique d'excitation et la cinétique de relaxation du plasma revient alors à l'étude des différents processus collisionnels ou radiatifs conduisant au retour à l'état fondamental.

L'identification des composantes spectrales rayonnées durant les périodes de décharge et de post-décharge (figure 35) montre une prédominance des raies atomiques appartenant aux systèmes de NeI, XeI et XeII. Aucune émission des molécules diatomiques Ne_2, Xe_2 ou NeXe n'a été détectée dans le domaine de longueur couvert par notre instrumentation (300 - 700 nm). Les raies les plus intenses de Ne, situées dans le rouge (585 - 672 nm), appartiennent toutes au groupe de transitions 3p-3s. Il est bien établi qu'elles proviennent, dans la post-décharge, de la recombinaison dissociative de l'ion Ne_2^+.

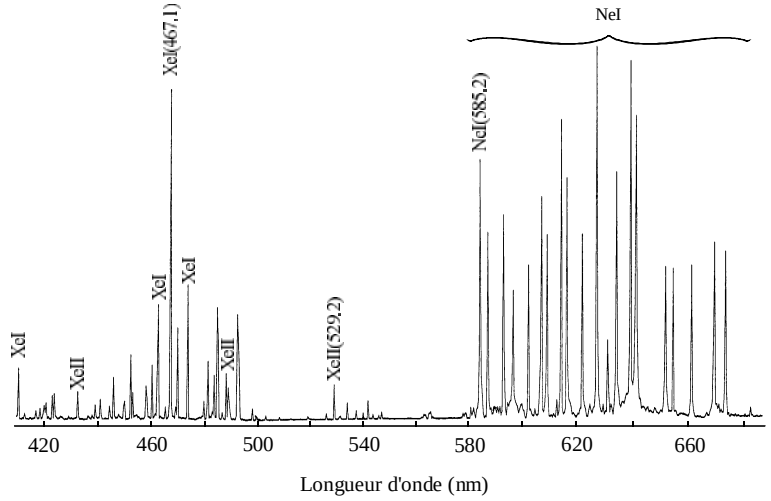

Figure 35 : Spectre d'émission d'un plasma Ne-Xe excité par décharge électrique rapide (P_{Ne} = 1.3 bar et P_{Xe} = 7 mbar).

Les raies de Xe neutre se trouvent essentiellement dans le bleu (412 - 483 nm), et la plupart d'entre elles appartiennent au groupe 7p-6s. Les niveaux supérieurs de ces transitions, situés à 1.16 eV seulement en dessous de la limite d'ionisation, se trouvent à des énergies d'excitation entre 10.9 et 11.0 eV, c'est à dire à seulement 0.1 - 0.2 eV en dessous du creux de potentiel pour l'ion moléculaire Xe_2^+. De ce fait, leur peuplement par recombinaison dissociative de cet ion est peu probable. Ces niveaux pourraient bien constituer un canal de sortie pour la recombinaison électronique des ions Xe^+. Le taux de recombinaison est essentiellement contrôlé par les processus de désexcitation, par collision électronique, de ces états très excités. Nous avons tout particulièrement étudié l'évolution de la raie du xénon à λ = 467.12 nm, susceptible de fournir des renseignements intéressants sur la cinétique des précurseurs ioniques des exciplexes XeCl. L'évolution temporelle de la raie XeI à 467.12 nm a été enregistrée pour une gamme étendue de pression de Ne et de Xe.

Ces émissions sont toujours constituées de deux composante distinctes à décroissance exponentielle (figure 36) : une première composante de décroissance rapide (quelques centaines de ns) suivi d'une composante qui être observée jusqu'à environ 20 µs après la fin de la décharge. Ces évolutions sont fortement dépendantes des concentrations de Ne et Xe.

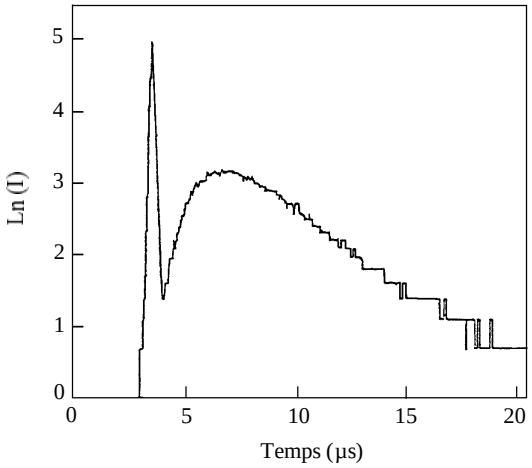

Figure 36 : E*volution temporelle de l'émission XeI à λ = 467.12 nm : P_{Ne} = 1.5 bar et P_{Xe} = 0.3 mbar.*

Il serait donc intéressant d'étudier l'évolution temporelle de ces deux composantes en fonction de la pression partielle de Xe, pour une pression de Ne constante et voir comment évolue la fréquence de destruction des ces deux composantes avec ces paramètres. L'une des méthodes employées utilise la notion de traceur qui permet, sous certaines conditions, de suivre une espèce donnée, inaccessible directement, à partir de la fluorescence d'une autre espèce accessible directement.

II. 1. Emission de XeI à λ = 467.12 nm

II. 1. a. Transfert de charge à 2 et 3 corps Ne_2^+/Xe

La première décroissance du signal de fluorescence de l'état $Xe^{**}(7p)$ (figure 36) reflète l'évolution temporelle des termes de destruction de l'ion Ne_2^+. En effet, dans les premiers instants de la post-décharge (≈ 500 ns) l'ion majoritaire du plasma est l'ion Ne_2^+, suivi en ordre de concentrations relatives par l'ion Xe^+ produit essentiellement par transfert de charge à 2 et 3 corps à partir de Ne_2^+ et détruit principalement par recombinaison électronique selon les réaction suivantes:

$$Xe^+ + e + e \xrightarrow{\delta} Xe^{**} + e \qquad (3)$$

$$Ne_2^+ + e \xrightarrow{k_1} Ne^* + Ne \qquad (4)$$

$$Ne_2^+ + Xe \xrightarrow{k_2} Xe^+ + 2Ne \qquad (5)$$

$$Ne_2^+ + Xe + Ne \xrightarrow{k_3} Xe^+ + 3Ne \qquad (6)$$

Le taux de décroissance de la première composante de XeI *à* λ = 467.12 nm est représenté sur la figure 37 en fonction de la pression partielle de Xe et de la pression totale. Pour les faibles pressions de Xe ce taux augmente proportionnellement au produit des concentrations de Ne et de Xe, suggérant l'implication d'un processus à trois corps. Pour des concentrations de Xe élevées, le taux semble présenter un phénomène de saturation, vers une valeur de $1.7\ 10^7\ s^{-1}$, qui pourrait être une signature d'une réaction inverse à déterminer.

En ne considérant que les termes pertes important pour l'ion Ne_2^+ (réactions 4 à 6), sa fréquence globale de destruction peut s'écrire,

$$\nu = k_1.[e] + (k_2 + k_3.[Ne]).Xe \qquad (7)$$

avec k_1, k_2 et k_3 représentant respectivement le coefficient de recombinaison dissociative, les coefficients de destruction bi et ter-moléculaire de Ne_2^+ par Xe.

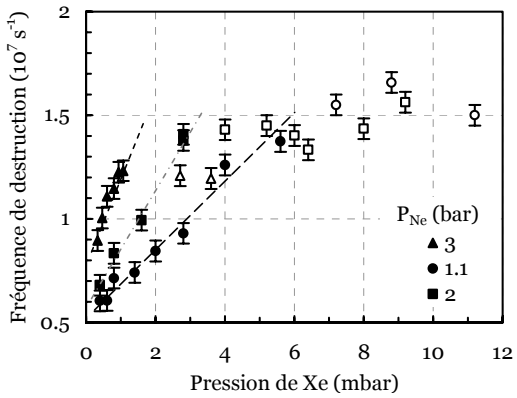

Figure 37 : *Diagramme de Stern-Volmer de la 1ère composante de l'émission des états $Xe^{**}(7p)$.*

En supposant qu'à l'instant initial la densité de population de l'ion Xe^+ est nulle, la résolution de l'équation différentielle régissant cette densité de population donne :

$$\left[Xe^+\right] = \frac{\nu_2}{\nu - \nu_1}.\left(e^{-\nu_1 t} - e^{-\nu t}\right).\left[Ne_2^+\right]_0 \qquad (8)$$

où $\nu_1 = \delta[e]$ avec δ représentant le taux de recombinaison électronique de Xe^+ :

$\delta = 3.8\ 10^{-9}\ T_e^{-4.5}$ [105] et $\nu_2 = k_e\,[Xe] = (k_2 + k_3[Ne]).[Xe]$.

Pour de faibles concentrations de Xe (quelques mbar) et dans nos conditions expérimentales ($T_e \approx 350$ K et une pression de Ne comprise entre 1 et 5 bar), la fréquence de destruction (ν_1) des ions Xe^+ par le processus de la réaction (3) est largement supérieure à celle (ν) de l'ion Ne_2^+ par les processus donnés par les réactions (4), (5), et (6). L'ion Xe^+ jouera donc le rôle de traceur de Ne_2^+ et l'intensité de la fluorescence de l'état Xe^+, qui est à tout instant proportionnelle à $[Xe^+]$, permettra de suivre l'évolution de $[Ne_2^+]$ dans les premiers instants de la post-décharge. Les pressions de xénon limites pour que cette notion de traceur soit appliquée ont été déterminées expérimentalement. Elles sont de 6, 2.7, et 1 mbar pour des pressions totales de 1, 2, et 3 bar, respectivement.

Un raisonnement identique pourra être fait pour les états excités $Xe^{**}(7p)$ qui sont détruits principalement par les processus collisionnels et radiatifs donnés par :

$$Xe^{**}(7p) + Ne \rightarrow Xe^{*} + Ne \qquad (9)$$

$$Xe^{**}(7p) \rightarrow Xe^{*} + h\nu \qquad (10)$$

avec des taux de réactions de 10^{-11} cm^3 s^{-1} [106] et $1.5\ 10^7$ s^{-1} [93] respectivement et où Xe^* est l'état métastable 6s.

Le taux global ν_o de destruction de $Xe^{**}(7p)$ par les processus (9) et (10) est très élevé comparé à ν_1 correspondant à la recombinaison électronique de l'ion Xe^+ ($\nu_o = 2.4\ 10^8$ s^{-1} et $\nu_1 = 2.4\ 10^7$ s^{-1}, pour $N_e = 3\ 10^{13}$ cm^{-3} et une pression de Ne de 1 bar). Dans ces conditions l'état $Xe^{**}(7p)$ sera un traceur de l'ion Xe^+. Finalement, dans la première phase de la post-décharge, et pour de faibles concentrations de xénon l'évolution temporelle de l'ion Ne_2^+, inaccessible directement par nos moyens expérimentaux, peut-être suivi à partir de la fluorescence de l'état $Xe^{**}(7p)$ à $\lambda = 467.12$ nm.

Le coefficient effectif ($k_{eff} = k_2 + k_3[Ne]$) de la réaction de transfert de charge de Ne_2^+ avec Xe (réactions 5 et 6) est représenté sur la figure 38 en fonction de la

pression de Ne. De cette figure sont extraits les coefficients bimoléculaire k_2 et termoléculaire k_3 :

$k_2 = (4.2 \pm 0.5)\ 10^{-12}\ cm^3\ s^{-1}$ et $k_3 = (2.6 \pm 0.3)\ 10^{-30}\ cm^6\ s^{-1}$

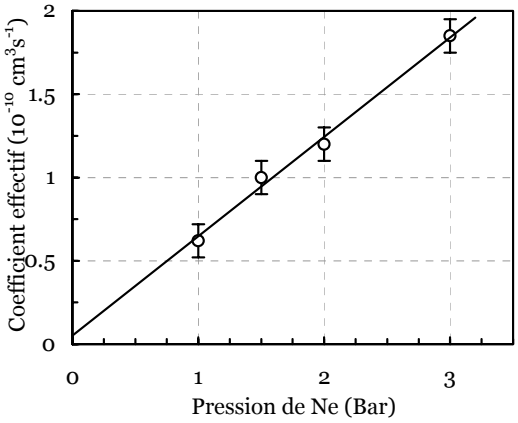

Figure 38 : *Coefficient effectif de transfert de charge de Ne_2^+ sur Xe.*

Ces résultats en bon accord avec ceux obtenus sur une gamme plus restreinte de pression par Collins et al [107], montrent clairement que le canal termoléculaire (réaction 6) ne peut pas être négligé dans la cinétique du laser XeCl quand le néon est utilisé comme gaz majoritaire. En effet, pour des pressions de Ne et de Xe typiquement employées dans ces lasers (quelques bar et quelques mbar, respectivement), la fréquence de destruction de l'ion Ne_2^+ par le processus bimoléculaire n'est de l'ordre que de quelques $10^6\ s^{-1}$ alors que dans les mêmes conditions, la fréquence de destruction associée au canal termoléculaire est deux ordres de grandeurs plus élevée. Ceci aura une influence directe sur le peuplement des ions Xe^+, précurseur des exciplexes XeCl, dont le taux de production est, bien sûr, augmenté de manière significative. Il apparaît donc que le transfert de charge des ions Ne_2^+ sur les Xe doit être considéré comme un processus important dans la chaîne cinétique conduisant au niveau supérieur de la transition laser.

Pour des pressions de Xe supérieures aux valeurs limites déterminées précédemment, l'état $Xe^{**}(7p)$ n'est plus traceur de l'ion Ne_2^+, mais reste toujours traceur de Xe^+. Le principal canal de dépeuplement de cet ion étant la réaction (3), sa destruction se trouve donc très peu affectée par la variation des concentrations de Xe et de Ne. Les résultats expérimentaux confirment bien ce phénomène et on observe une fréquence de destruction relativement constante pour toutes les pressions de Ne. Cette valeur est de l'ordre de $1.4\ 10^7\ s^{-1}$. Ce résultat est en bon accord avec la valeur du coefficient de recombinaison proposée par Stevefelt et al [105] pour une température de 350 K et une densité électronique de l'ordre de $3\ 10^{13}\ cm^{-3}$.

La fréquence de destruction estimée par extrapolation à pression de Xe nulle, dont les valeurs sont comprises entre $0.5\ 10^7\ s^{-1}$ et $0.8\ 10^7\ s^{-1}$, correspond bien à la recombinaison électronique de Ne_2^+ avec un taux de $(1.73 \pm 0.5)\ 10^{-7}\ cm^3\ s^{-1}$. Ce coefficient est en très bon accord avec la littérature [108].

II. 1. b. Processus associatif à 3 corps de $Xe^*(^3P_2)$ avec Ne

La décroissance lente de la deuxième composante (figure 36), s'étendant sur plusieurs microsecondes, traduit des phénomènes mettant en jeu des espèces excitées à très longue durée de vie: les métastables de Xe ou de Ne. Dans cette phase, le taux d'ionisation est maintenu élevé par le processus d'ionisation Penning de deux métastables atomiques du xénon (Xe^*), principal terme de peuplement des ions Xe^+. Le terme source issu des ions Ne_2^+ est pratiquement épuisé après environ

1 µs. Le peuplement des niveaux $Xe^{**}(7p)$ s'effectue donc principalement par recombinaison électronique de Xe^+ devenu l'espèce ionique majoritaire.

D'autre part, le principal terme de destruction des métastables Xe^* correspond à la réaction associative :

$$Xe^* + Xe + Ne \rightarrow Xe_2^* + Ne \qquad (11)$$

La fréquence globale de destruction de Xe^* reste largement inférieure à celle des ions Xe^+ dans nos conditions de pression et, pour les raisons exposées au paragraphe précédent, l'état $Xe^{**}(7p)$ sera traceur des ions Xe^+ et donc de Xe^*. La figure 39 montre la variation de la fréquence de destruction de l'état $Xe^{**}(7p)$ en fonction de la pression de Xe et de Ne.

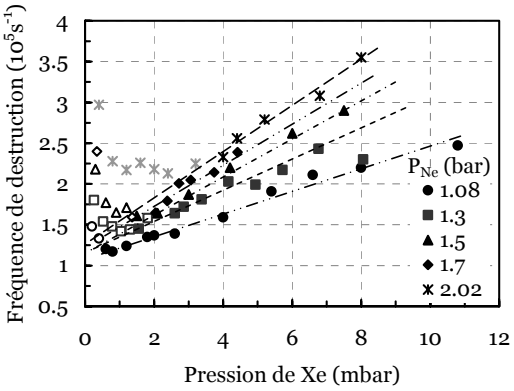

Figure 39 : *Diagramme de Stern-Volmer de la 2ème composante de l'émission des états $Xe^{**}(7p)$*

Il apparaît clairement deux régimes distincts. Le premier régime serait la conséquence de l'emprisonnement de rayonnement à 147 nm émis par l'état de résonance $Xe(^3P_1)$, lequel est couplé par collisions avec l'état métastable $Xe(^3P_2)$. Le second régime traduirait la destruction collisionnelle des atomes Xe^* par des processus faisant intervenir à la fois des atomes de Ne et de Xe.

La figure 40 rend compte de l'évolution du coefficient global de destruction de l'état $Xe^{**}(7p)$ en fonction de la pression de Ne et met en évidence le processus associatif à trois corps de $Xe^*(^3P_2)$ avec Xe. La valeur déterminée $(1.7 \pm 0.3)\ 10^{-32}\ cm^6\ s^{-1}$ est en bon accord avec les estimations de Johnson et al [93] et Aouame [109].

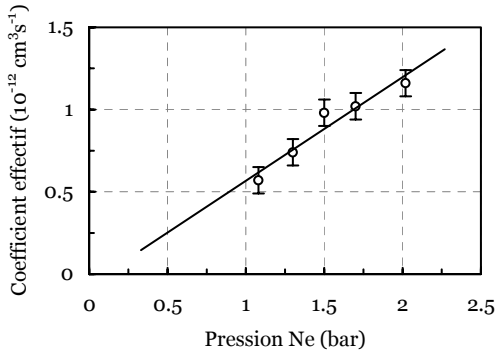

Figure 40 : *Coefficient effectif de destruction de l'état métastable $Xe^*(^3P_2)$ avec Xe.*

Il faut bien noter que les interprétations que l'on peut avancer concernant la cinétique de la post-décharge lointaine doivent être considérées avec prudence en raison de la grande complexité du milieu et du peu d'informations sur certains mécanismes. Une interprétation plausible peut se résumer par le schéma cinétique décrit dans ce qui suit.

II. 2. Schéma cinétique

Nous ne prétendons pas décrire un modèle exhaustif d'un plasma de Ne-Xe à haute pression. L'objectif est d'établir un schéma cinétique simple mais suffisamment complet pour simuler la relaxation des états atomiques et moléculaires de Xe et de Ne impliqués dans la cinétique du laser exciplexe XeCl. En effet, compte tenu du nombre de réactions élémentaires, impliquées dans ces systèmes, qui n'ont fait l'objet d'aucune détermination précise et de l'impossibilité ou de la difficulté d'accès à certaines données expérimentales, la prise en compte systématique de la totalité des espèces concernées et des divers mécanismes régissant la post-décharge serait illusoire ; la complexité même du modèle n'apporterait rien à la fiabilité de la comparaison modèle-expérience.

Ce modèle cinétique suppose que l'énergie d'excitation est déposée en partie dans les états ioniques Ne_2^+, Ne^+, Xe^+ et en partie dans les états métastables $Ne^*(3s)$ du néon. Le modèle prend en compte 26 réactions et permet de décrire l'évolution temporelle de 10 espèces : Ne^+, Ne_2^+, Xe^+, Xe_2^+, Ne^*, Ne_2^*, Xe^*, Xe^{**}, Xe_2^*, et la densité électronique n_e. Les états excités de Xe utilisés dans le modèle sont divisés en deux : l'état Xe^* correspond aux deux niveaux 6s ($^3P_1$ et $^3P_2$) dont le deuxième est métastable et, l'état Xe^{**} regroupe les niveaux 7p situés à une énergie d'environ 10.97 eV du niveau fondamental. La figure 41 représente le schéma réactionnel de relaxation de plasma de Ne-Xe à haute pression utilisé par le modèle. Les principaux canaux de réaction sont montrés en gras et les coefficients de réaction déterminés dans cette étude y sont spécifiés.

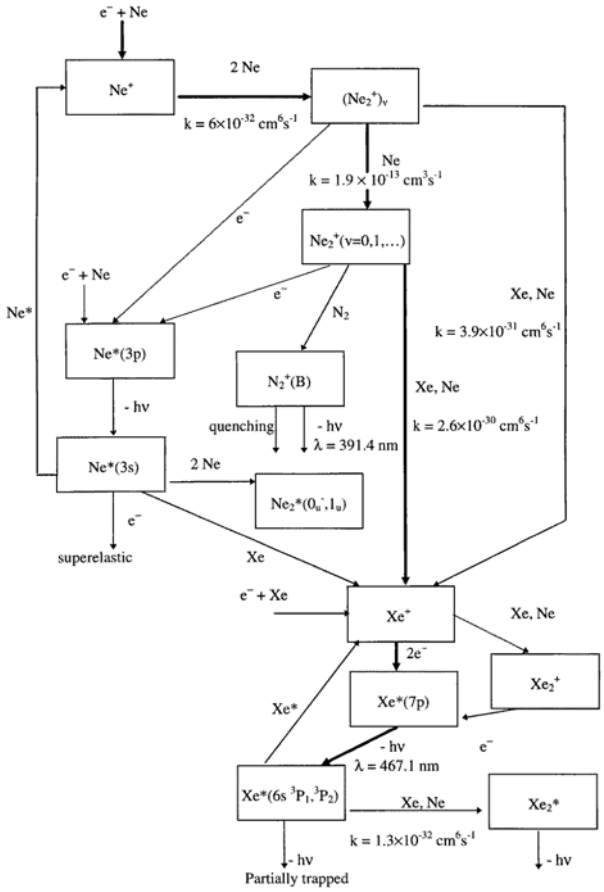

Figure 41 : *Schéma réactionnel montrant les principaux processus intervenant dans la relaxation de plasma de Ne-Xe à haute pression excité par décharge électrique.*

La densité électronique n_e dépend d'un nombre important de paramètres liés notamment au dépôt d'énergie dans le gaz. Elle peut-être estimée à partir des paramètres électriques de la décharge, mesurés expérimentalement. Elle est

donnée par [110] :

$$n_e = \frac{3N_a QdC\sqrt{2\pi m_e kT_e}}{2\tau Ae^2} \qquad (12)$$

où Q, N_a, m_e, A, d, C, τ, et T_e représentent respectivement la section efficace de transfert de la quantité de mouvement en collisions électron-atome, la densité d'atome neutre présents dans le plasma, la masse de l'électron, la section du plasma, la distance interélectrodes, la capacité de charge du système, la durée effective de la décharge ,et la température électronique, respectivement. Pour les champs électriques utilisés, la température électronique T_e dans la phase de création du plasma est d'environ 5 eV, et Q de l'ordre de 2 10^{-16} cm^2 dans le néon pur. L'adjonction de Xe jusqu'à des concentrations relatives de 1% n'est pas susceptible de modifier sensiblement ces valeurs.

La densité électronique maximale peut être estimée en utilisant les sections efficaces de transfert de quantité de mouvement calculées par Bordage et al [111] pour diverses valeurs du champ électrique réduit. Un exemple de résultats obtenus dans Ne pur à une tension de charge de 10 kV est montré dans le tableau 9. Dans ces conditions le maximum du courant de décharge correspondant à un champ électrique de 1.3 kV cm^{-1} et la durée effective de la décharge est d'environ 0.18 µs.

Pression (bar)	1	4
E/N (Td)	5.38	1.35
E_{moy} (eV)	7.18	5.33
Q (10^{-16} cm^2)	2.21	2.09
n_e (10^{13} cm^{-3})	3.96	13.35

Tableau 9 : *Densité électronique calculée pour différentes conditions expérimentales.*

La variation de la densité des particules d'un type donné obéit à l'équation de bilan :

$$\frac{d[n(r,t)]}{dt} = D.\nabla^2[n(r,t)] + S - P \qquad (13)$$

où D est le coefficient de diffusion et ∇^2 l'opérateur de Laplace appliqué à la variable d'espace. S et P représentent respectivement les termes sources et les termes pertes. Les temps caractéristiques de diffusion des espèces du plasma de Ne-Xe aux pressions atmosphériques sont de l'ordre de la milliseconde [102] alors que le temps de relaxation global du plasma dans la post-décharge est très inférieur à la trentaine de microseconde. La diffusion des particules peut donc être négligée dans cette étude.

Les équations d'évolution des différentes espèces se présentent sous la forme d'un système d'équations différentielles couplées du premier ordre qui peut se noter sous forme matricielle :

$$Y(t) = (A_{ij}).\chi(t) \qquad (14)$$

où le vecteur *Y(t)* est composé des dérivées temporelles des concentrations de chaque espèce, la matrice (A_{ij}) représente les différents taux de réaction multipliés par les rapports de branchement et le vecteur $\chi(t)$ est composé des produits de la concentration des réactants entrant dans les 26 réactions du modèle cinétique. La densité électronique n_e est gouvernée par la condition de quasi-neutralité du plasma.

Le système d'équations (14) a été résolu numériquement pour l'ensemble de coefficients donnés précédemment. Il rend bien compte de l'évolution des principales espèces dans une large gamme de pression de Ne, de Xe et de densité électronique. Les évolutions temporelles des concentrations en états ionisés et

excités ont pu être calculées sur des temps très longs atteignant 40 µs après la fin de la décharge. Un exemple de résultats obtenus sur 5 µs est montré sur les figures 42 et 43 pour différents conditions de pression.

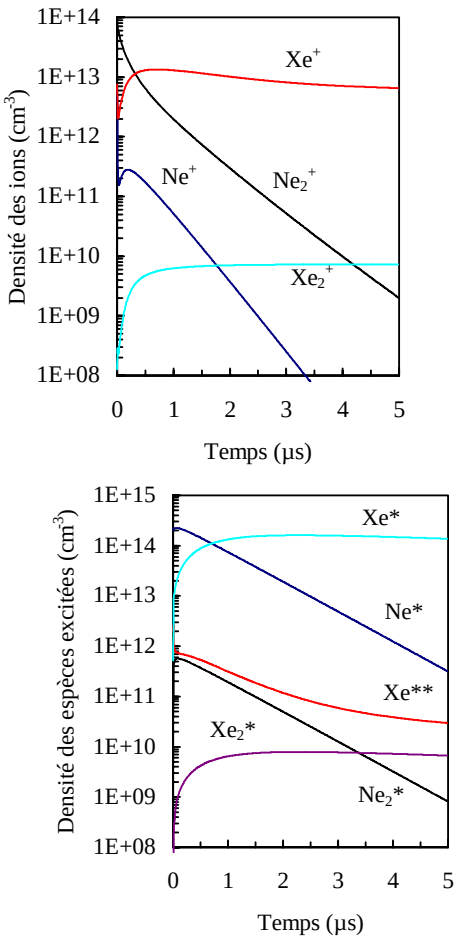

Figure 42 : *Evolutions temporelles calculées des ions et des espèces excités pour une pression de Ne et de Xe de 1 bar et 0.3 mbar respectivement*

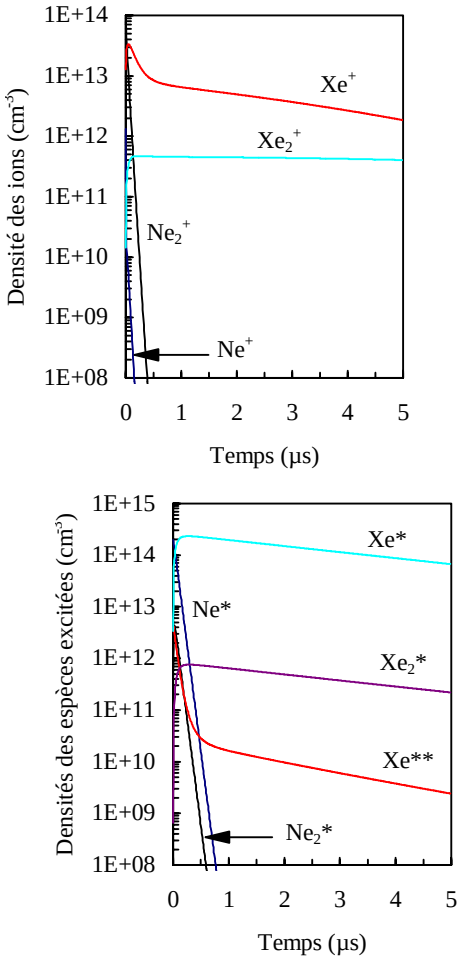

Figure 43 : *Evolutions temporelles calculées des ions et des espèces excités pour une pression de Ne et de Xe de 4 bar et 5 mbar respectivement.*

L'effet principal de l'augmentation des pressions de Xe et de Ne sur l'évolution temporelle des concentrations en états ionisés et excités est d'accélérer la cinétique de relaxation du plasma. A titre d'exemple à une pression de Ne de 1 bar, le maximum de concentration de l'ion Xe^+ précurseur des exciplexes XeCl est atteint 750 ns après la fin de la décharge pour une pression de Xe de 0.3 mbar. Ce temps est réduit à 80 ns pour une pression de Xe 17 fois plus élevée. Dans les mêmes conditions de pressions, la fréquence de destruction des états ioniques Ne^+ et Ne_2^+ augmente de plus d'un ordre de grandeur. Les transferts d'excitation à partir des états atomiques et moléculaires excités du néon (conduisant soit à de l'ionisation Penning soit à de l'ionisation associative), sont responsables de la disparition rapide de états du néon que l'on voit sur les figures 42 et 43.

Dans la mesure où le peuplement des états Xe^{**} émettant à $\lambda = 467.12$ nm résulte de réactions entre les derniers maillons de la chaîne cinétique, il parait très important de pouvoir tester la validité du modèle par une comparaison des prédictions théoriques avec les mesures effectuées sur les évolutions temporelles de la fluorescence de ces états pour des conditions expérimentales très variées.

Les études spectroscopiques sur l'état excité Xe^{**} ont montrés que dans la post-décharge, l'intensité émise dans les raies spectrales provenant de ces états, devrait suivre l'évolution I(t) telle que :

$$I(t) = c_1 [Xe^+] n_e + c_2 [Xe_2^+] n_e \qquad (15)$$

où c_1 et c_2 sont des fonctions de la température électronique T_e. Si l'on néglige la variation de T_e avec le temps l'intensité émise (deuxième composante de la raie)

sera alors proportionnelle au produit des concentrations des ions Xe^+ et des électrons. Dans le domaine des pressions atmosphériques, exploré au cours de ce travail, ces émissions s'effectuaient sur des temps relativement très longs, parfois dépassant 20 µs (figure 36). Ces observations quelque peu étonnantes au départ ont été confirmées par le modèle dans une large gamme de pressions partielles. Un exemple de comparaison des prédictions du modèle avec les mesures expérimentales effectuées sur les évolutions temporelles de la fluorescence des états atomiques excités Xe^{**} est montré figure 44. L'accord entre les résultats expérimentaux et ceux issus de la modélisation est satisfaisant sur un large domaine de pressions partielles. Il est cependant à noter que pour des pressions partielles de Xe élevées de fortes instabilités interviennent dans la décharge et les mesures deviennent imprécises. Cet effet pourrait expliquer, dans ces conditions, l'écart relativement important (≈30%) entre les résultats du modèle et ceux issus de l'expérience.

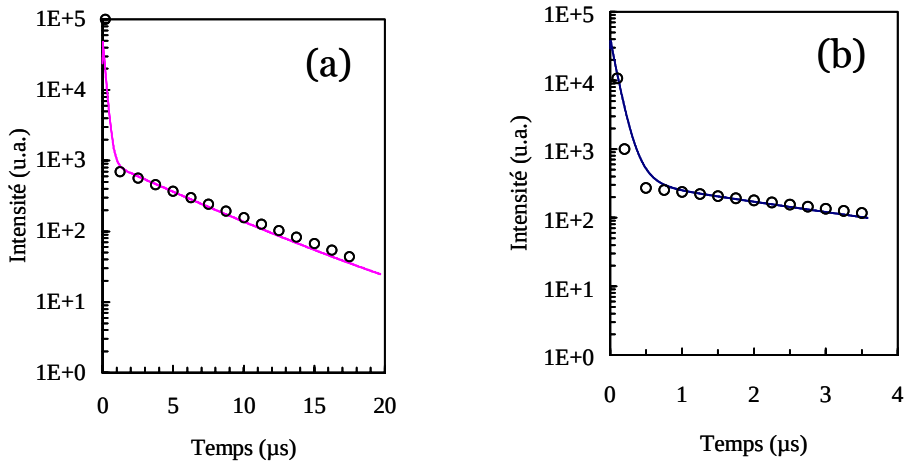

Figure 44 : *Comparaison des évolutions temporelles expérimentales (points) et calculées (trait) de la fluorescence de l'état Xe^{**} à λ = 467.12 nm pour :*
(a) : P_{Ne} = 1 bar et P_{Xe} = 3.2 mbar
(b) : P_{Ne} = 3 bar et P_{Xe} = 1.8 mbar

D'après ces résultats, il semble que les quelques réactions prises en compte soient suffisantes pour rendre globalement compte de la relaxation du plasma et des échelles de temps caractéristiques des différents processus mis en œuvre dans la cinétique réactionnelle de Ne-Xe à haute pression.

Comme il a été déjà souligné, les collisions à trois corps de transfert de charge des ions moléculaires Ne_2^+ avec Xe est un processus très important dans la cinétique des lasers exciplexes XeCl utilisant le néon comme gaz majoritaire à des pressions atmosphériques. Concernant la densité des états atomique Xe^{**} issus de la recombinaison électronique de Xe^+, la figure 45 montre les résultats du modèle correspondant à un calcul qui prend en compte les collisions à trois corps (pointillés) ou qui ne les prends pas en compte (trait plein) pour une pression de Ne de 1.08 mbar et une pression partielle de Xe de 2 mbar.

En plus de l'effet sur la densité de population de l'état émetteur Xe^{**} qui est diminuée de plus d'un ordre de grandeur, la simulation montre que le dépeuplement de cet état est plus de deux fois moins rapide quand $k_3 = 0$. Dans ces conditions les résultats issus de la simulation s'écartent considérablement des résultats expérimentaux

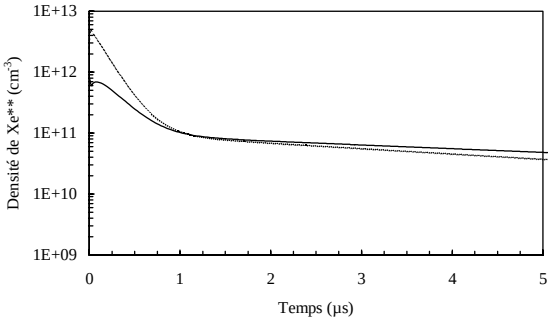

Figure 45 : *Evolutions temporelles calculées de la concentration de Xe^{**} pour une pression de Ne et de Xe de 1.08 bar et 2 mbar, respectivement dans le cas où $k_3 = 0$ (trait plein) et $k_3 = 2.5\ 10^{-30}$ $cm^6\ s^{-1}$ (pointillés).*

III. Conclusion

Les études concernant les plasmas de Ne-Xe que nous avons réalisées s'inscrivaient dans le cadre général d'études fondamentales consacrées à clarifier les mécanismes régissant les milieux excimères, menées par différents laboratoires publics regroupés au sein du *GDR 919*.

Le rôle des ions Ne_2^+ dans la cinétique est maintenant bien établi et les résultats de ces travaux confirment clairement que le canal termoléculaire de transfert de charge de Ne_2^+ sur Xe ne peut pas être négligé dans la chaîne cinétique conduisant au peuplement du niveau supérieur de la transition laser de l'excimère XeCl à 308 nm. Les réactions à trois corps à partir des ions moléculaires du néon ont été prises en compte dans les divers modèles de lasers excimères développés récemment, soulignant l'intérêt des expériences que nous avons menées. Les résultats obtenus ont permis une réelle avancée dans la compréhension des phénomènes mis en jeu et dans la mise au point de ces systèmes au niveau industriel.

CHAPITRE 4. REFERENCES BIBLIOGRAPHIQUES

[1] U. Kogelschatz, *Proc. 10th GD*, Swansea (GB), *972,* (1992)

[2] S.K. Dhali, I. Sardja, *J. Appl. Phys*. 69(9), 6319, 1991

[3] B.M. Penetrante, M.C. Hsiao, J.N. Bardsley, B.T. Merrit, G.E. Vogtlin, P.H. Wallman, A. Kuthi, C.P. Burkhart, J.R. Bayless, *Pure & Appl. Chem., 68(5), 1083*, 1996

[4] D. Evans, L.A. Rosocha, G.K. Anderson, J.J. Coogan, M.J. Kushner, *J. Appl. Phys., 74(9), 5378*, 1993

[5] *Groupe de Recherches sur l'Energétique des Milieux Ionisés - Orléans*, Equipe J.M. Cormier

[6] *Laboratoire de Physique des Gaz et des Plasma - Orsay*, Equipe S. Pasquiers

[7] B. Lacour, V. Puech, and S. Pasquiers, *Recent Res. Devel. Appl. Phys., 6, 149*, 2003

[8] *Laboratoire de Génie Electrique de Toulouse*, Equipe F. Massines

[9] F. Massines, A. Rabehi, P. Decomps, R. Ben Gadri, P. Ségur, C. Mayoux, *J. Appl. Phys., 83, 2950*, 1998

[10] I. Rusu, J. M. Cormier, *Chem. Eng. J., 91, 23* (2003)

[11] *Non-thermal Plasma Techniques for Pollution Control, part A and B*, ed. B. M. Penetrante and S. E. Schultheis (New York: Springer-Verlag), 1993

[12] A. Khacef, J.M. Cormier, J.M. Pouvesle, *J. Phys. D : Appl. Phys., 35, 1491*, (2002)

[13] A. Khacef, J.M. Cormier, J.M. Pouvesle, *J. Adv. Oxid. Technol., 8(2), 150*, (2005)

[14] A. Khacef, J.M. Cormier, *J. Phys. D: Appl. Phys., 39, 1078*, (2006)

[15] A. Khacef, J.M. Pouvesle, J.M. Cormier, *E. Phys. J.: Appl. Phys., 33, 195*, (2006)

[16] O. Gorce, H. Jurado, C. Thomas, G. Djéga-Mariadassou, A. Khacef, J.M. Cormier, J.M. Pouvesle, G. Blanchard, S. Calvo, Y. Lendresse, *SAE Technical paper N° 2001-01-3508*, (2001)

[17] I. Rusu, J.M. Cormier, A. Khacef, *http://preprint.chemweb.com/ inorgchem/ 0106001*, (2001)

[18] O. Aubry, C. Met, A. Khacef, J.M. Cormier, *Chem. Eng. J., 106(3), 241*, (2005)

[19] F. Ouni, A. Khacef, J.M. Cormier, *J. Chem. Eng. Technol.*, 29(5), 604, (2006)

[20] E. El Ahmar, C. Met, O. Aubry, A. Khacef, J.M. Cormier, *Chem. Eng. J., 116, 13*, (2006)

[21] A. Khacef, *Plasmas froids - Cinétiques, transports et transferts,* Publications de l'Université de Saint-Etienne, A. Granier et S. Mottin, Ed. 2005

[22] M.D. Amiridis, T. Zhang, R.J. Farrauto, *Appl. Catal. B, 10, 203*, 1996

[23] R.J. Baird, R.C. Ku, P. Wynblatt, *Surf. Sci., 97, 346*, 1980

[24] W. Held, A. König, T. Richter, L. Luppe, *SAE Technical Paper 900496*, (1990)

[25] M. Iwamoto, H. Yahiro, S. Shundo, Y. Yu-u, N. Mizuno, *Shokubai (catalyst), 32, 430,* (1990)

[26] B.M. Penetrante, R.M. Brusasco, B.T. Merrit, W.J. Pitz, F.E. Vogtlin, M.C. Kung, H.H. Kung, C.Z. Wan, K.E. Voss, SAE Technical Paper No. 982508, 57, (1998)

[27] H.H. Shin, W.S. Yoon, *SAE Technical Paper No. 2000-01-2969, 103*, (2000)

[28] R. Dorai, M.J. Kushner, *SAE Technical Paper No. 1999-01-3683, 81*, (1999)

[29] E.A. Filimonova, Y.H. Kim, S.E. Hong, Y.H. Song, *J. Phys. D: Appl. Phys., 35, 2795,* (2002)

[30] V. Puchkarev, G. Roth, M. Gundensen, *SAE Technical Paper No. 982516*, (1998)

[31] B.M. Penetrante, C.R. McLarno, *SAE Technical Paper No. 982433*, (1998)

[32] A.C. Gentile, M.J. Kushner, *J. Appl. Phys., 78(8), 2074,* (1995)

[33] R. Dorai, M.J. Kushner, *J. Phys. D : Appl. Phys., 34, 574*, (2001)

[34] M. Berger, *Thèse de Doctorat, Université Pierre et Marie Curie (Paris)*, (2000)

[35] O. Aubry, A. Khacef, J.M. Cormier, *Proc. Xth Hakone*, Saga(Japon), (2006)

[36] C. Liu, R. Mallison, L. Lobban, *J. Catal. , 179, 326*, (1998)

[37] X.S. Li, A.M. Zhu, K.J. Wang, Y. Xu, Z.M. Song, *Catal. Today, 98, 617,* (2004)

[38] M.G. Sobacchia, A.V. Saveliev, A.A. Fridman, L.A. Kennedy, S. Ahmed, T. Krause, *Int. J. of Hydogren Energy, 27, 635*, (2002)

[39] I. Rusu, J.M. Cormier, *Chem. Eng. J., 91, 23*, (2003

[40] H. Lesueur, A. Czernichowski, J. Chapelle, J. *of Hydogren Energy, 19, 139*, (1994)

[41] F. Richard, J.M. Cormier, S. Pellerin, J. Chapelle, *J. Appl. Phys., 79(5), 2245*, (1996)

[42] S. Pellerin, F. Richard, J. Chapelle, J.M. Cormier, K. Musiol, *J. Phys. D : Appl. Phys., 33(19), 2407*, (2000)

[43] J.M. Cormier, I. Rusu, A. Khacef, *Proc. 16th ISPC,* Taormina (Italie),*(*2003)

[44] F. Ouni, A. Khacef, J.M. Cormier, *Proc. 17th ISPC,* Toronto (Canada)*, (*2005)

[45] A. Khacef, F. Ouni, E. El Ahmar, O. Aubry, J. M. Cormier, *Proc. of the 9th Meeting on Combustion: Italian Section of the Combustion Institute*, Pise (Italie), (2006)

[46] F. Ouni, A. Khacef, J. M. Cormier, *Proc. 5th ISNTPT,* Ile d'Oléron (France)*, (*2006)

[47] F. Ouni, E. El Ahmar, A. Khacef, J.M. Cormier, *Proc. Xth Hakone, Saga (Japon), (*2006)

[48] O. Aubry, A. Khacef, J.M. Cormier, *Proc. 17th ISPC*, (2005)

[49] L. Bromberg, D.R. Cohn, A. Rabinovich, J. Heywood, *Int. J. of Hydogren Energy, 26, 1115*, (2001)

[50] E. El Ahmar, C. Met, A. Khacef, J.M. Cormier, *Proc. 17th ISPC*, Toronto (Canada), *(*2005)

[51] E. El Ahmar, A. Khacef, J. M. Cormier, *Proc. Xth Hakone*, Saga(Japon), (2006)

[52] E. Sato, A. Shikoda, S. Kimura, M. Sagae, T. Oizumi, K. Takahashi, Y. Hayasi, T. Shoji, K. Shishido, Y. Tamakawa, T. Yanagisawa, *SPIE, 1801, 628*, (1992).

[53] E. Sato, S. Kimura, S. Kawasaki, H. Isobe, K. Takahashi, Y. Tamakawa, T. Yanagisawa, *Rev. Sci. Instrum., 61, 2343*, (1990).

[54] C.B. Collins, F. Davanloo, T.S. Bowen, *Rev. Sci. Instrum., 57, 863,* (1986)

[55] J.M. Pouvesle, C. Cachoncinlle, E. Robert, R. Viladrosa, C.B. Collins, F. Davanloo, *Rev. Sci. Instrum., 64, 2320*, (1993)

[56] A. Ikhlef, M. Skowronek, *IEEE Trans. Plasma Sci., 21, 669,* (1993)

[57] R. Germer, *J. Phys. E: Sci. Instrum., 12, 336,* (1979)

[58] Q. Johnson, A.C. Mitchell, I.D. Smith, *Rev. Sci. Instrum., 51, 741,* (1980)

[59] F. Davanloo, T.S. Bowen, C.B. Collins, *Rev. Sci. Instrum., 58*, 2103, (1987)

[60] L.C. Bradley, A.C. Mitchell, Q. Johnson, I.D. Smith, *Rev. Sci. Instrum., 55, 25,* (1984)

[61] A. Khacef, R. Viladrosa, C. Cachoncinlle, E. Robert, J.M. Pouvesle, *Rev. Sci. Instrum., 68, 2292*, (1997)

[62] J.M. Pouvesle, C. Cachoncinlle, R. Viladrosa, E. Robert, A. Khacef, *Nucl. Instrum. Meth. Phys. Res. B, 113, 134*, (1996)

[63] E. Robert, A. Khacef, C. Cachoncinlle, J.M. Pouvesle, *Opt. Comm., 117, 179*, (1995)

[64] E. Robert, A. Khacef, C. Cachoncinlle, J.M. Pouvesle, *IEEE J. Quant. Electron., 33(11), 2119*, (1997)

[65] E. Robert, A. Khacef, C. Cachoncinlle, R. Viladrosa, J.M. Pouvesle, F. Davanloo, C.B. Collins, *Proc. XXIth ICPIG*, Bochum (Allemagne), *3, 237,* (1993)

[66] E. Robert, A. Khacef, C. Cachoncinlle, J.M. Pouvesle, *Bull. Am. Phys. Soc., 39, 1456*, (1994)

[67] C. Cachoncinlle, E. Robert, A. Khacef, J.M. Pouvesle, *An. Phys., 19, C1, 9,* (1994)

[68] E. Robert, A. Khacef, C. Cachoncinlle et J.M. Pouvesle, *Proc. XXIIth ICPIG*, Hoboken (USA), *4, 209,* (1995)

[69] J.M. Pouvesle, C. Cachoncinlle, A. Khacef, E. Robert, R. Viladrosa, *Bull. SFP, 100, 30,* (1995)

[70] A. Khacef, E. Robert, C. Cachoncinlle, R. Viladrosa, J.M. Pouvesle, *J. Phys. IV, 6, 747,* (1996)

[71] A. Khacef, R. Viladrosa, C. Cachoncinlle, E. Robert, J.M. Pouvesle, *Proc. 12th GD*, Greifswald (Allemagne), *I, 362,* (1997)

[72] E. Robert, C. Cachoncinlle, D. Arrivault, A. Khacef, and J.M. Pouvesle, *Proc. 12th GD,* Greifswald (Allemagne), *II, 516,* (1997)

[73] E. Robert, C. Cachoncinlle, A. Khacef, R. Viladrosa, J.M. Pouvesle, *Proc. XXIIIth ICPIG,* Toulouse (France), *3, 32*, (1997)

[74] R. Viladrosa, A. Khacef, C. Cachoncinlle, J.M. Pouvesle, *Proc. SPIE*, Santa-Fe (USA), *2869, 1086*, (1997)

[75] A. Khacef, R. Viladrosa, C. Cachoncinlle, E. Robert, J.M. Pouvesle, *An. Phys., 22, C1, 71,* (1997)

[76] R. Viladrosa, A. Khacef, C. Cachoncinlle, J.M. Pouvesle, *An. Phys., 22, C1, 77*, (1997)

[77] E. Robert, A. Khacef, C. Cachoncinlle, J.M. Pouvesle, *An. Phys., 22, C1, 135,* (1997)

[78] E. Robert, C. Cachoncinlle, A. Khacef, J.M. Pouvesle, *J. Phys. IV, 9, 13*, (1999)

[79] A. Khacef, R. Viladrosa, C. Cachoncinlle, J.M. Pouvesle, *J. Phys. IV, 9, 45,* (1999)

[80] E. Robert, C. Cachoncinlle, A. Khacef, R. Viladrosa, J.M. Pouvesle, F. Davanloo, C.B. Collins, *An. Phys., 19, C1, 167*, (1994)

[81] J.D. Monk, L.R. Beuchat, M.P. Doyle, *J. Food Protection, 58(2), 197*, (1993)

[82] G. Klein, M.J. Carvalho, *J. Phys. B: At. Mol. Phys., 14, 1283,* (1981)

[83] W. Krötz, A. Ulrich, B. Busch, G. Ribitzki, J. Wieser, *Phys. Rev. A, 43, 6089,* (1991)

[84] T. Griegel, H.W. Drotleff, J.W. Hammer, K. Petkau, *J. Chem. Phys., 93, 4581,* (1990)

[85] H. Langhoff, *Opt. Comm., 68, 31,* (1988)

[86] P. Millet, A. Birot, H. Brunet, H. Dijols, J. Galy, Y. Salamero, *J. Phys. B, 15, 2935,* (1982)

[87] C. Cachoncinlle, J.M. Pouvesle, F. Davanloo, J.J. Coogan, C.B. Collins, *J. Phys. D : Appl. Phys., 23, 984,* (1990)

[88] C. Cachoncinlle, J. M. Pouvesle, F. Davanloo, J. J. Coogan, C.B. Collins, *Opt. Comm., 79, 41,* (1990)

[89] A.K. Amirov, O.V. Korshunov, V.F. Chinnov, *J. Phys. B, 27, 1753*, (1994)

[90] Y. Tanaka, *J. Opt. Soc. Am., 45, 170*, (1955)

[91] Y. Tanaka, K. Yoshino, D.E. Freeman, *J. Chem. Phys., 62, 4484,* (1975)

[92] P. Millet, A. M. Barrie, A. Birot, H. Brunet, H. Dijols, J. Galy, Y. Salamero, *J. Phys. B: At. Mol. Phys., 14, 459,* (1981)

[93] T.H. Johnson, H.E. Cartland, T.C. Genoni, A.M. Hunter, *J. Appl. Phys., 66, 5707,* 1989)

[94] F. Kannari, W.D. Kimura, J.J. Ewing, *J. Appl. Phys., 68, 2615*, (1990)

[95] R. Riva, M. Legentil, S. Pasquiers, V. Puech, *J. Phys. D: Appl. Phys., 28, 856*, (1995).

[96] J.M. Pouvesle, A. Khacef, J. Stevefelt, V.T. Gylys, H.R. Jahani, C.B. Collins, *Bull. Am. Phys. Soc., 32, 1170*, (1987)

[97] J.M. Pouvesle, A. Khacef, J. Stevefelt, H.R. Jahani, V.T. Gylys, C.B. Collins, *Bull. Am. Phys. Soc., 32, 1646*, (1987)

[98] A. Khacef, J.M. Pouvesle, J. Stevefelt, H.R. Jahani, V.T. Gylys, C.B. Collins, *Proc. XVIIIth ICPIG*, Swansea (UK), *1, 42,* (1987)

[99] J.M. Pouvesle, A. Khacef, J. Stevefelt, H.R. Jahani, V.T. Gylys, C.B. Collins, *J. Chem. Phys., 88, 3061*, (1988)

[100] J.M. Pouvesle, A. Khacef, J. Stevefelt, H.R. Jahani, V.T. Gylys, C.B. Collins, *Bull. Am. Phys. Soc., 33, 127*, (1988)

[101] C. Cachoncinlle, E. Robert, A. Khacef, J.M. Pouvesle, *Bull. Am. Phys. Soc., 40, 1570,* (1995)

[102] A. Khacef, C. Cachoncinlle, R. Viladrosa, E. Robert, J.M. Pouvesle, *Proc. XXIIIth ICPIG,* Toulouse (France), *3, 30*, (1997)

[103] A. Khacef, O. Motret, J. Stevefelt, *J. Phys. D : Appl. Phys., 32, 176*, (1999)

[104] O. Motret, A. Khacef, J. Stevefelt, *J. Phys. D : Appl. Phys., 32, 471*, (1999)

[105] J. Stevefelt, J. Boulmer, J.F. Delpech, *Phys. Rev. A, 12, 1246*, (1975)

[106] F. Kannari, A. Suda, M. Obara, T. Fujioka, *IEEE J. Quant. Electron., 19, 1587*, (1983).

[107] C.B. Collins and F.W. Lee, *J. Chem. Phys., 72, 5381*, (1980)

[108] J.F. Delpech, J. Boulmer, and J. Stevefelt, *Adv. Elect. Phys. (Academic Press), 39, 121*, (1975)

[109] K. Aouame, *Thèse de doctorat*, Université Paul Sabatier, Toulouse, (1985)

[110] W.P. Allice, *Hanbuch der Physik, Tome 21, 413*, Spinger Verlag, Berlin, (1956)

[111] M.C. Bordage, A. Chouki, P. Segur, *Proc. XXth ICPIG,* Pise (Italie), *369*, (1991)

CHAPITRE 5. PERSPECTIVES

Les études présentées dans ce mémoire ont concernées de très larges domaines de la physique des plasmas (production de rayonnement, physico-chimie de milieux réactifs, dépollution, production d'hydrogène). Dans l'avenir nous nous consacrerons essentiellement aux thématiques développées au chapitre 1.

Bien que l'efficacité des décharges électriques, couplées ou pas à des catalyseurs, soit prouvée pour d'une part l'élimination de certaines molécules et d'autre part pour la valorisation des alcanes et de l'éthanol, les phénomènes mis en jeu restent dans la majorité des cas encore mal connus. Cette connaissance des processus physico-chimiques est pourtant essentielle pour une bonne maîtrise du procédé et pour son optimisation en termes de rendement et de coût énergétique. Sur le plan fondamental, les recherches futures seront essentiellement axées sur la compréhension de ces processus avec un questionnement sur le type de l'excitation électrique, la nature des espèces radicalaires clé dans la cinétique réactionnelle, la production d'espèces secondaires dans la post-décharge, la nature et l'emplacement du catalyseur, les processus d'activation du catalyseur, etc. L'ensemble de ces questions sont étudiées dans le cadre du GDR Cataplasme.

En parallèle, l'action sur la production du gaz de synthèse et de l'hydrogène sera orientée vers la valorisation de la biomasse et des ressources fossiles par des procédés plasma non thermique. Cette action de recherche sera développée sur la base des connaissances acquises lors du traitement plasma des alcanes et de l'éthanol. Elle sera concentrée dans un premier temps sur la valorisation de la biomasse dans le cadre du programme ANR PNRB "Pyroplasm : *Pyrolyse de la biomasse à haute température assistée par plasma non thermique*". Ce projet consiste à concevoir et à étudier en laboratoire un nouveau procédé d'abattement des matières condensables présentes dans les gaz issus de la pyrolyse ou de la gazéification de la biomasse. Cette étude mettra en œuvre l'association d'un réacteur à plasma non thermique avec un réacteur cyclone de pyrolyse rapide haute température. La finalité du projet est l'évaluation de l'applicabilité d'un tel système à plus grande échelle pour la production de gaz de synthèse dans des unités décentralisées, voire dans des unités centralisées.

Cette action englobe les procédés de production d'hydrogène et de gaz de synthèse ainsi que les procédés de purification qui mettront en œuvre les techniques développées dans le cadre de programmes sur la dépollution. La notion

de purification sera étendue d'une part à l'optimisation de la combustion et à l'amélioration des performances des combustibles, et d'autre part à la réduction des émissions polluantes par la voie plasma non thermique associé à un catalyseur. Cette orientation se situe dans la continuité de l'AC Energie du CNRS "Plasmhyrad: *Combustion assistée par hydrogène et radicaux générés par un plasma non thermique*".

Nos études récentes ont montré la possibilité de réaliser la réaction de *Water Gas Shift* dans un réacteur à décharge à barrière diélectrique impulsionnelle afin de convertir le monoxyde de carbone en hydrogène. Les études sur cette réaction seront complétées. Nous envisageons le couplage d'un réacteur DBD à un réacteur de pyrolyse (ou de gazéification) pour déterminer les conditions pour une réduction optimum du monoxyde de carbone.

Ces différentes thématiques mettent en œuvre deux types de réacteurs plasma : les réacteurs à décharges glissantes et les réacteurs à barrière diélectrique. Le savoir faire concernant l'étude et la réalisation d'alimentation adaptées, impulsionnelles rapides ou oscillantes entretenues, sera largement développé. La nécessité d'accéder à une compréhension fine des phénomènes mis en jeu dans de telles décharges nécessite la mise en place de techniques de diagnostic spectroscopiques adaptées et performantes. L'introduction de nouveaux dispositifs d'acquisition accompagnera la réalisation des réacteurs spécifiques à chaque application.

II. ACTIVITES D'ANIMATION DE LA RECHERCHE

II. 1. Encadrement et Co-encadrement

- Elise El Ahmar, Doctorante de l'Université d'Orléans, *Combustion assistée par hydrogène et radicaux générés par plasma non thermique*, depuis septembre 2004.
- Fakheddine Ouni, Doctorant de l'Université d'Orléans, *Production d'hydrogène et valorisation des alkanes par plasma non thermique*, septembre 2003–Novembre 2006.
- Djabirou Amadou, Master 1, Université d'Orléans, *Conception et réalisation d'une alimentation haute tension pour un réacteur à décharge à barrière diélectrique*, *Mai-Juillet 2005.*
- François Baudin, doctorant Université Pierre et Marie Curie (Paris VI), *Catalyse DeNOx assistée par plasma non thermique*, *Septembre 2001-Novembre 2004.*
- Etienne Gaultier, Maîtrise Université François Rabelais (Tours), *Traitement des gaz d'échappement des véhicules automobiles*, *Juin-Aout 2000*.
- Hervé Jurado, DEA Université Pierre et Marie Curie (Paris VI), *Elimination des oxydes d'azote en mélange pauvre (Lean Burn) par catalyse assistée par plasma,* Février-Juin 2000.

II. 2. Collaborations

II. 2. 1. Internationales

- IFP (Instituto di Fisica del Plasma), Milan, (G. Gervasini, N. Spinicchia)
- Institutului Politechnic de Iasi, (I. Rusu)
- INP (Institut für Niedertemperatur-Plasmaphysik), Greifswald, (M. Heintze, B. Pietruszka).
- Russian Research Center "Kurtchatov Institute", Moscou (B. Potapkin, M.A. Deminsky).
- Boreskov Institute of Catalysis, Novosibirsk, (V. A. Kirillov, T.M. Yurieva, A.A. Khassin).
- Center for Quantum electronics, University of Texas at Dallas, (C.B. Collins, F. Davanloo, H. Jahani).

II. 2. 2. Nationales

- LSCG, Nancy (J. Ledee)
- LRS, Paris VI (G. Djega-Mariadassou, C. Thomas, F. Baudin, P. Da Costa)
- LPGP, Orsay (S. Pasquiers, L. Magne, N. Blin-Simiand)
- LME, Orléans (C. Mounaim-Rousselle)
- LCSR, Orléans (I. Gokalp, P. Dagaut)
- LACCO, Poitiers (J.M. Tatibouët)
- LPTP, Ecole Polytechnique (A. Rousseau)
- CORIA, Rouen (P. Vervisch)
- LIMHP, Villetaneuse (K. Hassouni)

- INRA-CRITT Hyginov, Nouzilly (F. Lacroix)

II. 2. 3. Industrielles

- ATANOR, Irigny (G. Martin)
- PSA PEUGET CITROËN, La Garenne Colombes (Y. Lendresse, P. Rouveirolles, S. Schneider).
- RENAULT SA, Lardy (S. Calvo).
- SAINT GOBAIN Recherche, Aubervilliers (D. Lebellac).
- FEDERAL MOGUL, Orléans (A. Toumi).

II. 3. Diffusion

II. 3. 1. Conférences invitées, séminaires

- Hydrogen production by methane, propane and ethanol steam reforming in non-thermal plasma reactors, Workshop on the Plasma-Assisted Combustion and Plasma-Aftertreatment of Combustion Flue Gases for Power Industry, Gdansk (Pologne), 29-30 Mai 2006.
- Dépollution et DeNOx par plasma non thermique, Saint Gobain Recherche, 12 janvier 2006
- Hydrogen Generation from Alkanes and Alcohol by Non-Thermal Plasma Steam Reforming, 9th Meeting on Combustion: Italian Section of the Combustion Institute, Pise (Italie), 13-18 Juin 2006.
- On the use of non thermal plasma for hydrogen fuel enrichment, 17th International Symposium on Plasma Chemistry (ISPC 17), Toronto (Canada), 7-12 Août 2005.
- Plasma et catalyse pour la dépollution, 3ème Journées du Réseau Plasmas Froids, Bonascre (France), 17-20 Septembre 2004.
- Non-thermal plasma assisted catalytic NOx remediation from a lean model exhaust, Spring Fuels and Lubricants Meeting and Exhibition, Reno (USA), 6-9 Mai 2002.
- A table top, high intensity, short pulse flash X-ray source: development and characteristic studies, 12th International Conference on Gas discharges and their Applications, Greifswald (Allemagne), 8-12 Septembre 1997.
- Sources flash X compactes à haut taux de répétition, Rayons X et Matière, Strasbourg (France), 6-10 Novembre 1995.

II. 3. 2. Organisation de manifestations

- 15th International Symposium on Plasma Chemistry (ISPC 15), 9-13 Juillet, 2001, Orléans
- VIème Congrès Plasma de la Société Française de Physique (SFP), 7-9 Avril 1999, Orléans
- Colloque sur les Sources Cohérentes et Incohérentes UV, VUV et X. Applications et Développements récents (UVX 94), 13-16 Juin 1994, Nouan-Le-Fuzelier

II. 3. 3. Promotion des Sciences

- Journées "portes ouvertes" du GREMI : La Science en Fête 2005
- Journées "portes ouvertes" du GREMI : La Science en Fête 1998
- 2ème Forum "Images du Centre", 5 Décembre 1996, Tours
- Forum des transferts de technologie, 12 décembre 1996: Bourges

II. 4. Valorisation

II. 4. 1. Brevets

- Brevet Européen #05292350.5-2311 (7 Novembre 2005), Titre de l'invention: *Système de traitement des NOx de gaz d'échappement d'un moteur thermique de véhicule automobile*, F. Baudin, S. Schneider, Y. Lendresse, S. Calvo, P. Da Costa, G. Djega-Mariadassou, C. Thomas, A. Khacef, J.M. Cormier.

II. 5. Activités diverses

II. 5. 1. Jurys

- Membre du jury de thèse de Doctorat de F. Ouni, Université d'Orléans, 24 Novembre 2006
- Membre du jury de thèse de Doctorat de F. Baudin Université Paris VI, 8 Novembre 2004
- Membre du jury de Maitrise de E. Gaultier Université François Rabelais (Tours). 11 Juin 2001
- Membre du jury de DEA de H. Jurado Université Paris VI, 20 Juin 2000

II. 5. 2. Comités de lecture

Revues[11]

- Review of Scientific Instruments (American Institute of physics – AIP)
- Plasmas Sources Science and Technology (Institute of physics – IOP)
- Chemical Engineering Communications (Taylor & Francis Group)
- Environmental Science & Technology (ACS publications)

Conférences[12]

- SAE (Society of Automotive Engineers International), USA, 2000-2003
- International Advisory Commitee of the Central European Symposium on Plasma Chemistry (2006)
- Steering Committee of the International Workshop and Exhibition on Plasma-Assisted Combustion (IWEPAC), 2006.

II. 5. 3. Responsabilités administratives ou collectives

- Depuis 2002 : Membre élu du conseil de département GEA, IUT d'Orléans
- 1999-2000 et depuis 2004 : Membre élu au CDL (Conseil de Laboratoire), GREMI
- Depuis 2006 : Membre élu au Conseil de la Fédération EPEE (Energétique, Propulsion, Espace, Environnement)

[11]Evaluation régulière d'articles
[12]Membre

III. ACTIVITES D'ENSEIGNEMENT

III. 1. USTHB Université des Sciences et de la Technologie d'Alger

- *Electricité, Electrocinétique, Mécanique physique, Vibrations et Ondes Electromagnétiques*, Institut de Physique, (1977-1993).

III. 2. Institut National des Sciences Biomédicales d'Alger

- *Optique Géométrique et Biophysique, (1988-1993).*

III. 3. Université d'Orléans

III. 3. 1. IUT Département Gestion des Entreprises et des Administrations

- *Outils d'Information et de Communication-Outils informatiques pour la gestion, (depuis 1999).*

III. 3. 2. Faculté des Sciences

- *Instrumentation-Mesure et Analyses Physico-chimiques, Master 2 ICQM (Instrumentation-Contrôle-Qualité-Management), (2003-2005).*
- *Physique Générale, DEUG A cursus 1, (1995-1998).*
- *Electronique Générale, Licence de physique, (1995-1998).*
- *Electrotechnique, Licence d'ingénierie électrique, (1999-2000).*

III. 3. 3. Faculté des Sciences : Antenne de Bourges

- *Electromagnétisme-Electrocinétique, DEUG 2ème année, (2001-2002).*
- *Mécanique Vibratoire, Mécanique des Fluides, Licence TM (Technologie Mécanique), Licence SPI (Sciences pour la Production Industrielle), (2001-2002).*

IV. PUBLICATIONS

IV. 1. Articles de Revue

[1] A. Khacef and J.M. Cormier: Pulsed sub-microsecond dielectric barrier discharge treatment of flue gas simulated glass manufacturing industry: Removal of SO_2 and NOx, *Journal of Physics D: Applied Physics, 39, 1078, (2006)*

[2] F. Ouni, A. Khacef, and J.M. Cormier: Effect of oxygen on Methane Steam reforming in a Sliding Discharge Reactor, *Journal of Chemical Engineering and Technology*, 29(5), 604, (2006)

[3] A. Khacef, J.M. Pouvesle, and J.M. Cormier: Energy deposition effect on the NOx remediation in oxidative media using atmospheric non thermal plasmas, *European Physical Journal: Applied Physics*, 33, 195, (2006)

[4] E. El Ahmar, C. Met, O. Aubry, A. Khacef, and J.M. Cormier : Hydrogen enrichment of a methane-air mixture by atmospheric pressure plasma for vehicle applications, *Chemical Engineering Journal*, 116, 13, (2006)

[5] A. Khacef, J.M. Cormier, and J.M. Pouvesle: Non thermal plasma NOx remediation: From binary gas mixture to lean-burn gasoline and diesel engine exhaust, *Journal of Advanced Oxidation Technologies*, 8(2), 150, (2005)

[6] O. Aubry, C. Met, A. Khacef, and J.M. Cormier: On the use of a non thermal plasma reactor for ethanol steam reforming, *Chemical Engineering Journal*, 106(3), 241, (2005)

[7] A. Khacef, J.M. Cormier, and J.M. Pouvesle: NOx remediation in oxygen rich exhausts gas using atmospheric pressure non-thermal plasma generated by a pulsed nanosecond dielectric barrier discharge, *Journal of Physics D: Applied Physics* 35, 1491, (2002)

[8] I. Rusu, J.M. Cormier and A. Khacef: Hydrogen Production from simple compounds via plasma reactors, *http://preprint.chemweb.com/inorgchem/0106001*, (2001)

[9] O. Gorce, H. Jurado, C. Thomas, G. Djéga-Mariadassou, A. Khacef, J.M. Cormier, J.M. Pouvesle, G. Blanchard, S. Calvo, and Y. Lendresse: Non-thermal plasma assisted catalytic NOx remediation from a lean model exhaust, *SAE paper N° 2001-01-3508, Non-Thermal Plasma Aftertreatment (SAE Special Publication) Eds. M. L. Balmer, G. Fisher, and J. Hoard, Society of automotive Engineers, Warrendale,* (2001).

[10] A. Khacef, O. Motret, and J. Stevefelt: Characterization by emission spectroscopy of afterglow kinetics at atmospheric pressures: I. Reactions of neon ions with N_2, *Journal of Physics D: Applied physics*, 32, 176, (1999)

[11] O. Motret, A. Khacef, and J. Stevefelt: Characterization by emission spectroscopy of afterglow kinetics at atmospheric pressures: II. Reactions of neon ions with Xe, *Journal of Physics D: Applied Physics*, 32, 471, (1999)

[12] E. Robert, A. Khacef, C. Cachoncinlle and J.M. Pouvesle: Modeling of high pressure rare gas plasmas excited by an energetic flash X-ray source, *IEEE Journal of Quantum Electronics*, 33(11), 2119, (1997)

[13] A. Khacef, R. Viladrosa, C. Cachoncinlle, E. Robert and J.M. Pouvesle: High repetition rate compact source of nanosecond pulses of 5-100 keV X-ray photons, *Review of Scientific Instruments*, 68, 2292, (1997)

[14] J.M. Pouvesle, C. Cachoncinlle, R. Viladrosa, E. Robert and A. Khacef: Compact flash X-ray sources and their applications, *Nuclear Instruments and Methods in Physics Research B*, 113, 134, (1996)

[15] E. Robert, A. Khacef, C. Cachoncinlle and J.M. Pouvesle: Time-resolved spectroscopy of high pressure rare gases excited by an energetic flash X-ray source, *Optics Communications*, 117, 179, (1995)

[16] C. Cachoncinlle, E. Robert, A. Khacef, and J.M. Pouvesle: Fluorescence of rare gas exciplexe excited by dielectric controlled discharges, *Bulletin of the American Physical Society*, 40, 1570, (1995)

[17] E. Robert, A. Khacef, C. Cachoncinlle and J.M. Pouvesle: Flash X-ray excitation of high pressure gases, *Bulletin of the American Physical Society*, 39, 1456, (1994)

[18] M. Ganciu, E. Musa, O. Motret, A. Khacef, C. Cachoncinlle and J.M. Pouvesle; High voltage fast discharge in pure mercury for optimization of 254 nm radiation, *Bulletin of the American Physical Society*, 38, 2359, (1993)

[19] J.M. Pouvesle, A. Khacef, J. Stevefelt, H.R. Jahani, V.T. Gylys and C.B. Collins: Study of two body and three body channels for the reaction of metastable helium atoms with selected atomic and molecular species, *Journal of Chemical Physics*, 88, 3061, (1988)

[20] J.M. Pouvesle, A. Khacef, J. Stevefelt, H.R. Jahani, V.T. Gylys and C.B. Collins: Reactions of He_2^+ and $He(2^3S)$ with selected atomic and molecular species at atmospheric pressure, *Bulletin of the American Physical Society*, 33, 127, (1988)

[21] J.M. Pouvesle, A. Khacef, J. Stevefelt, V.T. Gylys, H.R. Jahani and C.B. Collins: Reactions of He_2^+ and $He(2^3S)$ with Ne, Ar, Kr, Xe, H_2, N_2, O_2, CO_2 and N_2O at atmospheric pressures, *Bulletin of the American Physical Society*, 32, 1170, (1987)

[22] J.M. Pouvesle, A. Khacef, J. Stevefelt, H.R. Jahani, V.T. Gylys and C.B. Collins: Reactions of He_2^+ and $He(2^3S)$ with selected atomic and molecular reactants, *Bulletin of the American Physical Society*, 32, 1646, (1987)

IV. 2. Chapitres de Livre

[23] A. Khacef : Plasmas froids - Cinétiques, transports et transferts : "Plasma et catalyse pour la dépollution", *Publications de l'Université de Saint-Etienne, A. Granier et S. Mottin*, Ed. 2005

IV. 3. Actes de Conférences Internationales (avec comité de lecture)

[24] F. Ouni, E. El Ahmar, A. Khacef, and J.M. Cormier: CO_2 reforming of CH_4 in non-thermal plasma reactor at atmospheric pressure, *Proc. of the X^th International Symposium on High Pressure Low Temperature Plasma Chemistry (Hakone X)*, Saga (Japon), 4-8 Septembre 2006

[25] E. El Ahmar, A. Khacef, and J.M. Cormier: *On the hydrogen enrichment of an air-methane mixture in a rotating discharge reactor*, *Proc. of the X^th International Symposium on High Pressure Low Temperature Plasma Chemistry (Hakone X)*, Saga (Japon), 4-8 Septembre 2006

[26] O. Aubry, A. Khacef, and J.M. Cormier: *Conversion of propane by pulsed dielectric barrier discharge in air, Proc. of the X^th International Symposium on High Pressure Low Temperature Plasma Chemistry (Hakone X)*, Saga (Japon), 4-8 Septembre 2006

[27] F. Ouni, A. Khacef, and J. M. Cormier: Application of three cathodes reactor for steam reforming of propane at atmospheric pressure, *Proc. of the V^th Non-Thermal Plasma Technology for Pollution Control and Sustainable Energy Development (ISNTPT 5)*, Ile d'Oléron (France), 19-23 Juin 2006

[28] O. Aubry, A. Khacef, and J. M. Cormier: CO conversion by a dielectric barrier discharges reactors using the water gas shift reaction, *Proc. of the V^th Non-Thermal Plasma Technology for Pollution Control and Sustainable Energy Development (ISNTPT 5)*, Ile d'Oléron (France), 19-23 Juin 2006

[29] E. El Ahmar, A. Khacef, and J. M. Cormier: Plasma aided combustion of air-natural gas mixture using an atmospheric pressure rotating discharge for vehicle applications, *Proc. of the V^th Non-Thermal Plasma Technology for Pollution Control and Sustainable Energy Development (ISNTPT 5)*, Ile d'Oléron (France), 19-23 Juin 2006

[30] F. Ouni, A. Khacef, and J. M. Cormier: Modeling of a nitrogen glow discharge at atmospheric pressure, *Proc. of the V^th Non-Thermal Plasma Technology for Pollution Control and Sustainable Energy Development (ISNTPT 5)*, Ile d'Oléron (France), 19-23 Juin 2006

[31] A. Khacef, F. Ouni, E. El Ahmar, O. Aubry, and J. M. Cormier: Hydrogen generation from alkanes and alcohol by non-thermal plasma steam reforming, *Proc. of the 9^th Meeting on Combustion: Italian Section of the Combustion Institute*, Pise (Italy), 13-18 Juin 2006

[32] F. Ouni, A. Khacef, and J.M. Cormier: Methane Steam Reforming with Oxygen in a Gliding Discharge Reactor, *Proc. of the 17^th International Symposium on Plasma Chemistry (ISPC 17)*, Toronto (Canada), 7-12 Août 2005.

[33] A. Khacef and J.M. Cormier: Removal of NOx and SO_2 from synthetic glass industry exhaust gases with pulsed dielectric barrier discharge, *Proc. of the 17^th International Symposium on Plasma Chemistry (ISPC 17)*, Toronto (Canada), 7-12 Août 2005.

[34] E. El Ahmar, C. Met, A. Khacef, and J.M. Cormier: On the Use of non thermal plasma for hydrogen fuel enrichment, *Proc. of the 17^th International Symposium on Plasma Chemistry (ISPC 17)*, Toronto (Canada), 7-12 Août 2005.

[35] O. Aubry, A. Khacef, and J.M. Cormier: Investigation on the water gas shift reaction in a dielectric barrier discharge reactor, *Proc. of the 17^th International Symposium on Plasma Chemistry (ISPC 17)*, Toronto (Canada), 7-12 Août 2005.

[36] F. Ouni, E. El Ahmar, C. Met, O. Aubry, A. Khacef, and J.M. Cormier: Non thermal plasmas and hydrogen production, *Proc. of the 17^th International Symposium on Plasma Chemistry (ISPC 17)*, Toronto (Canada), 7-12 Août 2005.

[37] F. Ouni, I. Rusu, A. Khacef, O. Aubry, C. Met, and J.M. Cormier: Steam reforming and cracking of methane by means of gliding discharges reactors, *Proc. of the XV^th International Conference on Gas Discharges and their applications*, Toulouse (France), 5-10 Septembre 2004.

[38] O. Aubry, C. Met, A. Khacef, and J.M. Cormier: Ethanol steam reforming: a plasma way for hydrogen production, *Proc. of the IX^th International Symposium on High Pressure Low Temperature Plasma Chemistry (Hakone IX), Padova (Italie)*, 23-27 Août 2004.

[39] C. Met, O. Aubry, A. Khacef, and J.M. Cormier: On the use of electric discharge reactors for hydrogen rich gas production in internal combustion engine, *Proc. of the IXth International Symposium on High Pressure Low Temperature Plasma Chemistry (Hakone IX), Padova (Italie)*, 23-27 Août 2004.

[40] A. Khacef, R. Viladrosa, J.M. pouvesle: Effect of ns pulsed X-ray irradiation on biological media, *Proc. of the 31stInternational Conference on Plasma Science (ICOPS)*, Baltimore (USA), 28 Juin-31 Juillet 2004.

[41] C. Met, J.M. Cormier, and A. Khacef: Adapted power electronic supply for cold plasma improving thermal engines operation, *Proc. of the IVth International Conference on optimization of Electrical and Electronic equipment (OPRIM'04), Brasov (Roumanie)*, 20-21 Mai 2004.

[42] A. Khacef, J.M. Cormier, J.M. Pouvesle: Non thermal plasma NOx remediation: From binary gas mixture to lean-burn gasoline and diesel engine exhaust, *Proc. of the IVth Non-Thermal Plasma Technology for Pollution Control and Sustainable Energy Development (ISNTPT 4)*, Panama City Beach (USA), 10-14 Mai 2004

[43] C. Met, O. Aubry, A. Khacef, and J.M. Cormier: Atmospheric non thermal plasma used for assisted combustion, *Proc. of the IVth Non-Thermal Plasma Technology for Pollution Control and Sustainable Energy Development (ISNTPT 4)*, Panama City Beach (USA), 10-14 Mai 2004

[44] J.M. Cormier, I. Rusu, and A. Khacef: Methane steam reforming in a gliding arc reactor, *Proc. of the 1st European Hydrogen Energy Conference*, Grenoble (France), 2-5 Septembre 2003.

[45] O. Martinie, J.M. Cormier and A. Khacef: Comparative study of energy deposition estimation in dielectric barrier discharge reactor, *Proc. of the 16th International Symposium on Plasma Chemistry (ISPC 16)*, Taormina (Italie), 22-27 Juin 2003.

[46] O. Martinie, J.M. Cormier and A. Khacef: Physical characteristics of a non-thermal plasma arc applied to NO reduction, *Proc. of the 16th International Symposium on Plasma Chemistry (ISPC 16)*, Taormina (Italie), 22-27 Juin 2003.

[47] A. Khacef, J.M. Cormier and J.M. Pouvesle: Investigation of nanosecond pulsed dielectric barrier discharges in various gas mixtures, *Proc. of the 16th International Symposium on Plasma Chemistry (ISPC 16)*, Taormina (Italie), 22-27 Juin 2003.

[48] J.M. Cormier, I. Rusu and A. Khacef: On the use of a magnetic blow out glidarc reactor for the syngas production by steam reforming, *Proc. of the 16th International Symposium on Plasma Chemistry (ISPC 16)*, Taormina (Italie), 22-27 Juin 2003.

[49] A. Khacef, J.M. Cormier, J.M. Pouvesle, O. Gorce, H. Jurado, C. Thomas, G. Djéga-Mariadassou, S Calvo, and Y. Lendresse, Plasma-catalyst system for NOx remediation in simulated lean exhaust, *Proc. of the VIIIth International Symposium on High Pressure Low Temperature Plasma Chemistry (Hakone VIII),* Pühajärve (Estonie), 21-25 Juillet 2002.

[50] A. Khacef, J.M. Cormier, O. Motret, and J.M. Pouvesle: Removal of NOx from synthetic engine exhaust by nanosecond pulsed dielectric barrier discharge reactor, *Proc. of the 15th International Symposium on Plasma Chemistry (ISPC 15)*, Orléans (France), 9-13 Juillet 2001.

[51] A. Khacef, J.M. Pouvesle, and J.M. Cormier: Energy deposition effect on the NOx efficiency treatment in atmospheric non thermal plasma, *Proc. of the 15th International Symposium on Plasma Chemistry (ISPC 15)*, Orléans (France), 9-13 Juillet 2001.

[52] A. Khacef, M. Nikravech, O. Motret, P. Lefaucheux, R. Viladrosa, J.M. Pouvesle, and J.M. Cormier: Plasma treatment of synthetic engine exhaust in atmospheric pressure non-equilibrium pulsed discharges, *Proc. of the VIIth International Symposium on High Pressure Low Temperature Plasma Chemistry (Hakone VII)*, Greifswald (Allemagne), 10-13 Septembre 2000.

[53] A. Khacef, R. Viladrosa, C. Cachoncinlle, E. Robert, and J.M. Pouvesle: A table top, high intensity, short pulse flash X-ray source: development and characteristic studies, *Proc. of the XIIth International Conference on Gas Discharges and their Applications*, Greifswald (Allemagne), 8-12 Septembre 1997.

[54] E. Robert, C. Cachoncinlle, D. Arrivault, A. Khacef, and J.M. Pouvesle: Fluorescence of argon based mixtures at multi-atmospheric pressures excited by an energetic flash X-ray source, *Proc. of the XIIth International Conference on Gas Discharges and their applications*, Greifswald (Allemagne), 8-12 Septembre 1997.

[55] A. Khacef, C. Cachoncinlle, R. Viladrosa, E. Robert, and J.M. Pouvesle: High energy photons emitted from high voltage fast discharge in vacuum and in low pressure gases, *Proc. of the 23rd International Conference of Physics of Ionized Gases (ICPIG 23)*, Toulouse (France), 17-22 Juillet 1997.

[56] E. Robert, C. Cachoncinlle, A. Khacef, R. Viladrosa, and J.M. Pouvesle: From the "third continuum" to the "molecular ion continua" of rare gases, *Proc. of the 23th International Conference of Physics of Ionized Gases (ICPIG 23)*, Toulouse (France), 17-22 Juillet 1997.

[57] R. Viladrosa, A. Khacef, C. Cachoncinlle, and J.M. Pouvesle: High repetition rate portable flash X-ray source, *Proc. of the 22nd International Congress on High-Speed Photography and Photonics, SPIE,* Santa-Fe (USA), 27 octobre-1er Novembre 1996)

[58] E. Robert, A. Khacef, C. Cachoncinlle et J.M. Pouvesle: Modeling of high pressure rare gas plasmas excited by an energetic flash X-ray source, *Proc. of the 22th International Conference of Physics of Ionized Gases (ICPIG)*, Hoboken (USA), 31 Juillet-5 Août 1995.

[59] E. Robert, A. Khacef, C. Cachoncinlle, and J.M. Pouvesle: Flash X-ray excitation of high pressure rare gases, *Proc. of the* 47th *Gaseous Electronic Conference* (GEC), Gaitherburg (USA), 18-21 Octobre 1994.

[60] E. Robert, A. Khacef, C. Cachoncinlle, and J.M. Pouvesle: Flash X-ray excitation of high pressure rare gases, *Proc. of the 16th European Sectional Conference on Atomic and Molecular Physics in Ionized Gases (ESCAMPIG)*, Noordwijkerhout (Pays Bas), 23-26 Août 1994

[61] E. Robert, A. Khacef, C. Cachoncinlle and J.M. Pouvesle: Study of the broad UV-VUV fluorescence of high pressure rare gas plasmas, *Proc. of the Future prospects for UV and VUV lasers Conference*, Santa Barbara (USA), 28 Février-3 Mars 1994.

[62] M. Ganciu, E. Musa, O. Motret, A. Khacef, C. Cachoncinlle and J.M. Pouvesle: High voltage fast discharge in pure mercury for optimization of 254 nm radiation, *Proc. of the 46*th *Gaseous Electronic Conference* (GEC), Montréal (Canada), 19-22 Octobre 1993.

[63] E. Robert, A. Khacef, C. Cachoncinlle, R. Viladrosa, J.M. Pouvesle, F. Davanloo and C.B. Collins: Energetic high repetition rate flash X-ray source: Application to UV-VUV fluorescence studies in high pressure gases, *Proc. of the 21th International Conference of Physics of Ionized Gases (ICPIG)*, Bochum (Allemagne), 19-24 Septembre 1993.

[64] J.M. Pouvesle, A. Khacef, J. Stevefelt, H.R. Jahani, V.T. Gylys and C.B. Collins: Reactions of He(2^3S) and He_2^+ with selected atomic and molecular

reactants, *Proc. of the 40th Gaseous Electronic Conference (GEC)*, Atlanta (USA), 13-16 Octobre 1987.

[65] A. Khacef, J.M. Pouvesle, J. Stevefelt, H.R. Jahani, V.T. Gylys, and C.B. Collins: Reactions of He(2^3S) and He_2^+ with N_2O at atmospheric pressures, *Proc. of the 18th International Conference of Physics of Ionized Gases (ICPIG)*, Swansea (Grande Bretagne), 13-17 Juillet 1987.

[66] J.M. Pouvesle, A. Khacef, J. Stevefelt, V.T. Gylys, H.R. Jahani, and C.B. Collins: Reactions of He_2^+ and He(2^3S) with Ne, Ar, Kr, Xe, H_2, N_2, O_2, CO_2 and N_2O at atmospheric pressures, *Proc. of the 39th Gaseous Electronic Conference*, Madison (USA), 7-10 Octobre 1986.

[67] J.M. Pouvesle, A. Khacef, R. Viladrosa and J. Stevefelt: Reactivity of helium metastable He(2^3S) and $He_2(a^3\Sigma_u)$ species in atmospheric pressure afterglow, *Proc. of the 8th European Sectional Conference on Atomic and Molecular Physics in Ionized Gases (ESCAMPIG)*, Greifswald, (Allemagne), 25-29 Août 1986.

IV. 4. Revues d'Impact national (avec Comité de Lecture)

[68] E. Robert, C. Cachoncinlle, A. Khacef, et J.M. Pouvesle : Productions d'impulsions de photons dans l'UV-VUV, *Journal de physique IV, 9*, 13 (1999).

[69] A. Khacef, R. Viladrosa, C. Cachoncinlle, et J.M. Pouvesle : Impulsions nanosecondes de rayons X durs à haut taux de récurrence et en mode rafale à partir d'un système compact et facilement transportable, *Journal de physique IV, 9*, 45 (1999).

[70] A. Khacef, R. Viladrosa, C. Cachoncinlle, E. Robert et J.M. Pouvesle: Etude paramétrique d'une source X impulsionnelle créée par décharge rapide dans le vide ou dans des gaz basse pression, *Annales de Physique, 22, C1*, 71, (1997).

[71] R. Viladrosa, A. Khacef, C. Cachoncinlle et J.M. Pouvesle : SPHINX : Générateur de rayons X pulsés, ultra compact à cadence élevée, *Annales de Physique, 22, C1*, 77, (1997).

[72] E. Robert, A. Khacef, C. Cachoncinlle et J.M. Pouvesle : Dépôt d'énergie par rayonnement X dans les gaz rares à haute pression, *Annales de Physique, 22, C1*, 135, (1997).

[73] A. Khacef, E. Robert, C. Cachoncinlle, R. Viladrosa et J.M. Pouvesle : Sources flash X compactes à haut taux de répétition, *Journal de Physique IV, 6*, 747, (1996)

[74] J.M. Pouvesle, C. Cachoncinlle, A. Khacef, E. Robert et R. Viladrosa : "Le "*troisième*" continu des gaz rares ou attention : un continu peut en cacher un autre", *Bulletin de la SFP, 100*, 30, (1995).

[75] C. Cachoncinlle, E. Robert, A. Khacef, et J.M. Pouvesle: Fluorescence des gaz rares à haute pression excités par flash X rapide, *Annales de Physique, 19, C1*, 9, (1994).

[76] E. Robert, C. Cachoncinlle, A. Khacef, R. Viladrosa, J.M. Pouvesle, F. Davanloo et C.B. Collins : Source flash X compacte impulsionnelle à haut taux de répétition, *Annales de Physique, 19, C1*, 167, (1994).

[77] O. Motret, A. Khacef, M. Ganciu, C. Cachoncinlle et J.M. Pouvesle : Caractérisation d'une décharge rapide dans Hg pur, *Annales de Physique, 17, C1*, 73, (1992).

[78] A. Khacef et J.M. Pouvesle : Plasmas de post-décharge créés par claquage rapide dans des mélanges hélium-argon-azote à haute pression : Expérience et modélisation, *Annales de Physique, 15, C3*, 105, (1990).

IV. 5. Publications Universitaires

[79] A. Khacef : Etude de plasmas à base de gaz rares à haute pression crées par décharge électrique rapide ou rayons X présentant un intérêt pour le développement de nouvelles sources UV-X ou lasers excimères : *Doctorat d'Etat en Electronique Quantique : Option physique des plasmas*. USTHB, Alger, (Décembre 1997).

[80] A. Khacef : Etude des transferts d'excitation et de charge dans des plasmas d'hélium à haute pression, *Magister (équivalent thèse de troisième cycle) en Electronique Quantique : Option physique des plasmas*. USTHB, Alger, (Juin 1988).

IV. 6. Livrables de Contrats ou de Projets

[81] O. Aubry, A. Khacef, O. Motret et J.M. Cormier : Conversion de l'éthylène et du propane par décharge à barrière diélectrique impulsionnelle, *Rapport final AC 2003 Non pollution, dépollution : nouveaux procédés/nouvelles méthodes : DECOV PAR PLASMAS, CNRS–Ministère de la Recherche* (Mars 2006).

[82] E. El Ahmar, C. Met, O. Aubry, A. Khacef et J.M. Cormier : "Plasmhyrad : Enrichissement en hydrogène d'un mélange méthane air par plasma non thermique, *Rapport final. ARC 2003 ENERGIE CNRS – Ministère de la Recherche*, (juin 2005)

[83] A. Khacef, O. Aubry et J.M. Cormier : Installation d'un dispositif de traitement par plasma froid et test de faisabilité pour la conversion du chlorure de méthylène, *Rapport d'étude FEDERAL MOGUL*, (octobre 2005).

[84] A. Khacef et J.M. Cormier : Application des plasmas froids au traitement des effluents gazeux issus des fours Verriers (DeSOx*), Rapport d'étude SAINT GOBAIN*, (Mai 2002).

[85] A. Khacef, J.M. Cormier et J.M. Pouvesle : Elimination des NOx en présence d'hydrocarbures dans diverses conditions plasmas: Couplage plasma/catalyseur. Synthèse finale, *Rapport de Synthèse ARC "DeNOx - DeSuie plasmas*", (Avril 2002).

[86] A. Khacef, P. Lefaucheux, O. Motret, M. Nikravech, J.M. Cormier, J.M. Pouvesle : Application des plasmas froids au traitement des gaz d'échappement de moteurs fonctionnant en mélange pauvre, *Rapport annuel ARC "DeNOx - DeSuie plasmas"*, (Mars 2000)

[87] A. Khacef, P. Lefaucheux, O. Motret, M. Nikravech, J.M. Cormier, J.M. Pouvesle : Application des plasmas froids au traitement des gaz d'échappement de moteurs fonctionnant en mélange pauvre, *Rapport d'activité ECODEV*, (2000).

[88] A. Khacef, P. Lefaucheux, O. Motret, M. Nikravech, J.M. Cormier, J.M. Pouvesle : Application des plasmas froids au traitement des gaz d'échappement de moteurs fonctionnant en mélange pauvre, *Rapport d'activité ECODEV*, (1999)

[89] A. Khacef, J.M. Pouvesle et R. Viladrosa : Générateur impulsionnel de rayons X durs à très haute cadence en mode rafale, *Rapport final, contrat DRET n°94.34.125.00.470.75.01*, (Mai 1998).

[90] A. Khacef, J.M. Pouvesle et R. Viladrosa : Générateur impulsionnel de rayons X durs à très haute cadence en mode rafale, *Rapport à 1 an, contrat DRET n°94.34.125.00.470.75.01*, (Juillet 1996).

[91] A. Khacef, J.M. Pouvesle et R. Viladrosa : Développement d'un générateur impulsionnel de rayons X, *Rapport final, contrat d'aide à l'innovation n°A9305100F00 ANVAR*, (Décembre 1995).

[92] A. Khacef, J.M. Pouvesle et R. Viladrosa : Générateur impulsionnel de rayons X durs à très haute cadence en mode rafale, *Rapport à 6 mois, contrat DRET n°94.34.125.00.470.75.01*, (Novembre 1995).

[93] A. Khacef, J.M. Pouvesle et R. Viladrosa : Développement d'un générateur impulsionnel de rayons X, *Rapport à 12 mois, contrat d'aide à l'innovation n°A9305100F00 ANVAR*, (Décembre 1994).

[94] A. Khacef, J.M. Pouvesle et R. Viladrosa : Développement d'un générateur impulsionnel de rayons X, *Rapport à 6 mois, contrat d'aide à l'innovation n°A9305100F00 ANVAR*, (Juin 1994).

[95] A. Khacef, O. Motret, R. Viladrosa et J. Stevefelt : Lasers à excimères de grandes puissances pour applications industrielles, *Rapport final, GDR 919 - CNRS*, (1992).

[96] A. Khacef, O. Motret, R. Viladrosa et J. Stevefelt : Lasers à excimères de grandes puissances pour applications industrielles, *Rapport d'avancement n°2, GDR 919 - CNRS*, (1991).

[97] A. Khacef, O. Motret, R. Viladrosa et J. Stevefelt : Lasers à excimères de grandes puissances pour applications industrielles, *Rapport d'avancement n°1, GDR 919 - CNRS*, (1990).

[98] A. Khacef, O. Motret, R. Viladrosa et J. Stevefelt : Lasers à excimères de grandes puissances pour applications industrielles, *Rapport final Programme EUREKA/EUROLASER, Proposition N°89/MS/MM/679*, (Octobre 1989).

[99] J. Stevefelt, O. Motret, A. Khacef et R. Viladrosa : Etude spécifique de la réaction de transfert de charge à trois corps : $Ne_2^+ + Xe + Ne \rightarrow Xe^+ + 3Ne$, *Rapport Projet EUREKA Lasers Excimères de grande puissance pour applications industrielles, Contrat CGE n°219/C/86*, (Janvier 1988).

IV. 7. Autres Publications

[100] J. M. Cormier, A. Khacef, et O. Motret : Dépollution des effluents gazeux par plasma, *Images de la Physique 2003-2004 Publication du CNRS*, 130, avril 2004.

[101] J.M. Pouvesle, C. Cachoncinlle, R. Viladrosa, E. Robert et A. Khacef : SPHINX : Source de PHotons Impulsionnelle Nanoseconde X, *CNRS Info, N°336, 7*, 1er février 1997.

V. PUBLICATIONS ANNEXEES

1 A. Khacef, J.M. Cormier, *J. Phys. D: Appl. Phys., 39, 1078, (2006)*

2 F. Ouni, A. Khacef, J.M. Cormier, *J. Chem. Eng. Technol.*, *29(5), 604*, (2006)

3 A. Khacef, J.M. Pouvesle, J.M. Cormier, *Eur. Phys. J.: Appl. Phys.*, *33, 195,* (2006)

4 E. El Ahmar, C. Met, O. Aubry, A. Khacef, J.M. Cormier, *Chem. Eng. J.*, *116, 13*, (2006)

5 A. Khacef, J.M. Cormier, J.M. Pouvesle, *J. Adv. Oxid. Technol., 8(2), 150*, (2005)

6 O. Aubry, C. Met, A. Khacef, J.M. Cormier, *Chem. Eng. J.*, *106(3), 241,* (2005)

7 A. Khacef, J.M. Cormier, J.M. Pouvesle, *J. Phys. D: Appl. Phys., 35, 1491,* (2002)

8 O. Gorce, H. Jurado, C. Thomas, G. Djéga-Mariadassou, A. Khacef, J.M. Cormier, J.M. Pouvesle, G. Blanchard, S. Calvo, Y. Lendresse, *SAE paper N° 2001-01-3508,* (2001).

9 A. Khacef, O. Motret, J. Stevefelt, *J. Phys. D: Appl. Phys.*, *32, 176*, (1999)

10 A. Khacef, R. Viladrosa, C. Cachoncinlle, E. Robert, J.M. Pouvesle, *Rev. Sci. Instrum.*, *68, 2292*, (1997)

11 E. Robert, A. Khacef, C. Cachoncinlle, J.M. Pouvesle, *Opt. Comm.*, *117, 179,* (1995)

INSTITUTE OF PHYSICS PUBLISHING JOURNAL OF PHYSICS D: APPLIED PHYSICS
J. Phys. D: Appl. Phys. 39 (2006) 1078–1083 doi:10.1088/0022-3727/39/6/013

Pulsed sub-microsecond dielectric barrier discharge treatment of simulated glass manufacturing industry flue gas: removal of SO_2 and NOx

A Khacef and J M Cormier

GREMI-Polytech'Orléans 14 rue d'Issoudun, B P 6744, 45067 Orléans Cedex 2, France

E-mail: ahmed.khacef@univ-orleans.fr

Received 23 December 2005, in final form 27 January 2006
Published 3 March 2006
Online at stacks.iop.org/JPhysD/39/1078

Abstract

Experiments were carried out to investigate the removal of SO_2 and NOx from simulated glass manufacturing industry flue gas containing O_2, N_2, NO, NO_2, CO_2, SO_2 and H_2O using a sub-microsecond pulsed dielectric barrier discharge (DBD) at atmospheric pressure. Removal efficiencies of SO_2 and NOx (NO + NO_2) were achieved as a function of gas temperature for two specific energies and two initial NO, NO_2 and SO_2 concentrations. The higher SO_2 and NOx removal efficiencies were achieved in a gas stream containing 163 ppm of SO_2, 523 ppm of NO, 49 ppm of NO_2, 14% of CO_2, 8% of O_2, 16% of H_2O and N_2 as balance. The experimental results were evaluated using the energy cost or *W*-value (eV/molecule removed). About 100% of SO_2 and 36% of NOx were removed at a gas temperature of 100 °C with an energy cost of about 45 eV/molecule removed and 36 eV/molecule removed, respectively. These results indicate that DBD plasmas have the potential to remove SO_2 and NOx from gas streams without additives.

1. Introduction

The reduction of pollutants, such as sulfur and nitrogen oxides—SO_2 and NOx (including NO and NO_2)—from industrial processes and vehicle exhausts is one of the critical and urgent topics in environmental and pollution control research. These molecules have adverse effects on human health and contribute greatly to acid rain which has had detrimental effects on ecosystems.

Removal of these pollutants from flue gases can be achieved by conventional methods combining wet scrubbers and catalytic converters. However, these methods require additives (ammonia, urea or lime), catalyst and additional waste water treatment processes.

In the last decade, many investigations [1–6] have paid attention to new technologies and suggested that the non-thermal plasma (NTP) could be one of the most effective methods for simultaneous removal of SO_2 and NOx (NO + NO_2) from flue gas at relatively low energy costs. NTP that has a low gas temperature and a high electron temperature can be produced by a variety of electrical discharge methods (pulsed corona discharge, barrier discharge and dc discharge) [7–10] or electron beam irradiation [1, 11]. The majority of electrical energy goes into the production of energetic electrons rather than into gas heating. The energy supplied into the discharge is directed preferentially to electron impact ionization and dissociation of the background gas to produce free radicals. Gas phase radicals such as hydroxyl (OH), hydroperoxyl (HO_2) and oxygen atoms (O) are generated and are consumed in chemical reactions, part of them promoting the desired conversion of pollutants. For example, these radicals can oxidize simultaneously SO_2 and NO to SO_3 and NO_2, respectively. The final step is the reactions with water to form acid molecules consisting of H_2SO_4 and HNO_3, respectively. In an industrial application of this process, the acid molecules could be chemically neutralized in the presence of ammonia (NH_3) to form salts like ammonium sulfate ($(NH_4)_2SO_4$) and ammonium sulfate nitrate ($(NH_4)2SO_4$-$2NH_4NO_3$) which can be recovered as a dry powder using a conventional particle

0022-3727/06/061078+06$30.00

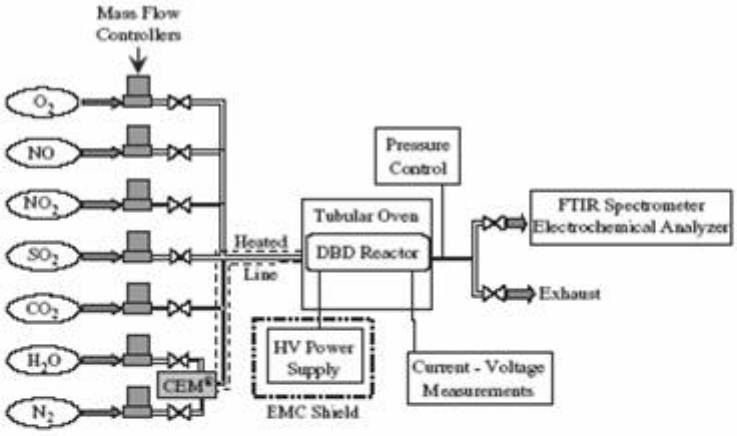

Figure 1. Experimental arrangement.

collector and can be sold as a useful product (agricultural fertilizer) [11].

Regarding their intrinsic properties, being well-adapted for treating large quantities of gas, the pulsed corona and dielectric barrier discharge (DBD) techniques are two of the more commonly used methods for producing electrical discharge plasmas.

As reported in the literature, the plasma discharge characteristics are greatly affected by the flue gas composition. Lowke and Morrow [12] investigated the various chemical reactions that occur in the corona discharge of an electrostatic precipitator operating in a typical flue gas. Their theoretical analysis shows that the presence of water vapour has a significant effect on the plasma chemistry of the removal of SO_2 and NOx. The investigations of Chang *et al* [13] using DBD and computer modelling show that the conversion of SO_2 primarily to H_2SO_4 is limited by the generation of OH radicals. Increasing the concentration of O_2 and H_2O increases the generation of OH radicals and results in further removal of SO_2 from flue gas streams. Based on such a NTP device, several pilot-plant tests on DeNOx and DeSOx were considered successful [14, 15].

In the present work, we report on an experimental study of the sub-microsecond pulsed DBD removal of SO_2 and NOx from simulated glass industry exhausts which contain large amounts of O_2 and H_2O (8% and up to 16%, respectively). The system performances of the DBD process were evaluated in terms of the SO_2 and NOx removal efficiencies combined with the energy costs (eV/molecule) or *W*-values. The effects of various conditions such as temperature, initial concentration and energy input will also be presented.

2. Experimental facility

The experimental system consists of a continuous flow gas generation system, a laboratory-scale DBD reactor, and a gas detection system (figure 1). The system was described in detail previously [16] but is briefly described here for clarity.

Synthetic gas containing mixtures of O_2, N_2, NO, NO_2, CO_2, SO_2 and H_2O was prepared in a gas handling system. The gas composition was controlled with calibrated high-precision mass flow controllers. Water vapour with controlled concentrations was added to the gas mixture using controlled evaporator mixer, CEM®. It consists of a liquid flow control, a carrier gas control, and a mixing chamber for liquid and carrier gas with heat exchanger for total evaporation. This device can provide high reproducibility and very stable water vapour flow. After mixing in the manifold, the gas then passes through a temperature-controlled line that preheats the gas and prevents condensation. The compositions of the gas mixtures studied are shown in table 1. Experiments were conducted at atmospheric pressure for two flow rates (3 and 10 L min^{-1}) corresponding to residence times of the flue gas in the DBD reactor of about 320 ms and 96 ms, respectively.

Table 1. Compositions of flue gases.

	Composition						
	O_2 (%)	H_2O (%)	CO_2 (%)	NO (ppm)	NO_2 (ppm)	SO_2 (ppm)	N_2 (%)
Gas mixture #1	8	16	14	523	49	163	62
Gas mixture #2	8	11.5	16.5	373	39	630	64

The DBD reactor geometry was of a wire-to-cylinder type. It consists of a 0.9 mm-diameter tungsten wire in a 16 cm-long quartz tube with inner and outer diameters of 11 mm and 13 mm, respectively. A brass mesh covers the dielectric tube and forms the other electrode. The length of the outer electrode can be adjusted and then used to determine the active volume of the DBD reactor. Results presented in this paper were obtained with a plasma volume of about 16 cm^3. The DBD reactor was placed inside a tubular furnace and the gas mixture temperature can be adjusted from room temperature to 500 °C.

The DBD reactor was powered by homemade high voltage pulses with amplitude up to 30 kV into 80 ns (FWHM) pulses and short rise times (40 ns) at variable pulse repetition rates (up to 200 Hz). The HV pulses were delivered by a transformer which is powered by ceramic knob capacitors disposed in a Blumlein-like configuration and switched by a triggered spark-gap. Details of this homemade HV-generator are given in [17]. The fast voltage rise time allows achieving significant overshoot of breakdown voltages (kilovolts per nanosecond) and allows working at larger reduced field values (E/n) than in ac-conventional DBD.

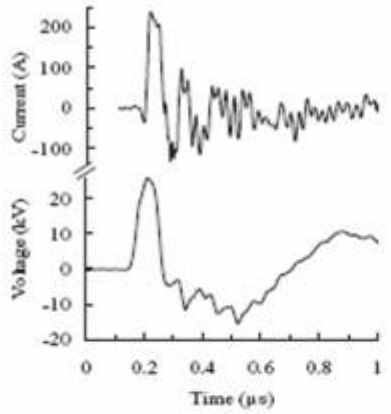

Figure 2. Typical voltage and current pulses for the DBD reactor.

The time-behaviour of the voltage and the current, shown in figure 2, was measured with a Tektronix P6015A high voltage probe (1000x) and current transformer, Europulse 9001. The signals from the probes were recorded on a Tektronix TDS 3034B digital oscilloscope. The discharge pulse energy into the plasma, about 32 mJ in the study, was determined by measuring the energy stored in the transfer capacitors of the system. The specific input energy, which is the discharge energy to unit volume of the treated gas, is given by

$$E_s = \frac{E_p \cdot f}{Q}, \qquad (1)$$

where E_p is the discharge pulse energy, f the pulse repetition frequency and Q the gas flow rate at standard conditions (25 °C and 1 atm). At a constant flow rate, changing the specific energy means changing either frequency and/or discharge pulse energy. In general, the experiments were performed with pulse energy of 32 mJ in the frequency range from 15 to 160 Hz.

The outlet gases were analysed online and quantified using Fourier transform infrared absorption spectrometer (FTIR, Nicolet Magna 550) equipped with a heated 10 m-multiple pass absorption cell. FTIR analysis collected 12 scans for each spectrum at a spectral resolution of about 0.5 cm^{-1}. Absorbencies were converted to concentrations using calibration plots. An electrochemical analyser (QUINTOX KM 9006) was also used for monitoring continuously SO_2, NO, NO_2, NOx as well as CO levels in the gas stream.

3. Discussion

Preliminary experiments were performed by plasma processing of a gas mixture without H_2O ('dry' gas mixture) at an energy of 10 J L^{-1}. Analysis of the gas composition at the outlet of the plasma reactor revealed the existence of compounds already reported in the literature. Besides the main products of the plasma such as NO_2, CO and CO_2, we should highlight the presence of by-products such as aldehydes (CH_2O, CH_3CHO), formic acid (CH_2O_2), ethyl nitrate ($C_2H_5ONO_2$) and methyl nitrate (CH_3ONO_2). Figure 3 shows an example of species observed in the 'dry mixture'. A small amount of

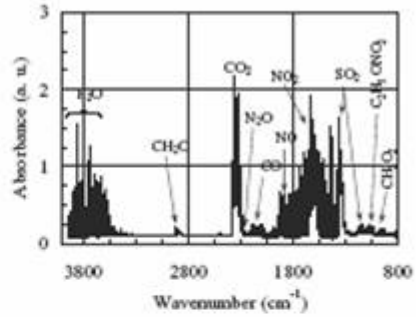

Figure 3. Typical FTIR spectrum: NTP processing of O_2 (8%)–CO_2 (14%)–NO (523 ppm)–NO_2 (49 ppm)–SO_2 (158 ppm)–N_2.

nitrous acid was measured indicating the presence of moisture in the system, possibly arising from the air supply or from moisture adsorbed onto the walls of the gas handling system.

The goal of treating SO_2 and NO contaminated gas streams is their conversion to H_2SO_4, HNO_2 and HNO_3 since these compounds are more easily removed from the gas stream in industrial installations. In the processing of humid gas mixture by non-thermal plasma, the formation of OH radicals via electron-impact dissociation of H_2O and reaction of H_2O with metastable oxygen atom become important and results in the formation of HNO_2, HNO_3 and H_2SO_4 by reactions with NO, NO_2 and SO_2, respectively [6, 12, 18, 19]. In the case of NOx conversion in the presence of N_2, O_2, H_2O and CO_2, it has been shown from detailed chemical kinetics analysis [20] that the role of H_2O in the formation of acids becomes more apparent when the H_2O concentration is 5% and above. In our case where the H_2O concentration is relatively high (11.5% and 16%), the analysis revealed a high acidity of the outlet solution (pH value ranging between 2.4 and 2.8).

From Chang *et al* [19], the overall kinetic scheme for the SO_2 conversion could be summarized into two channels:

(i) oxidation of SO_2 by OH producing HSO_3 and H_2SO_4 as shown in reactions (2) and (3).

$$OH + SO_2 \rightarrow HSO_3, \qquad (2)$$

$$OH + HSO_3 \rightarrow H_2SO_4, \qquad (3)$$

(ii) oxidation of SO_2 by O producing the hygroscopic specie SO_3 that can be hydrolysed to form H_2SO_4 as shown in reactions (4) and (5).

$$O + SO_2 + M \rightarrow SO_3 + M, \qquad (4)$$

$$SO_3 + H_2O \rightarrow H_2SO_4. \qquad (5)$$

The modelling of Lowke and Morrow [12] predicts that the principal channel for the removal of SO_2 is through the combination with the OH radical by reactions (2) and (3) rather than through oxidation of SO_2 by O to SO_3 by reaction (4).

The removal efficiency parameter is sometimes used instead of concentrations for the description of decomposition processes. For the molecule X (X could be SO_2, NO or NOx) this parameter is defined by the following equation where the subscripts indicate whether the discharge was turned on or turned off.

$$\eta(X) = \left(\frac{[X]_{off} - [X]_{on}}{[X]_{off}}\right). \qquad (6)$$

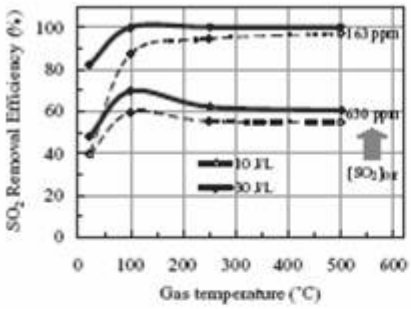

Figure 4. SO_2 removal efficiency as a function of gas temperature and specific energies for two different SO_2 initial concentrations (flow rate = 10 L min^{-1}).

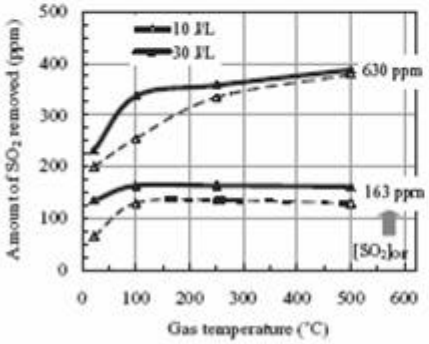

Figure 5. Amount of SO_2 molecules removed as a function of gas temperature for the two gas mixtures at flow rate of 3 L min^{-1} and specific energy depositions of 10 and 30 J L^{-1}.

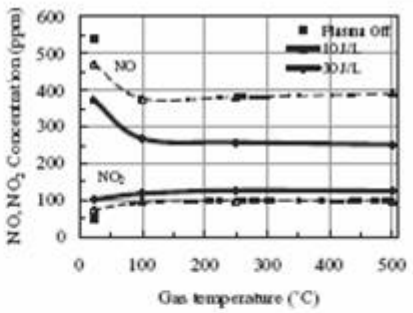

Figure 6. NO and NO_2 concentration as a function of gas temperature at two specific energies (10 and 30 J L^{-1}) for gas mixture #1 (flow rate = 10 L min^{-1}).

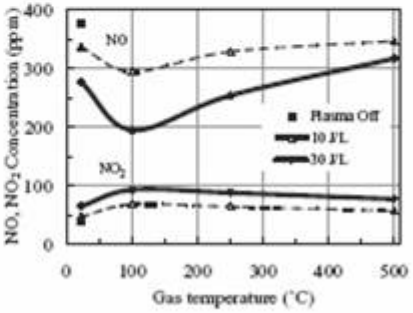

Figure 7. NO and NO_2 concentration as a function of gas temperature at two specific energies (10 and 30 J L^{-1}) for gas mixture #2 (flow rate = 10 L min^{-1}).

SO_2-removal efficiency $\eta(SO_2)$ as a function of gas temperature is shown in figure 4 for selected SO_2 inlet concentrations $[SO_2]_{off}$ (158 and 630 ppm) and specific energies, E_s (10 and 30 J L^{-1}). These measurements show that the highest SO_2 removal efficiency is obtained at temperatures above the condensation of water and remain constant in the range 100–500 °C. Even at relatively low specific energy (10 J L^{-1}), SO_2 removal efficiency higher than 80% was obtained at 163 ppm SO_2 inlet concentration. When the SO_2 inlet concentration increases, the SO_2 removal efficiency decreases to a value of about 60% at $[SO_2]_{off}$ = 680 ppm. Although $\eta(SO_2)$ is higher at a lower inlet SO_2 concentration, the amount of SO_2 molecules removed from the gas stream is larger for increasing inlet SO_2 concentration (figure 5). Note that the absolute SO_2 removal is a function of specific energy deposited into the gas. In our case, higher total removal can be achieved by operating at higher frequencies (see equation (1)).

These results could be compared with previous data obtained by Van Veldhuisen *et al* [5] in gas mixtures containing lower O_2 and CO_2 concentrations (6% and 8%, respectively) including the addition of up to 800 ppm of NH_3. These authors found that the maximum SO_2-removal rate was only 30% without NH_3 and 97% with the addition of 600 ppm of NH_3.

The removal of NO was investigated under the same experimental conditions as those for SO_2. With O_2 and H_2O in the gas mixture, a portion of NO is oxidized to form NO_2. The experimental data obtained at different NO and SO_2 inlet concentrations and gas flow rates exhibited similar trends. Examples of results are shown in figures 6 and 7 for plasma processing of the two gas mixtures at specific energy, E_s, of about 10 and 30 J L^{-1} for a gas flow rate of about 10 L min^{-1}. At a given temperature, the NO concentration decreases while that of NO_2 increases with increasing specific energy deposition. On the other hand, an increase in gas temperature appeared to have some significant effects on the NO to NO_2 conversion efficiency. In all the cases studied, maximum NO to NO_2 conversion occured when the gas temperature was around 100 °C. In the case of gas mixture #1 at a flow rate of 3 L min^{-1} and inlet concentration of NO of about 540 ppm, the maximum NO_2 concentration being about 80 ppm and 115 ppm at 10 J L^{-1} and 30 J L^{-1}, respectively, corresponding to NO to NO_2 conversion efficiency ranged between 16% and 36%. Increasing the gas flow rate by a factor of 3 increases the NO to NO_2 oxidation efficiency up to a factor of two (figure 6). In the case of mixture #2 (figure 7), the maximum NO to NO_2 conversion efficiency of about 48% was obtained at 30 J L^{-1} and 10 L min^{-1}.

The decrease in NO to NO_2 conversion with increasing gas temperature is primarily due to the back reactions that reduce NO_2 back to NO in the presence of oxygen with increasing gas temperature. From thermodynamics, if the temperature is high enough (above 400–500 °C), the rate of back reaction, such as $O + NO_2 \rightarrow NO + O_2$, should be great enough so that NO_2 is not stable and NO conversion is limited. The decreasing ozone concentration with increasing gas temperature could reinforce this limitation.

The maximum fraction of NOx (including NO and NO_2) removed was limited to a value of about 36% (figure 6). One possible way to enhance the NOx conversion is to introduce

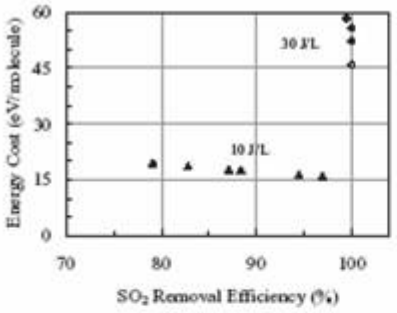

Figure 8. *W*-values for SO_2 as function of SO_2-removal rate in the gas mixture #1 for specific energy deposition of 10 and 30 J L^{-1}. Bold marks: 3 L min^{-1}; Open marks: 10 L min^{-1}.

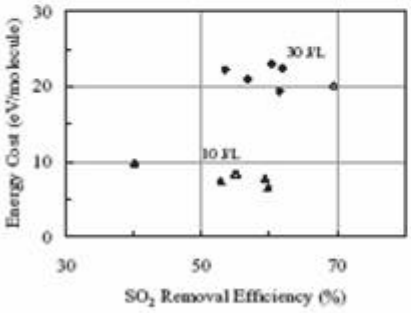

Figure 9. *W*-values for SO_2 as function of SO_2-removal rate in the gas mixture #2 for specific energy depositions of 10 and 30 J L^{-1}. Bold marks: 3 L min^{-1}; Open marks: 10 L min^{-1}.

a small amount of reducing agent (hydrocarbons or ammonia for example) as additive to increase the reactivity of the plasma [2, 5, 16, 19].

The removal efficiency is strongly correlated with the energy cost per removed molecule (*W*-value) [21]. In many previous studies, the energy yield (g kWh^{-1}), the *G*-value (molecule/100 eV) or the energy cost (eV/molecule) have been used to evaluate the system performance of a non-thermal plasma process [[3, 22, 23]. These parameters can be expressed as a function of the specific input energy (energy input to the unit gas volume) and the amount of gas molecules removed. The efficiency of the pulsed DBD reactor in removing pollutant molecules is expressed from the *W*-value (eV/molecule) given by the following formula [3, 24]:

$$W[\text{eV/molecule}] = \frac{250 \cdot E_p \cdot f}{Q\Delta(M)}, \qquad (7)$$

where E_p is the pulse energy in Joules, f the frequency in hertz, Q the gas flow rate in litres per second, and $\Delta(M)$ is the amount of gas molecules removed in parts per million (M could be NO, NOx or SO_2).

The *W*-values for SO_2 as a function of the removal rate for two specific energies (10 and 30 J L^{-1}) are shown in figures 8 and 9 in the case of the two gas mixtures at different flow rates (3 and 10 L min^{-1}).

At a given specific energy deposition, the energy cost seems to be a linear function of the SO_2 removal efficiency. Our measurements confirm that 500 °C is the temperature where the best cleaning (SO_2 removal) result is obtained at

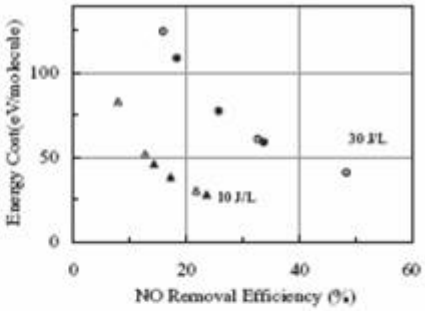

Figure 10. *W*-values for NO as function of NO-removal rate in the gas mixture #2 for specific energy deposition of 10 and 30 J L^{-1}. Bold marks: 3 L min^{-1}; Open marks: 10 L min^{-1}.

relatively low energy cost. Although the SO_2 conversion rates are completely different, no significant difference has been found in the energy cost when using different gas flow rates, except in the case of gas mixture #1 at 30 J L^{-1}. At a given temperature and energy deposition, the relative difference of the *W*-values does not exceed 10% between values obtained at 3 and 10 L min^{-1}. For example, for plasma processing of gas mixture #1 and gas mixture #2 at 10 J L^{-1}, the SO_2 energy cost ranges between 16–19 eV/SO_2-removed molecule (figure 6) and 6.6–9.8 eV/SO_2-removed molecule (figure 7), respectively. At higher energy deposition (30 J L^{-1}) in gas mixture #1, the totality of SO_2 has been removed with an energy cost ranging from 46 to 58 eV/SO_2-removed molecule.

Under initial concentration of NO of between 373 and 523 ppm, the removal efficiency η(NO) was less than 54% at the energy input to the gas of about 10 and 30 J L^{-1}. Figure 10 shows the *W*-values for NO as a function of removal rate for two specific energies (10 and 30 J L^{-1}) in the case of the gas mixtures #2 at flow rates of about 3 and 10 L min^{-1}. In the case of gas mixture #1 the data obtained at the same experimental conditions exhibited a similar trend. At the highest η(NO) obtained at a gas temperature of 100 °C, the energy cost of NO-removal was 41 eV/NO-removed molecule. These results could be compared with those obtained with the addition of NH_3 and performed by Civitano [18] and Van Veldhuisen *et al* [5]. These authors demonstrated NO efficiencies of 60% and 80% at an energy cost of 50 and 13 eV/NO-removed molecule, respectively.

4. Conclusion

An experimental investigation on removal of SO_2 and NOx simultaneously was carried out by sub-microsecond pulsed dielectric barrier discharge in simulated glass manufacturing industry exhausts (O_2, N_2, NO, NO_2, CO_2, SO_2, H_2O) containing a high concentration of H_2O (up to 16%) without additives. The effectiveness of using such a discharge to remove SO_2 and NOx from gas streams was evaluated with a laboratory scale reactor. Removal efficiencies of SO_2 and NOx are dependent on specific energy deposition, gas temperature and inlet concentration of SO_2 and NO. Higher SO_2 and NOx removal efficiencies, 100% and 38%, respectively, were achieved for plasma processing at about 30 J L^{-1} and SO_2 inlet concentrations of 163 ppm. The energy efficiencies for 100% SO_2 removal at a gas temperature of 100 °C were

lower than 58 eV/SO_2-removed molecule for all the treatment conditions explored. The highest NOx removal efficiency (38%) was obtained with an energy cost of about 36 eV/NOx-removed molecule. By-products such as aldehydes (CH_2O, CH_3CHO), formic acid (CH_2O_2), ethyl nitrate ($C_2H_5ONO_2$) and methyl nitrate (CH_3ONO_2) were determined by Fourier transform infra-red spectroscopy in a 'dry' gas mixture.

Results obtained in that study indicate that DBD plasmas have the potential to remove SO_2 and NOx from gas streams without additives. Scaling these results to industrial flow rates (1000 $m^3\,h^{-1}$) indicates that energy consumption three times lower than that of conventional technologies (selective catalytic reduction, selective non-catalytic reduction, reburning) can be obtained by DBD plasmas.

References

[1] Penetrante B M and Schultheis S E (ed) 1993 *Non-Thermal Plasma Techniques for Pollution Control* (Parts A and B) (Berlin: Springer)

[2] Park J Y, Tomicic I, Round G F and Chang J S 1990 *J. Phys. D: Appl. Phys.* 32 1006

[3] Kim H H, Prieto G, Takashima K, Katsura S and Mizuno A 2002 *J. Electrostat.* 55 25

[4] Urishima K and Chang J S 2000 *IEEE Trans. Dielect. Elect. Insul.* 7 602

[5] Van Veldhuizen E M, Zhou L M and Rutgers W R 1998 *Plasma Chem. Plasma Process.* 18 91

[6] Sun W, Pashaie B, Dhali S K and Honea F I 1996 *J. Appl. Phys.* 79 3438

[7] Masuda S and Nakao H 1990 *IEEE Trans. Ind. Appl.* 26 374

[8] Dhali S K and Sardja I J 1991 *Appl. Phys.* 69 6319

[9] Penetrante B M, Hsiao M C, Bardsley J N, Merrit B T, Vogtlin G E, Wallman P H, Kuthi A, Burkhart C P and Bayless J R 1996 *Pure Appl. Chem.* 68 1083

[10] Evans D, Rosocha L A, Anderson G K, Coogan J J and Kushner M J 1993 *J. Appl. Phys.* 74 5378

[11] Frank N W 1995 *Radiat. Phys. Chem.* 45 989

[12] Lowke J J and Morrow R 1995 *IEEE Trans. Plasma. Sci.* 23 661

[13] Chang M B, Balbach J H, Rood M J and Kushner M J 1991 *J. Appl. Phys.* 69 4409

[14] Dinelli G, Civitano L and Rea M 1990 *IEEE Trans. Ind. Appl. Soc.* 26 535

[15] Chang J S 1996 *IEEE Trans. Ind. Appl.* 32 131

[16] Khacef A, Cormier J M and Pouvesle J M 2002 *J. Phys. D: Appl. Phys.* 35 1491

[17] Khacef A, Viladrosa R, Cachoncinlle C, Robert E and Pouvesle J M 1997 *Rev. Sci. Instrum.* 68 2292

[18] Civitano L 1993 *Non-Thermal Plasma Techniques for Pollution Control, Part B: Electron Beam and Electrical Discharge Processing* ed B M Penetrante and S E Schultheis (Berlin: Springer) p 103

[19] Chang M B, Kushner M J and Rood M J 1992 *Plasma Chem. Plasma Process.* 12 568

[20] Penetrante B M and McLarno C R 1998 *SAE Technical Paper Series* No 982433

[21] Khacef A, Cormier J M and Pouvesle J M 2005 *J. Adv. Oxid. Technol.* 8 150

[22] Penetrante B M, Hsiao M C, Bardsley J N, Merrit B T, Vogtlin G E, Kuthi A, Burkhart C P and Bayless J R 1997 *Plasma Sources Sci. Technol.* 6 251

[23] Filimonova E A, Kim Y H, Hong S H and Song Y H 2002 *J. Phys. D: Appl. Phys.* 35 2795

[24] Puchkarev V, Roth G and Gundersen M 1998 *SAE Technical Paper Series* No 982516

C&E T Full Paper

Effect of Oxygen on Methane Steam Reforming in a Sliding Discharge Reactor

By *Fakhreddine Ouni**, *Ahmed Khacef*, and *Jean Marie Cormier*

DOI: 10.1002/ceat.200500333

Hydrogen-rich gas can be efficiently produced in compact plasma reformers by the conversion of a variety of hydrocarbon fuels, including natural gas and gasoline. This article describes experimental and modeling progress in plasma reforming of methane using a sliding discharge reactor (SDR). Experiments have been carried out in a compact device operating at low consumed power (1–2 kW). Previous studies of methane steam reforming using a SDR at atmospheric pressure show promising results (H_2 concentration higher than 55 %). In order to study the effect of oxygen on the methane conversion and thus hydrogen production, a small amount of oxygen in the range of 7–20 % was added to the CH_4-H_2O mixture. An unexpected result was that under our experimental conditions in the SDR oxygen did not have any influence on the methane conversion. Almost the totality of added oxygen is recovered intact. Moreover, part of the H_2 produced was transformed into water by reaction with O_2. A model describing the chemical processes based on classical thermodynamics is also proposed. The results indicate that the reactor design has to be improved in order to increase conversion and hydrogen production.

1 Introduction

Natural gas is attracting considerable attention as an alternative energy source to petroleum. One of the reasons why it is possible for natural gas to become the first resource is its high H to C ratio compared to those of coal and oil [1]. Accordingly, natural gas has the best future as a resource to produce hydrogen. However, due to the high stability of CH_4 molecules, it is difficult to induce a selective reaction to produce other molecules.

There are several methods to produce synthesis gas (syngas) but most of them (40 ×) are based on steam reforming (SR) [2]. The conventional catalytic technology presents several shortcomings, such as the large size of the equipment, high investments and exploitation costs, limitations on rapid response, catalyst sensitivity to poisons, and extreme operating conditions that limit the lifetime of reactors [3]. Therefore, a process which converts methane directly into syngas and other valuable products under "sweet" conditions is expected to be a challenge from the viewpoint of industry as well as science. Plasma reformers seem to be one of the proposed solutions [4, 5]. Non-thermal plasma, which is a very high energy density media, gives an attractive alternative for hydrogen and syngas production [6]. In this approach, the plasma could replace catalysts and accelerate chemical reactions due to both temperature and active species effects. Plasma reactors represent an incisive approach by their simplicity, compactness, and low energetic cost.

Hydrogen and syngas production via methane steam reforming has been experimentally investigated in various plasma reactor configurations [7]. A high level of H_2 production (up to 55 %) was obtained with this device.

Due to its high reactivity, oxygen was used in several processes based on hydrocarbon conversion into syngas in partial oxidation (POX) processes following the reaction (1):

$$CH_4 + \tfrac{1}{2}O_2 \rightleftarrows 2H_2 + CO \qquad \Delta H = -36\ \text{kJ/mol} \qquad (1)$$

Reaction (1) is exothermic. Neither a heat exchanger nor catalyst is needed because of its high temperature. It was used in auto-thermal reformers to provide heat for the steam reforming endothermic reaction given below (reaction (2)):

$$CH_4 + H_2O \rightleftarrows 3H_2 + CO \qquad \Delta H = 206\ \text{kJ/mol} \qquad (2)$$

The present work is a continuation of our previous studies regarding syngas production by steam reforming of methane [4]. In the set of experiments presented below, the effect of oxygen on methane conversion and hydrogen production using a SDR at atmospheric pressure was studied. The results were compared with a thermodynamic model describing the chemical evolution of the system.

2 Experimental

2.1 Sliding Discharge Reactor

The SDR used in this study was in a cylindrical configuration and is shown in Fig. 1. This geometry was chosen because of its simplicity. The reactor body was Pyrex or quartz tube (500 mm length, 100 mm external diameter) inserted between two stainless steel covers. Pyrex and quartz were used to enable us to visualize plasma evolution and to perform spectroscopy measurements. The SDR consists of three

[*] F. Ouni (author to whom correspondence should be addressed, fakhreddine.ouni@univ-orleans.fr), Dr. A. Khacef, Prof. J. M. Cormier, GREMI-Polytech'Orléans, 14 rue d'Issoudun, BP 6744, 45067 Orléans Cedex 2, France.

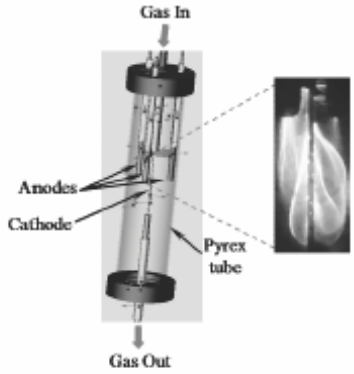

Figure 1. Schematic diagram of the sliding discharge reactor and photography of the produced discharge.

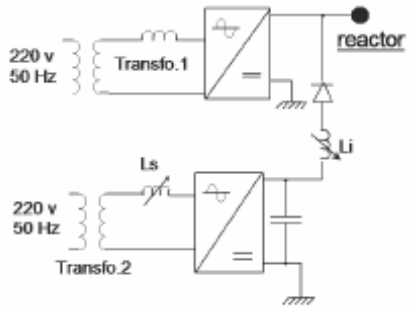

Figure 2. Simplified electric scheme of the power supply.

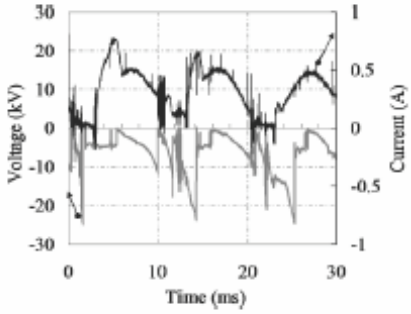

Figure 3. Typical voltage and current waveforms.

copper anodes arranged around a single 3 mm diameter tungsten cathode. To avoid arcing between the electrodes and reactor covers, ceramic shields are placed around part of the electrodes.

Discharges are ignited between the electrodes and then pushed by the gas flow. A magnet was inserted into the reactor in order to produce a rotating effect in the discharge region. The discharge column is a plasma string, with a visible diameter less than 1 mm, that slides in the gas flow and the magnetic field region (see Fig. 1). The plasma string performs a helix movement and looks like a wrapped wire around the cathode.

Using this type of reactor, plasma can sweep a large part of the inlet gas and maintain its non-equilibrium behavior. In the usual sliding discharges, plasma thermalization was avoided by using external current limitation.

The discharge behavior in a magnetic field is quite different from the usual gliding discharges. The first effect is the increase in the mixing properties of the reactor [7]. In the case of magnetic blow out, the force acting on the lengthening discharge column is proportional to the product between the current and the magnetic-field strength. This force produces a rapid lengthening of the discharge column. Due to the magnetic field, a self-limitation of the current intensity is produced.

2.2 Power Supply

In these experiments a three-channel power supply device was used, as already described in [7]. One channel consists of two transformers (see Fig. 2) with rectifiers that allow two running phases: the ignition at high voltage and low current intensity, and a complementary energy supply with higher current (about 2 A). This current intensity is sufficient to obtain a hot plasma string with a temperature up to 3000 K [7]. Current and voltage measurements were achieved using a Hall Effect probe and voltage divider (ratio of 0.01), respectively. The output signals were transmitted to a transient digitizer (Tektronix TDS 3034B) interfaced with a personal computer.

Typical voltage and current waveforms ($u(t)$ and $i(t)$, respectively) for one of the three discharges are shown in Fig. 3. For clarity, the high voltage is plotted as a negative signal. As can be seen from this figure, the discharge behavior is not definitely periodic due to the instabilities in the growing discharge. The mean electrical power ($P = 1/T = \text{u.i. d}t$) is obtained by averaging results over a large number of discharges.

2.3 Diagram of the Experimental Setup

Fig. 4 shows a diagram of the experimental setup. All experiments were conducted at atmospheric pressure. The water, methane, and oxygen are mixed before injection in a heating line. The gas temperature was fixed at about 150 °C for all the experiments. After plasma treatment the exhausts gas was passed through condensers.

The produced gases were analyzed online and quantified using two techniques: micro gas chromatography (μGC, Varian CP2003-P) and Fourier Transform Infra Red spectroscopy (FTIR, Nicolet Magna-IR 550 series II). The μGC analyzer was equipped with Molsieve 5 Å and PoraPlot Q columns and the detection was assured with a thermal conductivity detector (TCD) calibrated with standards of known composition. The major gas components identified were H_2, CH_4, and CO. Small amounts of CO_2 and C_2 hydrocarbons (C_2H_2,

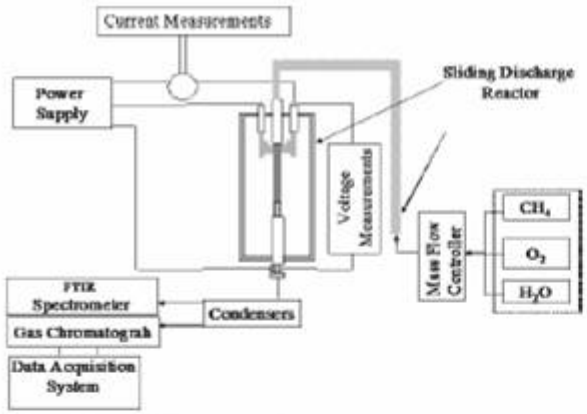

Figure 4. Diagram of the experimental setup.

C_2H_4, C_2H_6) have been detected with concentrations lower than 1 % in all cases studied.

2.4 Safety Aspects: Ignition Temperature and Explosibility

The addition of oxygen to methane requires consideration of the respective ignition temperatures, and lower and upper explosion limits (LEL, UEL).

The flammable (explosive) range is the range of a gas or vapor concentration that will burn or explode if an ignition source is introduced. Limiting concentrations are commonly called the "Lower Explosive or Flammable Limit" (LEL/LFL) and the "Upper Explosive or Flammable Limit" (UEL/UFL). Below the explosive or flammable limit the mixture is too lean to burn. Above the upper explosive or flammable limit the mixture is too rich to burn [8].

It is clear that for any CH_4-O_2 mixture, it is necessary to work below the LEL or above the UEL. We have to respect the explosion range shown in Tab. 1 [8]. In steam reforming processes, steam narrows the range of explosibility because of its "inerting" effect [9]. This effect allows one to work with a high amount of oxygen, up to 20 %.

Table 1. Ignition and explosibility characteristics of some gases in air/in oxygen [8].

Gas and vapors	Ignition temperature [°C]	LEL [%]	UEL [%]
Methane	225/215	5/5	15/61
Propane	480/470	2.2/2.3	10/45
Butane	285/275	1.8/1.8	8.4/49

2.5 Materiel Balance Equations

In order to verify the compatibility of different components between the inlet and the outlet of the reactor and to calculate experimental error, material balances of carbon, hydrogen, and oxygen atoms were considered. They led to the following material balance equations:

$$\Sigma C_i = [CH_4]_i = \Sigma C_f = [CO_2] + [CO] + [CH_4]_f + 2([C_2H_2] + [C_2H_4] + [C_2H_6]) \quad (3)$$

$$\Sigma H_i = 2[H_2O]_i + 4[CH_4]_i = \Sigma H_i = 2[H_2O]_i + 4[CH_4]_i + 2[C_2H_2] + 4[C_2H_4] + 6[C_2H_6] \quad (4)$$

$$\Sigma O_i = [H_2O]_i + 2[O_2]_i = \Sigma O_f = [H_2O]_f + 2[O2]_f \quad (5)$$

where brackets designate concentrations and the subscripts i and f indicate the initial and final states, respectively.

3 Results and Discussion

Fig. 5 shows an example of H_2, CO, CH_4, and CO_2 concentrations as a function of the inlet O_2 amount added in the CH_4-H_2O mixture. These results were compared with those obtained in the case of water-methane mixtures (0 % O_2) under the same experimental conditions. From that data, we note that adding up to 20 % of O_2 in methane-water mixtures does not significantly affect the CO, CH_4, and CO_2 concentrations obtained after plasma treatment, though the H_2 concentration slightly decreases in the presence of O_2. It seems that oxygen reacts preferentially with H_2 to form water vapor. This may be because the reactor walls worked as a catalyst for water formation, as reported in [10]. In addition, compared to the infrared spectrum obtained for the H_2O-CH_4 mixture, FTIR chemical analyses of H_2O-CH_4-O_2, shown in Fig. 6, do not indicate the formation of new oxygenated species. Gas chromatography analyses and material balance showed that a small amount of the added oxygen was reacted. More than 80 % of added oxygen remains intact without transformation in all studied cases.

Material balances were used to calculate the wet component concentrations after plasma treatment. Calculations were done with an average error of 10 %, as reported in Tab. 2.

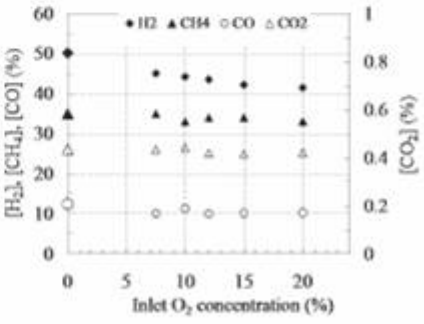

Figure 5. H_2, CH_4, CO, and CO_2 concentrations as a function of O_2 concentration in H_2O-CH_4-O_2 mixtures. (Inlet gas temperature: 150 °C, Average electrical power: 830 W, flow rate: 15 L/min, Initial CH_4 concentration: 30 %).

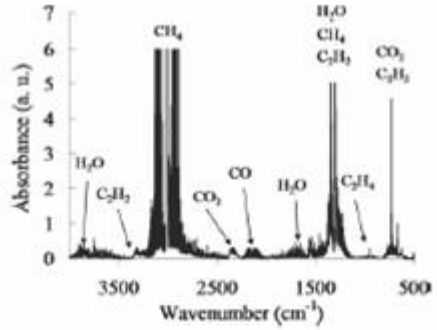

Figure 6. FTIR spectrum of H_2O-CH_4-O_2 (55 %-30 %-15 %) mixture after plasma treatment (Inlet gas temperature: 150 °C, Average electrical power: 830 W, Flow rate: 15 L/min).

Table 2. Inlet O_2 concentration and calculated wet outlet O_2 concentration via material balance.

Inlet O_2 concentrations [%]	Outlet O_2 concentrations [%]
7.5	7.1
10	8.6
12	9.6
15	12.2
20	16.1

Taking into account the main products identified in the reactor outlet by using chromatography and FTIR and the decrease of the outlet H_2 concentrations, characteristic parameters (conversion, selectivity) of the processes were calculated using the following main possible reactions:

- $CH_4 + H_2O \rightleftarrows 3\,H_2 + CO \quad \Delta H = 206$ kJ/mol (6)

Initial (moles) CH_4: 1
Consumed (moles) CH_4 :x
Final (moles) CH_4:1–x, H_2: 3x, CO: x

- $CH_4 \rightleftarrows 2\,H_2 + C \quad \Delta H = 74.6$ kJ/mol (7)

Initial (moles) CH_4: 1–x
Consumed (moles) CH_4: y
Final (moles) CH_4: 1–x--y, H_2: 2y

- $2\,H_2 + O_2 \rightleftarrows 2\,H_2O \quad \Delta H = -285.83$ kJ/mole (8)

Initial (moles) H_2: 3x+2y, O_2: w
Consumed (moles) H_2: 2z, O_2: w–z
Final (moles) H_2: 3x+2y–2z, O_2: w–z

The w, x, y, and z parameters represent the amount of inlet oxygen, the amount of methane consumed via the steam reforming reaction (Eq. (6)), the amount of methane consumed via the cracking reaction (Eq. (7)), and the amount of hydrogen converted in water, respectively. The parameters x, y and z can be calculated as functions of species concentrations given by chromatography analyses. They led to the following equations:

$$x = \frac{2 \times [CO] \times (1 - w)}{[H_2] - [CO] - 2 \times [O_2] + 2 \times [CH_4]} \quad (9)$$

$$y = 1 - \frac{x \times ([CH_4] + [CO])}{[CO]} \quad (10)$$

$$z = w - \frac{x \times [O_2]}{[CO]} \quad (11)$$

Accordingly, the total amount of methane converted will be equal to $(x + y)$. Fig. 7 presents the evolution of methane conversion as a function of the added O_2 concentration. It shows that methane conversion remained constant in all studied cases. The addition of O_2 does not seem to be the solution to improve CH_4 conversion.

In order to study the effect of oxygen on the steam reforming and cracking reactions, selectivities are calculated from the ratios given below:

Steam reforming selectivity: $\frac{x}{x+y}$ (12)

Craking selectivity: $\frac{y}{x+y}$ (13)

Fig. 8 gives the results of these calculations as a function of the O_2 concentration added to the CH_4-H_2O mixture. These results show that the addition of O_2 (up to 20 %) promotes the cracking reaction (Eq. (7)). In these experiments,

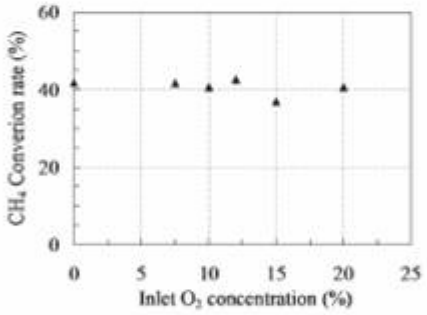

Figure 7. Calculated methane conversion rate as a function of the inlet oxygen concentration.

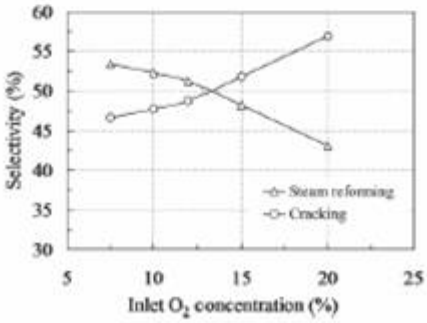

Figure 8. Steam reforming and cracking selectivities as a function of the inlet O_2 concentration.

a large quantity of soot was deposited on the plasma reactor wall in the case of high O_2 concentration. It could be explained by the decrease of the H_2O/CH_4 molar ratio (< 2.5) [11].

4 Modeling

The plasma chemical processes, occurring in the SDR, was simulated by means of chemical workbench code, version 3.2 (kinetic technologies Russia), using a Thermodynamic Equilibrium Reactor model (TER). The TER is designed for the calculation of the chemical equilibrium of multi-component heterogeneous systems. This thermodynamic system is considered as self-contained and closed. In this system, a state of thermodynamic equilibrium is achieved by internal chemical and phase transformations. It means that the system is under mechanical and energetic equilibrium. It is proposed also that the system under investigation is a heterogeneous one and consists of several uniform phases. The TER Code uses the common principle of entropy (S) maximum for the calculation of chemical and phase compositions. In accordance with this principle, the equilibrium state is characterized by the uniform distribution of the thermodynamic parameters in the system volume, and chemical composition corresponds to the maximum probability of energetic level distribution for macro particles. The method considers two hundred and sixty-eight atomic and ionic species that could appear in the C-H-O system. Calculations are made at atmospheric pressure for various temperatures.

The model is presented schematically in Fig. 9. We consider that the reactions occur in the discharge zone. If the a factor represents the percentage of gas passed through the discharge, the best fit with experimental data was obtained with a ranged between 45–55 %. The inlet gas stream is divided in two parts: 55–45 % remains at 423 K and 45–55 % is heated in the discharge. The assumption is made that both streams arrive at thermodynamic equilibrium and that the two resulting streams are afterwards perfectly mixed.

In order to compare the experimental results with modeled ones, the calculated variation of the chemical equilibrium composition was plotted as a function of temperature for different CH_4-H_2O-O_2 systems (see Fig. 10). These data show stabilization of concentrations in the temperature range 2000–3000 K that corresponds to the temperature of the outer surface of the discharge [12, 13]. In order to obtain the best fit with the experiments a is adjusted for each mixture.

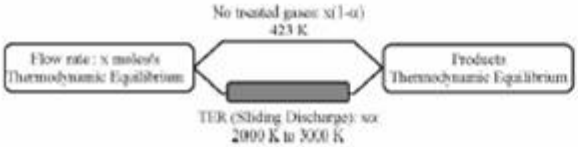

Figure 9. Simplified scheme of the theoretical model.

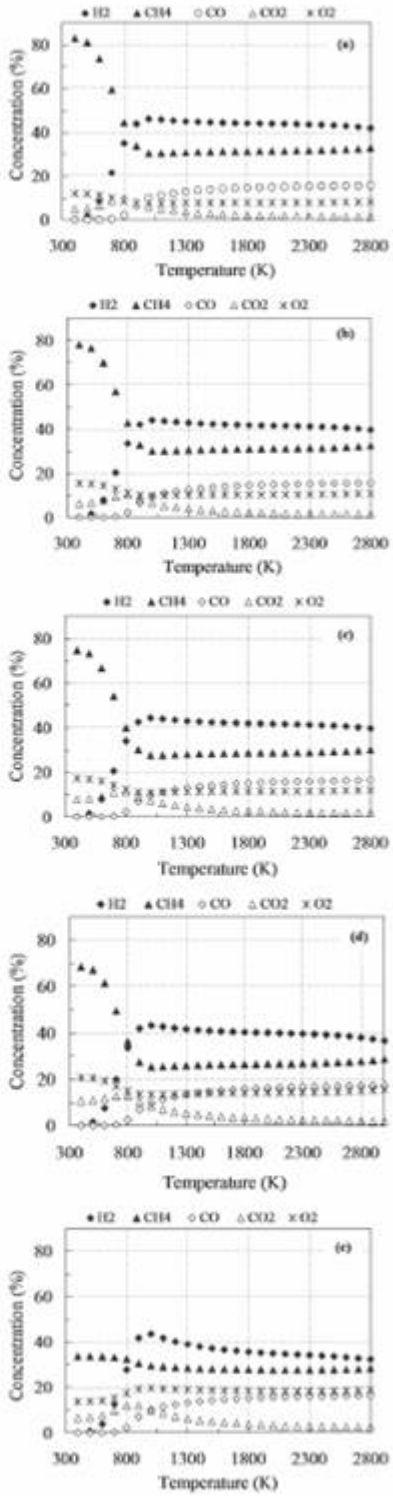

Figure 10. Calculated variation of the chemical composition versus temperature for the CH_4-H_2O-O_2 system: a) molar ratio = 30/62.5/7.5; b) molar ratio = 30/60/10; c) molar ratio = 30/58/12; d) molar ratio = 30/55/15; e) molar ratio = 30/50/20.

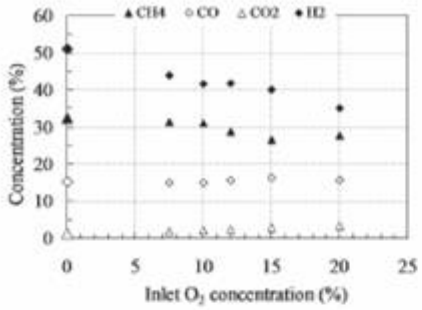

Figure 11. Calculated H_2, H_2O, CO, and CO_2 concentrations as a function of O_2 concentration in H_2O-CH_4-O_2 mixtures. (Temperature: 2000 K, flow rate: 15 L/min, Initial CH_4 concentration: 30 %).

Assuming a constant temperature of 2000 K in the TER, the chemical equilibrium composition versus inlet O_2 concentration is calculated. The results are plotted in the Fig. 11.

Results calculated at 2000 K showed that the model agrees well with experimental results for the CH_4 conversion and H_2 production, where agreement is within 10–15 %. O_2 added to H_2O-CH_4 mixture reacts with the produced hydrogen and promotes water formation. Therefore, the calculated CO and CO_2 concentrations are higher than the experimental results.

Plasma processing cannot be fully explained by equilibrium thermodynamics. However, one must note that the corresponding model demonstrates the possibility of obtaining higher conversions by increasing the *a* factor. However, new investigations are needed to find more adequate models for sliding discharge chemistry.

5 Conclusion

Compared with other processes, the sliding discharge rector showed promising results and seems to have a great future in the production of hydrogen from hydrocarbons (SR). More than 45 % of the inlet gas was treated, compared to previous reactors in which only 15–20 % passed through the discharge [14–16]. A high level of H_2 production (up to 55 %) was obtained with this device. The SDR is considered as a clean process. In all studied cases, CO_2 concentrations remained lower than 0.5 %. In the SDR, the addition of O_2 is not a solution to improving CH_4 conversion and increasing H_2 production. O_2 reacts preferentially with H_2 to produce water.

The thermodynamic calculations performed according to the proposed model fitted quite well with the chemical composition at the outlet of the reactors. According to the specific experimental conditions (the small plasma string volume, the high flow rate, and low temperature), the outlet gas contains unreacted components.

Therefore, further investigations must be performed in order to improve the correlation between model and experiment. In addition, reactor design must be improved in order to increase the plasma string volume, and then both conversion and selectivity.

Received: October 24, 2005

References

[1] S. Kado, K. Urasaki, Y. Sekine, K. Fujimoto, *Fuel* **2003**, *82*, 1377.
[2] C. Liu, R. Mallison, L. Lobbon, *J. Catal* **1998**, *179*, 326.
[3] M. A. Pena, J. P. Gomez, J. L. G. Fierro, *Appl. Catal., A* **1996**, *144*, 7.
[4] G. Kaske, L. Kerke, R. Muller, *Hydrogen Energy Prog. 6* **1986**, 1.
[5] T. Paulmier, L. Fulcheri, *Chem. Eng. J.* **2005**, *106*, 59.
[6] R. Muller, *Hydrogen Energy Prog. 6* **1982**, *3*, 885.
[7] I. Ruzu, J. M. Cormier, *Chem. Eng. J.* **2003**, *91*, 23.
[8] A. Cleuet, *Les Mélanges Explosifs*, INRS, Paris **1981**, 18.
[9] W. Bartknecht, *Explosions*, Springer-Verlag, New York **1981**, 4.
[10] S. Fukada, N. Nakamura, J. Monden, *Int. J. Hydrogen Energy* **2004**, *29*, 619.
[11] A. Berman, R. K. Karn, M. Epstein, *Appl. Catal., A* **2005**, *282*, 73.
[12] A. Pridman et al., *J. Phys. III* **1994**, *4*, 49.
[13] S. Pellerin et al., *J. Phys.* **2000**, *33*, 1.
[14] J. M. Cormier, I. Ruzu, M. Dudemaine, D. Sibiescu, *Proc. 4th Int. Conf Optimization of Electrical and Electronic Equipments OPTIM'1*, Brasov **2002**, 6.
[15] S. Potehin et al., *Preprint IAE-6023/12*, Kurchatov Institute, Moscow **1997**, p. 7.
[16] I. Ruzu, J. M. Cormier, *Chem. Eng. J.* **2003**, *91*, 23.

Eur. Phys. J. Appl. Phys. **33**, 195–198 (2006)
DOI: 10.1051/epjap:2006019

THE EUROPEAN PHYSICAL JOURNAL APPLIED PHYSICS

Energy deposition effect on the NOx remediation in oxidative media using atmospheric non thermal plasmas

A. Khacef[a], J.M. Cormier, and J.M. Pouvesle

Groupe de Recherche sur l'Énergétique des Milieux Ionisés, GREMI – Polytech'Orléans, 14 rue d'Issoudun, BP 6744, 45067 Orléans Cedex 2, France

Received: 3 November 2004 / Received in final form: 11 October 2005 / Accepted: 14 October 2005
Published online: 22 February 2006 – © EDP Sciences

Abstract. Dielectric barrier discharges (DBDs) have been investigated under a wide range of experimental conditions (pulsed and sinusoidal excitation, input energy, frequency, and residence time) to remediate NOx from atmospheric O_2 rich gas streams. In a given reactor under identical gas composition and equivalent energy density deposition, results show that the main parameter which controls the efficiency of the plasma process is the energy deposition mode. For example, in a pulsed DBD processing at energy density deposition of 30 J/L, 25% of NOx and 40% of C_3H_6 were converted at 35 mJ/pulse whereas, at 195 mJ/pulse these values were 0% and 15%, respectively. Furthermore, significantly different end products were observed when changing the nature of electrical excitation.

PACS. 52.80.-s Electric discharges – 82.33.Xj Plasma reactions – 92.60.Sz Air quality and air pollution

1 Introduction

Increasing environmental awareness and strict pollution control have motivated investigations into energy efficient method to remove oxides of nitrogen (NOx) from industrial systems. Among the systems proposed for NOx reduction are those based on atmospheric non-thermal plasma (NTP) discharge. NTP with a low gas temperature and high electron temperature can be produced by a variety of electrical discharge methods (pulsed corona discharge, barrier discharge, and D.C. discharge) [1–4] or electron beam irradiation [5,6]. Pulsed corona and dielectric barrier discharge (DBD) techniques are two of the more commonly used methods for producing electrical discharge plasmas. The critical parameter in the use of these plasmas in pollution control devices is the electrical energy consumption of the plasma reactors. This energy consumption depends on both the chemical reaction efficiency and the energy conversion efficiency from the main power source to the plasma. Many papers in the plasma processing literature present the NOx conversion efficiency as a function of parameters such as: input energy density, residence time of the gas into the reactor, or applied voltage to the plasma reactor [7–10].

In this work we will show the importance of the energy deposition conditions on the NOx and hydrocarbon conversion in NTP. Plasma was created in gas mixtures containing O_2, NO, C_3H_6 and N_2 as balance at room temperature using a DBD powered by a nanosecond pulsed generator and 50 Hz-sinusoidal transformer, respectively. While keeping the energy density constant, pulsed DBD are investigated in two regimes:

(i) low energy per pulse deposition and high repetition rate regime, and
(ii) high energy per pulse deposition and low repetition rate regime.

The experiments were conducted at two different flow gas rates (4 L/min and 16 L/min) corresponding to residence times of exhaust gas within the discharge volume of 240 ms and 60 ms, respectively.

2 Experimental set-up

The experimental system consists of a continuous flow gas generation system, laboratory-scale dielectric barrier discharge (DBD) reactor, and a gas detection system. The system was described in detail previously [11] and is briefly described here for clarity.

Synthetic exhaust gases (O_2, N_2, NO, and C_3H_6) were prepared and mixed in a gas handling system and their composition was controlled by calibrated high-precision mass flow controllers.

The electrical discharge reactor used is dielectric-barrier discharge (DBD) in cylindrical configuration. The inner electrode is a tungsten wire (0.9 mm diameter) and the outer electrode is a metal (aluminum foil or copper mesh) wrapped around a quartz tube (13 mm outer diameter, 1 mm thickness). The length of the outer electrode

[a] e-mail: Ahmed.khacef@univ-orleans.fr

can be adjusted and then determines the active volume of the DBD reactor.

Two high-voltage generators (pulsed Blumlein-like source and AC power source) were used for powering the reactors in that study. The AC power supply was a leakage transformer able to deliver a 50 Hz sinusoidal current of typically 100 mA. The voltage delivered by this system adjusts itself between 1 kV and 10 kV according the input voltage of the transformer. The power in the discharge could be varied by adjusting the input voltage. The second generator used is a home made HV power supply which is capable to deliver high voltage pulses up to 150 kV (open circuit) into 80 ns (FWHM) pulses and 40 ns rise times at a repetition rate which can reach 1 kHz. The fast voltage rise time (several kilovolts per nanosecond) allows achieving significant over-voltage at breakdown and allowing working at larger reduced field values (E/n) than in AC-conventional DBDs.

Details of the pulsed generator were given elsewhere [12]. Briefly, it consists in a line transformer powered by ceramic capacitors disposed in a Blumlein-like configuration and switched by a triggered spark gap. The discharge pulse energy into the plasma was measured with a capacitive circuit and was given by:

$$E_p = \frac{1}{2} CV^2 \quad (1)$$

where C is the transfer capacitance and V the charging voltage of the system. The energy deposition in the plasma reactor, Joules per liter (J/L), is given by:

$$E_d = \frac{E_p \cdot f}{Q} \quad (2)$$

where E_p is the discharge pulse energy, f is the pulse repetition rate, and Q is the gas flow rate at standard conditions (25 °C and 1 atm). In these experiments, E_p was varied from 35 mJ/pulse to 195 mJ/pulse, f from 1 up to 200 Hz, and Q from 1.6 to 16 L/min.

The major output gaseous components as NO, NO_2, CO, CO_2, and C_3H_6 were analyzed online and quantified using Fourier Transform Infrared Absorption Spectroscopy (FTIR). An electrochemical NOx analyzer was also used for monitoring the concentrations of nitrogen oxides (NO, NO_2, and NOx) as well as CO in the gas stream.

3 Results and discussion

The composition of the output gaseous components was recorded as a function of energy density which is the parameter commonly used to evaluate the NOx conversion efficiency in the plasma. However, if this parameter is important to characterize the electrical energy consumption of the process we should take into account how the energy is deposited into the plasma. In the case of pulsed DBD, the energy per pulse deposition combined with the voltage repetition frequency is the main control parameter that should be used.

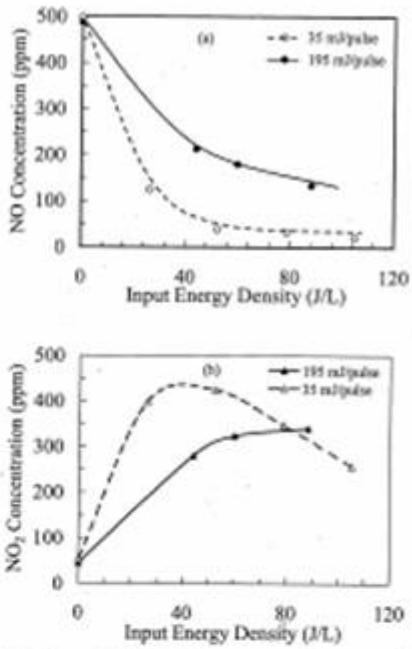

Fig. 1. NO (a) and NO_2 (b) concentrations as a function of input energy density for 35 mJ/pulse and 195 mJ/pulse in the case of pulsed excitation in gas mixture containing 20% O_2, 500 ppm NO, 500 ppm C_3H_6 and N_2 as balance (flow rate = 4 L/min).

Three types of experiment have been used. Two of them used a pulsed excitation and the third one used an AC excitation.

In the case of pulsed excitation, the first set of experiments was realized with a gas mixture containing 500 ppm NO, 500 ppm C_3H_6 in 20% O_2 and N_2 as balance. The residence time of the exhaust gas within the discharge volume was 240 ms. Due to the strongly oxidative action of hydrocarbon radicals, NO_2 is the main product in that case. The NO and NO_2 concentrations plotted as a function of the energy density for two different energies per pulse deposition (35 mJ/pulse and 195 mJ/pulse) are shown in Figures 1a and 1b, respectively. At a given energy density, the conversion of NO to NO_2 depends strongly of the effective energy per pulse deposition in the plasma. For the 35 mJ/pulse and high repetition rate (up to 200 Hz) case, about 95% of NO is converted to NO_2 at energy densities of 50 J/L and above. This conversion is only around 60% for 195 mJ/pulse and low repetition rate (up to 30 Hz) case. For specific energy higher than 40 J/L (Fig. 1b, 35 mJ/pulse), NO_2 concentration decrease. This loss of NO_2 molecules is due to the formation of organic nitrates and nitrites as well as nitrous acid.

In the second set of experiments, the oxygen concentration and the residence time of the exhaust gas within the discharge volume were reduced at 10% and 60 ms, respectively. NOx concentration (sum of NO and NO_2 concentrations) and C_3H_6 conversion as a function of the

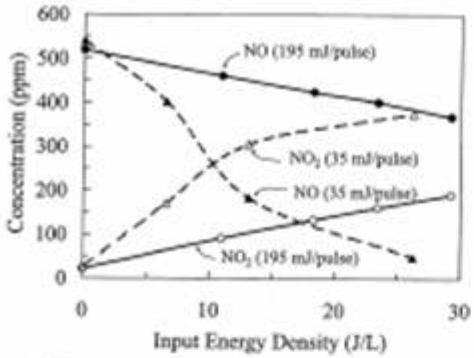

Fig. 2. NO and NO_2 concentrations as a function of input energy density for 35 mJ/pulse and 195 mJ/pulse in the case of pulsed excitation in gas mixture containing 10% O_2, 500 ppm NO, 500 ppm C_3H_6 and N_2 as balance (flow rate = 16 L/min).

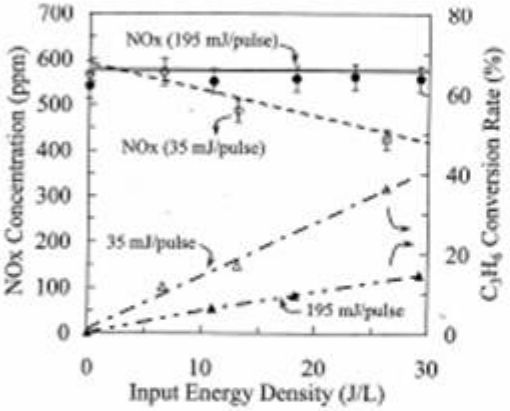

Fig. 3. NOx concentration and C_3H_6 conversion as a function of input energy density for 35 mJ/pulse and 195 mJ/pulse in the case of pulsed excitation in gas mixture containing 10% O_2, 500 ppm NO, 500 ppm C_3H_6 and N_2 as balance (flow rate = 16 L/min).

energy density for 35 mJ/pulse and 195 mJ/pulse energy deposition are shown in Figure 2. These data obtained in different experimental conditions confirm the importance of the energy per pulse deposition in the plasma chemistry. In the high energy per pulse and low repetition rate regime, the NO_2 concentration increased from 25 ppm to 200 ppm but the NOx concentration was unchanged as shown in Figure 3. This indicated that the totality of the NO molecules was oxidized into NO_2 without forming another nitrogen compounds such as N_2O. In that case the hydrocarbon conversion is around 15%.

The NOx and C_3H_6 conversion efficiencies were greatly improved by plasma processing at low energy per pulse and high repetition rate regime. Plasma processing at about 26 J/L (35 mJ/pulse and 200 Hz) shows that approximately 25% of NOx and 40% of C_3H_6 were converted, respectively (Fig. 3). Due to the large amount of O_2 in the gas mixture (10%), plasma processing of NOx is dominantly oxidative. The decreasing of NOx concentration is due to the reaction of NOx and C_3H_6 oxidation by-products and corresponds to the formation of R-NOx compounds (R = hydrocarbon radical) such as methyl nitrate (CH_3ONO_2) and nitromethane (CH_3NO_2) [13]. It appears from these experimental results that if the energy is deposited in small fractions more often, the energy utilization is more efficient. This behavior confirmed the multi-pulse effect studied numerically by Kushner et al. [14,15] and explained as a cumulative effect of the process. When using multiple pulses, reactions occur in the latter pulses with reaction products from previous pulses which are not accessible with a single pulse.

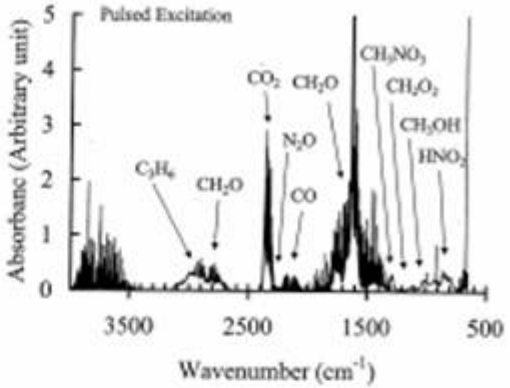

Fig. 4. Typical FTIR spectrum of the by-products from pulsed plasma at 90 J/L input energy density (10% O_2, 500 ppm NO, 500 ppm C_3H_6 and N_2 as balance).

As expected, under these oxygen rich conditions, in addition of the main products of the plasma (NO_2, CO, and CO_2), the plasma partially oxidizes the hydrocarbons (Fig. 4). The by-products such as formaldehyde (CH_2O), methanol (CH_3OH), methyl nitrate (CH_3ONO_2), formic acid (CH_2O_2), methanol (CH_3OH) and nitrous acid (HONO) are formed with marked differences in final concentrations according the case (35 mJ/pulse – 200 Hz or 195 mJ/pulse – 30 Hz).

In the case of 50 Hz-AC excitation, a single experiment using the same gas mixture and the same reactor configuration than previously has been conducted at an energy density of 90 J/L. In this AC discharge mode, the average number of discharge per period is about 52 [16]. Data obtained are presented in Table 1. In these conditions, results show that after plasma processing, the NOx concentration was unchanged and the hydrocarbon removal efficiency was only around 7%. These results could be compared with results obtained at lower energy density as shown in Figure 3 (for example at 30 J/L, 25% of NOx and 40% of C_3H_6 were converted, respectively). The FTIR spectrum given in Figure 5 shows that the partial oxidation of C_3H_6 leads to formation of formaldehyde (CH_2O) and no other by-products are detected. The comparison of these results to those obtained when using a pulsed discharge, confirmed that the energy deposition method is one of the

Table 1. Emission data obtained with 50 Hz-sinusoidal DBD in gas mixture containing 10% O_2, 500 ppm NO, 500 ppm C_3H_6 and N_2 as a balance (energy density deposition = 90 J/L).

	Species Concentration (ppm)					
	NO	NO_2	NOx	CO	CO_2	C_3H_6
Plasma OFF	533 ± 27	26 ± 5	559 ± 28	6 ± 5	2 ± 2	506 ± 10
Plasma ON	470 ± 24	103 ± 5	574 ± 29	21 ± 5	7 ± 2	473 ± 10

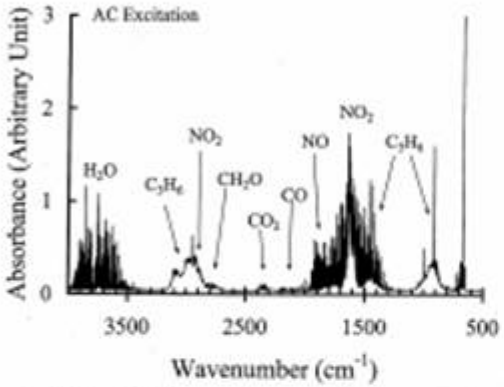

Fig. 5. Typical FTIR spectrum of the by-products from 50 Hz AC plasma at 90 J/L input energy density (10% O_2, 500 ppm NO, 500 ppm C_3H_6 and N_2 as balance).

main factors which control the plasma chemical processes including the nature of by-products and the efficiency of the NOx removal processes.

4 Summary

In summary, we have observed that the input energy density is not the only relevant parameter when comparing the performance of the plasma reactor using different plasma discharge conditions. The main parameter which controls the efficiency of the plasma processing is how the energy is deposited into the plasma. In a given reactor, different results on efficiencies and nature of by-products can be obtained if the experiments are performed under different discharge conditions. The best results on NOx and hydrocarbon removal efficiencies have been obtained when using a pulsed DBD reactor at low energy per pulse and high repetition rate regime, instead of sinusoidal one at the same equivalent energy density. In the case, the optimization of these two parameters (energy/pulse and frequency) leads to lowering the energy cost of NOx conversion.

References

1. S. Masuda, H. Nakso, IEEE T. Ind. Appl. **26**, 374 (1990)
2. S.K. Dhali, I. Sardja, J. Appl. Phys. **69**, 6319 (1991)
3. B.M. Penetrante, M.C. Hsiao, J.N. Bardsley, B.T. Merrit, G.E. Vogtlin, P.H. Wallman, A. Kuthi, C.P. Burkhart, J.R. Bayless, Pure Appl. Chem. **68**, 1083 (1996)
4. D. Evans, L.A. Rosocha, G.K. Anderson, J.J. Coogan, M.J. Kushner, J. Appl. Phys. **74**, 5378 (1993)
5. *Non-thermal Plasma Techniques for Pollution Control*, edited by B.M. Penetrante, S.E. Schultheis (Springer-Verlag, New York, 1993), Part A and B
6. N.W. Frank, Radiat. Phys. Chem. **45**, 989 (1995)
7. *Plasma Exhaust Aftertreatment* (SAE Special Publication SP 1395), edited by J. Hoard, H. Servati (Society of automotive Engineers, Warrendale, 1998)
8. *Non-Thermal Plasma for Exhaust Emission Control* (SAE Special Publication SP 1483), edited by M.L. Balmer, G. Fisher, J. Hoard (Society of automotive Engineers, Warrendale, 1999)
9. *Non-Thermal Plasma* (SAE Special Publication SP 1566), edited M.L. Balmer, G. Fisher, J. Hoard (Society of automotive Engineers, Warrendale, 2000)
10. C.R. Mc Larnon, B.M. Penetrante, SAE Technical Paper Series No. 982434 (1998)
11. A. Khacef, J.M. Cormier, J.M. Pouvesle, J. Phys. D Appl. Phys. **35**, 1491 (2002)
12. A. Khacef, R. Viladrosa, C. Cachoncinlle, E. Robert, J.M. Pouvesle, Rev. Sci. Instrum. **68**, 2292 (1997)
13. A. Khacef, J.M. Cormier, J.M. Pouvesle, J. Adv. Oxid. Technol. **8**, 150 (2005)
14. R. Dorai, M.J. Kushner, J. Phys. D Appl. Phys. **34**, 574 (2001)
15. A.C. Gentile, M.J. Kushner, J. Appl. Phys. **78**, 2074 (1995)
16. O. Martinle, Ph.D. Thesis, Orléans University, France, 2000

ELSEVIER

Chemical Engineering Journal 116 (2006) 13–18

Chemical Engineering Journal

www.elsevier.com/locate/cej

Hydrogen enrichment of a methane–air mixture by atmospheric pressure plasma for vehicle applications

E. El Ahmar*, C. Met, O. Aubry, A. Khacef, J.M. Cormier

GREMI-Polytech'Orléans, 14 rue d'Issoudun, B.P. 6744, 45067 Orléans, Cedex 2, France

Received 19 July 2005; received in revised form 13 October 2005; accepted 14 October 2005

Abstract

During the last few years, the control of motor vehicles pollution has generated considerable research oriented towards the efficiency and the yield of the combustion techniques. A relatively new technology based on the plasma treatment of inlet gases appears to improve the operating conditions of internal combustion engines. The primary focus of this technique is the transformation of methane–air mixture into hydrogen-rich gas before the admission in the cylinder of the vehicle engine.

This work describes an experimental investigation in CH_4–air mixture using a 20 kHz sliding discharge plasma reactor at atmospheric pressure. After plasma treatment, the major gaseous: H_2, CH_4, CO, CO_2 and H_2O were analyzed and quantified using a micro-gas chromatograph (μGC) and Fourier transform infrared absorption spectrometer (FTIR). Plasma treatment results show H_2 enrichment in the range of 4–10% of the inlet gas mixture.

The next step of this preliminary laboratory study will be the engine test bench.

Keywords: Non-thermal plasma; Combustion; Sliding discharges

1. Introduction

Among the existing pollution sources, motor vehicles are seen as a major contributor to air pollution by nitrogen oxides (NO_x), carbon oxides (CO and CO_2), unburned hydrocarbons (UHC) and fine particles matter (PM). The more and more constraining environmental regulations have motivated investigations for decreasing the fuel consumption and reduce drastically pollutant emissions. These objectives require the improvement of the combustion processes and a better understanding of ignition and combustion chemistry.

Thermal plasmas have been applied to combustion over the past three decades with success, particularly in the conversion of fuel–air mixtures into H_2 and CO in efforts to increase internal combustion engine efficiency and to reduce NO_x emissions [1,2].

Non-equilibrium plasmas created by electrical discharge are potentially useful for promoting combustion. In such plasma, the formation of reactive species eventually accelerates the chemical conversions and the reforming reactions. The result is the production of H_2-rich mixture. A broad range of hydrocarbons can be treated by this way. Plasma treatment may favor partial oxidation by reducing the production of soot. The on-board production of hydrogen could thus favor the ignition of combustion in lean burn engines [1–4]. Hydrogen significantly increases the flame propagation rate flame and enlarges the possibilities of using lean-burn mixtures by avoiding misfiring. This approach seems particularly attractive for gasoline and natural gas engines since a small quantity of hydrogen could enable correct operation in the case of lean-burn mixtures.

The objective of the present work is to evaluate the plasma treatment of air–fuel mixture applied to internal combustion engines. Preliminary results obtained in a laboratory scale reactor operating at conditions close to those of thermal engines are presented. These results show the possibilities to obtain an H_2-rich mixture from CH_4–air mixture.

2. Experimental setup

A sliding discharge reactor operates according to the principle of "Glidarc" discharge previously studied in GREMI laboratory for several types of applications [5–10]. The construction of the reactor was simplified in order to rapidly assess the reactor

* Corresponding author. Tel.: +33 2 38 49 46 00; fax: +33 2 38 41 71 54.
E-mail address: elise.el-ahmar@univ-orleans.fr (E. El Ahmar).

1385-8947/$ – see front matter © 2005 Elsevier B.V. All rights reserved.
doi:10.1016/j.cej.2005.10.005

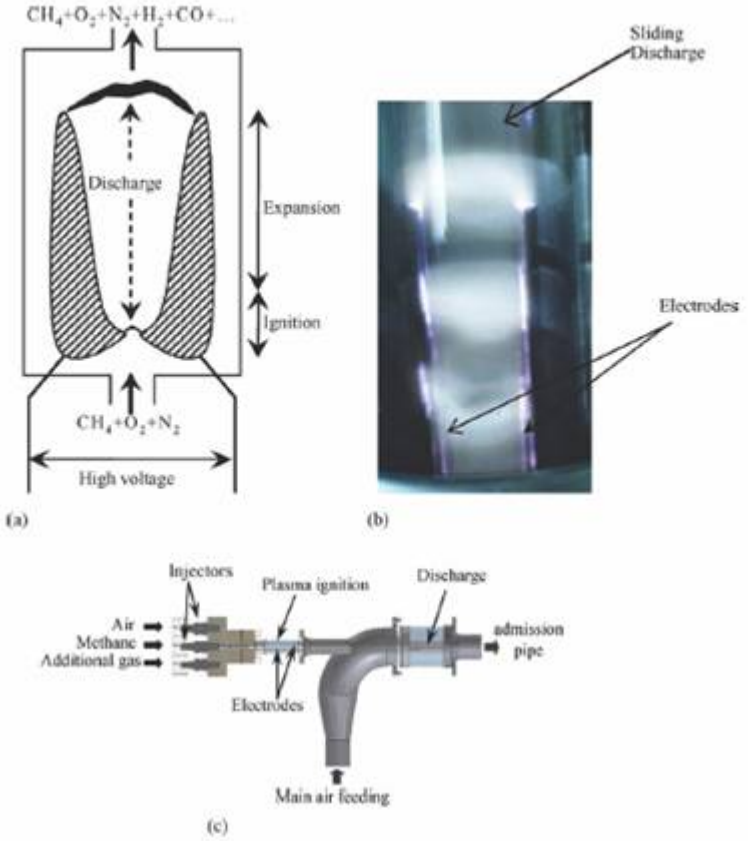

Fig. 1. Experimental reactor. (a) Schematic of sliding discharge, (b) photography of sliding discharge and (c) motor bench reactor.

possibilities for the planned application. The reactor consists of a quartz tube (length, 300 mm; inner diameter, 22 mm) in which two parallel electrodes are laid out. The electrode gap is about 1 mm near the gas mixture injector (ignition; Fig. 1a) in order to ignite the discharge. The plasma column thus created is carried along the electrodes and is elongated at their extremities before being extinguished, giving rise to a new discharge in the ignition space [11–14]. The phenomenon is periodic and the lifetime of a discharge decreases with increasing the gas flow rate.

Fig. 1a and b shows the schematic of the sliding discharge device and photography of the reactor in operation, respectively. Fig. 1c presents a schematic of the test motor bench reactor.

The power supply operating conditions must be flexible in order to allow a synchronization between the discharge and the admission of gases in the engine combustion chamber. According to the engine regime, the plasma treatment duration must be regulated. At a speed of 2000 rounds per minute, this duration is approximately 15 ms. This power supply consists of a symmetric square waveform voltage with a step-up transformer. The discharge is directly connected to the secondary coil of the transformer. Because of leakage fluxes, discharge current waveform is determined by the primary voltage, reactance and resistance of winding.

Voltages and currents were measured with an ST500 probe connected to a voltage divider (ratio, 0.01) and a Hall effect probe Tektronix TCP 202, respectively. The signals from the probes were recorded on a Tektronix TDS 460A digital oscilloscope and processed in a PC.

On Fig. 2, typical voltage and current are plotted with a phase angle of 180° in order to clarify the presentation (real phase angle is 0°). The voltage and current oscillations over the mean waveform are typical of backbreakdown phenomenon [15]. Backbreakdown number is a function of the gas velocity and it is about 13 per cycle in our experiments. The electrical power is calculated from voltage–current recordings and deter-

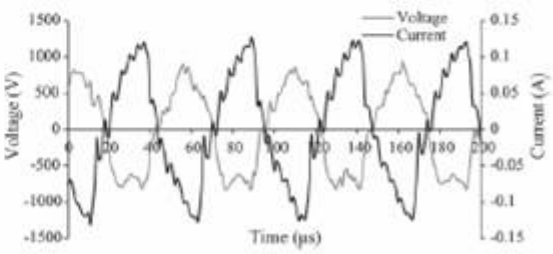

Fig. 2. Current and voltage with CH_4 (19%)–air.

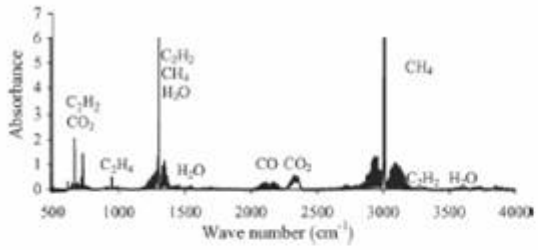

Fig. 3. Typical IR spectrum (CH_4 (19%)–air, electrical power = 50 W).

mined by averaging the instantaneous power over two sliding periods.

The experiments were conducted at atmospheric pressure and room temperature. Air–methane experiments were carried out with methane concentrations higher than the upper explosive limit (15%) [16], i.e. ranging from 16 to 35%. Mixtures with higher CH_4 concentration had been not studied because of carbon deposition phenomena.

After plasma treatment, the output gases were taken over and cooled down in order to eliminate water. Dry output gases (O_2, N_2, H_2, CH_4, CO and CO_2) were analyzed and quantified with Fourier transform infrared spectroscopy (FTIR, Nicolet Magna 550, equipped with a heated 10 m multiple pass absorption cell) and micro gas chromatography (μGC, Varian CP2003P) [16,17]. The H_2O concentration was estimated by considering material balance.

The mean exhaust gas temperature was measured by thermocouples (type K) placed at the outlet of the plasma reactor.

3. Experimental results and discussion

Analyses of formed species were carried out for two series of experimental conditions:

(i) input electrical power varying from 35 to 75 W while CH_4 and air concentrations remain constant;
(ii) CH_4 concentration varying from 16 to 35% while electrical power and air flow rate remain constant.

The major products observed by FTIR spectroscopy were CO, CO_2 and H_2O and the by-products were C_2H_2, C_2H_4 and C_2H_6. A typical IR spectrum is shown in Fig. 3.

3.1. Electrical power effect on CH_4 conversion and H_2 production

Since the device implanted in a thermal engine must be a low energy consumer, we arbitrarily set the electrical power used in these preliminary experiments at several tens of watts (35–75 W).

An example of the mole fractions variation for different species observed after the CH_4 (19%)–air plasma processing as a function of the electrical power are shown in Fig. 4 (symbols). For the maximal power (75 W), CH_4 conversion is about 58% and H_2 production is about 9%. One can note that the changes in CH_4 conversion and H_2 production are not linear since for a power of 35 W, the CH_4 conversion rate is about 13% and H_2 production is 2.5%. The CH_4 conversion and the H_2 production are increasing functions of power supplied to the plasma.

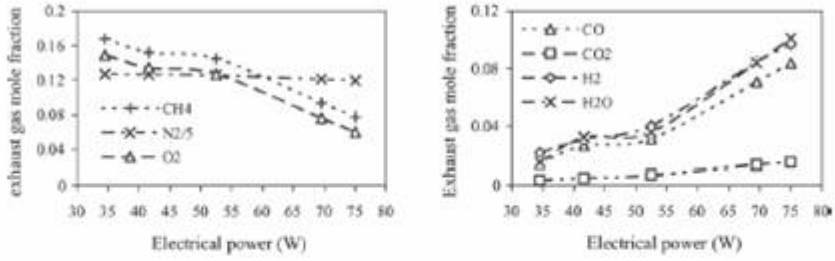

Fig. 4. Experimental (symbols) and adjusted (dashed lines) exhaust gas composition as a function of electrical power (total flow rate = 41 l/min) (CH_4, N_2, O_2, H_2, CO and CO_2 are expressed in dry basis, H_2O is estimated).

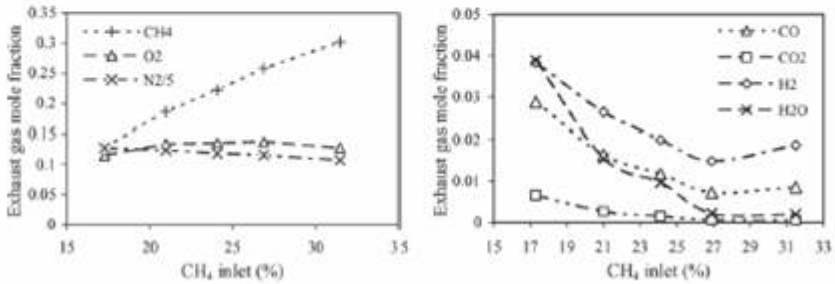

Fig. 5. Experimental (symbols) and adjusted (dashed lines) exhaust gas composition as a function of CH_4 inlet (air flow rate = 33 l/min and electrical power = 50 W) (CH_4, N_2, O_2, H_2, CO and CO_2 are expressed in dry basis, H_2O is estimated).

3.2. Initial CH_4 mole fraction effect on CH_4 conversion and H_2 production

The mole fractions variation for different species observed after CH_4–air plasma processing as a function of initial CH_4 mole fractions are shown in Fig. 5 (symbols). In these experiments the air flow rate and the electrical power were maintained constant at 33 l/min and 50 W, respectively. H_2O, H_2, CO and CO_2 concentrations increase with decreasing the initial CH_4 concentration. H_2O production indicates that a combustion process has been ignited.

4. Three reactions model

The above results show that H_2 enrichment causes a significant CH_4 consumption, a part of which is totally oxidized. The calorific capacity of the combustible mixture is thus considerably modified, explaining the necessity to present an energy balance study in order to discuss the efficiency of the method.

Taking into account the chemical results presented in paragraph 3, a set of three chemical reactions is used to compare the electrical power consumed in the system with the chemical energy exchanged per unit of time.

$$CH_4 + 2O_2 \rightarrow CO_2 + 2H_2O, \quad \Delta H_1 = -802.34\,\text{kJ/mol} \quad (1)$$

$$CH_4 + 1/2O_2 \rightarrow CO + 2H_2, \quad \Delta H_2 = -35.72\,\text{kJ/mol} \quad (2)$$

$$CH_4 + 3/2O_2 \rightarrow CO + 2H_2O, \quad \Delta H_3 = -519.36\,\text{kJ/mol} \quad (3)$$

The change in the composition of the outlet gas mixture can be expressed in terms of progress variables, which represent the proportion of limiting reagent (CH_4) transformed in the reaction. We defined α, β and γ as the progress variables of reactions 1, 2 and 3, respectively. Each chemical species concentration can thus be expressed as a function of α, β and γ.

The α, β and γ coefficients was calculated from the experimental data and the calculated mole fraction using the least square method. The validity of the description using these three coefficients (also called fitting model) is shown by the following results.

4.1. Electrical power effect

Fig. 6 shows the progress variables as a function of the input electrical power. From this data, CH_4 partial oxidation (reaction 2) seems to be the predominant reaction. The coefficients α, β and γ increase with increasing the electrical power. For the lower power used in these experiments (34 W), values of α, β and γ values reach their minima. The validity of the description using progress variables is shown in Fig. 4, where experimental results (symbols) are compared to fitting model (dashed lines).

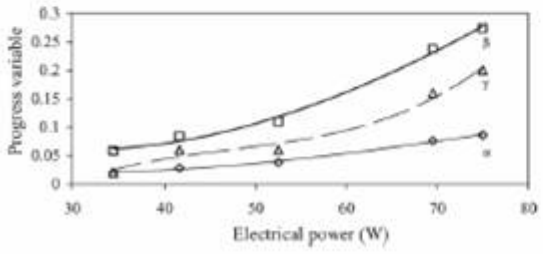

Fig. 6. Progress variables as function of electrical power (total flow rate = 41 l/min).

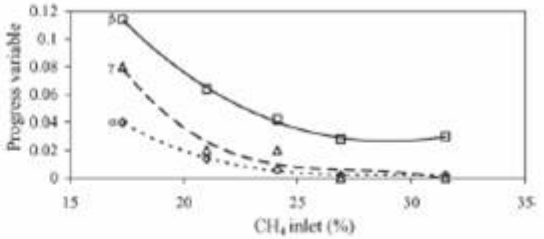

Fig. 7. Progress variables as function of CH_4 inlet (air flow rate = 33 l/min and electrical power = 50 W).

4.2. Initial CH_4 mole fraction effect

Fig. 7 shows the progress variables as a function of the initial CH_4 concentration. As mentioned in the previous paragraph, the data of Fig. 7 shows that CH_4 partial oxidation is the predominant reaction. O_2 consumption increases considerably in the depleted mixtures since the N_2/O_2 ratio increases from 4.2 to 5.5 for the most depleted mixture. Probably an O_2 proportion reacts with CH_4 to form H_2 and CO.

The α and γ values approach zero when CH_4 concentration reaches 30%. The decrease of coefficient β is also significant. These three progress variables reach their maximal values for the minimal CH_4 composition. In that case, the CH_4 consumption is maximal.

The experimental mole fractions of outlet gases were compared to those calculated from the progress variables. Results are given in Fig. 5 (experimental results, symbol; fitting model, dashed lines) and shows that the simplified three chemical reactions correctly describe the process.

5. Absorbed power and physical characterization

5.1. Exhaust gas temperature

The discharge produces a heating of the system. The heating is supplied from two main sources: (i) the electrical energy furnished to the plasma by Joule effect and (ii) the energy supplied by exothermal reactions ignited by the plasma. The exhaust gas temperature was measured using thermocouple placed at 6 cm from the discharge.

Fig. 8 shows the exhaust gas temperature as a function of the initial CH_4 mole fraction. The outlet gas temperature decreases with increasing the initial CH_4 mole fraction. The maximum gas temperature was observed for a CH_4 concentration of about 17%, which corresponds to a strong reactivity of the system. This rise in exhaust gas temperature, which increases when one

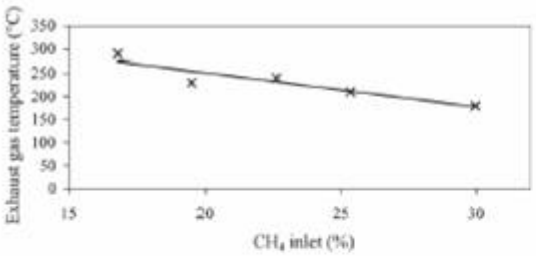

Fig. 8. Outlet reactor gas temperature as a function of CH_4 (air flow rate = 33 l/min and electrical power = 50 W).

approaches the high explosive limit, is probably related to the starting of the combustion process.

5.2. Energy balance

The energy balance of the system is presented by introducing the different power contributions:

(i) P_e, electrical power determined from current–voltage waveforms;

(ii) P_c, power generated by the chemical reactions (in standard conditions) calculated from α, β and γ, as a function of standard enthalpy ΔH^0 (kJ/mol) and CH_4 flow rate D (mol/s);

$$P_c = \Delta H^0 D \quad (4)$$

where the standard enthalpy ΔH is given by:

$$\Delta H^0 = \alpha \Delta H_1 + \beta \Delta H_2^0 + \gamma \Delta H_3 \quad (5)$$

(iii) P_p, power lost by heating products, calculated from α, β and γ, as a function of enthalpy ΔH (kJ/mol) and of the methane flow-rate D (mol/s).

$$\Delta H = \alpha C_{p1} \Delta T + \beta C_{p2} \Delta T + \gamma C_{p3} \Delta T \quad (6)$$

where C_{pi} and ΔT are the calorific capacity of each species and temperature variation between initial and final states, respectively.

$$P_p = \Delta H D \quad (7)$$

P_c and P_p are decreasing functions of the initial CH_4 mole fraction (Fig. 9). By adding P_c and P_e, we obtain the total power

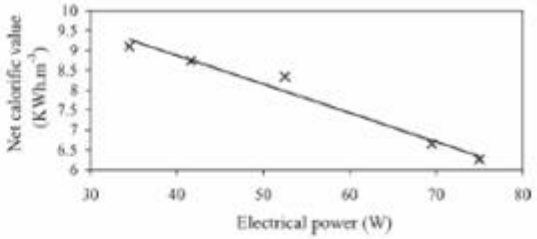

Fig. 10. Net calorific value of CH_4–H_2 mixture as a function of electrical power (total flow rate = 41 l/min).

furnished to the system (P_t). Taking into account a perfect energy balance, this power (P_t) must correspond to the sum of the heating products power P_p and the power loss in the reactor (P_l). Then, the power loss in the reactor (P_l) is derived from the following relation:

$$P_l = P_e + P_c - P_p \quad (8)$$

Fig. 9 shows that the power generated by the chemical reactions (P_c) is higher than the electrical one (P_e) for CH_4 concentration lower than 23.5%. Also, it is shown that the power losses (P_l) and the one used for heating the products (P_p) have the same order of magnitude.

5.3. Calorific value of the outlet mixture (CH_4–H_2)

The mixture net calorific value (C_m) is calculated from the relation:

$$C_m = \sum (X_i C) \quad (9)$$

where X_i and C are the mole fraction and the net calorific value of each component, respectively.

The net calorific values of H_2 and CH_4 are 2.98 and 9.95 kWh/m^3, respectively. The net calorific value of the outlet CH_4–H_2 mixture was calculated and results are presented as a function of electrical power (Fig. 10). C_m is a decreasing function of the electrical power provided to plasma. Indeed, as previously announced, the CH_4 to H_2 conversion efficiency is as high as the electrical power provided to plasma is high. The weakest C_m value (6.25 kWh/m^3) was obtained for the maximum power (75 W in that study). This result shows that the H_2 enrichment generates fuel mixtures releasing less energy (C_m value) than methane (C value).

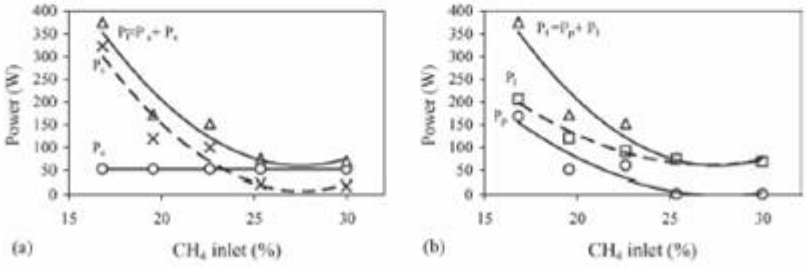

Fig. 9. Various powers as function of CH_4 inlet (air flow rate = 33 l/min and electrical power = 50 W). (a) Total input power and (b) total output power.

6. Conclusion

The treatment of methane–air mixture by plasma at atmospheric pressure, as well as the chemical analysis of the gas products, was carried out. Only, the major products: H_2, CO, CO_2 and H_2O were presented. The hydrogen mole fraction in outlet gas is about 9% for an electric power supplied of 75 W. The reduction of the net calorific value shows that the only interest would be to support the ignition of combustion and the emission reduction.

More work is needed in order to enhance the H_2 concentration produced as well as the energy efficiency. Beside the optimization of the discharge parameters, experiments on the motor bench are envisaged soon.

Acknowledgment

This work was performed within the framework of the French energy program "improvement of the combustion techniques". The authors are grateful to CNRS and to the Ministère de la recherche for their financial support.

References

[1] L. Bromberg, D.R. Cohn, A. Rabinovich, J.E. Surma, J. Virden, Int. J. Hydrogen Energy 24 (1999) 341–350.
[2] L. Bromberg, D.R. Cohn, A. Rabinovich, J. Heywood, Int. J. Hydrogen Energy 26 (2001) 1115–1121.
[3] R. Breashers, H. Cotrill, J. Rupe, First Symposium on Low Pollution Power Systems Development, Ann Arbor SEMI, 1973.
[4] D.R. Cohn, A. Rabinovich, C.H. Titus, L. Bromberg, Int. J. Hydrogen Energy 22 (1997) 715–723.
[5] F. Richard, J.M. Cormier, S. Pellerin, J. Chapelle, J. Appl. Phys. 79 (1996) 2245–2250.
[6] F. Richard, J.M. Cormier, S. Pellerin, J. Chapelle, J. High Temp. Mater. Process. 2 (1997) 239–248.
[7] F. Richard, J.M. Cormier, S. Pellerin, V. Dalaine, J. Chapelle, Prog. Plasma Process. Mater. (1997) 343–351.
[8] V. Dalaine, J.M. Cormier, P. Lefaucheux, J. Appl. Phys. 83 (1998) 2435–2441.
[9] I. Rusu, J.M. Cormier, Chem. Eng. J. 91 (2003) 23–31.
[10] I. Rusu, J.M. Cormier, Int. J. Hydrogen Energy 28 (2003) 1039–1043.
[11] E. Hnatiuc, V. Dalaine, J.M. Cormier, S. Pellerin, Proceedings of the 6th International Conference on Optimisation of Electrical and Electronic Equipments, OPTIM, 1998.
[12] S. Pellerin, J.M. Cormier, F. Richard, K. Musiol, J. Chapelle, J. Phys. D: Appl. Phys. 32 (1999) 891–897.
[13] S. Pellerin, F. Richard, J. Chapelle, J.M. Cormier, K. Musiol, J. Phys. D: Appl. Phys. 33 (2000) 2407–2419.
[14] A. Kaminska, J.M. Cormier, S. Pellerin, O. Martinie, J. High Temp. Mater. Process. 5 (2001).
[15] S. Pellerin, O. Martinie, J.M. Cormier, J. Chapelle, P. Lefaucheux, J. High Temp. Mater. Process. 3 (2) (2001) 167–180.
[16] C. Met, A. Khacef, J.M. Cormier, Proceedings of the 4th International Symposium of Non-Thermal Plasma Technology for Pollution Control and Sustainable Energy Development, 2004.
[17] C. Met, O. Aubry, A. Khacef, J.M. Cormier, Proceedings of the 9th International Symposium on High Pressure, Low Temperature Plasma Chemistry, 2004.

Non Thermal Plasma NOx Remediation: From Binary Gas Mixture to Lean-Burn Gasoline and Diesel Engine Exhaust

A. Khacef*, J. M. Cormier, and J. M. Pouvesle

GREMI, CNRS-Polytech'Orléans, 14 rue d'Issoudun, B.P. 6744, 45067 Orléans Cedex 2, France

Abstract: Experiments are presented on the plasma removal of NOx (sum of NO and NO_2 concentrations) and hydrocarbons in atmospheric pressure gas streams by sub-microsecond pulsed dielectric barrier discharge processing. This investigation presents the effects of electrical input energy, hydrocarbon addition, and water addition on the NOx chemistry and by-products formation. Exhaust gas mixtures with composition containing up to seven gases (CO, CO_2, NO, O_2, H_2O, C_3H_6, N_2) were synthesized. The objective is to use synthetic gas exhaust simulating diesel and Lean Burn gasoline engine exhaust with propene as a reductant agent. It was established that the observed chemistry in the plasma includes conversion of NO to NO_2 as well as the partial oxidation of hydrocarbon. In a given reactor under identical gas composition and equivalent energy density deposition, experimental results show that the main parameter which controls the efficiency of the plasma process is the energy deposition mode. The best results on NOx and hydrocarbon removal efficiencies have been obtained at low input energy per pulse and high discharge frequency. NOx removal improves with increasing input energy deposition and the presence of water in the gas mixture appears to essentially enhance the chemistry process efficiency, reducing by this way the energy cost of the processes. For example, for an input energy density of 27 J/L, the fraction of NOx removed was about 60% with an energy cost less than 30 eV/molecule in the case of simulated diesel engine exhaust. The data obtained suggest that aldehydes (CH_2O and CH_3CHO) are formed in concert with NO oxidation to NO_2 in the plasma phase. Methyl nitrate (CH_3ONO_2) and nitromethane (CH_3NO_2) are the main R-NOx compounds produced and small amounts of nitrous acid (HNO_2) and formic acid (CH_2O_2) were also detected.

Introduction

Among the existing pollution sources, motor vehicles are seen as a major contributor to air pollution by nitrogen oxides (NOx), unburned hydrocarbons (UHC), and fine particulate matter (PM). The relatively new methods being widely investigated for cleaning exhaust gases are based on non-thermal plasma (NTP) processing. Many applications of NTP have been developed for plasma-processing chemistry and pollution control applications (*1-5*). In the automotive domain, the primary focus of plasma after-treatment studies has been upon the removal of NOx and sulfur oxides (SOx), and treatments for diesel and gasoline engine exhausts under lean conditions have been proposed (*6-9*). Further works on plasma chemical reaction kinetics have been carried out. For example, pulsed corona kinetics has been carried out by Lowke and Morrow (*10*) for NOx and SOx removal, and pulsed barrier discharge modeling of formation and destruction of NO has been performed by Heron (*11*).

NTP that has a low gas temperature and a high electron temperature can be produced by a variety of methods (pulsed corona discharge, barrier discharge, dc discharge, electron beam irradiation) (*12-14*). Pulsed corona and dielectric barrier discharge (DBD) techniques are two of the more commonly used methods for producing electrical discharge plasmas. Regarding their intrinsic properties DBDs appear very well adapted to treat large gas quantities with relatively low energy cost. In these plasmas, the chemistry is initiated by high-energy free electrons. These electrons form N, O, OH and other radicals through molecular electron-impact dissociation. These radicals are the active species of the plasma that eventually lead to the chemical conversion of NOx. Due to the presence of H_2O and O_2, plasma processing of NOx is dominantly oxidative resulting primarily in NO_2 and acids (HNO_2, HNO_3). Also, hydrocarbons in exhausts have been found to play an important role in the NOx removal processes (*6, 8, 15-19*).

This paper will present the results of an extensive series of experiments aimed towards understanding the effect of gas composition on the NOx conversion chemistry in plasma.

Experiments have been conducted in synthetic exhaust gas mixtures prepared from N_2, O_2, NO, CO, CO_2, H_2O, and C_3H_6 at temperatures ranging

*Corresponding author;
E-mail Address: ahmed.khacef@univ-orleans.fr

ISSN 1203-8407

from 20 °C to 300 °C using a sub-microsecond pulsed DBD. The goal is to reach synthetic gas exhaust simulating diesel (12% O_2, 10% CO_2, 10% H_2O, 500 ppm CO, 10% CO_2, 300 ppm NO, 300 ppm C_3H_6, N_2) and lean burn gasoline engine exhaust (6% O_2, 10% CO_2, 10% H_2O, 3000 ppm CO, 1000 ppm NO, 1000 ppm C_3H_6, N_2). This investigation studies the effects of electrical input energy, hydrocarbon addition, and water addition on the NOx chemistry and by-products formation.

Experimental Arrangement

The experimental apparatus is shown in Figure 1 and consists of a gas manifold, an electric discharge reactor, and gas analyzers.

Synthetic gas mixtures preparing from O_2, N_2, NO, CO, CO_2, H_2O, and C_3H_6 (propene) were prepared in a gas handling system and their composition was controlled with calibrated high-precision mass flow controllers. Water vapor with controlled concentrations was added to the gas mixture using Controlled Evaporator Mixer CEM®. This device can provide a high reproducibility and a very stable vapor flow. After mixing in the manifold, the gas then passes through a temperature controlled line which preheats the gas and prevent condensation.

The plasma reactor uses a dielectric-barrier discharge (DBD). The reactor geometry was one of a wire to cylinder type. It consists of a 0.9 mm-diameter tungsten wire in a 16 mm-long quartz tube with inner and outer diameters of 11 mm and 13 mm, respectively. An aluminum foil coating the outside of the dielectric tube form the other electrode. The DBD reactor was placed inside a tubular furnace. The gas mixture temperature can be adjusted from room temperature to 500 °C.

The DBD reactor is driven by a line transformer powered by high-voltage ceramic capacitors disposed in Blumlein-like configuration. This power supply is capable of delivering open circuit voltage up to 150 kV output into 80 ns (FWHM) pulses and short voltage rise time (40 ns). The shapes of pulse voltage and current in the plasma reactor are displayed in Figure 2. The pulse repetition rate is adjustable from single shot regime to 1 kHz. The results presented in this work are obtained at a discharge voltage of about 20 kV and a repetition rate up to 200 Hz.

The discharge pulse energy was measured with a capacitive circuit and the energy density (J/L) is given by the ratio of the power deposited into the gas to the gas flow rate at standard conditions (25 °C and 1 atm). The average electrical power is the product of the discharge pulse energy and the pulse

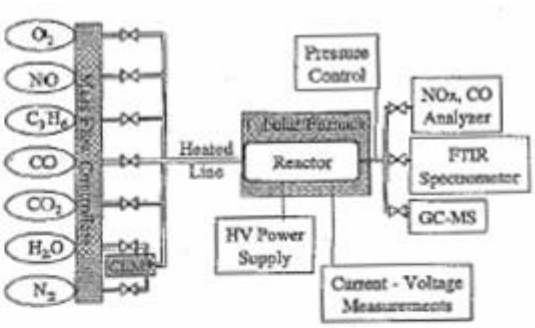

Figure 1. Schematic diagram of the experimental set-up.

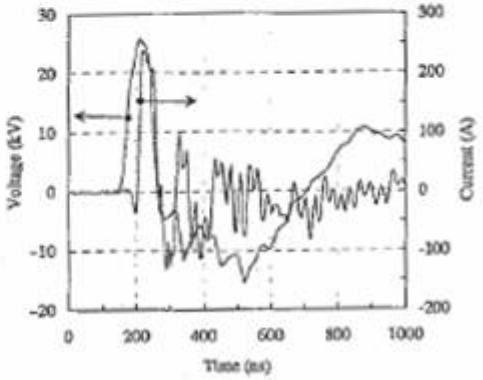

Figure 2. Typical waveforms of pulse voltage and current in the plasma reactor.

frequency. At a given gas flow rate, the input energy density was varied by varying the repetition rate of the high voltage pulses.

The major gaseous components as NO, NO_2, CO, CO_2, and C_3H_6 were analyzed online and quantified using Fourier Transform Infrared Absorption Spectrometer (FTIR) equipped with a heated 10 m-multiple pass absorption cell. An electrochemical NOx analyzer was also used for monitoring continuously NO, NO_2, NOx as well as CO levels in the gas stream. Cold trap (liquid nitrogen) could be inserted in the output line to obtain condensed products. Soluble species were sampled to be further analyzed by Gas Chromatography coupled with Mass Spectrometer (GC-MS) measurements.

Results and Discussion

This Investigation presents the effects of electrical input energy, hydrocarbon addition, and water addition on the NOx chemistry and by-products formation.

Different set of experiments were conducted to investigate gas mixtures with composition more and more complex ($NO-C_3H_6-N_2$, $CO-NO-N_2$, $O_2-NO-C_3H_6-N_2$, $CO-NO-O_2-N_2$, $CO-NO-O_2-C_3H_6-N_2$, ...).

The goal is to reach synthetic gas exhaust simulating diesel and lean burn gasoline engine exhaust based on O_2-CO_2-H_2O-CO-NO-C_3H_6-N_2 mixture. The high value of NO concentration (500 ppm) was used because it represents typical levels in a modern heavy-duty diesel engine.

Figure 3 shows an example of typical FTIR spectra for plasma processing at room temperature and energy deposition of 27 J/l of C_3H_6-N_2 (a), NO-C_3H_6-N_2 (b), and O_2-C_3H_6-NO-N_2 (c). In the case (a), the propene conversion (50% at 53 J/L) leads to the production of hydrogen cyanide (HCN). When 500 ppm of NO were added to N_2-C_3H_6 mixture (case b), oxidation processes take place and NO_2, CO, CO_2, formaldehyde (HCHO) and nitrous oxide (N_2O) were observed. In that case, NO to NO_2 oxidation is very weak (< 5%) and NO could be chemically reduced into nitrogen. The partial oxidation of propene (18%) leads to the production of small amounts of CO (30 ppm), CH_2O (15 ppm) and CO_2 (8 ppm).

When 10% O_2 was added to the NO-C_3H_6-N_2 mixture (case c), NO oxidation results in the formation of NO_2. Under these oxygen rich conditions, a significant fraction of input plasma energy is dissipated in the dissociation of O_2 which become the dominant process because O_2 dissociation is much more efficient than N_2 dissociation in the electron energy range studied. Detailed kinetic schemes and discussions of the mechanisms involved in gas phase chemistry in the plasma processing O_2, NO, N_2, and hydrocarbon mixtures were studied extensively (*6, 15-16*).

At energy deposition of about 27 J/L, measured NO to NO_2 conversion was about 90% and the C_3H_6 conversion rate was around 36.3%. As expected, the plasma partially oxidizes the hydrocarbons to form CH_2O, CH_3OH, CH_3ONO_2, CH_2O_2, and HNO_2. Carbon products could be quantified as follows: 42.4% CH_2O, 36.6% CO, 4.6% CO_2 and 16.4% "others". "Others" represents the by-products like formic acid and methyl nitrate which were not quantified in this study. This data are consistent with previously published results (*17, 20*).

Hydrocarbon Effect

As reported previously (*15-19*), some hydrocarbon additives are required for the promotion of NO to NO_2 conversion. In these investigations, as in some others, the best NOx conversion occurs with C_3H_6 and ethylene (C_2H_4).

Experimental data of Figure 4 shows that the maximum of NO to NO_2 conversion occurs when the

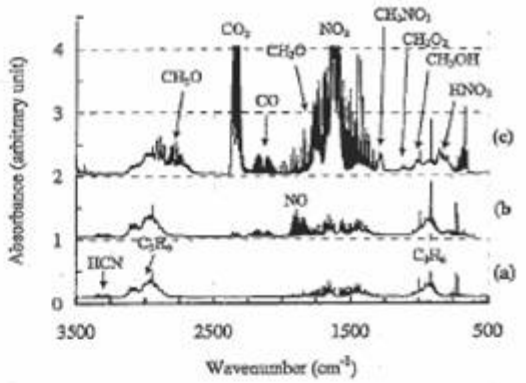

Figure 3. Typical FTIR spectra produced by plasma processing (27 J/L) at room temperature of: (a) C_3H_6 (500 ppm)-N_2. (b) NO (500 ppm)-C_3H_6 (500 ppm)-N_2. (c) O_2 (10%)-NO (500 ppm)-C_3H_6 (500 ppm)-N_2.

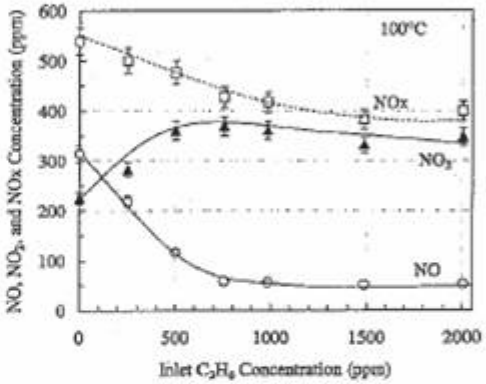

Figure 4. Effect of inlet propene concentration on the conversion of NO to NO_2 in plasma processing of 500 ppm NO, in 94% air and N_2 as balance. T = 100 °C and energy deposition = 44 J/L (195 mJ/pulse - 15 Hz).

gas mixtures contain at least 500 ppm of hydrocarbon. The increase of initial C_3H_6 concentrations above 500 ppm does not influence the NO to NO_2 oxidation as reported in the literature (*15, 19*). This is the reason why the inlet C_3H_6 concentration was fixed at 500 ppm as reported in the following sections.

The NO concentrations as functions of energy density for the cases without propene and with 500 ppm propene are shown in Figure 5 (energy per pulse of 195 mJ and repetition rate of pulses up to 40 Hz). In the absence of hydrocarbons, the oxygen radicals are the responsible for the oxidation of NO to NO_2 and less than 54% of the initial NO is converted to NO_2 even for the highest energy densities (up to 103 J/L). However, NOx (sum of NO and NO_2) removal remains nearly constant. The increase in NO conversion obtained with increasing energy deposition is counteracted by the increase in NO_2

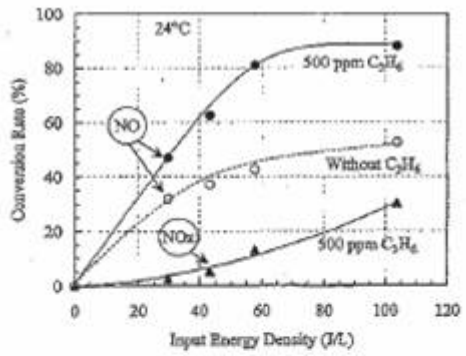

Figure 5. Effect of input energy density on NO and NOx conversion at room temperature. Gas mixture (19.6% O_2, 500 ppm NO, N_2 as balance) without propene and with 500 ppm propene. In the case without propene NOx conversion is 0%. (195 mJ/pulse and pulse repetition rate up to 40 Hz).

concentration resulting in an almost constant NOx level. In that case, the energy cost for NO removal or W-value for NO, calculated from formula given by Puchkarev et al (*21*), is about 42 eV.

When 500 ppm of propene is added to the gas stream the oxidation of NO to NO_2 was enhanced and energy cost for this oxidation lowered. The radical responsible for the oxidation of NO to NO_2 is no longer the O radical. From chemical kinetics analysis, Penetrante et al (*6*) showed that the hydrocarbon acts as a getter of O and OH radicals, with the resulting products reacting with O_2 to yield peroxyl radicals HO_2 which efficiently convert NO to NO_2.

In that case, the W-values obtained for NO are ≈ 25 eV compared to 42 eV for a gas mixture without hydrocarbon. Maximum NOx conversion rate was ≈ 30% and the W-value for NOx was ≈ 165 eV. One can see that the electrical consumption is very high with respect to the fraction of NOx removed. The selection of the gas mixture composition and the electrical conditions could lead to a significantly reduced energy cost of the plasma process in relation with the NOx fractional removed. This aspect is especially important for a future automotive development.

Water Effect

Plasma processing of 500 ppm NO and 500 ppm C_3H_6 in 10% O_2, 10% H_2O and N_2 as balance was performed. The gas flow rate was 16 L/min corresponding to a space velocity of 60 000 h^{-1} and the energy density was less than 30 J/L. In this humid gas mixture, the formation of OH radicals via electron-impact dissociation of H_2O and reaction of H_2O with metastable oxygen atom become important and results in the formation of HNO_2 and HNO_3 by reactions with NO and NO_2. The role of H_2O in the formation of acids becomes more apparent when the H_2O concentration is 5% and above (*22*). When propene is present in the gas mixture, the OH radical becomes the main radical consuming propene. The radical responsible for the oxidation of NO to NO_2 is no longer the O radical. It has been shown from detailed chemical kinetics analysis (*22-23*) that the HO_2 radicals, produced from reactions involving hydrocarbon intermediates of propene oxidation, are the radicals that oxidize NO to NO_2. The HO_2 radical concentration is a function of both the energy density input to the plasma and the hydrocarbon concentration in the gas mixture. The OH radical reacts preferentially with the hydrocarbon, then the oxidation of NO and NO_2 to nitric and nitrous acids is minimized.

Figures 6(a) and 6(b) show the GCMS chromatogram plots of liquid and gaseous phases of the exhaust gas. The products of hydrocarbons processing are those reported commonly in the literature. These products are acetaldehyde (CH_3CHO), propene oxide (C_3H_6O) and a large variety of species such as, formic acid, methyl nitrate, and nitromethane (CH_3NO_2). However, due the strongly oxidative action of hydrocarbon radicals, NO_2, CO, and CO_2 are the main products in that case. Nitromethane was predicted as a major by-product from propene induced NO to NO_2 conversion in the modeling reported by Shin et al (*15*). However, in our knowledge, that specie has never been observed experimentally.

OH radicals produced from water vapor by the plasma play a major role in the NOx removal chemical reactions. NO and NO_2 concentrations as a function of energy deposition in dry and humid (10% H_2O) gas mixture at 260 °C is shown in Figure 7. With increasing energy deposition, the NO conversion and NO_2 formation efficiencies have been improved by adding 10% H_2O in the dry gas mixture.

For example, at 260 °C, the energy deposition of only 7 J/L was required to achieve maximum NO to NO_2 oxidation efficiency (up to 92%). This efficiency rate is only 61% when no water is present in the gas stream. The W-values for humid plasma induced NO removal are dramatically reduced to values scaling from ≈ 15 eV at 27 J/L down to ≈ 4 eV at 7 J/L. These results could be compared with previous data obtained by S. Bröer et al (*24*) in synthetic gas mixture containing a higher O_2 concentration (18%), C_2H_4 instead of C_3H_6 and at higher repetition (1 kHz). These authors found that the maximum NO-removal rate was 92% with a W-value for NO around 100 eV.

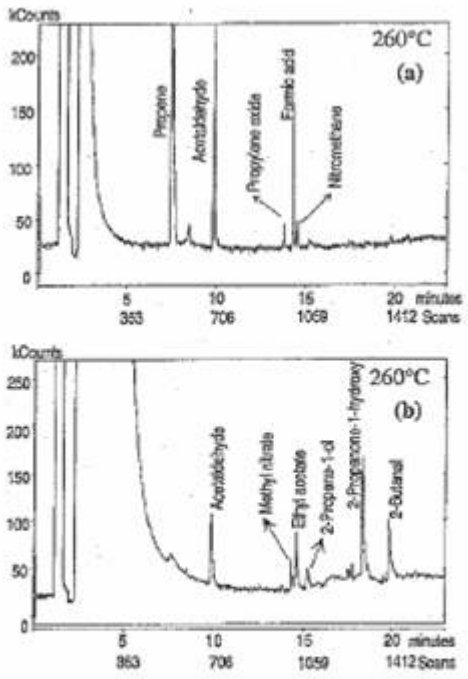

Figure 6. GCMS chromatogram plots of gaseous (a) and liquid (b) phases of the exhaust gas. Plasma processing of 500 ppm NO, 500 ppm C_3H_6, 10% O_2, 10% H_2O and N_2 at 260 °C.

Data of Figure 7 serve to validate the calculations made by Doraï and Kushner (*25*). The computed NO concentrations agree well with the experiments whereas agreement for the case of NO_2 is within 15-20% at 260 °C. At this temperature, the maximum NOx conversion rate (43%) is reached at energy deposition of 27 J/L. The energy cost was reduced by a factor 2.2 in comparison with results obtained in plasma processing without water in the similar experimental conditions. The W-value for NOx calculated in that case was around 30 eV.

Synthetic Diesel and Lean Burn Gasoline Exhaust

Experiments with gas mixtures simulating diesel (12% O_2, 10% CO_2, 10% H_2O, 500 ppm CO, 10% CO_2, 300 ppm NO, 300 ppm C_3H_6, N_2) and lean burn gasoline (6% O_2, 10% CO_2, 10% H_2O, 3000 ppm CO, 1000 ppm NO, 1000 ppm C_3H_6, N_2) engine exhaust were conducted as functions of temperature (150 °C and 300 °C). Figures 8(a) and 8(b) summarize the data obtained at 150 °C and 300 °C in the simulated diesel exhaust. The fraction of NOx removed significantly increases with increasing input energy density. Approximately 50% of the NOx was removed by the DBD discharge at energy density of about 27 J/l.

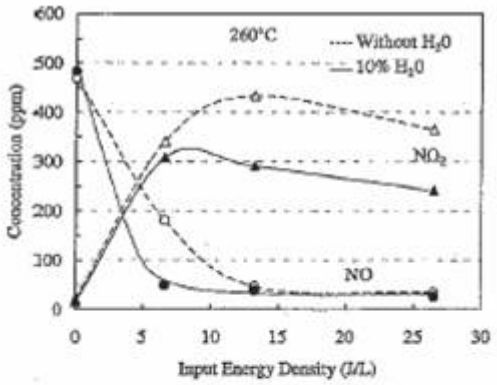

Figure 7. Effect of input energy density on NO conversion at 260 °C. Gas mixture (10% O_2, 500 ppm NO, 500 ppm C_3H_6, balance N_2) without H_2O and with 10% of H_2O. (195 mJ/pulse and pulse repetition rate up to 200 Hz).

The energy costs as a function of NOx-removal rates in simulated diesel engine exhaust at 150 °C and 300 °C are shown in Figure 9. This figure illustrates how the important parameters - the fraction of NOx removed and energy cost per removed molecule - are strongly correlated. At high temperature (300 °C), the energy cost increase rapidly with NOx-removal. It appears that the plasma processing of diesel exhaust is much more efficient at low temperature. At 150 °C around 60% of NOx are removed at an energy cost of only 24 eV/molecule.

Energy Deposition Effect

Many papers in the plasma processing literature present the fraction of NOx removed as a function of parameters such as the input energy density, the residence time of the gas in the reactor, or the applied voltage to the plasma reactor (*26-28*). The composition of the output gaseous components was recorded as a function of energy density which is the parameter commonly used to evaluate the NOx conversion efficiency in the plasma. However, if this parameter is important to characterize the electrical energy consumption of the process we should take into account how the energy is deposited into the plasma. In a given reactor and at an equivalent energy density, different results on efficiencies and nature of by-products can be obtained if the experiments are performed under different discharge conditions. In the case of pulsed DBD, we will show that the energy per pulse deposition combined with the voltage repetition frequency is the main control parameter that should be used.

In order to show the importance of the energy deposition into the plasma on the chemistry processes, experiments in gas mixtures containing O_2,

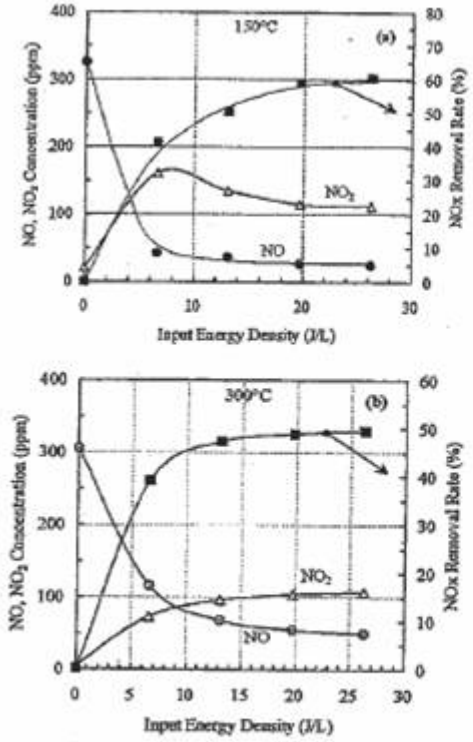

Figure 8. NO, NO_2 concentrations and NOx removal rate as a function of input energy density in plasma processing of simulated diesel exhaust at (a) 150 °C and (b) 300 °C. (195 mJ/pulse and pulse repetition rate up to 200 Hz).

NO, C_3H_5 and N_2 as balance at room temperature using a sub-microsecond pulsed DBD were conducted. While keeping the energy density constant, two discharge regimes were investigated:

(i) low energy per pulse and high repetition rate, and

(ii) high energy per pulse and low repetition rate.

Experiments were conducted in O_2 rich mixtures (10% and 20% O_2) and different space velocities (15 000 h^{-1} and 60 000 h^{-1}).

NO concentration and C_3H_6 conversion rate plotted as a function of the energy density for two different discharge pulse energies (35 mJ/pulse and 195 mJ/pulse) are shown in Figure 10. From these data at a given energy density (J/L), NO and C_3H_6 conversion efficiencies were greatly improved by plasma processing at low energy per pulse and in the high repetition rate regime. For example, plasma processing at about 27 J/L (35 mJ/pulse and 200 Hz) shows that more than 90% of NO molecules and 36% of C_3H_6 molecules were converted, respectively. Those conversions are only around 29% and 15%, respectively, for 195 mJ/pulse and 30 Hz case.

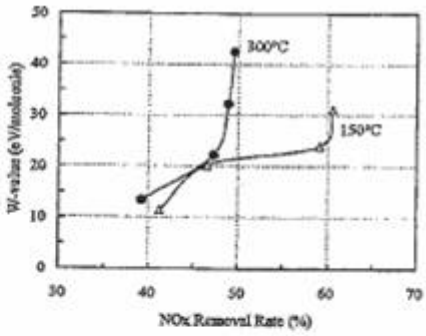

Figure 9. Energy cost as function of NOx removal rate in plasma processing of simulated diesel exhaust at 150 °C and 300 °C.

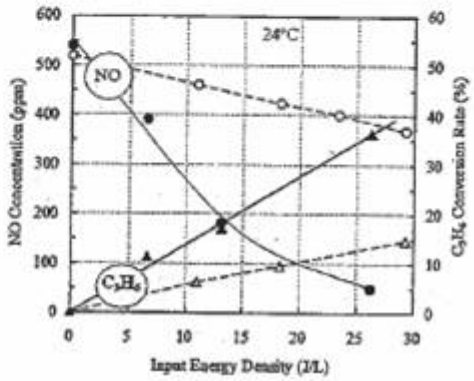

Figure 10. NO concentration and C_3H_6 conversion rate as a function of input energy density in the case of pulsed excitation in gas mixture containing 10% O_2, 500 ppm NO, 500 ppm C_3H_6 and N_2 as balance at room temperature (flow rate = 16 l/min). Solid lines: 35 mJ/pulse and pulse repetition rate up to 200 Hz, Dashed lines: 195 mJ/pulse and pulse repetition rate up to 40 Hz.

It appears from these experimental results that if the energy is deposited in small fractions more often, the energy utilization could be more efficient. The optimization of these two parameters (energy/pulse and frequency) leads to lowering the energy cost of NOx conversion which is one of the determinant parameters in pollution control processes. The energy cost of one removed toxic molecule or W-value (eV/molecule) mainly depends on the efficiency of the energy transfer from the power source to the plasma reactor, configuration of electrodes, and efficiency of chemical reactions (*21*).

As expected, under these oxygen rich conditions, in addition of the main products of the plasma (NO_2, CO, and CO_2), the plasma partially oxidizes the hydrocarbons. Formaldehyde (CH_2O), methanol (CH_3OH), methyl nitrate (CH_3ONO_2), formic acid (CH_2O_2), methanol (CH_3OH) and nitrous acid (HONO) are formed with marked differences in final

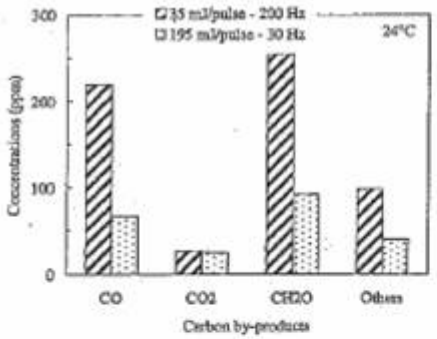

Figure 11. Carbon by-products concentrations obtained in plasma processing at 27 J/L of gas mixture (10% O_2, 500 ppm NO, 500 ppm C_3H_6 and N_2 as balance) at room temperature in the cases of 35 mJ/pulse - 200 Hz and 195 mJ/pulse - 30 Hz. "others" represents the by-products like formic acid (CH_2O_2) and methyl nitrate (CH_3NO_3) which were not quantified in that study.

concentrations in the two cases (35 mJ/pulse - 200 Hz and 195 mJ/pulse - 30 Hz). Figure 11 presents an example of data of carbon products CO, CO_2, CH_2O, and "others" identified by-products (CH_2O_2, CH_3NO_3) obtained at input energy deposition of 27 J/L for the two operation modes.

In the case of 50 Hz-sinusoidal excitation in the same reactor configuration and gas mixture, the NOx concentration was unchanged and the fraction of hydrocarbon removed was only around 7% (*29*). The partial oxidation of C_3H_6 leads to formation of formaldehyde. The by-products detected in the case of pulsed excitation such as, methyl nitrate, formic acid, and methanol are not observed. These results confirmed that the energy deposition method is one the main factors which control the plasma chemical processes including the nature of by-products. In that case, it affects the fractional removal of NOx and hydrocarbon.

Summary

Experimental results on sub-microsecond pulsed plasma processing of gas mixtures containing up to seven gases (N_2, NO, O_2, C_3H_6, H_2O, CO, and CO_2) have been presented. Results show that the main parameter which controls the efficiency of the plasma process is the energy deposition mode. The lowering of energy cost of NOx conversion was obtained for low input energy per pulse and high discharge repetition rate and could be optimized by these parameters.

It was established that the observed chemistry in the plasma includes conversion of NO to NO_2 as well as the partial oxidation of hydrocarbon. The hydrocarbon added to the gas mixture plays two essential functions in the plasma: first it assists the gas phase oxidation of NO to NO_2 by electric discharge in excess oxygen and, secondly, it lowers the energy cost for this oxidation. Total NOx removal improves with increasing input energy deposition. The presence of water (10%) in the gas mixture appears to essentially enhance the chemistry process efficiency reducing by this way the energy cost of the processes.

Data obtained under rich O_2 conditions suggest that aldehydes (CH_2O and CH_3CHO) are formed in concert with NO oxidation to NO_2 in the plasma phase. Methyl nitrate (CH_3ONO_2) and nitromethane (CH_3NO_2) are the main R-NOx compounds produced and small amounts of nitrous acid (HONO) and formic acid (CH_2O_2) were also detected.

References

(*1*) Vogtlin, F. E.; Penetrante, B. M. In *Non-thermal Plasma Techniques for Pollution Control*, part A, eds.; Springer-Verlag, 1993; pp 187-198.

(*2*) Rosocha, L.A.; Korzekwa, R. A. *J. Adv. Oxid. Technol.* **1999**, *4*, 247-264.

(*3*) Rosocha, L. A.; Korzekwa, R. A. In *Electrical Discharges for Environmental Purposes – Fundamentals and Applications*; E.M. Van Veldhuizen, eds.; Nova Science Publishers, Inc.: Huntington, NY, 2000; pp 245-278.

(*4*) Chang, J. S.; Lawless, P. A.; Yamamoto, T. *IEEE Trans. Plasma Sci.* **1991**, *19*, 1152-1156.

(*5*) Chang, J. S. *Sciences and technology of advanced Materials* **2001**, *2*, 571-576.

(*6*) Penetrante, B. M.; Brusasco, R. M.; Merrit, B. T.; Pitz, W. J.; Vogtlin, F. E.; Kung, M. C.; Kung, H. H.; Wan, C. Z.; Voss, K. E. *SAE Technical Paper Series No. 982508*, 1998; pp 57-66.

(*7*) Hoard, J.; Balmer, M. L. *SAE Technical Paper Series No. 982429*, 1998; pp 13-19.

(*8*) Balmer, M. L.; Tonkin, R.; Yoon, S.; Kolwaite, A.; Barlow, S.; Maupin, G.; Hoard, J. *SAE Technical Paper Series No. 1999-01-3640*, 1999; pp 67-73.

(*9*) Penetrante, B. M.; Brusasco, R. M.; Merrit, B. T.; Pitz, W. J.; Vogtlin, F. E.; *SAE Technical Paper Series No. 1999-01-3637*, 1999; pp 45-50.

(*10*) Lowke, J. J.; Morrow, R. *IEEE Trans. Plasma Sci.* **1995**, *23*, 661-671.

(*11*) Herron, J. T. *Plasma Chem. & Plasma Process* **2001**, *21*, 581-609.

(*12*) Dhali, S. K.; Sardja, I. *J. Appl. Phys.* **1991**, *69* (9), 6319-6324.

(*13*) Evans, D.; Rosocha, L.A.; Anderson, G. K.; Coogan, J. J.; Kushner, M. J. *J. Appl. Phys.* **1993**, *74* (9), 5378-5386.

(*14*) Frank, N. W. *Radiat. Phys. Chem.* **1995**, *45*, 989-1002.

(15) Shin, H. H.; Yoon, W. S. *SAE Technical Paper Series No. 2000-01-2969*, 2000; pp 103-110.

(16) Khacef, A.; Cormier, J. M.; Pouvesle, J. M. *J. Phys. D: Appl. Phys.* **2002**, *35*, 1491-1498.

(17) Dorai, R.; Kushner, M. J. *SAE Technical Paper Series No. 1999-01-3683*, 1999; pp 81-87.

(18) Penetrante, B. M.; Hsiao, M. C.; Bardsley, J. N.; Merritt, B. T.; Vogtlin, G. E.; Wallman, P. H.; Kuthi, A.; Burkhart, C. P.; Bayless, J. R. *Pure & Appl. Chem.* **1996**, *68* (5), 1083-1087.

(19) Filimonova, E. A.; Kim, Y. H; Hong, S. H.; Song, Y. H. *J. Phys. D: Appl. Phys.* **2002**, *35*, 2795-2807.

(20) Park, K. S.; Kim, D. I.; Lee, H. S.; Chun, K. M.; Chun, B. H. *SAE Technical Paper Series No 2001-01-3515*, 2001; pp 59-67.

(21) Puchkarev, V.; Roth, G.; Gundensen, M. *SAE Technical Paper Series No. 982516*, 1998; pp 107-111.

(22) Penetrante, B. M.; McLarno, C. R. *SAE Technical Paper Series No. 982433*, 1998; pp 37-48.

(23) Gentile, A. C.; Kushner, M. J. *J. Appl. Phys.* **1995**, *78* (8), 2074-2085.

(24) Bröer, S.; Hammer, T.; Kishimoto, T. In *Proceedings of the 12th International Conference of Gas Discharges and Their Applications*, 1997; pp 188-191.

(25) Dorai, R.; Kushner, M. J. *J. Phys. D: Appl. Phys.* **2001**, *34*, 574-583.

(26) *Plasma Exhaust Aftertreatment* (SAE Special Publication SP 1395) eds.; Society of automotive Engineers: Warrendale, 1998.

(27) *Non-Thermal Plasma for Exhaust Emission Control* (SAE Special Publication SP 1483) eds.; Society of automotive Engineers: Warrendale, 1999.

(28) *Non-Thermal Plasma* (SAE Special Publication SP 1566) eds.; Society of automotive Engineers: Warrendale, 2000.

(29) Khacef, A.; Pouvesle, J. M.; Cormier, J. M. In *Proceedings of the 15th International Symposium on Plasma Chemistry*, 2001; pp 3079-3084.

Received for review, November 10, 2004. Accepted December 12, 2004.

ELSEVIER

Chemical Engineering Journal 106 (2005) 241–247

Chemical Engineering Journal

www.elsevier.com/locate/cej

On the use of a non-thermal plasma reactor for ethanol steam reforming

O. Aubry*, C. Met, A. Khacef, J.M. Cormier

GREMI-Polytech'Orléans, 14 rue d'Issoudun, B.P. 6744, 45067 Orléans Cedex 2, France

Received 21 July 2004; received in revised form 28 October 2004; accepted 4 December 2004

Abstract

This work is dedicated to the steam reforming study of ethanol in a non-thermal plasma reactor at low temperature and at atmospheric pressure. The plasma reactor was powered by a high voltage 50 Hz AC power supply with a 155 mA sinusoidal current. The voltage delivered by this system was self-adjusted between 0.4 and 1 kV according to the primary voltage of the transformer. Outlet concentration species, mainly H_2, CO and CO_2, were determined using chemical analysis apparatus and studied as functions of the electrical power and electrical discharge characteristics. Reactor behaviour and plasma product distribution are strongly determined by the electrical power and ethanol/water ratio. Chemical species and physical parameter variations have been described using two overall reactions: the ethanol steam reforming and endothermic cracking reactions. This present paper shows interesting results in comparison with catalytic processing of ethanol steam reforming.

Keywords: Hydrogen; Non-thermal plasma; Steam reforming; Ethanol

1. Introduction

Fuel cells are considered as a clean energy source. Nevertheless, since hydrogen is difficult to transport and store, its production in situ from an easily transported liquid feedstock can be an efficient alternative. The use of ethanol for energy production is an effective solution for the reduction of CO_2 emissions and preserves the fossil energy resources. Taking these aspects into consideration, the bio-ethanol steam reforming seems to be a promising technique [1,2]. Ethanol can be obtained by fermentation of surplus or agricultural residues and therefore is a renewable energy source that can be used to the H_2 production. During last decade, studies showed that hydrogen present a potential use as a fuel for electricity generation and transportation purposes. Moreover, H_2 is a renewable energy source and do not contribute to the green house effect [3,4]. The use of ethanol catalytic reactors for H_2 production had been presented in previous studies [1,2,5–8]. Nevertheless, some authors have performed the possibility to use plasma reactors for the hydrogen production from water and hydrocarbons [9–12].

The aim of the present paper is to study the steam-reforming from ethanol with a non-thermal plasma reactor to perform chemical analysis of the exhausts gas by micro gas chromatography (μGC) and Fourier transform infrared techniques (FTIR) and to identify the main ways implicated.

2. Experimental

The experiments were conducted at atmospheric pressure with a liquid ethanol/water mixture heated by graphite electrodes in a plasma reactor. The electrode gap was 10 mm. The length and diameter of the electrode were 150 and 25 mm, respectively. Fig. 1 is a schematic representation of the experimental reactor. The ethanol and water mole fractions ratio of the inlet mixture studied was in the range from 0–0.72.

* Corresponding author. Tel.: +33 238 494609; fax: +33 238 417154.
E-mail address: olivier.aubry@univ-orleans.fr (O. Aubry).

1385-8947/$ – see front matter © 2004 Elsevier B.V. All rights reserved.
doi:10.1016/j.cej.2004.12.003

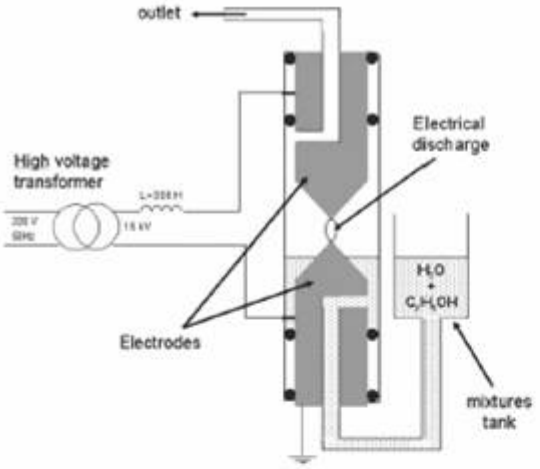

Fig. 1. Schematic reactor experimental.

The outlet gas composition was analysed using two techniques: micro gas chromatography (μGC, Varian CP2003-P) and Fourier transform infra-red (FTIR, Nicolet Magna-IR 550 series II). The μGC analyser contained 5 Å Molecular sielve and Plot Q columns. Both columns were equipped with thermal conductivity detectors (TCD) calibrated with standards of known composition. The temperatures of the column and injector for the analysis of H_2, CH_4 and CO on the Molecular sielve 5 Å column were 70 and 85 °C for Poraplot Q and the analysis of hydrocarbons and CO_2. The 10 m long FTIR analysis cell was maintained at 110 °C. The species detected and analyzed were H_2, CH_4, C_2H_2, C_2H_4, C_2H_6, CO, CO_2, C_2H_5OH and H_2O. The latter two were detected only in humid gas. The H_2O concentration at reactor output was estimated from the C, H and O balances, since no other specie was detected in our work.

The exhaust gas was sampled through a hole, in the second electrode, which was linked to μGC via a heating pipe (110 °C) to quantify the moisture gas or via the heating pipe until a cryogenic trap (−30 °C) to analyse the desiccated gas.

The current and voltage waveforms were measured using a TCP202 Tektronix Hall effect probe and a P5205 Tektronix high voltage differential probe connected to a voltage divider with a ratio of 0.01. The signals from the probes were recorded on a Tektronix TDS 460A digital oscilloscope and processed in a PC.

The gas discharge power was determined from voltage and current measurements. The electrical discharge was powered by a 50 Hz high voltage step-up transformer with leakage flux (AUPEM SEFLI high voltage transformer: primary 230 V, 10000/100, I_2 = 155 mA). The sinusoidal current remains at a constant value of 155 mA. In order to verify the running stability, several voltage and current recording were performed for each liquid mixture. Finally, the signal processing was performed on a PC.

3. Results

3.1. Chemical analysis

3.1.1. Dry gas

The dessicated gas mole fractions as functions of the inlet mole fractions ratio are displayed Fig. 2. FTIR and μGC were associated in this study. The species detected were: H_2, CO, CO_2, CH_4 and C_2 hydrocarbons. No reactive species (C_2H_5OH and H_2O) were detected with the use of the cryogenic trap.

As the inlet ethanol/water ratio rises, the mole fractions of H_2 and CO_2 decrease, from 0.72 to 0.62 and from 0.10 to 0.013, respectively. The concentration of the others species

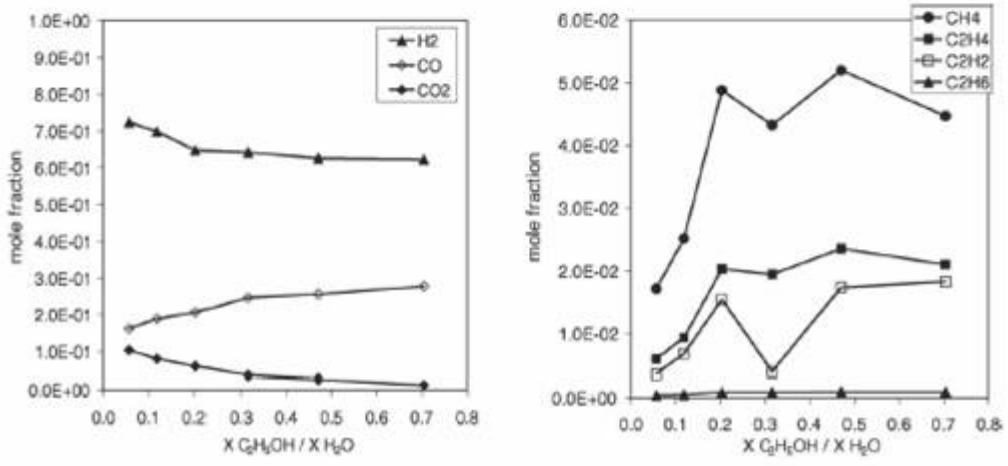

Fig. 2. Composition of the dried exhaust gas vs. the inlet ethanol/water ratio.

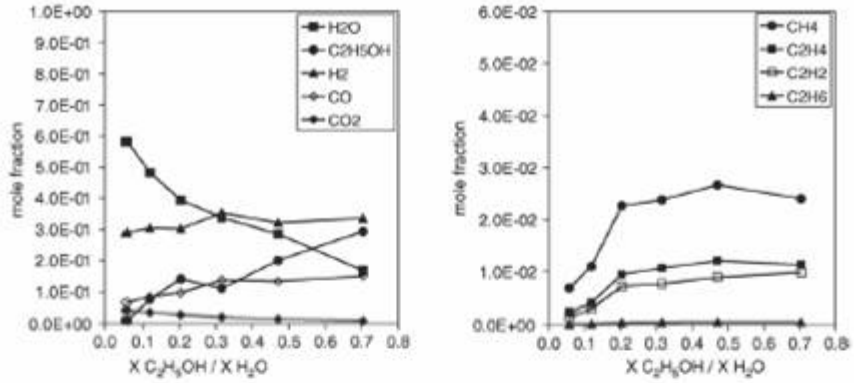

Fig. 3. Composition of the wet exhaust gas vs. the inlet ethanol/water ratio.

increase: CO mole fraction rises from 0.16 to 0.28 and the concentration of the hydrocarbons species stays below 0.05 in the entire studied domain.

3.1.2. Wet gas

The study of dry gases does not enable all species present at reactor output to be quantified. Indeed, to analyse all the products and especially the no-consumed species (H_2O and C_2H_5OH), we have studied the wet exhaust gas composition. Mole fractions of these species are presented in Fig. 3 as functions of the inlet mole fractions ratio.

H_2 concentration slightly increases from 0.29 to 0.34 when the ethanol/water ratio rises. Simultaneously, the mole fractions of CO, CH_4, C_2H_2, C_2H_4 and C_2H_6 rise from 0.06 to 0.15, 6.8×10^{-3} to 2.4×10^{-2}, 2.4×10^{-3} to 1.14×10^{-2}, 1.46×10^{-3} to 9.86×10^{-3} and 1.56×10^{-4} to 5.32×10^{-4}, respectively. The CO_2 decreases from 4.16×10^{-2} to 8.74×10^{-3}.

Trends in mole fractions variations for the others species are similar to the dried gas results. Low concentrations of hydrocarbons are observed in the outlet gas.

Our dry results show that there were high mole fractions of H_2 at reactor output, of the order of 0.6 to 0.7. In order to carry out the complete energy balance involved in this process, however, it is necessary to take into account all species present at reactor output, i.e. wet gas. Dry and wet gas comparisons of no-condensed species show that the mole fractions in the wet outlet gas are nearly divided by 2. In the wet case, the concentrations of H_2, CO, CO_2, CH_4 and of C_2 compounds decreased because H_2O and C_2H_5OH were included in the quantification of species at reactor output. This shows that it is important to take all species present and not only dry gases into account, in order to establish a complete material and energy balance in this type of process. Moreover, the precursors (C_3, C_4) of aromatic or polyaromatic species that lead to the formation of soot are absent, explaining the absence of carbon deposit.

C_2H_5OH and H_2O are not fully converted. The corresponding conversion rates, τ, are defined by the following expression:

$$\tau = \frac{n_{cons}}{n_i} \quad (1)$$

where n_{cons} represents the consumed number of moles of each reactant and n_i is the number of moles of inlet reactant. Results are shown in Table 1. Conversion rates depend on the inlet ethanol/water ratio. Ethanol conversion decreases and water conversion increases when C_2H_5OH/H_2O ratio rises.

Table 1
Examples of C_2H_5OH and H_2O conversion rates

Inlet XC_2H_5OH/XH_2O	0.12	0.32	0.70
τ C_2H_5OH	0.39	0.27	0.22
τ H_2O	0.15	0.23	0.36

3.2. Characteristics of the discharge

Fig. 4 shows the variations of the voltage and current as functions of the time for a given liquid mixture: ethanol/water ratio = 0.12.

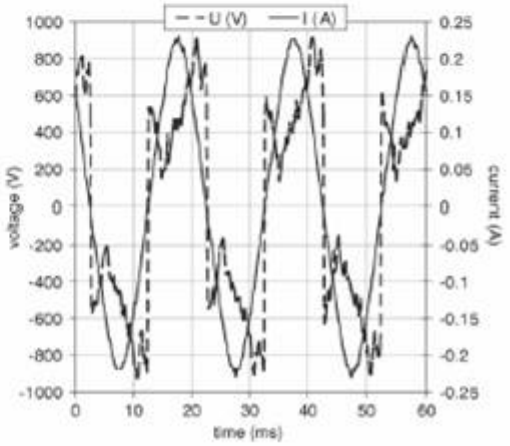

Fig. 4. Variation of the voltage and current as functions of the time. Ethanol/water = 0.12.

The plasma reactor is powered by a 50 Hz step-up transformer. Root mean square (RMS) value of the sinusoidal current is 155 mA. The secondary voltage applied to the discharge gap is self-adjusted as an effect of leakage flux in the range: 0.4–1.0 kV. Periodic ignition of the discharge is corresponding to a voltage pulse. The ignition pulses magnitude values are in the range 400–500 V. A characteristic parameter of the plasma was determined, corresponding approximately to the maximum degree of ionization, by measuring the resistance value of the ionized column when current is maximal. This value in a steam plasma is 1600 Ω when the length of the ionized column is 15 mm. The voltage drop at the electrodes is 60 V. The instantaneous discharge resistance changes with time during each half-period of current.

As the plasma is recombining the resistance is increasing and greatest voltage values are observed for a corresponding time of about 10 ms. Pulses magnitude and maximum voltages are linked to the inlet ethanol/water ratio.

Fig. 4 shows voltage and current variations of the plasma discharge. Ignition values and maximum of voltage can be observed. Due to the leakage flux effect, a large inductance appears and the current remains at a nearly constant RMS value of 155 mA with a sinusoidal waveform. Voltage is determined by ionization properties of the gaseous mixture. Previous studies [13–15] had shown a non-thermal plasma behaviour in which electrons temperature (8000–1000 K) is higher than the gas temperature. Plasma column looks like a plasma string with 1 and 10 mm for diameter and length, respectively. The order of magnitude of the maximum gas temperature is 2000 K and the average temperature at the reactor outlet is about 600 K. In light of the voltage drop at the electrodes and of the temperature difference between electrons and the gas, it can be said that the discharge is a "glow discharge", illustrating the non-thermal nature of the plasma.

In the case of Fig. 4, the average power provided to plasma discharge is about 66 W. A non-linear behaviour of the plasma discharge can be observed. This non-linear effect is shown in Figs. 4 and 5.

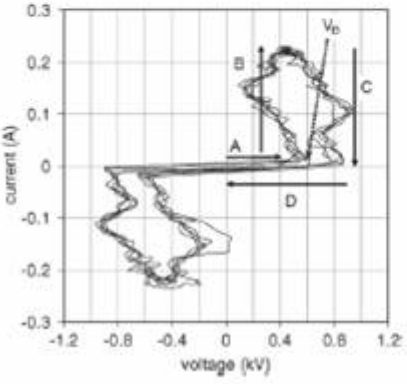

Fig. 5. Dynamical current–voltage characteristic. Ethanol/water = 0.12.

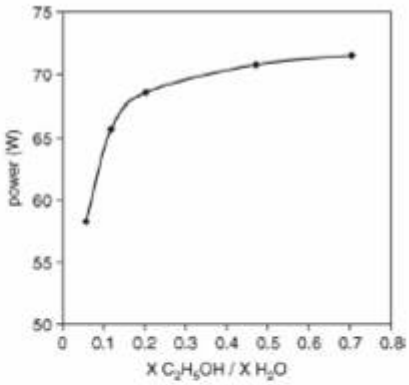

Fig. 6. Power of the discharge vs. the inlet composition.

Fig. 5 shows four phases are observed corresponding to the following effects:

(A) increasing voltage without significant current;
(B) full ionisation region corresponding to current increasing;
(C) recombination region with increasing of the plasma column resistance;
(D) weak ionisation region.

Transition from A to B is characterized by a breakdown potential V_B (ignition of the discharge). This potential is a function of the gas mixture. V_B is increasing as the C_2H_5OH concentration increases.

The input electrical discharge power, P_i, is calculated from voltage and current measured for each mixture: $P_i = \frac{1}{T}\int_o^T u_{(t)} i_{(t)}\,dt$; with $u_{(t)}$ and $i_{(t)}$ voltage and current, respectively.

As shown in Fig. 6, P_i strongly depends on the inlet composition. P_i rapidly increases from 57 to 69 W when the inlet ethanol/water mole fractions ratio rises from 0.05 to 0.20. Above this upper limit, the input power slightly increases up to 72 W. This means that the voltage is linked to the inlet composition because of a constant value of the current. Therefore, the average voltage increases when the input power rises.

4. Interpretation and energy balance

The fine interpretation of the reaction mechanisms involved in this type of reactor requires the use of a kinetic model coupled with a hydrodynamic model of the plasma that includes electron reactions. This study is complex and requires the participation of specific high level competence. Our current understanding does not enable us to present the comparison between a model and local measurements of the density of different species. Taking the context into account, we present only the overall experimental results, describing the principal parameters of system advancement. So, to estimate the energy balance, we represented the chemical

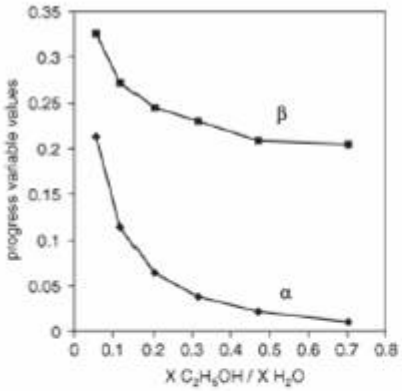

Fig. 7. Conversion degree of the overall reactions Eqs. (2) and (3).

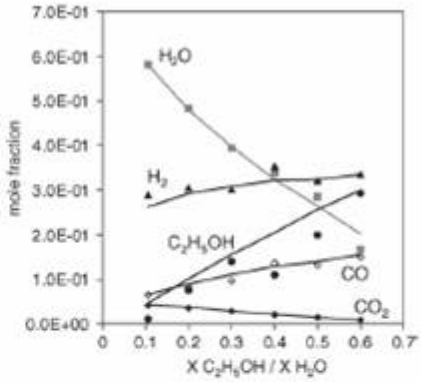

Fig. 8. Experimental mole fractions (symbols) and calculated values (solid lines) vs. the inlet composition.

system from two global reactions. Indeed, from our experimental data, the general evolution observed for the main species in the wet gas could be described by considering two overall reactions:

$$C_2H_5OH + 3H_2O \rightarrow 2CO_2 + 6H_2 \quad (2)$$

$$C_2H_5OH + H_2O \rightarrow 2CO + 4H_2 \quad (3)$$

For each C_2H_5OH–H_2O mixture, H_2, CO, CO_2, C_2H_5OH and H_2O mole fractions can be expressed in terms of the progress variables α, β of reactions (2) and (3). A least square procedure has been used to derive α and β values to minimize the sum $\sum (Xi_{exp} - Xi_{calc})^2$. In order to calculate the relative importance of the two global reactions representing changes of major species (H_2, CO, CO_2, C_2H_5OH, H_2O) and to calculate the energy involved in the chemical process, we determined the consumption of reactants in the two reactions. We calculated the mole fractions of species, noted Xi_{calc}, versus the progress values (α and β) of the two reactions (2) and (3). This provides the lowest sum $\sum (Xi_{exp} - Xi_{calc})^2$ for each reaction mixture. The Xi_{exp} values are the mole fractions measured of the species analyzed. The results are shown in Fig. 7.

α decreases down to 0 and β decreases to a stable value (0.22) for the highest ethanol mole fraction. This latter explains the nearly constant H_2, CO and CO_2 mole fractions. H_2O and C_2H_5OH are consumed by these reactions. For the lowest inlet ethanol mole fraction, the consumption of ethanol occurs by reactions (2) and (3) in same part and contribute to form H_2.

When inlet C_2H_5OH mole fraction increases, reaction (3) dominates the consumption of ethanol which explains the lowest CO_2 mole fractions in favour of the CO production.

The experimental mole fractions are compared with the mole fractions calculated from the progress variables (Fig. 8). The results in Fig. 8 show that the description using two reactions mentioned above, combined with α and β, is sufficient for an overall description of the effect of the plasma. We can thus use these degrees of advancement to calculate an energy balance.

By taking into account the progress variables of the two overall reactions, power balance of the reactor can be performed. Fig. 9 displays different powers: input power, P_i, power used to vaporize the inlet mixture, P_v, and power implied in the two overall chemical reactions, P_r.

The vaporization power, P_v, is calculated from the liquid volume consumed, ethanol and water vaporization enthalpies (−42.3 and −44 kJ mol^{-1}) and the inlet mole fraction of ethanol. The vaporization power calculated is in the range from 58 to 72 W when ethanol/water ratio increases from 0.05 to 0.72.

Previous studies showed that theses electrical discharges imply low electron densities, high electron temperature and low gas temperature. We assumed a maximum gas temperature in the plasma column of about 2000 K [13–15]. The enthalpies of the overall reactions (2) and (3) were calculated at 2000 K: $\Delta_r H_2$ and $\Delta_r H_3$ are 220.05 and 272.1 kJ mol^{-1}, respectively.

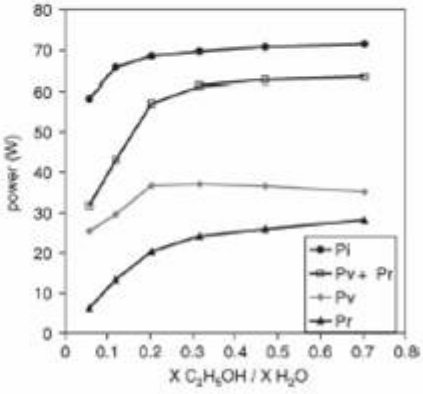

Fig. 9. Input, vaporization, reaction and vaporization + reaction powers vs. ethanol/water ratio.

Thus, the overall enthalpy in the reactions is expressed by the equation (4):

$$\Delta_r H = \alpha \Delta_r H_1 + \beta \Delta_r H_2 \quad (4)$$

α and β are the progress values obtained previously (Fig. 7).

From $\Delta_r H$ calculated, the power used in the chemical reactions, P_r, can be estimated. P_r is a function of the inlet ethanol mole fraction. This power is in the range from 6 to 28 W.

Our results showed that the vaporization of the ethanol/water mixtures require more energy than that implied in the chemical process. These powers are strongly influenced by the composition of the inlet mixture. As lowest ethanol/water ratio, the power implicated in the hydrogen production is decreasing. If we compare input power and the sum of P_v and P_r as functions of inlet ratio, we can observe that $P_v + P_r$ is close to P_i when the inlet ethanol/water ratio is above 0.2. As it is shown in Fig. 9, main part of the input power is used to the vaporisation and chemical reactions.

A dramatic influence of the inlet mixture was observed in input power and applied voltage. The rise of the ethanol/water ratio leads to an increase of the electric resistance in the ionized gas phase. Moreover, the ionized gas phase composition in the electric discharge is an important factor on plasma and gas phase temperatures. Electron densities and temperatures depend on the inlet parameters and electrical properties. Thus, an increase of the hydrocarbon species concentration can lead to a decrease of these temperatures. Therefore, the decrease of the electrical resistance of the ionized gas phase can be understood.

A comparison between the results of this plasma steam reforming and catalytic steam reforming appears to be interesting.

Nevertheless, it is very difficult to find in the literature results on the concentrations of the species produced in wet gases. Therefore, Table 2 presents the mole fractions of main species present in the dry gas in different ethanol steam reforming processes.

The catalytic and non-thermal plasma results show a same order of magnitude for H_2, CO, CO_2 and CH_4 concentrations. We observe that plasma technology allows to achieve a good level of H_2 mole fraction in a great range of ethanol/water ratio comparing to the catalytic techniques. Llorca et al. [5] obtained gas exhaust without CO in the case of Co/ZnO catalysts while plasma method implies relative high CO mole fractions. The others species present same concentration levels.

Table 2
Comparative H_2, CO, CO_2, CH_4 mole fractions in the dry outlet gas vs. inlet ethanol/water ratio and vs. steam reforming techniques used

	This work	Auprètre et al. [1]	Llorca et al. [5]
Inlet ethanol/water ratio	0.05–0.72	0.33	0.07
H_2	0.62–0.72	0.44–0.72	0.65–0.738
CO	0.16–0.28	0.07–0.20	–
CO_2	0.10–0.12	0–0.21	0.216–0.242
CH_4	0.017–0.052	0–0.21	0.003–0.008

This comparison indicates that plasma steam reforming of the ethanol is a competitive way to produce H_2 with CO and CO_2. Nevertheless, the CO concentration is the main drawback because of concentrations higher than 10 ppm. This value is considered as a limit in order to avoid poisoning fuel cells.

5. Conclusions

This work shows that non-thermal plasma steam reforming of the ethanol at atmospheric pressure is a promising technique for H_2 production. Our results are very close to ones obtained in the catalytic reactors.

Chemical analysis of the outlet gas and characteristics of the discharge had been studied. We quantified the wet and dry exhaust gas composition. Thus, several species had been quantified: no-consumed reactive species (C_2H_5OH and H_2O), oxygenated, and hydrocarbon products (H_2, CO, CO_2, CH_4, C_2H_2, C_2H_4, C_2H_6). The mole fractions of CO and CO_2 depended on the inlet composition while H_2 concentrations remained constant. These results showed that the optimization of the process was important to reduce the CO mole fraction. Indeed CO was poisoning specie for the fuel cells; its concentration must be limited near 10 ppm. Chemical interpretation of the results in term of two overall reactions showed that parallel reactions could describe the conversion of the inlet ethanol and water. For the lowest inlet ethanol mole fractions, the progress variable values were in the same order of magnitude. For the highest ethanol mole fraction, the reaction leading to the CO_2 production becomes negligible. The method for producing hydrogen from ethanol with the plasma reactor described here is interesting and could, after additional work and depending on the results obtained, be developed at the industrial scale. Compared to conventional techniques, its principal advantages would be ease of use and uncomplicated control of the various operating parameters. We can envision the regulation of gas flows by adding auxiliary heating, combined with a command suited to the power delivered by the plasma. In addition, the plasma system eliminates problems related to the use of catalysts prepared from costly materials (Pt, Rh, Ru, Co, ...) and that require precautions in use and operation in order to optimize conversion rates and avoid the inactivation of catalysts by poisoning. The energy balances show that it is possible to reach yields very close to those calculated from the laws of thermodynamics. These balances carried out with a laboratory scale reactor are a determinant element that should arouse the interest of industries concerned in order to continue investigations on the possible applications of this technology.

The non-thermal plasma appears as a good technique for the steam reforming from bio-ethanol with a high H_2 concentration. Energetic costs could be decreased by re-injecting

the condensed gas phase containing water and ethanol. Moreover, to achieve low CO mole fractions, studies on others inlet mixtures with hydrocarbon-ethanol and/or a plasma-catalysis technique can be envisaged.

References

[1] F. Auprêtre, C. Descorme, D. Duprez, Catal. Commun. 3 (2002) 263–267.
[2] G.A. Deluga, J.R. Salge, L.D. Schmidt, X.E. Verykios, Science 303 (2004) 993–997.
[3] J. Benemann, Nat. Biotechnol. 14 (9) (1996) 1101–1103.
[4] J.-J. Lay, Y.-J. Lee, T. Noike, Water Res. 33 (11) (1999) 2579–2586.
[5] J. Llorca, N. Homs, J. Sales, P. Ramirez de la Piscina, J. Catal. 209 (2002) 306–317.
[6] J.P. Breen, R. Burch, H.M. Coleman, Appl. Catal. B: Environ. 39 (2002) 65–74.
[7] F.J. Marino, E.G. Cerrella, S. Duhalde, M. Jobbagy, M.A. Laborde, Int. J. Hyd. Energy 23 (12) (1998) 1001–1095.
[8] E.Y. Garcia, M.A. Laborde, Int. J. Hyd. Energy 16 (5) (1991) 307–312.
[9] J.M. Cormier, I. Rusu, J. Phys. D: Appl. Phys. 34 (2001) 2798–2803.
[10] F.N. Pekhota, V.D. Rusanov, S.P. Malyshenko, Int. J. Hyd. Energy 23 (10) (1998) 967–970.
[11] K. Meguernes, J. Chapelle, A. Czernichowski, J. High Temp. Mater. Proc. 5 (3) (2001) 363–374.
[12] A. Huang, G. Xia, J. Wang, S.L. Suib, Y. Hayashi, H. Matsumoto, J. Catal. 189 (2000) 349–359.
[13] A. Kaminska, J.-M. Cormier, S. Pellerin, O. Martinie, J. High Temp. Mater. Proc. 5 (3) (2001) 403–409.
[14] S. Pellerin, J.-M. Cormier, F. Richard, K. Musiol, J. Chapelle, J. Phys. D 32 (1999) 891–897.
[15] J.M. Cormier, I. Rusu, A. Kaminska, J. High Temp. Mater. Proc. 6 (4) (2002) 421–429.

INSTITUTE OF PHYSICS PUBLISHING JOURNAL OF PHYSICS D: APPLIED PHYSICS
J. Phys. D: Appl. Phys. 35 (2002) 1491–1498 PII: S0022-3727(02)34538-8

NO_x remediation in oxygen-rich exhaust gas using atmospheric pressure non-thermal plasma generated by a pulsed nanosecond dielectric barrier discharge

A Khacef[1], J M Cormier and J M Pouvesle

Groupe de Recherche sur l'Enérgétique des Milieux Ionisés, GREMI-ESPEO,
14 Rue d'Issoudun BP 6744, 45067, Orléans Cedex 2, France

E-mail: Ahmed.Khacef@univ-orleans.fr

Received 5 March 2002
Published 18 June 2002
Online at stacks.iop.org/JPhysD/35/1491

Abstract

It is clearly seen that the application of non-thermal plasmas (NTP) to remove NO_x from gas mixture containing a large amount of oxygen (O_2) is dominated by NO to NO_2 oxidation. Experiments have been conducted using a NTP generated by a nanosecond pulsed dielectric barrier discharge in synthetic exhaust gas, prepared from N_2, O_2, NO, H_2O, and C_3H_6, over a large range of gas temperature (20–300°C). Results show that the NO_x removal rate significantly increased with increasing specific energy deposition. For example, at a temperature of 100°C and an energy deposition of 27 J l^{-1}, 92% of the NO molecules have been removed. The W values for NO is dramatically reduced to values scaling from ≈15 eV at 27 J l^{-1} down to ≈4 eV at 7 J l^{-1}. NO_x removal efficiency around 43% was obtained at a temperature of 260°C and a space velocity of 60 000 h^{-1} for a specific input energy of 27 J l^{-1}. W values for NO_x were less than ≈30 eV. Such treatments in exhaust gas with and without the presence of water vapour induced reactions leading to the production of a large variety of by-products such as acetaldehyde, propylene oxide, formic acid, methyl nitrate, and nitromethane.

1. Introduction

Non-thermal plasmas (NTP) appear to be potent technology for the removal of air pollutants such as nitrous oxides (NO_x), sulphur oxides (SO_x), and volatile organic compounds (VOCs) in the exhaust gas stream under atmospheric pressure in particular when the environmental regulations became more and more constraining. NO_x, which is an ozone precursor and one of the most difficult air pollutants to suppress, remains the most serious hazard to human health than any other regulated compound.

Among the existing pollution sources, motor vehicles are seen as a major contributor to air pollution by NO_x, unburned hydrocarbons (UHC), and fine particles matter (PM). Many applications of NTP have been developed [1] and treatments for diesel and gasoline engine exhausts under lean conditions have been proposed [2–6]. The primary focus of plasma aftertreatment studies has been on the removal of NO_x. Because of the significant oxygen and water vapour levels in lean exhaust, rendering conventional three way catalyst (TWC) ineffective for the NO_x treatment, the reduction of NO_x to N_2 in plasma was drastically limited [7–9]. A relatively new approach to promote chemical reduction of the NO_x to N_2 is the application of plasma-catalyst hybrid systems [2, 4, 10, 11]. In that case the plasmas could be used as a pretreatment step to a catalyst bed. The process by which plasma catalysis takes place can be separated into two distinct parts: (a) plasma induced oxidation of NO to NO_2 at low temperature and (b) selective catalytic reduction (SCR) of NO_x to N_2 by consumption of hydrocarbons even in oxygen-rich condition [12, 13].

[1] Author to whom correspondence should be addressed.

0022-3727/02/131491+08$30.00

NTP that has a low gas temperature and a high electron temperature can be produced by a variety of electrical discharge methods (pulsed corona discharge, barrier discharge, and dc discharge) [14–17] or electron beam irradiation [1, 18]. Pulsed corona and dielectric barrier discharge (DBD) techniques are two of the more commonly used methods for producing electrical discharge plasmas. Regarding their intrinsic properties, DBDs appear very well adapted to treat large gas quantities with relatively low energy cost. In these plasmas, the electrons do not react directly with the NO_x molecules. The kinetic energy of the electrons is deposited mainly into the background gas molecules like N_2, O_2, and H_2O. The most useful deposition of energy is associated with the production of N, O, and OH radicals through electron-impact dissociation. These radicals are the active species of the plasma that eventually lead to the chemical conversion of NO_x. Due to the presence of H_2O and O_2, plasma processing of NO_x is dominantly oxidative resulting primarily in NO_2 and some extent in HNO_2, HNO_3. Also, hydrocarbons in exhausts have been found to play an important role in the NO_x removal processes. For example, Penetrante *et al* [2] investigated the consequence of propene (C_3H_6) in a NO_x–air mixture and found that, at 300°C, almost 100% of the initial NO (500 ppm) was converted to NO_2, whereas in the absence of propene, only 7% of NO were remediated. Niessen *et al* [19] found that addition of ethene (C_2H_4) in NO_x–humid air mixture improve the NO removal efficiency with most of the remediated NO being converted to NO_2.

This paper will present the results of an extensive series of experiments aimed towards understanding the effect of gas composition of the NO_x conversion chemistry in plasma. Experimental results in dry and humid oxygen-rich gas mixtures are presented using a nanosecond-pulsed DBD plasma reactor combined with external heating. Species such as NO, NO_2, CO, CO_2, C_3H_6, and CH_2O have been analysed and quantified.

2. Experimental set-up

Figure 1 shows a schematic diagram of experimental arrangement. Synthetic gas mixtures containing O_2, N_2, NO, and C_3H_6 (propene) were prepared in a gas handling system and their composition was controlled by calibrated high-precision mass flow controllers (MFC Brooks). Water vapour with controlled concentrations was added to the gas mixture using controlled evaporator mixer CEM® (Bronkhorst Hi-Tec). It consists of a liquid flow control, a carrier gas control and a mixing chamber for liquid and carrier gas with heat exchanger for total evaporation. This device can provide a high reproducibility and a very stable vapour flow. After mixing in the manifold, the gas then passes through a temperature-controlled line which preheat the gas and prevent condensation.

The electrical discharge reactor used is DBD. The reactor geometry was one of a wire to cylinder type. It consisted of a tungsten wire (0.9 mm diameter) in a long dielectric (quartz) tube with inner and outer diameters of 11 mm and 13 mm respectively. An aluminium foil to form the outer electrode covered the dielectric tube. The length of the outer electrode can be adjusted and then determines the active volume of the DBD reactor. The DBD reactor was placed inside a tubular furnace. The gas mixture temperature can be adjusted from room temperature to 500°C.

The DBD reactor is driven by a cable transformer powered by high-voltage ceramic capacitors disposed in Blumlein-like configuration. Details of this homemade high-voltage generator are given in [20]. This pulse generator is capable of delivering open circuit voltage up to 150 kV output into 80 ns (FWHM) pulses and short voltage rise time (40 ns). Figure 2 shows an example of the time-behaviour of the voltage and the current. The fast voltage rise time allows achieving significant over-voltage at breakdown. The pulse repetition rate could be adjusted from single shot regime to 1 kHz. The results presented in this paper are obtained at a discharge voltage of about 20 kV and a repetition rate up to 200 Hz.

The applied voltage and current were measured using a high voltage probe (Tektronix P6015A, 1000x) and a current probe (Europulse 9001), respectively. The output signals were transmitted to a digitizing oscilloscope (Tektronix 2440). The discharge pulse energy into the plasma was measured with a capacitive circuit. The energy deposition in the plasma reactor

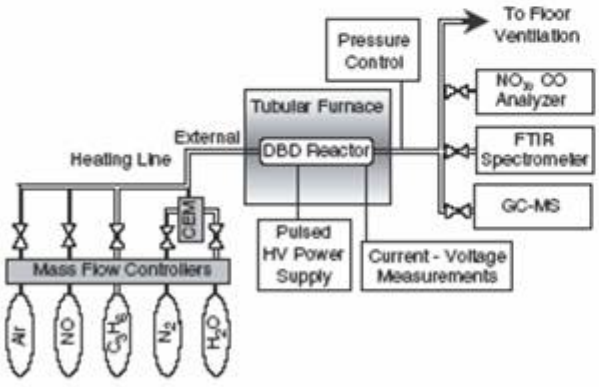

Figure 1. Schematic diagram of the experimental set-up.

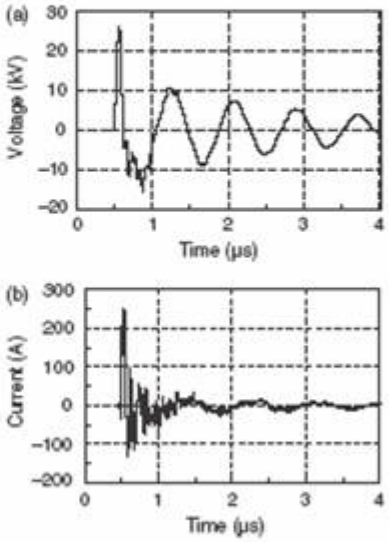

Figure 2. Typical recording of voltage (*a*) and current (*b*) pulses as a function of time.

$J1^{-1}$ is given by

$$E_d = \frac{E_p f}{Q} \quad (1)$$

where E_p is the discharge pulse energy, f is the pulse repetition frequency, and Q is the gas flow rate at standard conditions (25°C and 1 atm).

The major gaseous components as NO, NO_2, CO, CO_2, and C_3H_6 were analysed online and quantified using Fourier transform infrared (FTIR) absorption spectrometer equipped with a heated 10 m-multiple pass absorption cell. An electrochemical NO_x analyser was also used for monitoring continuously NO, NO_2, and NO_x, as well as CO levels in the gas stream. Cold trap (liquid nitrogen) could be inserted in the output line to obtain condensed products. Soluble species were sampled to be further analysed by gas chromatography coupled with mass spectrometer (GCMS) measurements.

3. Experimental results

Detailed kinetic schemes and discussions of the mechanisms involved in gas phase chemistry in the plasma processing O_2, NO, N_2, and hydrocarbon mixtures were studied extensively [2, 22, 23]. New pathways for NO oxidation are introduced, most of which primarily result in the formation of NO_2. Briefly, when the O_2 concentration is higher than 5% the plasma gas phase chemistry is initiated mainly by the production of oxygen radicals via electron induced dissociation of O_2. The dissociation of O_2 promotes the gas-phase oxidation of NO to NO_2. In the absence of hydrocarbons, the efficiency of NO_2 production via three body reaction of NO with O will be reduced as a result of the reverse reaction of NO_2 with O and also by conversion of NO_2 to acid in the presence of water vapour in the gas exhaust. It is well known that when hydrocarbon is added to the gas mixture, NO to NO_2 oxidation is enhanced to a large extent as the amount of hydrocarbon increases. The hydrocarbon acts as a getter of O and OH radicals, with the resulting products reacting with O_2 to yield peroxy radicals (HO_2) which efficiently convert NO to NO_2.

In the following, we first present experiments performed at high energy density in order to show how the hydrocarbon (propene in our case) affect the non-thermal plasma treatment of NO_x in oxygen-rich exhausts. Then, experimental results at lower energy density are presented.

3.1. Hydrocarbon effect on NO to NO_2 oxidation

Preliminary experiments were performed by plasma processing of dry gas mixtures (19.6% O_2, 500 ppm NO, 500 ppm C_3H_6, N_2 as balance gas) at an energy deposition of 195 mJ per pulse and a repetition rate of about 15 Hz. Figure 3 illustrates the NO to NO_2 conversion when propene is used. It can be seen that some hydrocarbons are required for complete oxidation of NO to NO_2, consistent with previous works [2, 4]. Maximum NO to NO_2 conversion occurs when gas mixtures contain at least 500 ppm propene (at 3 : 1 ratio of C_1 to NO_x).

The NO_x concentrations (sum of NO and NO_2 concentrations) as a function of residence time and energy density deposition for the cases without propene and with 500 ppm propene are shown in figures 4(*a*) and (*b*),

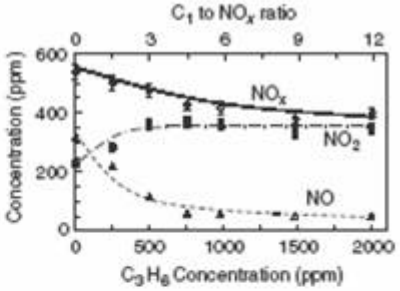

Figure 3. Effect of inlet propene concentration on the conversion of NO to NO_2 in plasma processing of 19.6% O_2, 500 ppm NO, and N_2. T = 100°C and energy deposition = 44 $J1^{-1}$.

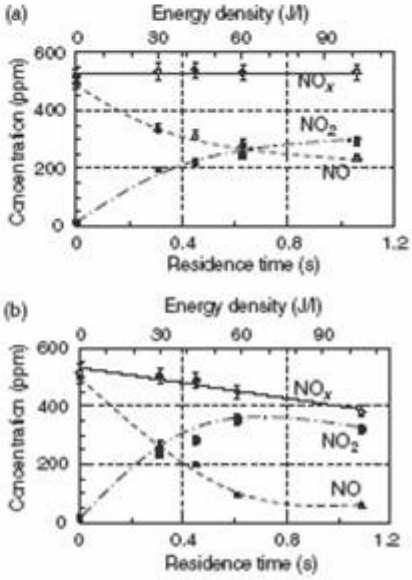

Figure 4. The effect of residence time (or energy deposition) on the plasma oxidation of NO at room temperature. Plasma processing of 500 ppm NO in 19.6% O_2, balance N_2, (*a*) without propene, and (*b*) with 500 ppm propene.

respectively, for plasma processing at room temperature. In the absence of hydrocarbons, the oxygen radicals are responsible for the oxidation of NO to NO_2. Figure 4(*a*) shows that less than 50% of the initial NO is converted to NO_2 even for the highest energy densities (up to 103 $J1^{-1}$). However, NO_x removal remains nearly constant. The increase in NO conversion obtained with increasing energy deposition is counteracted by the increase in NO_2 concentration resulting in an almost constant NO_x level.

The efficiency of these processes can be quantified by W values. W values (eV/molecule) are the amount of energy required to remove one molecule of the compound. The lower values correspond to more efficient processes. In that case, W value for NO is about 42 eV.

As shown in figure 4(*b*), the addition of 500 ppm of propene in the gas mixture enhances the oxidation of NO to NO_2, and lower is the energy cost for this oxidation. The radical responsible for the oxidation of NO to NO_2 is no longer the O radical. From chemical kinetics analysis, Penetrante *et al* [2] show that HO_2 is the radical that oxidizes NO to NO_2 when

the plasma processing is done in the presence of hydrocarbons. In that case, the W values for NO are ≈25 eV compared to 42 eV for gas mixture without hydrocarbon. Maximum NO_x conversion rate was ≈30% and W value for NO_x was ≈165 eV. One can see that the electrical consumption is very high with respect to NO_x removal efficiency. So, by properly selecting the gas mixture composition and the electrical conditions, it is possible to significantly reduce the energetic cost of the plasma process in relation with the NO_x removal efficiency. This aspect is especially important for a future automotive development. In a recent paper [23], we established that the main parameter, which controls the efficiency of the plasma process, is the energy deposition way into the gas. These experiments showed that at constant energy density, a large number of pulses with small amount of energy per pulse result in a higher NO_x and hydrocarbon removal efficiency than in the case of small number of pulses with large amount of energy per pulse.

In the following sections, DBDs in high repetition rate regime and low energy per pulse deposition were investigated by maintaining the gas flow rate at 16 litre min^{-1} corresponding to a space velocity of 60 000 h^{-1} (typical of the one of a running car engine). The electrical energy was 35 mJ per pulse and the repetition rate was varied between single shot regime up to 200 Hz. In all cases, the energy deposition was less than 30 $J l^{-1}$. The inlet gas conditions to the plasma reactor were typically 500 ppm NO, 500 ppm C_3H_6, 10% O_2, 0 or 10% H_2O, and N_2 as balance gas. The high value of NO concentration was used because it represents typical levels in a modern heavy-duty diesel engine. The pressure was 1 atm and four reactor temperatures were considered in this study: 22°C, 100°C, 173°C, and 260°C.

3.2. Dry gas mixture: O_2 (10%)–NO (500 ppm)–C_3H_6 (500 ppm)–N_2

The first set of experiments examined plasma processing of 500 ppm NO and 500 ppm C_3H_6 in 10% O_2, and balance N_2. Figure 5 shows the typical FTIR spectrum illustrating the plasma processing effect on the NO_x and hydrocarbons at ambient temperature and for an energy deposition of 27 $J l^{-1}$. Similar spectra were observed at higher temperatures (up to 260°C). Under these oxygen-rich conditions (10%), a significant fraction of input plasma energy is dissipated in the dissociation of O_2 which become the dominant process because O_2 dissociation is much more efficient than N_2 dissociation in the electron energy range produce. This dominant oxidation process leads to the formation of the main products of the plasma such as NO_2, CO, and CO_2. As expected, the plasma partially oxidizes the hydrocarbons. This partial oxidation processes lead to the formation of formaldehyde (CH_2O) and a large variety of by-products, such as methyl nitrate (CH_3ONO_2), formic acid (CH_2O_2), and nitrous acid (HONO).

The small amount of nitrous acid produced indicated the presence of moisture in the system, possibly arising from the air supply or from moisture adsorbed onto the walls of the gas handling system. Also, weak signals were observed in the absorption bands ranging 2140–2270 cm^{-1} and 2000–2300 cm^{-1} and attributed to N_2O and HCNO, respectively. Also, one can note the overlapping of peaks attributed to different species in different spectral regions highlighting the difficulties of this type of analysis.

3.2.1. NO_x removal. The NO, NO_2, and NO_x concentrations in dry conditions as a function of energy deposition are shown in figures 6(*a*) and (*b*), respectively, for room temperature and 260°C. NO_x concentration refers to the sum of individual concentrations of NO and NO_2. One can note the small amounts of NO_2 (less than 25 ppm) produced by oxidation of NO even without plasma. The NO to NO_2 oxidation was increased as the energy deposition increased. The gas temperature has a significant effect on the NO conversion though it has a small effect on NO_x conversion. At a given energy deposition, the increase in NO conversion obtained with increasing temperature is counteracted by the increase in NO_2 concentration resulting in an almost constant NO_x level.

At the maximum energy deposition used in that study (27 $J l^{-1}$), the measured NO_x conversion rate was ≈26% and

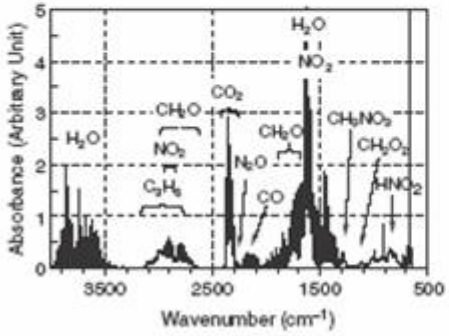

Figure 5. Typical FTIR spectrum produced by plasma processing of standard dry gas mixture at room temperature and an energy deposition of 27 $J l^{-1}$.

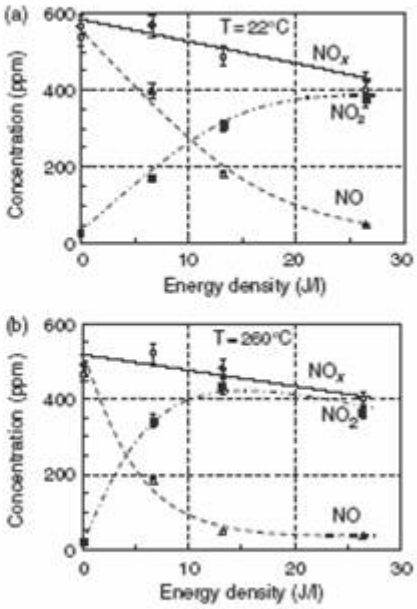

Figure 6. NO, NO_2, and NO_x output concentrations as a function of energy deposition at: (*a*) 22°C and (*b*) 260°C. Inlet gas contains 500 ppm NO, 500 ppm C_3H_6, 10% O_2, and balance N_2.

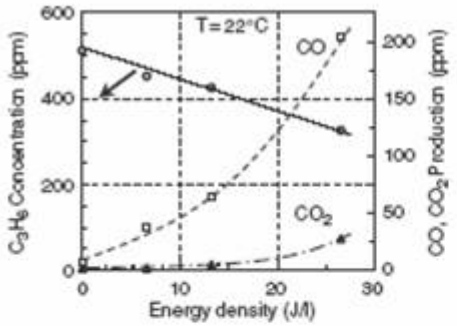

Figure 7. CO, CO_2, and C_3H_6 concentrations as a function of energy deposition. Inlet gas contains 500 ppm NO, 500 ppm C_3H_6, 10% O_2, and balance N_2 at room temperature.

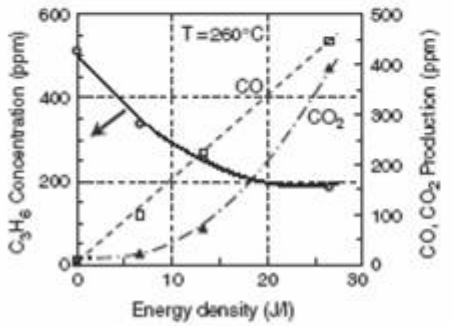

Figure 8. CO, CO_2, and C_3H_6 concentrations as a function of energy deposition. Inlet gas contains 500 ppm NO, 500 ppm C_3H_6, 10% O_2, and balance N_2 at 260°C.

W value for NO_x was ≈65 eV. The W values for plasma induced NO_x molecule removal were calculated from the formula given by Puchkarev *et al* [24]:

$$W(\text{eV/molecule}) = \frac{250 \times E_p \times f}{Q \times \Delta(NO_x)} \qquad (2)$$

where E_p is the pulse energy in J, f the frequency in Hz, Q the gas flow rate in litre s^{-1}, and $\Delta(NO_x)$ is the NO_x removal in ppm.

3.2.2. C_3H_6 removal and CO, CO_2 production. Figures 7 and 8 show the concentrations of C_3H_6, CO, and CO_2 as a function of energy deposition at room temperature and at 260°C. The consumption of propene increases with increasing input energy and is mainly influenced by the gas temperature. At an energy deposition of about 27 J l^{-1}, the measured reduction of C_3H_6 concentration is about 36% at room temperature while being 64% at 260°C. Large amounts of CO and CO_2 is formed during the oxidation of the hydrocarbon. This production may be higher at higher input energy and temperature. As much as 450 ppm of CO and 400 ppm of CO_2 were produced at energy deposition of 27 J l^{-1} and a temperature of 260°C. These results are consistent with modelling of Pitz *et al* [25] obtained at 300°C in 1000 ppm C_3H_6, 500 ppm NO, 10% O_2, and balance N_2.

Formaldehyde is one of the major by-products of the partial oxidation of propene in the plasma. Figure 9 presents the result of carbon products as a function of gas temperature

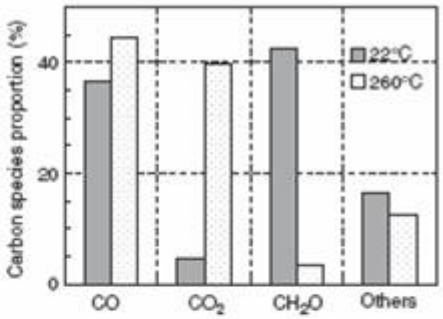

Figure 9. Effect of temperature on the carbon species proportion. Inlet gas contains 500 ppm NO, 500 ppm C_3H_6, 10% O_2, and balance N_2 at 27 J l^{-1}.

for plasma processing of standard dry gas mixture at 27 J l^{-1}. 'Others' represent the by-products like formic acid and methyl nitrate which were not quantified in that study. At room temperature, about 42% of oxidized hydrocarbons form formaldehyde. This amount was dramatically reduced at higher temperatures to reach around 3% at 260°C as shown in figure 9.

3.3. Humid gas mixture: O_2(10%)–H_2O (10%)–NO (500 ppm)–C_3H_6 (500 ppm)–N_2

The second set of experiments examined plasma processing of 10% H_2O, 500 ppm NO and 500 ppm C_3H_6 in 10% O_2 and balance N_2. For gas mixtures containing per cent level of water vapour, it is not possible to use the FTIR system due to strong interference from water bands. However, the by-products were detected by the GCMS in the liquid and gaseous phase of the exhaust gas but without quantification of each compound. Only NO, NO_2, NO_x, and CO were quantified in these experiments.

In humid gas mixture, the formation of OH radicals via electron-impact dissociation of H_2O and reaction of H_2O with metastable oxygen atom become important and results in the formation of HNO_2 and HNO_3 by reactions with NO and NO_2. The role of H_2O in the formation of acids becomes more apparent when H_2O concentration is 5% and above. When propene is present in the gas mixture, the OH radical becomes the main radical consuming propene. The radical responsible for the oxidation of NO to NO_2 is no longer the O radical. It has been shown from detailed chemical kinetics analysis [21, 26] that the HO_2 radicals, produced from reactions involving hydrocarbon intermediates of propene oxidation, is the radical that oxidizes NO to NO_2. The HO_2 radical concentration is a function of both the energy density input to the plasma and the hydrocarbon concentration in the gas mixture. Because the OH radical reacts preferentially with the hydrocarbon, the oxidation of NO and NO_2 to nitric and nitrous acids is minimized.

However, particular care must be observed when comparing the different results published in the literature. In a recent publication, F Fresnet [27], using a single pulse discharge, found that the presence of H_2O does not change significantly the gas composition after the plasma treatment. Doraï and Kushner [28] numerically investigated the consequences of multiple discharge pulses on the

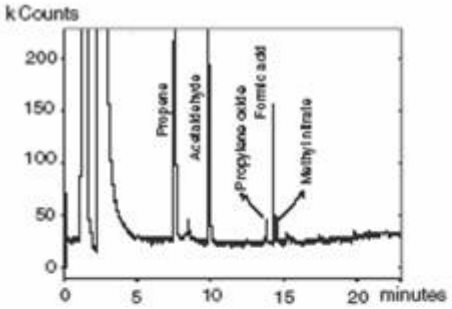

Figure 10. Chromatogram plot of a gas phase. Plasma processing of 500 ppm NO, 500 ppm C_3H_6, 10% O_2, 10% H_2O, and N_2 at 260°C.

plasma remediation of NO_x in the presence of water and hydrocarbons. Comparison of the products of single- and multiple-pulse discharges showed marked differences in the final concentrations of NO_2, HNO_x, C_3H_6, and CO. This behaviour can be explained by the fact that when using multiple pulses, reactions occur in the latter pulses with reaction products from previous pulses which are not accessible with a single pulse. These reactions produce significantly different end products. These conclusions reinforce the fact that when comparing the performance of the DBD reactors at different discharge conditions, the input energy density is not the relevant parameter. The main control parameter is how the energy is deposited into the plasma [23].

As shown in figure 10, the products of hydrocarbons processing are those reported commonly in the homogeneous gas phase processing of diesel exhaust containing propene [12–14]. These products are acetaldehyde (CH_3CHO), propylene oxide (C_3H_6O) and a large variety of species such as, formic acid, methyl nitrate, and nitromethane (CH_3NO_2). However, due to the strongly oxidative action of hydrocarbon radicals, NO_2, CO, and CO_2 are the main products in that case. To our knowledge, CH_3NO_2 has not been observed in any other reported experiments. That species was however predicted as a major by-product from propene induced NO to NO_2 conversion by Shin *et al* [29].

3.3.1. NO_x removal. OH radicals produced from water vapour by the plasma plays a major role in the NO_x removal chemical reactions. Output NO and NO_2 concentrations as a function of energy deposition in standard humid (10% H_2O) gas mixture is shown in figure 11 for three gas temperatures: 100°C, 173°C, and 260°C. With increasing energy deposition, the NO concentration decreases while that of NO_2 initially increases and decreases. These results served to validate the model conducted by Dorai and Kushner [28]. The computed NO concentrations agree well with the experiments whereas agreement for the case of NO_2 is within 15–20% at 260°C.

The NO conversion efficiency has been improved by increasing the gas temperature. For example, at 260°C, the energy deposition of only $7\,J\,l^{-1}$ was required to achieve maximum oxidation efficiency (figure 11(*c*)). As mentioned before [23], the NO_x and C_3H_6 conversion efficiencies (*W* values) were greatly improved by plasma processing at high repetition rate regime consistent with the modelling of Dorai and Kushner [28] for gas mixture containing 8% O_2, 6% H_2O,

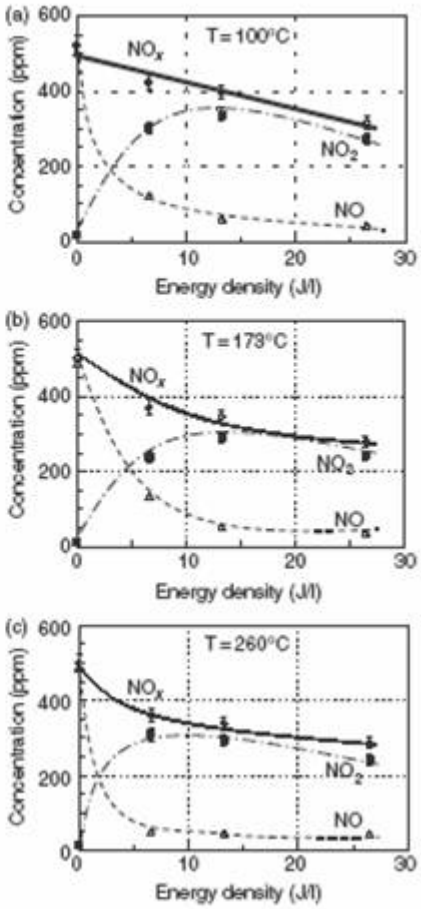

Figure 11. NO, NO_2, and NO_x output concentrations as a function of energy deposition at three gas temperature (*a*) 100°C, (*b*) 173°C, and (*c*) 260°C. Inlet gas contains 500 ppm NO, 500 ppm C_3H_6, 10% O_2, 10% H_2O and balance N_2 at 260°C.

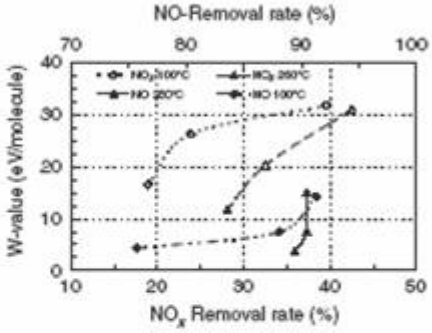

Figure 12. *W* values for NO and NO_x as a function of NO- and NO_x-removal rate in a standard humid (10% H_2O) gas mixture at 100°C and 260°C.

7% CO_2, 400 ppm CO, 260 ppm NO, 133 ppm H_2, 500 ppm C_3H_6, and 175 ppm C_3H_8 (propane) with N_2 as balance. In that model, the *W* values for NO_x remediation decrease from 240 eV for a single pulse ($58\,J\,l^{-1}$) to 185 eV when the same energy was distributed over 20 pulses.

The *W* values for NO and NO_x as a function of removal rates are shown in figure 12 at two temperatures

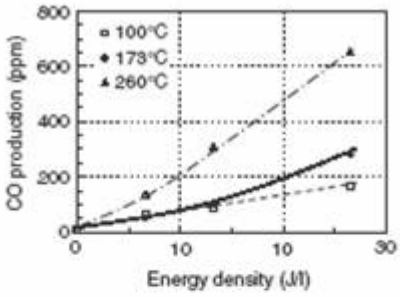

Figure 13. CO production as a function of energy deposition produced by plasma processing of standard humid (10% H_2O) gas mixture at 100°C, 173°C, and 260°C.

(100°C and 260°C). The W values decrease with increasing temperature. Using a processing frequency of 200 Hz, up to 92% of the NO have been removed at a specific energy input of about 27 $J l^{-1}$, which was the maximum energy input for all measurements. This removal has been mainly caused by oxidation to NO_2. In that case, the W values for plasma induced NO removal are dramatically reduced to values scaling from ≈15 eV at 27 $J l^{-1}$ down to ≈4 eV at 7 $J l^{-1}$. These results could be compared with previous data obtained by S Bröer *et al* [30] in synthetic gas mixture containing a higher O_2 concentration (18%), C_2H_4 (ethene), instead of C_3H_6 and at higher repetition (1 kHz). These authors found that the maximum NO-removal rate was 92% with a W value for NO around 100 eV.

The maximum NO_x conversion value (43%) is reached at 260°C and an energy deposition of 27 $J l^{-1}$. The energy cost was reduced by a factor 2.2 in comparison with results obtained in plasma processing without water in similar experimental conditions. The W value for NO_x measured was ≈30 eV.

3.3.2. CO production. Figure 13 shows the CO production in the plasma as a function of energy deposition with temperature as parameter. The CO production increases with increasing energy deposition in the plasma. The rate of rise of CO concentration is more important for high temperature. CO production increases from a few ppm to 160 ppm at 100°C, while it reaches 650 ppm at 260°C. These results give an idea of the acceleration of propene combustion reactions with the temperature.

4. Conclusion

Pulsed DBD appears to be a very promising technology for exhaust gas aftertreatment. Plasma processing of gas mixtures without water vapour (NO, C_3H_6, O_2, N_2) and with H_2O were performed at relatively low energy deposition (up to 27 $J l^{-1}$) in the temperature range from room temperature to 260°C. Besides CO and CO_2, significant amounts of formaldehyde, acetaldehyde, propylene oxide, formic acid, methyl nitrate, nitromethane, and ethyl acetate are formed in the plasma-initiated gas-phase reaction.

The oxidative potential of non-thermal plasma in gases with excess oxygen results in an effective conversion of NO to NO_2. The hydrocarbon added to the gas mixture plays two essential functions in the plasma: firstly, it assists the gas-phase oxidation of NO to NO_2 by electric discharge in excess oxygen and, secondly, it lowers the energy cost for this oxidation. Total NO_x removal improves with increasing input energy deposition, while the temperature has a smaller effect on the total NO_x conversion. However, these parameters affect significantly the concentrations of NO, C_3H_6, and CO. The measured NO_x conversion was about 43% with energy cost down to 30 eV per NO_x molecule destroyed. Higher energy costs were obtained with more conventional DBDs. These results, obtained in very high voltage short rise time pulsed DBD, become compatible with motorist specifications.

More work is needed in order to enhance the energy efficiency as well as yields of the NO_x reduction reactions. Beside the optimization of the discharge parameters, the coupling of the DBD plasma with selected catalysts is an important parameter. Studies have been done and results will be presented in a forthcoming paper.

Acknowledgments

The authors gratefully appreciate the technical assistance of A Bonnet, J C Pellicer and B Dumax from GREMI, and of A Gremy from CBM (CNRS, Orléans), and wish to express their sincere thanks.

This work was performed in the frame of the French ECODEV—PREDIT program (CNRS) with financial support of the Groupement d'Intérêt Economique (GIE) PSA Peugeot-Citroën-RENAULT SA under contract number 97DI0024.

References

[1] Penetrante B M and Schultheis S E (ed) 1993 *Non-thermal Plasma Techniques for Pollution Control* (part A and B) (New York: Springer) p 187
[2] Penetrante B M, Brusasco R M, Merrit B T, Pitz W J, Vogtlin G E, Kung M C, Kung H H, Wan C Z and Voss K E 1998 *SAE Technical Paper Ser.* No 982508
[3] Hoard J and Balmer M L 1998 *SAE Technical Paper Ser.* No 982429
[4] Balmer M L, Tonkin R, Yoon S, Kolwaite A, Barlow S, Maupin G and Hoard J 1999 *SAE Technical Paper Ser.* No 1999-01-3640
[5] Higashi M, Uchida S, Suzuki N and Fujii K 1992 *IEEE. Trans. Plasma Sci.* **20** 1
[6] Penetrante B M, Brusasco R M, Merrit B T, Pitz W J and Vogtlin G E 1999 *SAE Technical Paper Ser.* No 1999-01-3637
[7] Chang M B, Kushner M J and Rood M 1992 *Environ. Sci. Technol.* **26** 777
[8] Vogtin G E and Penetrante B M 1993 *Non-thermal Plasma Techniques for Pollution Control, part B: Electron Beam and Electrical Discharge Processing* ed Penetrante B M and Schultheis S E (New York: Springer) p 187
[9] Penetrante B M, Hsiao M C, Merrit B T and Vogtlin G E 1997 *Workshop on Diesel Engine Emissions Reduction* (San Diego, 28–31 July)
[10] Hammer T and Bröer S 1999 *SAE Technical Paper Ser.* No 1999-01-3633
[11] Fisher G B, DiMaggio C L and Sommers J W 1999 *SAE Technical Paper Ser.* No 1999-01-3685
[12] Petunchi J O and Hall W K 1993 *Appl. Catal. B: Environ.* **2** L17
[13] Shelef M, Montreuil C N and Jen H W 1994 *Catal. Lett.* **26** 277
[14] Masuda S and Nakao H 1990 *IEEE Trans. Ind. Appl.* **26** 374
[15] Dhali S K and Sardja I 1991 *J. Appl. Phys.* **69** 6319

[16] Penetrante B M, Hsiao M C, Bardsley J N, Merrit B T, Vogtlin G E, Wallman P H, Kuthi A, Burkhart C P and Bayless J R 1996 *Pure Appl. Chem.* 68 1083
[17] Evans D, Rosocha L A, Anderson G K, Coogan J J and Kushner M J 1993 *J. Appl. Phys.* 74 5378
[18] Frank N W 1995 *Radiat. Phys. Chem.* 45 989
[19] Niessen W, Wolf O, Schruft R and Neiger M 1998 *J. Phys. D: Appl. Phys.* 31 542
[20] Khacef A, Viladrosa R, Cachoncinlle C, Robert E and Pouvesle J M 1997 *Rev. Sci. Instrum.* 68 2292
[21] Gentile A C and Kushner M J 1995 *J. Appl. Phys.* 78 2074
[22] Dorai R and Kushner M J 1999 *SAE Technical Paper Ser.* No 1999-01-3683
[23] Khacef A, Pouvesle J M and Cormier J M 2001 *Proc. 15th International Symp. on Plasma Chemistry (ISPC15)* p 3079
[24] Puchkarev V, Roth G and Gundensen M 1998 *SAE Technical Paper Ser.* No 982516
[25] Pitz W J, Penetrante B M, Hsiao M C and Vogtlin G E 1997 *Fall Meeting of the Western States Section of the Combustion Institute (Diamond Bar, California, 23, 24 October)*
[26] Penetrante B M and Mclarno C R 1998 *SAE Technical Paper Ser.* No 982433
[27] Fresnet F 2001 *PhD Thesis* Paris Sud University, France
[28] Dorai R and Kushner M J 2001 *J. Phys. D: Appl. Phys.* 34 574
[29] Shin H H and Yoon W S 2000 *SAE Technical Paper Ser.* No 2000-01-2969
[30] Bröer S, Hammer T and Kishimoto T 1997 *Proc. 12th International Conf. on Gas Discharges and Their Applications (Greifswald)* p 188

2001-01-3508

Non-thermal plasma assisted catalytic NO_x remediation from a lean model exhaust

O. Gorce, H. Jurado, C. Thomas and G. Djéga-Mariadassou
Laboratoire de Réactivité de Surface, Université Pierre et Marie Curie

A. Khacef, J.M. Cormier and J.M. Pouvesle
Laboratoire GREMI, Université d'Orléans

G. Blanchard
Rhodia

S. Calvo[1], Y. Lendresse[2]
GIE PSA Peugeot Citroën [2] – Renault [1]

ABSTRACT

No efficient catalyst presently exists for deNO$_x$ in lean burn conditions. Furthermore, actual catalysts generally deactivate during reaction. A cylindrical DBD non-thermal plasma reactor was coupled with a stable three-function catalyst in order to verify the nature of the effect of the plasma on the catalytic process. A mixture of $NO/O_2/C_3H_6$ in N_2 was used as a lean model exhaust. The plasma was found to perform two of the three functions: NO oxidation to NO_2 and propene activation through the partial oxidation of the hydrocarbon to aldehyde or alcohol. A complete catalyst containing the first two previous functions and the associative chemisorption of NO (third function) was used, as well as a simplified catalyst containing only the third function. Results suggest an advantageous plasma-catalyst coupling effect on NO_x remediation in accordance with the proposed catalytic model.

INTRODUCTION

No stable and sufficiently active catalyst has yet been designed to reduce the NO_x ($NO+NO_2$) emission from automotive exhaust gases in lean conditions.

The coupling of a non-thermal plasma to a catalyst is one of the engineering processes which has attracted much attention over the last few years. The present paper tries to answer the following questions :

(i) Why can a plasma help the catalytic deNO$_x$reaction ?

(ii) How can one design a catalyst taking into account the gas composition at the outlet of the plasma reactor ?

(iii) How can one design a catalyst, which does not deactivate with time on stream, to prove the plasma effect contribution to the catalytic process ?

Several catalytic models for the deNO$_x$ process can be encountered in the literature. For a NO/O_2/hydrocarbon feed, they generally depend on the nature of the active site. Over a zerovalent precious metal such as well-reduced platinum, NO is considered to dissociate and the hydrocarbon cleans the oxygen atoms left by NO to regenerate the metallic site Pt(0) [1]. Another way considers cations as active sites (such as cobalt, copper, and iron... or any other transition metal cation on an acidic support such as zeolites). In this case, nitro or nitroso organic intermediates are invoked [2] leading to N_2 or N_2O during the NO "reduction" in the presence of hydrocarbon. Joubert et al. [3] recently reported the presence of minor intermediates such as $C_xH_yO_z$, $C_xH_yN_z$, $C_xH_yN_zO_t$ detected in course of the $C_3H_6/NO/O_2/H_2O$ reaction over Pt/Alumina.

Unfortunately, zeolite supported catalysts deactivate rapidly and cannot be used at this point for industrial deNO$_x$ applications (Deactivation can occur due to coking or dealumination-sintering of the zeolite support during reaction at high temperature in the presence of water vapor).

We recently proposed a general kinetic approach from Three-Way Catalysis (TWC) to deNO$_x$ reaction [4]. Berger [5] has shown that three catalytic functions are necessary for deNO$_x$ assisted by methane, over a Co-Pd/HMOR catalyst (HMOR = acidic mordenite) patented by IRMA and Gaz de France [6]:

- ✓ 1st function : oxidation of NO to NO_2 (over cobalt oxide)
- ✓ 2nd function : hydrocarbon activation, owing to NO_2, through a mild oxidation step leading to $C_xH_yO_z$ intermediate species such as aldehydes or alcohols (over palladium oxide)
- ✓ 3rd function : associative chemisorption of 2 NO molecules - on a transition metal cation stabilized by the support - followed by the formation of N-N bond and subsequent scissions of either 1 N-O bond (leading to N_2O) or 2 N-O bonds (leading to N_2). The previous $C_xH_yO_z$ intermediate species can achieve their own total oxidation by cleaning the oxygen atoms left by NO.

In the present work, a new catalyst - named A - was designed including these three functions [7]. This catalyst is a Rh^{III}/CeO_2-ZrO_2 based material, as previously described elsewhere [4], to which a second and a third function were added. Furthermore, it will be shown in this paper that its activity remains stable during runs in the presence of both hydrocarbon and water vapor. This catalyst was coupled at the outlet of the plasma reactor.

A second catalyst - named B - was designed to contain only the third function assuming that the plasma would provide the first two as already suggested by Penetrante et al. [8]. This B material is typically Rh^{III}/CeO_2-ZrO_2 [4].

The catalyst support, i.e. CeO_2-ZrO_2, is not acidic and therefore does not deactivate in the presence of hydrocarbon (no coking). In addition, such a support was found to be highly stable in the presence of water.

EXPERIMENTAL

The electrical discharge reactor used was a dielectric-barrier discharge (DBD). The reactor geometry was one of a wire to cylinder type. It consisted of a tungsten wire (0.9 mm diameter) in a long dielectric (quartz) tube with inner and outer diameters of 11 mm and 13 mm, respectively. The dielectric tube was covered by an aluminum foil to form the outer electrode. The length of the outer electrode can be adjusted and then determines the active volume of the DBD reactor. The results presented in this paper were obtained with a volume of 16 cm^3. The DBD reactor was placed inside a tubular furnace (SR-A, Nabertherm) and the gas mixture temperature can be adjusted from room temperature to 500°C.

The DBD reactor was powered by a high-voltage power supply. This pulse generator is capable of delivering open circuit high voltage pulses up to 150 kV output into 80 ns (FWHM) pulses and short voltage rise times (40 ns) at variable repetition rates up to kilohertz. The fast voltage rise time allows for significant over-voltage at breakdown. The pulse repetition rate could be adjusted from single shot regime to 1 kHz (up to 200 Hz in the present work).

The voltage and current wave-forms were recorded by an oscilloscope (Tektronix 2440) using Tektronix P6015A high voltage probe (1000x) and Europulse 9001 current probe, respectively.

The electrical energy deposition in the plasma reactor was measured with a capacitive circuit. The input energy density, Joules per liter ($J.L^{-1}$), is the ratio of the product of the discharge pulse energy and the pulse repetition frequency to the gas flow rate in standard conditions (25°C and 1 atm). In these experiments, the input energy density (typically up to around 30 $J.L^{-1}$ for all measurements) can be modified by changing the pulse repetition frequency from single shot regime to 200 Hz. The discharge pulse energy was maintained constant at about 35 $mJ.pulse^{-1}$.

The catalysts were placed downstream of the plasma device in the oven as shown in Figure 1 and the catalyst volume was chosen in order to obtain a space velocity of 45000 h^{-1}.

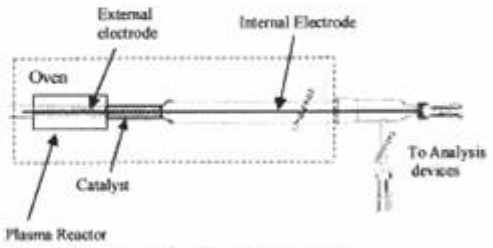

Figure 1. Dielectric Barrier Experimental device

Reactant gases were fed from independent mass flow controllers (Brooks 5850TR) and the total flow rate was set to 150 $NL.h^{-1}$. The Temperature Programmed Surface Reaction (TPSR) experiments were carried out from 30°C up to 350°C with a heating rate of 1°C.min^{-1}.

The NO_x ($NO + NO_2$) products were quantified by a QUINTOX KM9606 analyzer equipped with an electrochemical cell. This does not analyze N_2O on line. However separate experiments carried out in a different experimental device allowed us to follow N_2O on line in the absence of plasma (see hereafter).

All the different experimental parameters are summarized in Table 1. These values were given by natural gas combusters. They were used in this study for a sake of comparison with Berger's data [5].

TABLE 1: EXPERIMENTAL CONDITIONS

Catalyst Weight	5 g
NO	340 vol. ppm
O_2	8 vol. %
C_3H_6	1900 vol. ppm C_3
N_2	Balance
Temperature	From 30 to 350°C (1°C.min^{-1})
Space Velocity	45000 h^{-1}
Energy Deposition	36 J.L^{-1}

Some additional experiments (Figures 4 and 5) were performed in a different experimental set up. These experiments were carried out in a U-type quartz reactor using 0.5 g of catalyst and the different flow rates were adjusted to maintain both the same reactant concentrations and space velocity as reported in Table 1. However in these cases, the heating rate was set to 10°C.min^{-1}.

The reactor outflow was analyzed using a combination of three different detectors. A Eco Physics CLD 700 AL NO_x chemiluminescence analyzer (for NO and total NO_x (i.e. NO + NO_2)) allowed the simultaneous detection of both NO and NO_x. An Ultramat 6 IR analyzer was used to monitor N_2O and a FID detector was used to follow the propene concentration. The use of a mass spectrometer (Hiden HPR 20) in a separate set of experiments did not show the presence of aldehydes nor alcohols in the reactor outlet gas mixture. Since these species were detected as traces in Berger's work [5], this was interpreted in terms of high reactivity of such intermediates.

RESULTS AND DISCUSSION

The aim of this paper is to show the role of plasma, taking into account both the reaction pathway already established [4] and the composition of gases at the outlet of a plasma reactor. To show that the plasma gas exhaust produces the active intermediates needed for scavenging of oxygen species left on the active site (3rd function) by $(NO)_2$ dissociation, it is convenient to develop here a general scheme for deNO_x reaction.

The general scheme considers, on the 3rd function, the co-adsorption of two NO molecules, acting as ligands for Rh^{z+}. This co-adsorption is called a "associative NO adsorption" process [4]. The two NO molecules having an unpaired electron, the N-N bond is formed at this point. The associative NO adsorption is followed by subsequent N-O bond scissions and N_2 production whereas oxygen species left by this NO dissociation inhibit the Rh^{z+} site.

Activated hydrocarbon species - called $C_xH_yO_z$ and detected by Berger [5] as alcohol and aldehyde - are necessary to remove the oxygen species left by $(NO)_2$ dissociation. In the case of catalytic experiments carried out without plasma and in the presence of the complete catalyst A, those $C_xH_yO_z$ species are formed due to a mild oxidation of HC by NO_2. This latter reaction is generally admitted by the international community working on deNO_x processes.

As the plasma gas exhaust contains both NO_2 and $C_xH_yO_z$ species (Figure 3), we can expect that the coupling of a plasma and a suitable catalyst provides the aldehyde and/or alcohol necessary to clean the active site from the adsorbed oxygen species allowing NO to adsorb again. Therefore the catalytic cycle could turn over. NO_2 can oxidize, over the catalyst, the HC molecules which have not been transformed to $C_xH_yO_z$ species yet.

In order to clean the adsorbed oxygen atoms left by the dissociation of two NO molecules, the three functions (Figure 2) should occur simultaneously in order to provide $C_xH_yO_z$ species, the activated form of the reducer. The support must be able to stabilize a transition metal cation, as for a zeolite support. However it must not be acidic as to avoid the hydrocarbon cracking which leads to coke formation and consequently to a strong deactivation of the catalyst. We have already shown [4] that CeO_2-ZrO_2 is able to stabilize 100% surface Rh^{z+} species.

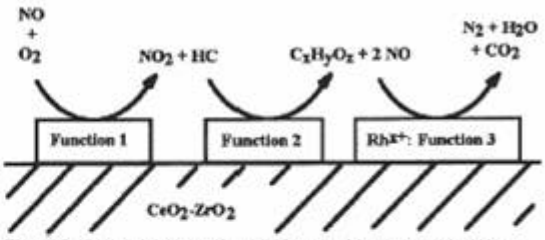

Figure 2. General scheme for deNOx reactions as deduced from Berger [5], over CoPd/HMOR. HC = Hydrocarbon, $C_xH_yO_z$ = mainly aldehyde or alcohol.

1. COMPOSITION OF PLASMA EXHAUST GASES

Analysis of gas composition at the outlet of the plasma reactor revealed the existence of compounds already reported in the literature [9,10]. On Figure 3, we should highlight the presence of aldehyde (CH_2O), RNO_x (CH_3ONO_2), formic acid (CH_2O_2) and nitrogen dioxide (NO_2). Small amounts of nitrous acid (HNO_2) were also observed indicating the presence of moisture in the analytical system.

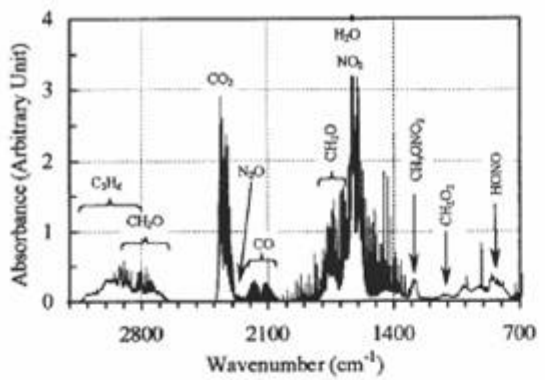

Figure 3. Typical FTIR spectrum measured in the presence of plasma in a NO(340ppm)/O_2(8%)/C_3H_6(1900ppm) mixture at room temperature – empty reactor – SV=45000 h^{-1}

2. DENO$_x$ REACTION OVER THE COMPLETE CATALYST "A" (THREE FUNCTIONS)

After flowing the NO/O_2/C_3H_6 mixture at room temperature on the catalyst to recover the initial feed composition, Figure 4 shows the NO_x and propene concentrations (ppm) versus reaction temperature. After a first desorption of NO, NO_2 and N_2O around 101°C, which releases after NO adsorption during the initial reactor flushing with the feed, propene is mildly oxidized up to 225°C where the deNO$_x$ process starts. A maximum of 55% consumption of NO_x including 13% towards N_2O is observed at a temperature of 300°C. In this transient temperature programmed surface reaction (TPSR), the nitrogen balance thus corresponds to 42% deNO$_x$ to N_2 at 300°C.

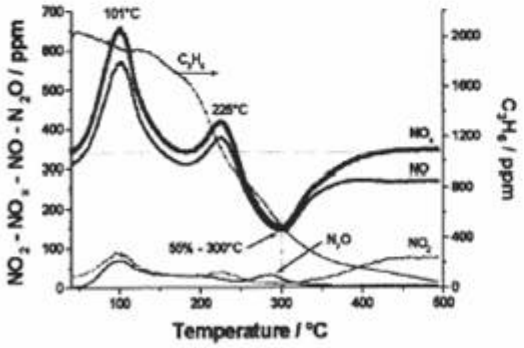

Figure 4. TPSR (10°C.min^{-1}) of NO(340ppm)/O_2(8%)/C_3H_6(1900ppm) from 30 to 500°C - Catalyst A – SV=45000 h^{-1}

3. STABILITY OF CATALYST "A" (THREE FUNCTIONS) WITH TIME ON STREAM IN THE PRESENCE OF WATER VAPOR AT 270°C

Figure 5 reports the stability of the complete catalyst "A" in the presence of 1.7 vol. % water for a 36 hour period. It can be seen that the catalyst activity is stable. In order to evidence the role of plasma, we needed a stable catalyst.

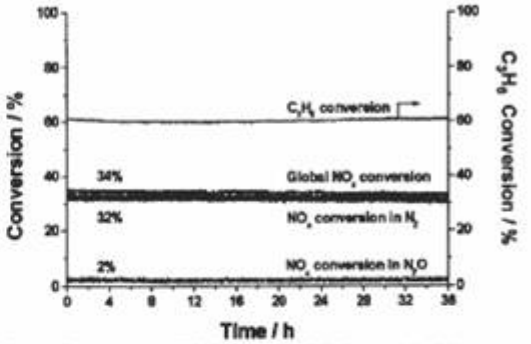

Figure 5. Isotherm at 270°C under a NO(340ppm) / O_2(8%) / C_3H_6(1900ppm) / H_2O(1.7%) mixture – Catalyst A – SV=45000 h^{-1}

4. FORMATION OF RNO$_x$ SPECIES BY THE PLASMA IN THE ABSENCE OF A CATALYTIC MATERIAL

Figure 6 shows the NO_x concentration at the outlet of the plasma reactor, as measured at the outlet of the empty catalytic reactor. The upper plot shows the 340 ppm NO_x mixture in the absence of plasma which corresponds to the initial synthetic feed and is quite stable as the temperature rises.

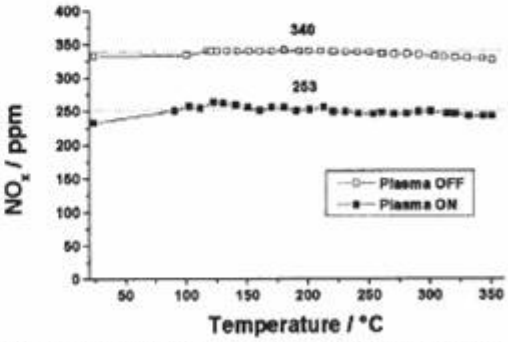

Figure 6. NO_x concentration versus reaction temperature in the presence or absence of plasma (36 J.L^{-1}) during a TPSR (1°C.min^{-1}) of NO(340ppm)/O_2(8%)/C_3H_6(1900ppm) – Empty reactor

When the plasma was applied, it can be seen that 87 ppm of NO_x were consumed. From a detailed gas

chromatography analysis of the mixture at the outlet of the reactor, it appears that this NO_x consumption must mainly be attributed to the formation of RNO_x species as already suggested in previous work [10].

5. SUPPORT ALONE IN THE CATALYTIC REACTOR

In the absence of plasma in the first reactor, the catalyst support is shown to store (chemisorption) NO_x between 125 and 170°C (Figure 7), then to release NO_x in two steps, from 170 to 240°C and from 240 to 320°C.

If plasma is applied, storage of NO_x, probably as NO, NO_2 and RNO_x (as described for the plasma alone in section 4) occurs from room temperature up to around 170°C. A loss of NO_x then occurs up to 350°C probably due to a RNO_x formation.

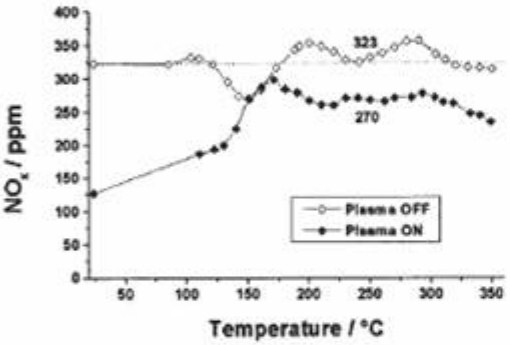

Figure 7. NO_x concentration versus reaction temperature in the presence or absence of plasma (36 $J.L^{-1}$) during a TPSR (1°C.min^{-1}) of NO(340ppm)/O_2(8%)/C_3H_6(1900ppm) – Catalyst Support – SV=45000 h^{-1}

6. ACTIVITY OF THE SIMPLIFIED CATALYST "B" CONTAINING ONLY THE THIRD FUNCTION (NO ASSOCIATIVE ADSORPTION FOLLOWED BY ITS DISSOCIATION, AND OXYGEN REMOVAL BY THE PARTIALLY OXIDIZED HYDROCARBON)

In the absence of plasma, this catalyst "B" exhibits a low $deNO_x$ activity. The upper plot in Figure 8 shows a NO_x chemisorption at about 125°C, similar to that observed on the support alone (Fig. 7). Then the $deNO_x$ reaction occurs at about 280°C, with a very low conversion (about 8%).

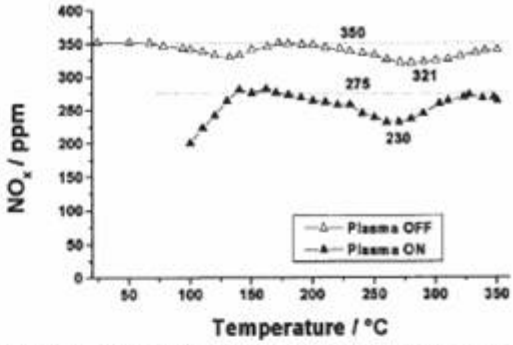

Figure 8. NO_x concentration versus reaction temperature in the presence or absence of plasma (36 $J.L^{-1}$) during a TPSR (1°C.min^{-1}) of NO(340ppm)/O_2(8%)/C_3H_6(1900ppm) – Catalyst B - SV=45000 h^{-1}

In the presence of plasma (Fig. 8, lower plot), the NO_x chemisorption observed on the support (Fig. 7) occurs up to 125°C and a global $deNO_x$ reaction is detected at around 270°C. At this latter temperature, 230 ppm of NO_x are still present at the outlet of the catalytic reactor, corresponding to a 34 % global consumption of NO_x (considering the initial feed composition without plasma). Taking into account the RNO_x produced by the plasma itself (Fig. 6), a true $deNO_x$ conversion can be calculated, considering the RNO_x baseline at about 275 ppm NO_x. The conversion to N_2 is then equal to 13% ([275-230]/340), instead of 8% previously found in the absence of plasma (Fig. 9). Thus, it can be assumed that the plasma provides the NO_2 (first function of the complete catalyst "A") and $C_xH_yO_z$ species (second function of the complete catalyst "A") necessary over this simplified catalyst "B" (including only the third function) to proceed to the $deNO_x$ reaction to N_2.

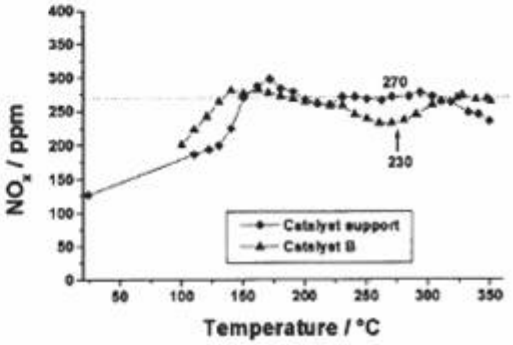

Figure 9. NO_x concentration versus reaction temperature in the presence of plasma (36 $J.L^{-1}$) during a TPSR (1°C.min^{-1}) of NO(340ppm)/O_2(8%)/C_3H_6(1900ppm) – Catalyst Support and Catalyst B - SV=45000 h^{-1}

7. EFFECT OF PLASMA ON THE COMPLETE CATALYST "A" (THREE FUNCTIONS)

The upper plot in Figure 10 reports the $deNO_x$ activity of catalyst "A" in the absence of plasma. At 270°C, a 32% NO_x consumption is observed. By extrapolating the data from Figure 5, this NO_x consumption can be attributed to a 30% N_2 formation and a 2% N_2O formation.

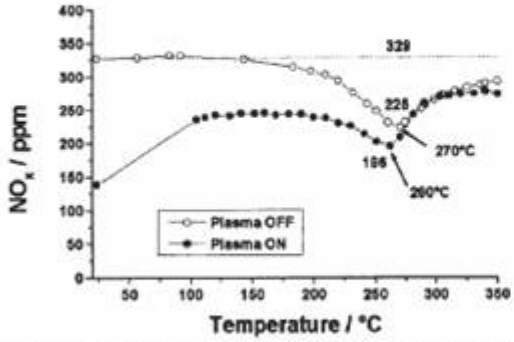

Figure 10. NO_x concentration versus reaction temperature in the presence or absence of plasma (36 $J.L^{-1}$) during a TPSR (1°C.min^{-1}) of NO(340ppm)/O_2(8%)/C_3H_6(1900ppm) – Catalyst A - SV=45000 h^{-1}

If plasma is applied, the lower plot in Figure 10 again shows a chemisorption of NO_x or/and RNO_x up to 110°C over the catalyst, then a steady-state is observed, corresponding to 250 ppm of NO_x as detected over the catalyst support (Figure 7). At a higher temperature, the $deNO_x$ process occurs and the effect of plasma is quite clear. Indeed, the global NO_x consumption is now 40% ([329-196]/329) and it occurs at a lower temperature (260°C) than that observed without plasma (270°C).

Once more, the general features of the global $deNO_x$ process to N_2 are observed, as shown in Figure 4 even though this experiment has been carried out in a different experimental setup.

8. COMPARISON BETWEEN THE SIMPLIFIED CATALYST "B" (THIRD FUNCTION ONLY) BEHAVIOR IN THE PRESENCE OF PLASMA, AND THE COMPLETE CATALYST "A" IN THE ABSENCE OF PLASMA

If our assumption that the plasma provides the first two functions (NO_2 formation and production of $C_xH_yO_z$ intermediates) to the catalyst, the $deNO_x$ activity of catalyst "B" in the presence of plasma must be comparable to that of catalyst "A" in the absence of plasma. Indeed, NO_2 is able to partially oxidize HC. $C_xH_yO_z$ produced by the plasma reactor suffers a deeper oxidation to CO_2 and H_2O thereby cleaning the active site from the oxygen left by NO dissociation. We were able to verify in this work by flowing propan-2-ol instead of C_3H_6 over Rh^{III}/CeO_2-ZrO_2 (catalyst B). It was found that the $deNO_x$ reaction occurs at the same temperature as for the complete catalyst in the absence of plasma.

Figure 11 shows that the $deNO_x$ conversion at about 270°C is almost the same for both catalysts. Nevertheless, the behavior between room temperature and 170°C is quite different, due to the probable RNO_x formation in the plasma and their subsequent adsorption on the catalyst support, as evidenced by Beutel et al. [2].

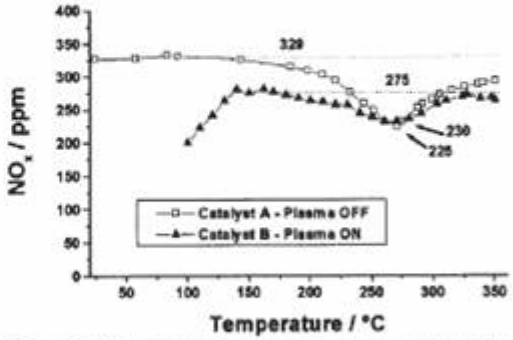

Figure 11. NO_x concentration versus reaction temperature in the presence of plasma (36 $J.L^{-1}$) (Catalyst B) and in the absence of plasma (Catalyst A) during a TPSR (1°C.min^{-1}) of NO(340ppm)/O_2(8%)/C_3H_6(1900ppm) - SV=45000 h^{-1}

CONCLUSION

A general model for $deNO_x$ reaction was proposed. It assumed, by extrapolating the results obtained by Berger in our group [5], that three functions are necessary for a catalyst to proceed to a $deNO_x$ reaction : (i) oxidation of NO to NO_2; (ii) usage of NO_2 for partial oxidation of the hydrocarbon (reductant of NO); (iii) associative chemisorption of 2 NO molecules leading to a surface dinitrosyl intermediate species and subsequent N-O bond scissions leading to N_2 (or N_2O if the catalyst is not efficient enough); then the partial oxidized hydrocarbon (aldehyde and/or alcohol) proceeds to the cleaning of residual oxygen atoms left by NO dissociation.

A complete catalyst "A" including the three functions and a simplified catalyst "B" including the third function were coupled to a cylindrical DBD non-thermal plasma reactor. These two kinds of catalysts were found to be stable under the experimental conditions, allowing a reliable evaluation of the effect of the plasma on the catalytic process.

It was found that the plasma, leading to the formation of both NO_2 and $C_xH_yO_z$ intermediate species, could substitute for the first two functions of the complete catalyst "A". As a consequence, catalyst "B" in the presence of plasma was found to be equivalent to catalyst "A" in the absence of plasma. This result demonstrates

what can be the role of plasma in non-thermal plasma assisted catalytic NO_x remediation. Furthermore, plasma is able to provide both NO_2 and $C_xH_yO_z$ intermediate species at low temperature.

However, the behavior of the RNO_x species formed in the plasma still remains to be studied. Indeed, in order to definitely confirm that the NO_x removal leads mainly to dinitrogen, a complete nitrogen balance would be needed.

ACKNOWLEDGMENTS

This program was performed with the financial support of the Groupement d'Intérêt Economique (GIE) PSA Peugeot Citroën et Renault. The catalyst support was provided by Rhodia.

REFERENCES

[1] "Mechanism of the selective reduction of nitrogen monoxide on platinum-based catalysts in the presence of excess oxygen"; R. Burch, P.J. Millington and A.P. Walker, Appl. Catal. B, 4, 65 (1994)
[2] "Potential reaction paths in NO_x reduction over Cu/ZSM5"; T. Beutel, B. Adelman and S. Sachtler, Catal. Lett., 37 (1998) 125
[3] "GC-MS identification of organic by-products of the NO SCR by propene"; E. Joubert, J.C. Menezo, D. Duprez and J. Barbier, CAPOC V (2000) pp 149-158
[4] "A general model for both three-way and deNO_x catalysis: dissociative or associative nitric oxide adsorption, and its assisted decomposition in the presence of a reductant – Part I. Nitric oxide decomposition assisted by CO over reduced or oxidized rhodium species supported on ceria" G. Djéga-Mariadassou, F. Fajardie, J.-F. Tempère, J.-M. Manoli, O. Touret, G. Blanchard, J. Mol. Catal. A, 161 (2000) 179
[5] M. Berger, PhD Thesis, Pierre et Marie Curie University (1999)
[6] C. Hamon, O. Le Lamer, N. Morio, J.Saint-Just, 1998, PCT WO 98/15339
[7] O. Gorce, C. Thomas, G. Djéga-Mariadassou, G. Blanchard, French Patent Registered # 0009678 (July 24th, 2000)
[8] "Plasma-assisted catalytic reduction of NO_x"; B. Penetrante, R.M. Brusasco, B.T. Merritt, W.J. Pitz, G.E. Vogtlin, M.C. Kung, H.H. Kung, C.Z. Wan and K.E. Voss, SAE Paper 982508
[9] "Analysis of plasma-catalysis for diesel NO_x remediation"; J. Hoard, M. Lou Balmer, SAE Paper 982429
[10] "Effect of propene on the remediation of NO_x from engine exhausts"; R. Doraï and M.J. Kushner, SAE Paper 1999-01-3683

CONTACT

For further information please contact:
Pr G. Djéga-Mariadassou
Laboratoire de Réactivité de Surface
Université Pierre et Marie Curie
4 Place Jussieu –Case 178
75252 Paris Cedex 05
France
Tél.: (33) 1 44 27 36 26
Fax.: (33) 1 44 27 60 33
e-mail: djega@ccr.jussieu.fr

J. Phys. D: Appl. Phys. 32 (1999) 176–182. Printed in the UK PII: S0022-3727(99)93066-8

Characterization of afterglow kinetics at atmospheric pressures by emission spectroscopy. I: reactions of neon ions with N_2

A Khacef, O Motret and J Stevefelt

Groupe de Recherches sur l'Energétique des Milieux Ionisés, Université d'Orléans, BP 6759, 45067 Orléans Cedex 2, France

Received 6 April 1998, in final form 10 August 1998

Abstract. The afterglow of a 1 kA, 10 ns duration discharge in neon at 1–4 bar pressure containing up to 10 mbar of reactant admixture N_2 was studied by time-resolved emission spectroscopy. Destruction rates of neon ions have been experimentally determined from the selectively excited fluorescence of N_2^+ emitted as the result of charge transfer. Reasonable agreement with previously reported results was obtained over the smaller range of nitrogen pressures (below 0.8 mbar) used in those studies. Data obtained at reactant pressures higher than about 1.2 mbar were consistent with a kinetic model in which vibrationally excited Ne_2^+ ions play an important role. The slow collisional relaxation of these ions (rate coefficient 3.7×10^{-13} cm^3 s^{-1}) would limit the rate of Ne^+ to Ne_2^+ conversion at neon pressures higher than about 0.2 bar.

1. Introduction

In the past, the development of high-pressure gas lasers has emphasized the importance of charge and excitation transfer mechanisms in atmospheric pressure plasmas. Continued interest in the subject has been stimulated by research on discharge lamps, plasma displays, and other opto-electronic devices.

A buffer gas such as He, Ne or Ar is usually used to improve discharge characteristics. Plasma kinetics are then dominated by energy-storing ionic and metastable excited species, and many of their key features are determined by various transfer mechanisms. Among the large number of reactions of interest, those involving helium ions and metastables have been most extensively studied both at low pressures (Fehsenfeld *et al* 1966, Bohme *et al* 1970, Schmeltekopf and Fehsenfeld 1970) and high pressures (Chen *et al* 1977b, Collins and Lee 1978, Jahani *et al* 1988, Pouvesle *et al* 1988). Fewer direct measurements of the reaction rates concerning the corresponding neon species have been made (Chen *et al* 1977a, Collins and Lee 1980, Mayhew 1992). In the kinetic modelling of high-pressure lasers using neon or argon as the buffer gas, many reaction rates remain unknown and are simply extrapolated from measured low-pressure data, or from the better known rates in helium. However, high-pressure studies have revealed the existence of previously unsuspected reaction channels, involving atoms of the background gas acting as third bodies (Lee *et al* 1976) or diatomic molecules in high vibrational states (Pouvesle *et al* 1985) that may become important at pressures of a few hundreds of millibar. This paper reports an extension of our studies of charge transfer reactions and the rates at which they occur to the case of atmospheric pressure neon afterglows.

As a convenient method to monitor the time evolution of neon ions, previous workers (Chen *et al* 1977a, Collins and Lee 1980) used the fluorescence $N_2^+(B\,^2\Sigma_u)_{v=0} \rightarrow N_2^+(X\,^2\Sigma_g)_{v=0,1}$, emitted when an appropriate amount of nitrogen is added to the gas mixture. The reactivity of atomic Ne^+ ions with N_2 in its lowest vibrational states $v = 0$ and 1 has been shown (Albritton *et al* 1973) to be undetectably low ($<10^{-14}$ cm^3 s^{-1}). These authors explained their finding in terms of the poor Franck–Condon factors that exist because of the high vibrational levels ($v>10$) of the $N_2^+(B\,^2\Sigma_u)$ ions that would have to be populated in order to provide energy resonance. The low reactivity of Ne^+ with N_2 has been confirmed more recently (Mayhew 1992). In contrast, the diatomic Ne_2^+ ion is known to react with N_2 at a rate that is close to the value of 7.7×10^{-10} cm^3 s^{-1} calculated using Langevin theory for non-polar molecules (Bohme *et al* 1970, Collins and Lee 1980, Mayhew 1992). In this case, the energy available in the vertical transition from the $(Ne_2^+)_{v=0}$ state to the repulsive Ne_2 ground state $X\,^1\Sigma_g$ at the equilibrium internuclear separation $R_e = 3.3a_0$ is equal to about 19 eV (Cohen and Schneider 1974), providing close resonance with the $N_2(X\,^1\Sigma_g)_{v=0} \rightarrow N_2^+(B\,^2\Sigma_u)_{v=0,1}$ transition for which the Franck–Condon factor is large.

The afterglow plasma is also expected to contain a high concentration of metastable neon atoms, having enough energy to produce only the $N_2^+(X\,^2\Sigma_g)$ and $(A\,^2\Pi_u)$

0022-3727/99/020176+07$19.50

states in their lowest vibrational levels through Penning reactions. Hence, time-resolved observation of the $N_2^+(B\,^2\Sigma_u)$ fluorescence would provide a selective monitor of the Ne_2^+ ion concentration in a neon–nitrogen plasma.

Nevertheless, using a weak proton beam excitation at neon pressures of 31 and 100 Torr, Chen *et al* (1977a) reported a rate coefficient of only 7.2×10^{-11} cm^3 s^{-1} for the charge transfer to nitrogen, whereas at higher pressures of 300 and 600 Torr the rate coefficient increased to 7.5×10^{-10} cm^3 s^{-1} and 9.7×10^{-10} cm^3 s^{-1} respectively. They ascribed the first value to the reaction of Ne^+, assumed to be the majority ion at those pressures, and they decomposed the high-pressure results in bimolecular and termolecular coefficients 5.3×10^{-10} cm^3 s^{-1} and 2.3×10^{-29} cm^6 s^{-1}, corresponding to the reactions

$$Ne_2^+ + N_2 \rightarrow N_2^+(B\,^2\Sigma_u)_{v=0} + 2\,Ne \qquad (1)$$

$$Ne_2^+ + N_2 + Ne \rightarrow N_2^+(B\,^2\Sigma_u)_{v=0} + 3\,Ne. \qquad (2)$$

Collins and Lee (1980) used intense electron beam discharges to excite high-pressure neon–nitrogen mixtures and they also found that two different ions might be involved in producing the N_2^+ fluorescence. Over the range of pressures from 1000 to 1500 Torr their data could be interpreted in terms of reactions (1) and (2), with bimolecular and termolecular rate coefficients of 8.6×10^{-10} cm^3 s^{-1} and 3.6×10^{-30} cm^6 s^{-1} respectively. At lower pressures, between 500 and 1000 Torr, the N_2^+ fluorescence decayed more slowly, and in a way that could be linearly extrapolated to a very small rate at zero neon pressure. This suggested that these lower pressure data were characteristic of the reaction of Ne^+, or of some population in kinetic equilibrium with Ne^+. This result was quite surprising because of the rapid termolecular process

$$Ne^+ + 2\,Ne \rightarrow (Ne_2^+)_v + Ne \qquad (3)$$

which would convert the initial Ne^+ population with a lifetime of ~15 ns at a pressure of 1000 Torr, unless the rate coefficients for reaction (3) obtained at low pressures (Johnsen *et al* 1980) are inappropriate at atmospheric pressures. In fact, as pointed out by Collins and Lee (1980), reaction (3) actually produces $(Ne_2^+)_v$ in a high vibrational state and a pressure dependent saturation of the subsequent relaxation process could exist.

These are, to our knowledge, the only studies of high-pressure neon–nitrogen afterglows performed so far. They obviously create some ambiguities which motivated the present work, focusing on the reactions of neon ions with N_2 over a much wider range of neon pressures and nitrogen concentrations. While this work confirms the data reported in earlier studies reasonably well, the extended parameter space makes it possible to construct a theoretical model to give a better understanding of experimental results.

2. Experimental method

The experimental arrangement that was used in this work is shown schematically in figure 1. Ultrahigh purity gas mixtures were prepared in a gas handling system including calibrated high-precision mass flowmeters. Nitrogen relative concentrations up to 0.25% could be obtained while the total pressure was set in the range from 1 to 4 bar. The gas was transversely excited between two aluminium electrodes 9 cm in length, spaced 5 cm apart, and having a flat profile over a width of 1 cm. Fast pulsed discharges were driven by a plate transmission line in a Blumlein-like circuit charged to 8–12 kV, corresponding to 0.03–0.07 J stored energy, and electrically switched by a hydrogen thyratron. Single pulses of 1 kA peak current and ~10 ns duration were produced at a repetition rate that could be varied between 1 and 16 Hz, and that was kept low enough to prevent gas heating. Hence, throughout this work gas densities were deduced from the measured pressures assuming a temperature of 300 K.

Plasma homogeneity was improved by using a corona preionization. A high-voltage pulse (10–60 kV), developed by a cable transformer which was driven by a thyratron switching a low-inductance capacitor, was applied to an external electrode separated from the gas by the dielectric material of the discharge cell. The time delay between preionization and the main discharge could be continuously varied to optimize the discharge characteristics. In direct observations the discharge appeared as a homogenous layer of 2–3 mm thickness, slightly decreasing with increasing neon pressure.

Visible light from the discharge was analysed with a 1 m high-resolution grating monochromator in a direction parallel to the plasma axis. The monochromator was provided with a fast rise time photomultiplier whose output was recorded with a 325 MHz oscilloscope (Tektronix 2440) connected to a computer. An optical fibre was used to synchronize the data acquisition system with the discharge.

3. Results and analysis

The time evolution of the (0, 0) vibrational component of the $N_2^+(B \rightarrow X)$ fluorescence at 391.4 nm, as typified by the data shown in figure 2, generally displayed an exponential decay over at least one decade, beginning rather rapidly after termination of the discharge current pulse. This behaviour defined a decay rate, ν, that was a function of the neon and nitrogen partial pressures only, and that had values in the range 10^7–10^8 s^{-1} as illustrated in figure 3.

In addition to spontaneous emission at a rate of 1.5×10^7 s^{-1}, the $N_2^+(B\,^2\Sigma_u, v = 0)$ state would be quenched in collisions with both Ne and N_2. The corresponding rate coefficients have been determined in low-pressure experiments ($P_{Ne} \leqslant 10$ Torr, Plain and Jolly 1984) to be 3.1×10^{-11} cm^3 s^{-1} and 8.2×10^{-10} cm^3 s^{-1} respectively. Even if these values were inappropriate at atmospheric pressures, where they would extrapolate to quenching rates in excess of 10^9 s^{-1}, it seems very unlikely that they should saturate at the destruction rates shown in figure 3. Rather, then, these results represent the decay rate of the reactant neon ion that produces the N_2^+ fluorescence, as was concluded in previous work (Lee *et al* 1976, Chen *et al* 1977a, b, Collins and Lee 1978, 1980).

Similarly to what was found previously, the data in figure 3 (except for the one point at $P_{Ne} = 1.2$ bar, $P_{N2} = 8.5$ mbar, see discussion below) could be described by linear

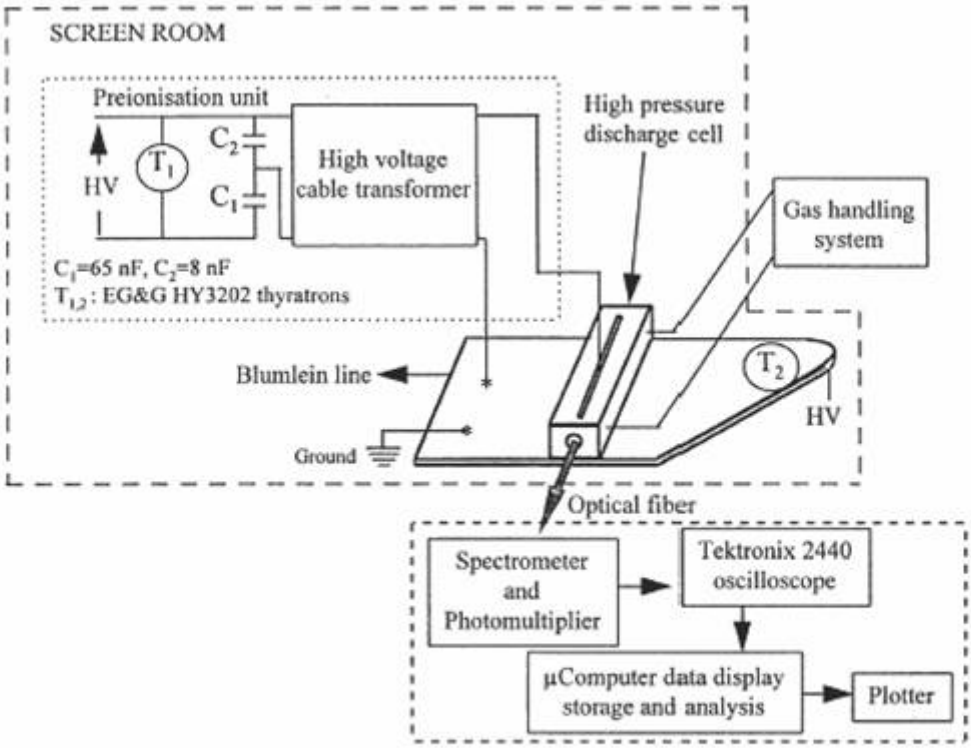

Figure 1. Experimental arrangement used for studying afterglow kinetics at atmospheric pressures.

approximations, but over two different ranges of nitrogen pressures:

$$\nu = \nu_0 + K_1[\mathrm{Ne}] + K_2[\mathrm{N_2}] \qquad (4)$$

where for low pressures, $P_{N2} < P^*_{N2}$ (see also figure 4),

$$\nu_0 = (3.2 \pm 1.0) \times 10^6\ \mathrm{s^{-1}}$$

$$K_1 = (1.2 \pm 0.2) \times 10^{-13}\ \mathrm{cm^3\ s^{-1}}$$

$$K_2 = (3.5 \pm 1.2) \times 10^{-10} + (2.6 \pm 2.0) \times 10^{-30}[\mathrm{Ne}]\ \mathrm{cm^3\ s^{-1}}$$

and for $P_{N2} > P^*_{N2}$

$$\nu_0 = 0 \qquad K_1 = (3.7 \pm 0.2) \times 10^{-13}\ \mathrm{cm^3\ s^{-1}}$$

$$K_2 = (2.6 \pm 0.1) \times 10^{-10}\ \mathrm{cm^3\ s^{-1}}.$$

In these expressions, square brackets denote concentrations in $\mathrm{cm^{-3}}$ and P^*_{N2} is the pressure at which the two linear approximations cross. The numerical values extracted from this analysis are not in concordance with values reported in the literature.

On the other hand, it should be stressed that our measured decay rates ν agree with those previously reported (Chen *et al* 1977a, Collins and Lee 1980) to within experimental error in the overlapping region of partial pressures ($P_{Ne} < 2$ bar, $P_{N2} < 0.8$ mbar). This is more readily apparent in figure 4, which is a blow-up of this region, and where we have compared our decay rates with those from previous works. Hence, a kinetic model that is able to describe our results would also, in principle, apply to the previously reported measurements.

In constructing such a model, we assumed the following three facts to be well established from experimental studies.

(i) At low neon pressures the three-body association, reaction (3), occurs with the rate coefficient $k_a \approx 6 \times 10^{-32}\ \mathrm{cm^6\ s^{-1}}$ reported in several papers, even if it could be impeded at high pressures by the inverse dissociation process having a rate coefficient k_d:

$$(\mathrm{Ne_2^+})_v + \mathrm{Ne} \rightarrow \mathrm{Ne^+} + 2\ \mathrm{Ne}. \qquad (5)$$

(ii) The reactivity of atomic $\mathrm{Ne^+}$ ions with $\mathrm{N_2}$ is vanishingly small.

(iii) $\mathrm{Ne_2^+}$ ions in their ground vibrational state $v = 0$ react with $\mathrm{N_2}$, the corresponding rate coefficient being close to the classical Langevin value of $k_g = 8 \times 10^{-10}\ \mathrm{cm^3\ s^{-1}}$.

Obviously, reactions (1)–(3) and (5) cannot alone explain the observed phenomenology displayed in figure 3. Instead, the possibility of two different neon species, both yielding the observed $\mathrm{N_2^+}$ fluorescence, must be considered. The more reactive species would dominate in the production of the detected radiation at low concentrations of $\mathrm{N_2}$, whereas at some sufficiently high pressure of $\mathrm{N_2}$ the formation of that species would become limited by the reaction of the other species, being a precursor or kinetic intermediate in the formation of the first species.

After due consideration of several possibilities, detailed agreement between experimental data and the kinetic model was achieved by identifying the more reactive species as being the $\mathrm{Ne_2^+}$ ion in its first vibrational states (which in the following we denote simply by $\mathrm{Ne_2^+}$), and the other species as a manifold of rovibrational states $(\mathrm{Ne_2^+})_v$ being formed by reaction (3). The transition from the low to the high $\mathrm{N_2}$

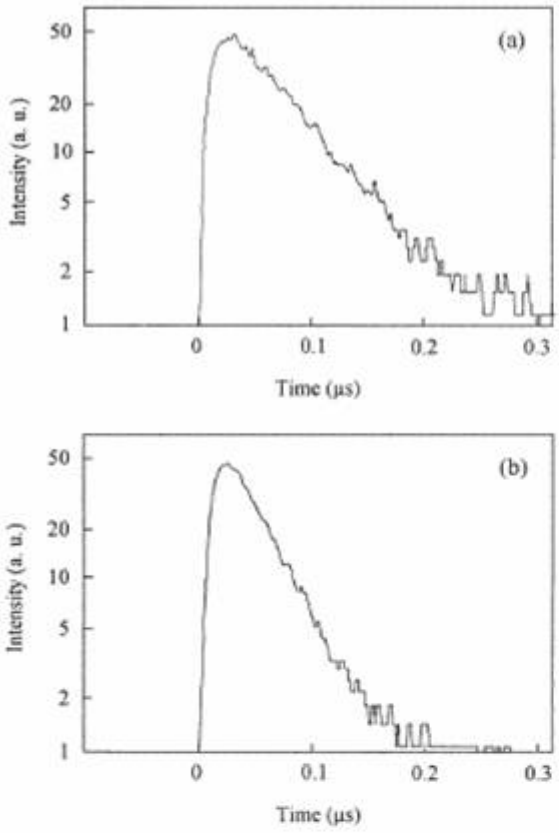

Figure 2. Time-resolved emission of the $N_2^+(B\,^2\Sigma_u)_{v=0} \rightarrow N_2^+(X\,^2\Sigma_g)_{v=0}$ transition at a wavelength 391.4 nm from the afterglow of 2.1 bar of neon with (a) 0.67 mbar and (b) 1.67 mbar of nitrogen.

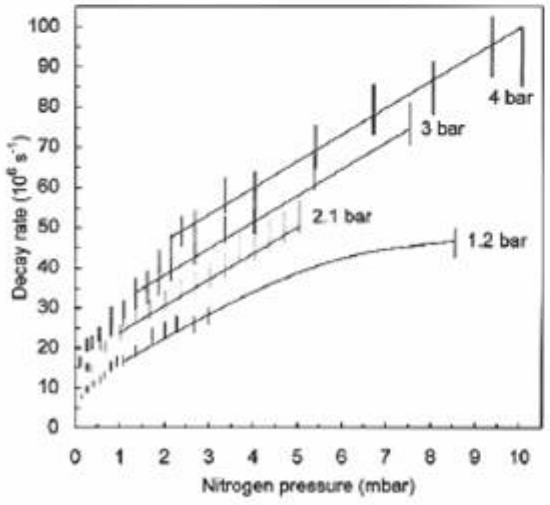

Figure 3. Exponential decay rates of $N_2^+(B\,^2\Sigma_u)$ as function of nitrogen partial pressure and for four different neon pressures. The full lines show decay rates calculated using equation (9).

concentration regimes in figure 3 would then occur when the reaction

$$(Ne_2^+)_v + N_2 \rightarrow N_2^+(B) + 2\,Ne \qquad (6)$$

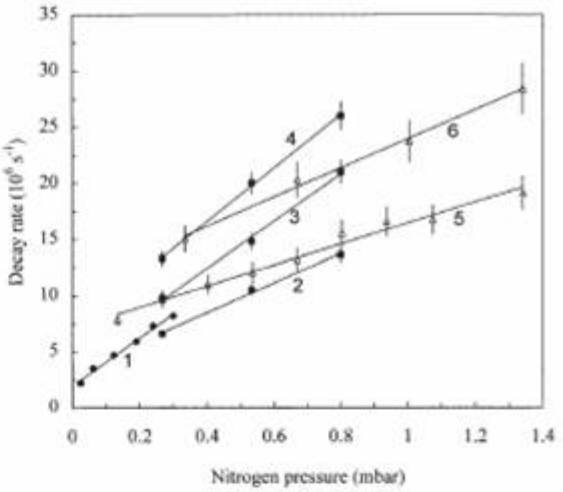

Figure 4. Comparison of our decay rates with those reported in previous studies: 1, Chen *et al* 1977a, $P_{Ne} = 0.8$ bar; 2–4, Collins and Lee 1980, $P_{Ne} = 0.8$, 1.2 and 1.9 bar; 5, 6, this work, $P_{Ne} = 1.2$ and 2.1 bar.

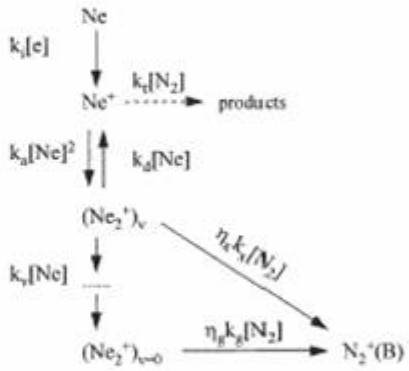

Figure 5. Major reaction pathways in Ne/N_2 discharge plasmas. Reaction rates are indicated along the arrows. Electronic recombination and quenching processes of $N_2^+(B)$ are not shown.

becomes more rapid than the vibrational relaxation

$$(Ne_2^+)_v + Ne \rightarrow \cdots \rightarrow Ne_2^+ + Ne. \qquad (7)$$

Vibrational transfer (V–V′) from $(Ne_2^+)_v$ to N_2 would be rather unlikely because of the large difference in vibrational frequencies (~ 300 cm^{-1} and 2330 cm^{-1} respectively).

The reaction pathways included in this kinetic model are illustrated schematically in figure 5.

Exact identification of the $(Ne_2^+)_v$ manifold would require a detailed theoretical investigation. Schneider and Cohen (1974) determined the location of 32 bound vibrational states, together with their rotational constants, for the Ne_2^+ ion having a dissociation energy $D_e = 1.17$ eV according to *ab inttio* calculations including spin–orbit coupling (Cohen and Schneider 1974). A slightly deeper well, with $D_e = 1.347$ eV, was calculated by Michels *et al* (1978) and agrees with the experimental results of Connor and Biondi (1965).

From considerations of energy resonance and Franck–Condon overlap, as indicated in the section 1, one may conclude that the reactivity of the highest vibrational states of Ne_2^+ would not be much different from that of the atomic ion Ne^+. However, when descending the vibrational 'ladder' there might be an increasing overlap between the bound $(Ne_2^+)_v$ state and the repulsive ground state $Ne_2(X\,^1\Sigma_g)$ near the inner turning point for $(Ne_2^+)_v$, together with an increasing resonance with the $N_2(X\,^1\Sigma_g)_{v=0} \rightarrow N_2^+(B\,^2\Sigma_u)_{v=0,1}$ transition. Since these conditions for efficient charge transfer are met only during part of the vibrational cycle, the corresponding rate coefficient which we shall denote by k_x will be smaller than the value k_g that applies to the low vibrational states. The location of the manifold $(Ne_2^+)_v$ was further suggested, *a posteriori*, by the fact that the best fit to experimental data was obtained by taking the value $k_d \sim 5\times10^{-14}$ cm^3 s^{-1} for reaction (5) (see below), yielding an equilibrium constant $[(Ne_2^+)_v]_{eq}/[Ne^+][Ne] = k_a/k_d \sim 1\times10^{-18}$ cm^3. In terms of the spectroscopic constants given by Schneider and Cohen (1974), this implies that the manifold $(Ne_2^+)_v$ would include rovibrational states situated at about 0.25 eV below the dissociation limit of Ne_2^+. At high pressures these states probably correspond to a sort of 'bottleneck' in the ion conversion from Ne^+ to Ne_2^+, in the sense that the capture process (3), producing molecules in weakly bound vibrational states and having a rate scaling as $[Ne]^2$, becomes faster than the subsequent relaxation process (7) that only increases linearly with [Ne].

We shall now proceed to a quantitative analysis of our data, within the framework of the kinetic model shown in figure 5.

Considering all the processes, and also the loss of Ne_2^+ ions due to electronic recombination with the well known rate coefficient $\alpha = 1.7\times10^{-7}$ cm^3 s^{-1} ($T_e = 300$ K, Frommhold *et al* 1968), the rate equations for the $[Ne^+]$, $[(Ne_2^+)_v]$ and $[Ne_2^+]$ populations could be formulated to read:

$$\begin{aligned}
(d/dt)[Ne^+] &= k_d[Ne][(Ne_2^+)_v] - k_a[Ne]^2[Ne^+]\\
(d/dt)[(Ne_2^+)_v] &= k_a[Ne]^2[Ne^+] - k_d[Ne][(Ne_2^+)_v]\\
&\quad -k_v[Ne][(Ne_2^+)_v] - k_x[N_2][(Ne_2^+)_v]\\
(d/dt)[Ne_2^+] &= k_v[Ne][(Ne_2^+)_v] - \alpha[e][Ne_2^+]\\
&\quad -k_g[N_2][Ne_2^+] \qquad (8)
\end{aligned}$$

where k_v is the overall rate coefficient for vibrational relaxation of the $(Ne_2^+)_v$ manifold, reaction (7), and [e] is the electron concentration. A 10 ns discharge pulse produces an initial population of Ne^+ ions, with $[Ne^+] = [e]$ at time $t = 0$, that is rapidly converted by reaction (3) to $(Ne_2^+)_v$ at the rate $\nu_a = k_a[Ne]^2$, ranging from $\sim 5\times10^7$ s^{-1} at $P_{Ne} = 1.2$ bar to $\sim 6\times10^8$ s^{-1} at $P_{Ne} = 4.0$ bar. After a certain time a transient equilibrium will be reached between $[Ne^+]$ and $[(Ne_2^+)_v]$, and thereafter they will continue decaying together at the common rate $\nu_x = k_v[Ne] + k_x[N_2]$. In the range of high nitrogen pressures, $P_{N2} > P^*_{N2}$, where N_2^+ fluorescence is supposed to follow the $[(Ne_2^+)_v]$ concentration, the decay rate ν_x should be identified with expression (4), yielding $k_v = (3.7\pm0.2)\times10^{-13}$ cm^3 s^{-1} and $k_x = (2.6\pm0.1)\times10^{-10}$ cm^3 s^{-1}. Hence, $k_x < k_g$, as required.

In general, also, $\nu_x < \nu_a$, as can be seen in figure 3. However, bypassing the mass flowmeter that controls the nitrogen concentration, it was possible to obtain a single measurement at a higher N_2 partial pressure of 8.5 mbar. Rather interestingly, the corresponding decay rate appears to be saturated near the value ν_a, as would be expected from the kinetic model. The eigenvalues of the first two equations of (8) are

$$\nu_{+,-} = \tfrac{1}{2}(\nu_d + \nu_a + \nu_x) \pm \tfrac{1}{2}[(\nu_d - \nu_a + \nu_x)^2 + 4\nu_d\nu_a]^{1/2} \qquad (9)$$

where the lower eigenvalue ν_- describes the late time decay of $[Ne^+]$ and $[(Ne_2^+)_v]$, and $\nu_d = k_d[Ne]$. This expression was used to calculate the full lines in figure 3, where the value of k_d, taken equal to 5×10^{-14} cm^3 s^{-1}, intervenes in causing a gradual transition from the linear regime with slope k_x to the saturated regime $\nu = \nu_a$. Due to the lack of experimental

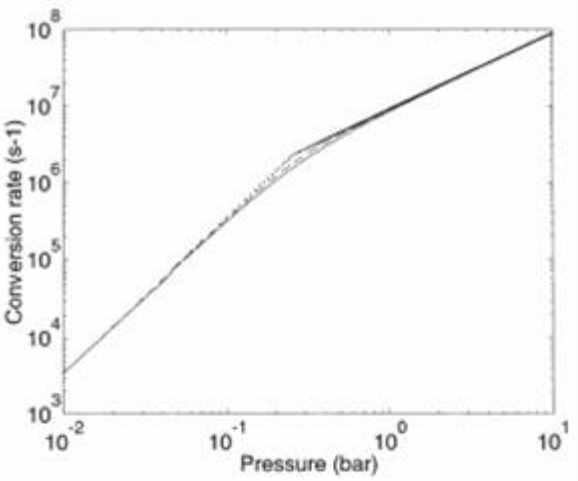

Figure 6. Dependence of Ne^+–Ne_2^+ conversion rate on neon pressure, as predicted by our kinetic model. Dotted curve, $k_d = 0$; dashed curve, $k_d = 0.3\times10^{-13}$ cm^3 s^{-1}; full curve, $k_d = 1.0\times10^{-13}$ cm^3 s^{-1} (k_d = rate coefficient for reaction (5)).

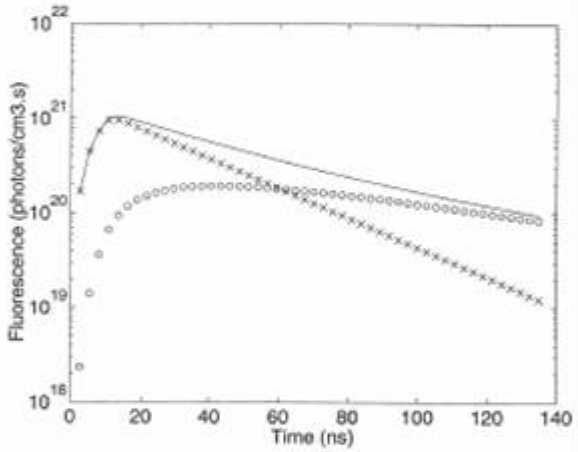

Figure 7. Result of a simulation of plasma evolution for a neon pressure of 4.0 bar and a nitrogen pressure of 0.37 mbar. $N_2^+(B \rightarrow X)$ fluorescence resulting from the reaction of Ne_2^+ in its lower vibrational states, assuming a branching efficiency $\eta_g = 0.15$, is shown as circles, whereas the crosses represent the contribution from the vibrationally excited states with an efficiency $\eta_v = 1$. The full curve shows the sum of the two components.

data in this transition range of nitrogen concentrations, the uncertainty in our value of k_d is fairly high (~100%). In the limit of zero nitrogen concentration, expression (9) describes the overall conversion rate of Ne^+ ions into diatomic Ne_2^+ ions through reactions (3) and (7), shown in figure 6 as function of neon pressure. For $k_d = 0$, $|\nu|$ is the smaller of ν_a or ν_x, leading to an abrupt transition from a P_{Ne}^2 dependence at low pressures to a linear dependence above the pressure where $\nu_a = \nu_x$, or $[Ne] = k_v/k_a$. Again, a non-vanishing value for k_d will cause a more gradual transition, with little difference between the curves for $k_d = 0.3 \times 10^{-13}$ and 1.0×10^{-13} cm^3 s^{-1}. For these small values of k_d, one has for low densities [Ne],

$$\nu_- \approx \nu_a[1 - \nu_d/(\nu_x - \nu_a)] \qquad (10)$$

so that the value of k_a has to be slightly increased in order to recover the experimental low-pressure values of the conversion rate. This was done in preparing figure 6.

At the lowest values of nitrogen pressure, $P_{N2} < P_{N2}^*$, N_2^+ fluorescence would follow the time evolution of the Ne_2^+ ions in their first vibrational states. The expected decay rate would then be $\nu_g = \alpha[e]+k_g[N_2]$. Comparing this expression with the experimental results (4), one may conclude that the electron concentration, $[e] = (\nu_0+K_1[Ne])/\alpha$, increases with neon pressure from a value ~ 4×10^{13} cm^{-3} at $P_{Ne} = 1.2$ bar to ~ 9×10^{13} cm^{-3} at $P_{Ne} = 4.0$ bar. These values, of course, represent an average over the ~ 0.2 μs afterglow period, but are entirely self-consistent. Chen *et al* (1977a) reported a similar increase with neon pressure of the intercept value of decay rate at zero N_2 concentration, which they interpreted as indirect evidence of the existence of Ne_3^+. More recently, however, the stability of such rare gas cluster ions has been the subject of much research, and for the reaction

$$Ne_2^+ + 2\,Ne \rightarrow Ne_3^+ + Ne \qquad (11)$$

the equilibrium ratio $[Ne_3^+]/[Ne_2^+]$ was measured over a range of temperatures from 72 K to 112 K (Hiraoka and Mori 1990). Extrapolating their results to $T = 300$ K and $P_{Ne} = 4$ bar leads to an estimation of the equilibrium ratio $[Ne_3^+]/[Ne_2^+] = 0.02$. The time evolutions presented by these authors also indicate that reaction (11) probably proceeds with a rate coefficient that is comparable to that of (3), so that equilibrium between $[Ne_3^+]$ and $[Ne_2^+]$ would be reached very rapidly. The small Ne_3^+ population could then be expected to play the role of a minor additional degeneracy of the Ne_2^+ state, having little influence on the overall kinetics.

The second term, $k_g[N_2]$ in the expression for ν_g, should correspond to $K_2[N_2]$ in (4), when $P_{N2} < P_{N2}^*$. As it appears there, K_2 would be the sum of a bimolecular component whose value is significantly smaller than the generally accepted rate coefficient k_g, and a termolecular component that seems to agree fairly well with the value reported by Collins and Lee (1980). However, in order to obtain a better understanding of this range of partial nitrogen pressures, we performed a numerical solution of the rate equations (8) with the rate coefficients deduced above. Detailed agreement between these simulations and the experimental fluorescence curves (such as those shown in figure 2) could be obtained by assuming that the reactions (1) and (6) produce the $N_2^+(B\,^2\Sigma_u)$ state with certain efficiencies η_g and η_x, averaged over the corresponding vibrational states v since in general η would be a function of v, and also assuming that their ratio η_g/η_x was only ~ 0.15. The resulting contributions to the $N_2^+(B \rightarrow X)$ fluorescence are shown in figure 7 for a typical case with $P_{Ne} = 4$ bar and $P_{N2} = 0.37$ mbar. This illustrates how the combined reaction channels yield a nearly exponential decay curve with a slope intermediate between ν_0 and ν_x, in agreement with the measured temporal evolution. Unfortunately, this implies that our data cannot be used to determine the value of k_g precisely, or to confirm the existence of a termolecular component in the reaction of Ne_2^+ with nitrogen.

4. Conclusions

Fast pulsed discharges in well controlled high-pressure neon–nitrogen gas mixtures have been used to study (by time-resolved emission spectroscopy) the reactions of neon ions with N_2 and the rates at which they occur. The measured afterglow decay rates for the resulting N_2^+ fluorescence agree with those previously reported (Chen *et al* 1977a, Collins and Lee 1980) in the common region of partial pressures ($P_{Ne} < 2$ bar, $P_{N2} < 0.8$ mbar). For higher Ne and N_2 densities the data were found to deviate from simple extrapolations of previous results. A kinetic model, in which vibrationally excited Ne_2^+ ions play an important role, was able to describe all of the results in some detail. In this model the rate coefficients for charge transfer from $Ne^+(k < 10^{-14}$ cm^3 s$^{-1})$ and $(Ne_2^+)_{v=0}(k = 8 \times 10^{-10}$ cm^3 s$^{-1})$ were taken as well established, as was the coefficient for three-body ion conversion measured at low pressures.

From the data obtained at N_2 pressures higher than 1–2 mbar, a rate coefficient of $(2.6 \pm 0.1) \times 10^{-10}$ cm^3 s^{-1} was obtained for the reaction of a manifold of rovibrational states of Ne_2^+ with N_2. Also, the vibrational relaxation rate coefficient for these states, tentatively located at about 0.25 eV below the dissociation limit, was obtained as $(3.7 \pm 0.2) \times 10^{-13}$ cm^3 s^{-1}. As a result, the P_{Ne}^2 dependence of the Ne^+ to Ne_2^+ conversion rate, measured in several low-pressure experiments, should gradually change into a linear pressure dependence over the range from 0.1 to 1 bar.

References

Albritton D L, Bush Y A, Fehsenfeld F C, Ferguson E E, Govers T R, McFarland M and Schmeltekopf A L 1973 *J. Chem. Phys.* **58** 4036

Bohme D K, Adams N G, Mosesman M, Dunkin D B and Ferguson E E 1970 *J. Chem. Phys.* **52** 5094

Chen C H, Judish J P and Payne M G 1977a *J. Chem. Phys.* **67** 2713

——1977b *J. Chem. Phys.* **67** 3376

Cohen J S and Schneider B 1974 *J. Chem. Phys.* **61** 3230

Collins C B and Lee F W 1978 *J. Chem. Phys.* **68** 1391

——1980 *J. Chem. Phys.* **72** 5381

Connor T R and Biondi M A 1965 *Phys. Rev.* A **140** 778

Fehsenfeld F C, Schmeltekopf A L, Goldan P D, Schiff H I and Ferguson E E 1966 *J. Chem. Phys.* **44** 4087

Frommhold L, Biondi M A and Mehr F J 1968 *Phys. Rev.* **165** 44

Hiraoka K and Mori T 1990 *J. Chem. Phys.* **92** 4408
Jahani H R, Gylys V T, Collins C B, Pouvesle J M and Stevefelt J 1988 *IEEE J. Quant. Electron.* **24** 568
Johnsen R, Chen A and Biondi M A 1980 *J. Chem. Phys.* **73** 1717
Lee F W, Collins C B and Waller R A 1976 *J. Chem. Phys.* **65** 1605
Mayhew C A 1992 *J. Phys. B : At. Mol. Opt. Phys.* **25** 1865
Michels H H, Hobbs R H and Wright L A 1978 *J. Chem. Phys.* **69** 5151
Plain A and Jolly J 1984 *Chem. Phys. Lett.* **111** 133
Pouvesle J M, Khacef A, Stevefelt J, Jahani H, Gylys V T and Collins C B 1988 *J. Chem. Phys.* **88** 3061
Pouvesle J M, Stevefelt J and Collins C B 1985 *J. Chem. Phys.* **82** 2274
Schmeltekopf A L and Fehsenfeld F C 1970 *J. Chem. Phys.* **53** 3173
Schneider B and Cohen J S 1974 *J. Chem. Phys.* **61** 3240

High repetition rate compact source of nanosecond pulses of 5–100 keV x-ray photons

A. Khacef,[a] R. Viladrosa, C. Cachoncinlle, E. Robert, and J. M. Pouvesle
GREMI, CNRS/Université d'Orléans, B.P. 6759, 45067 Orléans Cedex 2, France

(Received 20 December 1996; accepted for publication 3 March 1997)

A powerful, compact, and repetitive flash x-ray system based on a cable transformer technology powered by ceramic capacitors in a Blumlein-like configuration has been developed. Open circuit voltages in excess of 100 kV can be achieved while commutation occurs at low voltage (<20 kV). The x-ray emission from a low impedance x-ray diode with a hollow cathode configuration was observed under a wide range of experimental conditions. The critical parameters limiting the flash x-ray performances are mainly the pressure in the x-ray diode and the anode–cathode space. This true table top device is able to produce doses up to 1 R per shot, measured at the output window, of x-rays between 5 and 100 keV. The pulse widths were about 20 ns and the maximum repetition rate was about 60 Hz. Operation is possible in air or in other gases (He, Ne, Ar, Kr, Xe, H_2, N_2) at pressures varying from 10^{-3} mbar for xenon to about 1 mbar for helium. [S0034-6748(97)05006-5]

I. INTRODUCTION

Due to the large number of potential applications, the development of flash x-ray sources has received particular attention during the last few years. These sources are very useful in the investigation of high-speed phenomena, biomedical radiography, preionization of high pressure gas discharge lasers, and more recently, in the photoexcitation of molecular and atomic systems for fluorescence studies and time-resolved x-ray diffraction studies.[1–8] Depending on the application, systems with specific characteristics (high-dose, high repetition rate, short pulse duration, and wide energy spectrum) are required. Currently available systems based upon synchrotrons,[9] laser plasmas,[10] and e-beam discharges,[11] while presenting very interesting performances, are often large, complex, and expensive devices. Thus, the challenge is the development of small size systems capable of operation at high repetition rates and emitting a high-dose per shot of x rays with energy ranging from a few keV to a few hundred keV while minimizing cost and maintenance.

The generation of short x-ray pulses at high repetition rate realized by discharge techniques[12] seems to be very attractive if obtained with devices of laboratory scale. Basically, the conventional x-ray diode operates in vacuum (or low gas pressure) with closely spaced electrodes that are powered with a high-voltage pulse discharge. Various kinds of flash x-ray generators using different pulse forming networks have been reported in the literature[13–20] with storage energies ranging between several hundreds of millijoules to several hundred joules.

Based around Blumlein technology, the devices developed by the University of Texas at Dallas group[17,21–23] were able to emit average powers of radiation approaching 1 kR min^{-1} (R: roentgen, 1 R=2.58×10^{-4} C/kg) with photon energy up to 300 keV, operating at 70 kV charging voltage.[23] These systems exhibited repetition rates up to 100 Hz and generated x-ray fluxes with pulse widths on the order of a few tens of nanoseconds. The characteristics of these devices are very attractive but their size remains relatively large (line of about 3.7 m long). Pouvesle *et al.*[14] developed a flash x-ray machine based on Blumlein configuration close to the ones designed by the Dallas group, but with a big improvement in the ratio of x-ray output to the size and weight of the source less than 0.15 m^3 and 80 kg, respectively. With dose rates exceeding 1.4 kR min^{-1} at the output window with photon energies up to 50 keV, from pulses of tens of nanoseconds duration, this device is easily transportable and can be included in various types of industrial systems or laboratory experiments. A big improvement of the system that allows a longer lifetime with stable x-ray doses was readily obtained with the use of a sliding–rotating anode.[24]

In the field of high-speed radiography in the biomedical area, the Sato group from the Iwate Medical University of Japan has developed compact repetitive flash x-ray sources based upon many kinds of high-voltage pulsers and flash x-ray tubes. A detailed review of the different types of systems they developed can be found in Ref. 25. For example, one of these sources[2] uses a modified two-stages Marx generator characterized by a pulse duration ranged from 40 to 100 ns, a repetition rate less than 50 Hz, and an x-ray intensity of about 1.0 μC/Kg per pulse at 0.3 m from the source (corresponding to about 4 mR).

In this article, we report the detailed study of a new very compact flash x-ray system developed around a cable transformer technology,[26] powered by ceramic capacitors disposed in a Blumlein-like configuration and switched by a fast commutation system. The size and the weight of this device including the high-voltage power supply and the vacuum pump were less than 0.13 m^3 and 60 kg, respectively.

The vacuum diode employing a conical anode can operate in transmission mode (TM) or in reflection mode (RM) with a conical hollow cathode. The x-ray diode can be directly connected to the generator or deported from the device through 4.5 m cable line. Dose rates exceeding 3.6 kR min^{-1} at the output window were obtained with

[a]Electronic mail: khacef@univ-orleans.fr

 0034-6748/97/68(6)/2292/6/$10.00

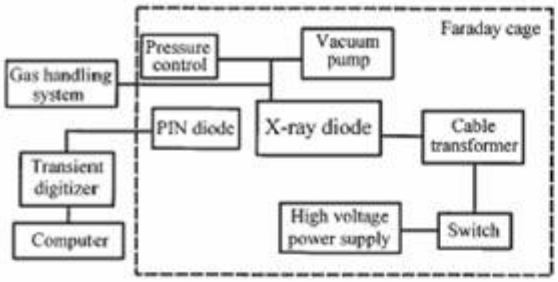

FIG. 1. Block diagram of experimental setup.

rather low input energy per shot (900 mJ) from pulses of 20 ns duration at a charging voltage of only 15 kV. In the present device, the open circuit voltage reaches 100 kV.

The effects of critical parameters such as voltage characteristics, electrodes material and geometry, anode–cathode (A–C) separation, diode vacuum pressure, and gas that can influence the characteristics of the x-ray emission are detailed here. We also measured the angular distribution of the x-ray emission.

II. EXPERIMENTAL ARRANGEMENT AND INSTRUMENTATION

The schematic diagram of the repetitive flash x-ray system is illustrated in Fig. 1. This generator consists of the following essential components: a high-voltage cable generator, a switching system capable of operating at a high repetition rate, a low impedance cold cathode x-ray diode, and a primary vacuum pump.

A cross-sectional view of the x-ray diode is shown in Fig. 2. The flash tube was made of a quartz cylinder with 3 mm wall thickness, 35 mm outside diameter, and 130 mm length. Various combinations of electrodes with different materials and geometries were used.

In RM, the anode consists of an 8 mm diam (ϕ_a) rod with a conical shaped tip; made of copper (Cu), molybdenum (Mo), or tungsten (W) with different angular profiles [$\theta = 20°$, 40°, or 60°, see inset of Fig. 7(a)]. The cathode, made of different materials (W, Cu, stainless steel), is of the conical hollow-cathode configuration. Experiments with different hollow-cathode diameters ($\phi_c = 5$, 8, and 11 mm) were performed. Best performances were obtained with $\phi_a = \phi_c$ $= 8$ mm. An increase of ϕ_c leads to unstable arc ignition in vacuum, yielding x-ray tube damage due to unwanted discharge. Operations at a high-dose rate and high repetition rate during a long period of time requires the use of a W anode for which the erosion is weakest.

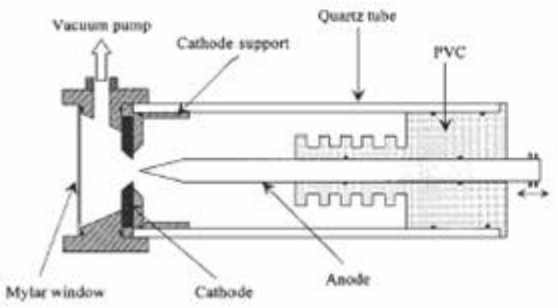

FIG. 2. Schematic drawing of the flash x-ray diode.

The x-ray diode is of demountable type and the electrodes can easily be changed. The anode–cathode distance can be adjusted from the outside of the x-ray diode with an accuracy of 0.1 mm. The x rays were detected through a 350 μm mylar window with a cutoff energy around 6 keV. A small mechanical vacuum pump is used to maintain the residual pressure in the discharge volume in the order of 10^{-3} mbar. The x-ray diode can be operated close to the system or at long distance from it through cable line (4.5 m) with a weak (20%) decrease in the emitting dose.

The x-ray diode is powered by a high-voltage generator, which is the main element of the device. It is composed of two parts. The first one is a bank of ceramic knob storage and transfer capacitors of 4 nF each one, connected in a Blumlein-type configuration. The second one is the cable transformer system. It consists of six Dielectric Sciences 2012 SST coaxial cables. The storage capacitors were charged by a home made high-voltage, low current dc power supply (50 mA, 18 kV) and commuted with a fast switching element. After commutation, the Blumlein circuit produces pulses with a peak voltage of about 1.1–1.2 times the charged voltage. Then, this high voltage was fed through the cable transformer and a maximum open circuit voltage of six times the charging voltage of each cable was achieved.

The typical charging voltage was about 15 kV and the high-voltage open circuit pulse was about 100 kV with 60 ns duration full width at half-maximum (FWHM). The repetition rate of the system mainly depended on the circuit time constant of the high-voltage power supply. The maximum repetition rate was about 60 Hz in this experiment, yet it can be easily increased by using a power supply with higher performances.

The switching of the high voltage was affected by hydrogen thyratron, spark-gap (SG), or rotating spark-gap (RSG) switches. For the performances describe in this work, RSG or SG switches were used because of the low commutation time ($\leqslant$10 ns). Operating at atmospheric pressure, these simple devices easily allowed voltage commutation up to 20 kV and pulse repetition frequencies of hundreds of hertz in the case of RSG. Voltage measurements were achieved with a high-voltage short rise time Tek P6015A probe connected to a Tektronix 2440 or TDS 620 transient digitizers interfaced with a personal computer.

The x-ray outputs were measured in the forward direction of the x-ray diode by two different methods. First, the integrated doses were obtained by using SEQ5, SEQ6, and SEQ7 Saphymophy dosimeters with cutoff energies of 30, 10, and 5 keV, respectively, and sensitivities of 0.2 and 1 R full scale. Second, the temporal evolutions of the x-ray outputs were obtained with a 1 ns rise time Hamamatsu S1722-03 Si pin diode from which the protective window had been removed in order to detect the maximum range of energies of the x-ray photons. Being inserted in a small metallic box playing the role of a Faraday cage, it was carefully

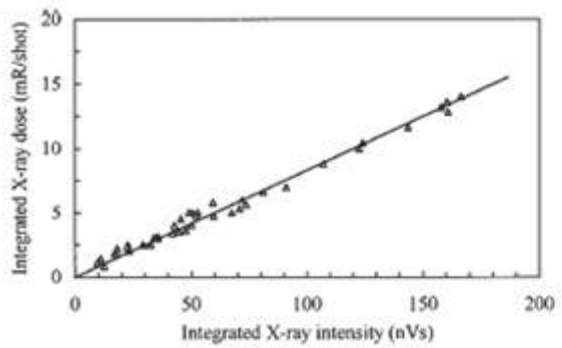

FIG. 3. Dependence of the integrated dose on the PIN diode integrated signal. The minimum source-to-detector distance was 16 cm.

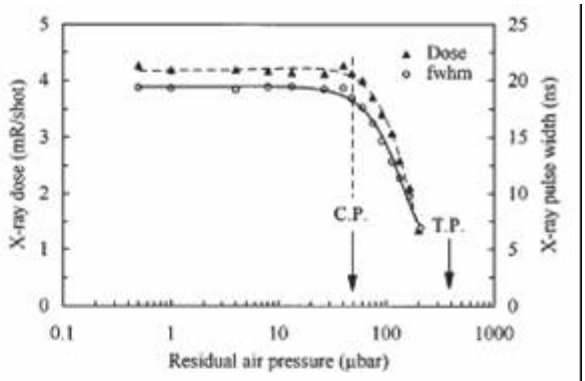

FIG. 4. Effect of the residual pressure in the x-ray diode on the x-ray dose per shot and on the x-ray pulse width for a charging voltage of 15 kV and an A–C space d_0 of 2 mm, when operating with a W(60°) anode.

protected from the remaining rf noise. The necessary window for x-ray detection was covered with a thin aluminum foil. This foil also prevented any visible light from being detected.

Electrical signals were recorded with the fast digitizers mentioned above. A signal-to-noise ratio greater than 50 was readily attained with this approach. The time response of the whole detection system was of the order of 3 ns.

Use of the pin diode was simpler for dose measurements versus repetition rate than was the dosimeter, which had to be reset after each shot or predetermined sequence of shots. This required systematic calibrations of the pin diode against the measured dose at a given distance from the x-ray window. For any given x-ray pulse width, a linear relation between the integrated dose measured with the dosimeters and the pin diode integrated signal at a given distance from the x-ray tube was verified. Figure 3 demonstrates the high degree of linearity of the pin diode response over the emitted x-ray spectral range. In the course of this work, the pin diode response has been checked frequently. No radiation damage with the accumulated dose to the pin diode was observed.

For any given experimental conditions leading to emitted doses of interest, the pulse-to-pulse fluctuations remained at an acceptable level of less than 10% of the average value in most cases. The stability of the average dose rate was proven by measurements that showed that the system could be run for hours at 10 Hz without any significant decrease in the x-ray output when using a W anode. However, this was not the case when using brass or Mo anodes because material ablation modified the gap setting, and probably the direction of the x-ray output, when the shape of the anode was changed.

III. RESULTS AND PERFORMANCES

In order to reach high efficiency x-ray production, the x-ray output characteristics were studied as a function of critical parameters, such as the pressure in the x-ray diode, the nature of gases introduced with controlled pressure in the x-ray diode, the A–C distance, and the electrode materials and shapes.

Figure 4 shows the dependence of the x-ray dose per pulse and the duration in time (FWHM) of the output pulse, respectively, as functions of the residual air pressure in the x-ray diode. The x-ray emission appears below threshold pressure (TP) of about 0.4 mbar for most of electrode spacing having some practical utility. Below the characteristic pressure (CP) of about 0.05 mbar, the x-ray production efficiency is high and the x-ray output remains constant exhibiting a *plateau*. The x-ray pulse duration exhibits the same behavior as the x-ray dose versus the residual pressure.

This indicates that in such experimental conditions a high vacuum is not necessary, as indicated in previous studies.[2,19,27] One can note that when the residual pressure varies from 0.4 to 0.05 mbar, the duration (FWHM) of the x-ray emission increases by nearly one order of magnitude. This behavior gives us the possibility of adjusting the pulse length from 4 to 20 ns at the expense of the emitted dose for the shorter pulse duration. This makes the flash x-ray system applicable to specific fields of research such as, for example, photoexcitation of gaseous matter and observations of ultrashort phenomena.

Measurements of the shorter x-ray duration is limited by the time response of the system (PIN diode, oscilloscope). A typical record of the x-ray power output as a function of time is shown in Fig. 5 for one of the lowest pressures of Fig. 4.

Otherwise, it is interesting to characterize the influence of the nature of gas, introduced with controlled pressure in-

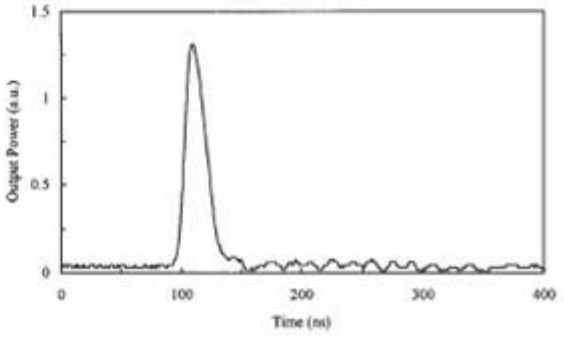

FIG. 5. Typical recording of the x-ray output as a function of time. The system was operated with a W(60°) anode at a charging voltage of about 12.5 kV and residual pressure in the x-ray diode around 10^{-2} mbar.

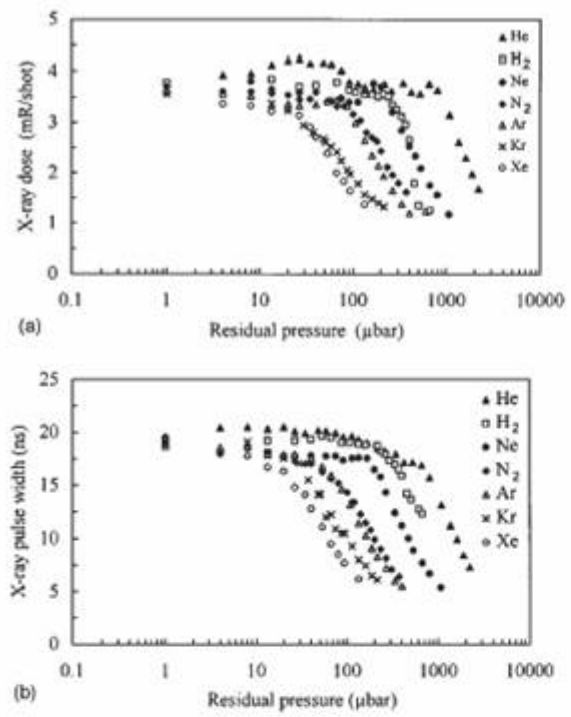

FIG. 6. Flash x-ray characteristics as a function of the residual gas pressure in the x-ray diode. This data was obtained with a W(60°) anode when operating with different gases such as He, Ne, Xe, Kr, Ar, H_2, and N_2, as indicated. The A–C space d_0 and the charging voltage were 2 mm and 15 kV, respectively. (a) Flash x-ray dose per shot measured at 0.25 m from the x-ray source. (b) Corresponding x-ray pulse width (FWHM).

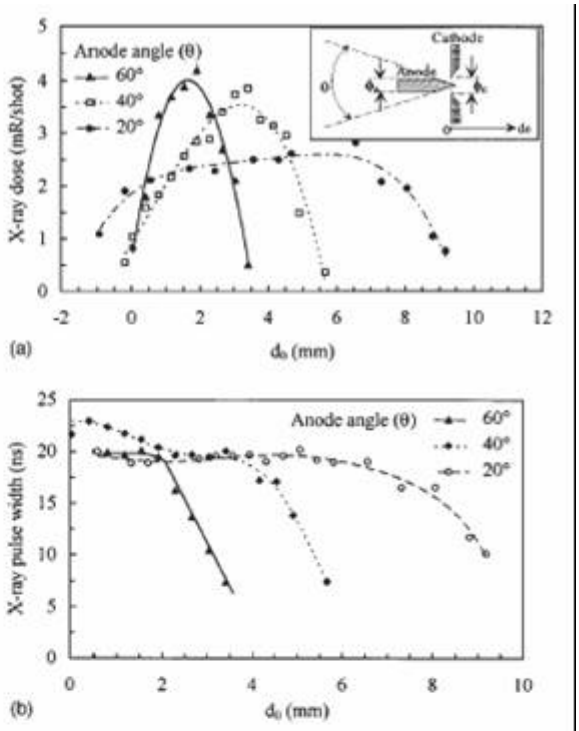

FIG. 7. Flash x-ray characteristics as a function of the A–C space d_0 when operating at a charging voltage of about 15 kV and residual pressure around 10^{-2} mbar. Cu cathodes and W anodes with angular profiles of 20°, 40°, and 60° were used, as indicated. The inset is the anode–cathode geometry. (a) Flash x-ray dose per shot measured at 0.25 m from the x-ray source. (b) X-ray pulse width (FWHM).

side the x-ray diode, on the x-ray output. An example of data obtained with He, Ne, Ar, Kr, Xe, H_2, and N_2 is given in Figs. 6(a) and 6(b). As can be seen, the working pressure range can be largely extended to higher pressures when using lighter rare gases without changing the emitted dose (CP changes of about two orders of magnitude from xenon to helium). One can note that the CP seems strongly correlated to the ionization potential of the considered gases. The higher values of the ionization potential correspond to the higher CP's except in the case of hydrogen. Below the CP, the x-ray pulse duration exhibits a *plateau* and tends to a constant value of 20 ns, whatever the gas used.

For a given charging voltage, the A–C distance appears to be the second critical parameter in maximizing the x-ray output. The optimum value varied with electrode materials and geometries. At a charging voltage of 15 kV, the x-ray dose does not exceed 134 mR per shot at the x-ray diode window when a 20° Mo anode tip angle is used. In this case, the x-ray signal drops after only a few tens of shots due to the anode erosion. When the system operates with a 30° brass anode tip angle, the maximum x-ray dose was similar to those obtained with Mo.

The best performances in this work were obtained with the tungsten anode. Figures 7(a) and 7(b) show the variation of x-ray dose per pulse and x-ray duration (FWHM), respectively, when changing the anode–cathode space (d_0) and anode tip angle (θ) in the case of the tungsten anode. d_0 is defined as the distance between the extremity of the anode tip and the plane of the cathode, as shown in the inset of Fig. 7(a). We see that the x-ray dose increases with increasing θ. As Fig. 7(a) indicates, in our experimental conditions, the maximum value for the x-ray dose is reached at $\theta = 60°$ and d_0 of approximately 2 mm, which correspond to a real A–C distance of 2.5 mm. In this experiment, the maximum x-ray dose was 1 R per pulse at the output window at 15 kV of charging voltage. For the smallest value of θ, the x-ray dose was weaker and remained constant for A–C separations ranged from 2 to 7 mm. Figure 7(b) indicates that the output pulse duration, in the case of small angles, is rather constant over a large domain of d_0, even if the x-ray dose is weak. Short pulse widths were obtained for a larger value of d_0 and could be interesting in particular applications where large x-ray doses are not required.

The optimum A–C separation for a maximum x-ray dose [Figure 7(a)] is constant and independent of the filling gas at residual pressure below the CP. An example of the results is shown in Fig. 8.

The spatial homogeneity of the x-ray beam has been checked. The x-ray dose has been measured at different angles from the diode axis. Results are presented in Fig. 9. These data show a very homogeneous beam between $-30°$ and $+30°$. Note that this output angle of x-rays is limited by the geometry of the diode. The effective focal spot varies

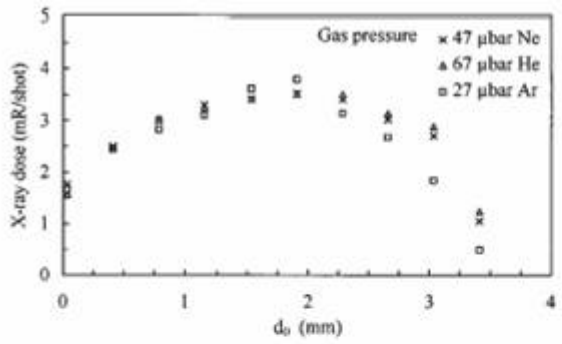

FIG. 8. Flash x-ray dose per shot at 0.25 m from the x-ray source as a function of the A–C space d_0 with a W(60°) anode and charging voltage of 15 kV, for residual gas pressures in the x-ray diode of 27 μbar of Ar, 47 μbar of Ne, and 67 μbar of He, as indicated.

according to the charging voltage, d_0, and the anode shape. In the high-dose regime, when the anode tip is 1.75 mm inside the hollow cathode, the effective focal spot seems to be large (2–3 mm). It can be reduced to less than 1 mm in diameter for the low-dose regime ($d_0 < 1$ mm).

The x-ray dose versus the source-to-detector distance follows the $(1/d^2)$ law, which is the characteristic law for a small size point source. The source images were achieved by using a 300 μm pinhole camera and a high-speed ISO 3000 Polaroid film.

The system has been also tested, without any consideration of optimization, in TM with a 0.1 mm thick aluminum disk anode placed between two 350 μm thick mylar foils. The maximum dose obtained in that configuration was 2.5

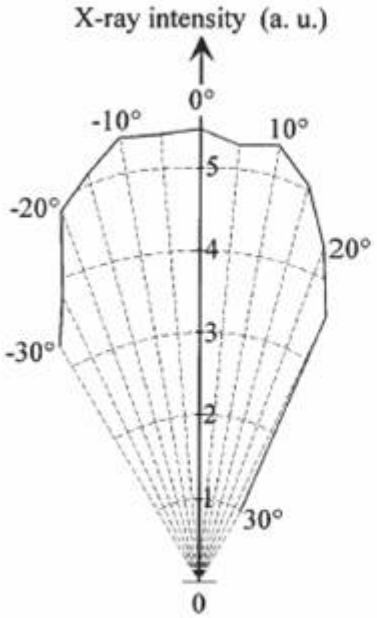

FIG. 9. Angular x-ray emission distribution in front of the x-ray diode in arbitrary units.


(a)

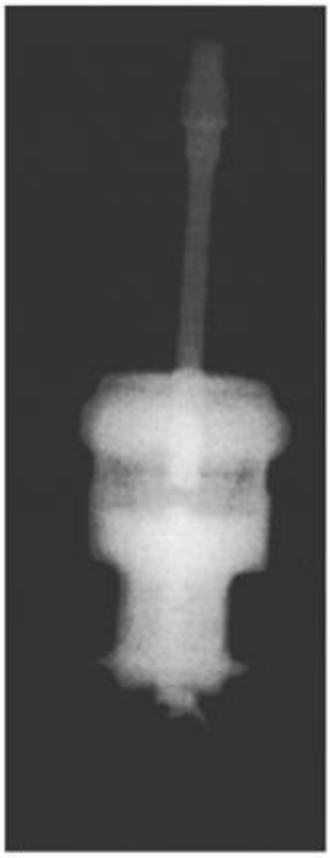
(b)

FIG. 10. Single shot radiographs achieved with 15 kV charging voltage. (a) Human fingers at 63 cm from the x-ray source. (b) Car spark plug at 14 cm from the x-ray source.

times smaller than those obtained in RM when operating with the W anode under the same other experimental conditions.

The emitted x-ray spectra were not precisely determined in this work. However, in RM, measurements performed with various dosimeters with different cutoff energies indicate that around 90% of the total x-ray energy is radiated in characteristic lines of the anode material (K lines for Cu and Mo, and L lines for W). The 10% remaining are distributed over a large bremsstrahlung continuum with an endpoint energy corresponding to the voltage across the electrodes.

Figures 10(a) and 10(b) show radiographs of a human finger and a car spark plug achieved with one shot of flash x-rays using an ISO 3000 Polaroid film. These images (without filtering) were obtained in RM with x-ray pulses of 20 ns duration at a charging voltage of 15 kV and a distance between the film and x-ray source of 63 and 14 cm, respectively. These high contrast radiographs clearly show the efficacy of the system for two different absorbing materials that need different photon energies.

The operation of the flash x-ray device developed in this work was only limited by the charging voltage power supply available at the time of the study. It is clear from these scaling studies that operations at much higher charging voltage and repetition rates can be easily achieved. Presently, another system that includes a 12 cable transformer is in progress and results will be published in a forthcoming paper.

ACKNOWLEDGMENTS

The authors would like to thank M. Ganciu Petcu of the Plasma Department of the Institute of Atomic Physics, Bucharest (Romania) for his fruitful collaboration in the development of the rotating spark gap. The authors gratefully appreciate the technical assistance of A. Bonnet, B. Dumax, and M. Dudemaine from GREMI, and of A. Quilgars from LCSR (CNRS, Orléans), and wish to express to them their sincere thanks. This work was supported by ANVAR Grant No. A9309100F00.r

[1] E. Sato, H. Isobe, and F. Hoshino, Rev. Sci. Instrum. 57, 1399 (1986).
[2] E. Sato, S. Kimura, S. Kawasaki, K. Takahashi, Y. Tamakawa, and T. Yanagisawa, Rev. Sci. Instrum. 61, 2343 (1990).
[3] E. Sato, A. Shikoda, S. Kimura, M. Sagae, H. Isobe, K. Takahashi, Y. Tamakawa, T. Yanagisawa, K. Honda, and Y. Yokota, Rev. Sci. Instrum. 62, 2115 (1991).
[4] J. I. Levatter and Z. Li, Rev. Sci. Instrum. 52, 1651 (1981).
[5] C. Cachoncinlle, J. M. Pouvesle, F. Davanloo, J. J. Coogan, and C. B. Collins, J. Phys. D 23, 984 (1990).
[6] E. Robert, A. Khacef, C. Cachoncinlle, and J. M. Pouvesle, Opt. Commun. 117, 179 (1995).
[7] I. V. Tomov, P. Chen, and P. M. Rentzepis, Rev. Sci. Instrum. 66, 5214 (1995).
[8] J. M. Pouvesle, C. Cachoncinlle, R. Viladrosa, E. Robert, and A. Khacef, Nucl. Instrum. Methods Phys. Res. B 113, 134 (1996).
[9] I. L. Spain and D. R. Black, Rev. Sci. Instrum. 56, 1461 (1985).
[10] H. Milchberg, R. R. Freeman, and S. C. Davey, in *Advances in Laser Science II*, Proceedings of the Second International Laser Science Conference, Seattle, October, 1986, edited by M. Lapp, W. C. Stwalley, and G. A. Kenny-Wallace, AIP Conf. Proc. No. 160 (AIP, New York, 1987), pp. 179–181.
[11] J. D. Ivers and J. A. Nation, Rev. Sci. Instrum. 54, 1509 (1983).
[12] R. Germer, J. Phys. E 12, 336 (1979).
[13] A. Khacef, E. Robert, C. Cachoncinlle, R. Viladrosa, and J. M. Pouvesle, J. Phys. (France) IV 6, 747 (1996).
[14] J. M. Pouvesle, C. Cachoncinlle, E. Robert, R. Viladrosa, C. B. Collins, and F. Davanloo, Rev. Sci. Instrum. 64, 2320 (1993).
[15] L. C. Bradley, A. C. Mitchell, Q. Johnson, and I. D. Smith, Rev. Sci. Instrum. 55, 25 (1984).
[16] Q. Johnson, A. C. Mitchell, and I. D. Smith, Rev. Sci. Instrum. 51, 741 (1980).
[17] C. B. Collins, F. Davanloo, and T. S. Bowen, Rev. Sci. Instrum. 57, 863 (1986).
[18] M. Sworonek and P. Romeas, IEEE Trans. Plasma Sci. 15, 589 (1987).
[19] A. Ikhlef and M. Skowronek, IEEE Trans. Plasma Sci. 21, 669 (1993).
[20] A. Shikoda, E. Sato, M. Sagae, T. Oizumi, Y. Tamakawa, and Y. Yanagisawa, Rev. Sci. Instrum. 65, 850 (1994).
[21] F. Davanloo, T. S. Bowen, and C. B. Collins, Rev. Sci. Instrum. 58, 2103 (1987).
[22] F. Davanloo, J. J. Coogan, T. S. Bowen, R. K. Krause, and C. B. Collins, Rev. Sci. Instrum. 59, 2260 (1988).
[23] J. J. Coogan, F. Davanloo, and C. B. Collins, Rev. Sci. Instrum. 61, 1448 (1990).
[24] E. Robert, C. Cachoncinlle, A. Khacef, R. Viladrosa, J. M. Pouvesle, C. B. Collins, and F. Davanloo, Ann. Phys. (Paris) 19, 167 (1994).
[25] E. Sato, A. Shikoda, S. Kimura, M. Sagae, T. Oizumi, K. Takahashi, Y. Hayasi, T. Shoji, K. Shishido, Y. Tamakawa, and T. Yanagisawa, Proc. SPIE 1801, 628 (1992).
[26] V. N. Ishchenko, V. N. Lisitsyn, and V. N. Starinskiy, Opt. Technol. 41, 155 (1974).
[27] C. S. Wong, C. X. Ong, S. Lee, and P. Choi, IEEE Trans. Plasma Sci. 20, 405 (1992).

ELSEVIER

15 May 1995

OPTICS COMMUNICATIONS

Optics Communications 117 (1995) 179–188

Full length article

Time-resolved spectroscopy of high pressure rare gases excited by an energetic flash X-ray source

E. Robert, A. Khacef [1], C. Cachoncinlle, J.M. Pouvesle

GREMI, CNRS/Université d'Orléans, BP 6759, 45067 Orléans Cedex 2, France

Received 20 September 1994

Abstract

Fluorescence from high pressure (0.1–30 bar) rare gas plasmas has been excited using an intense flash X-ray source specially developed and optimized for this experiment. Spectral analysis of the so-called "third continuum" of rare gases is presented. Time-resolved spectroscopy, absorption measurements and pressure dependence studies have provided an extended database on this longer wavelength continuum of rare gases. These data allow us to understand some of the previously contradictory results reported in the literature. They strongly support a multi-component spectral aspect of the previously called "third continuum". In fact, the observed fluorescence result from the superposition of several continua whose relative intensities are strongly dependent upon pressure. This suggests that different species are at its origin. The name of "third continuum" does not seem anymore appropriate when speaking of the whole fluorescence emitted in the longer wavelength continuum by high pressure rare gas plasmas. Generally speaking, the flash X-ray device was proven to be a very convenient and powerful tool for the study of high pressure plasmas resulting in UV–VUV fluorescence.

1. Introduction

Since the pioneering work of Tanaka [1] in the 50's, rare gas (Rg) plasmas have been extensively studied because of their ability to produce broad spectral bands of intense UV–VUV fluorescence. In the 70's, they have been shown to produce laser oscillations in the VUV region when excited by energetic means. Stimulated emissions have been observed in Ar (126 nm), Kr (146 nm) and Xe (178 nm) [2]. These laser transitions have been extensively studied theoretically and experimentally both in gas and in condensed phases. Wavelengths mentioned above correspond to the wavelength of the maximum of the well known "second continuum" of Rg which originate from transitions between the lowest excited states of the neutral dimer towards the repulsive ground state.

Other very broad spectral features, named third continua of rare gases, that cover a great part of the UV–VUV domain have often been reported since the sixties but their exact origin remains unknown. Interest in their study was recently reawakened by Laghoff [3] who proposed that transitions in the doubly ionized molecular system (transitions from Rg_2^{++} to $Rg^+ + Rg^+$) could be at the origin of these emissions and suggested the possibility of a new class of tunable UV–VUV ionic excimer laser. A great number of theoretical [4–8] and experimental [9–15] works have been very recently published on this subject. In the following, the designation "third continuum" will be employed for convenience, as usually done in the literature, to describe the continua at

[1] LPMI, Institut de Physique, USTHB, BP 32 El Alia, Alger, Algeria.

SSDI 0030-4018(94)00664-4

longer wavelength than the second continuum even if it does not appear the most appropriate as will be shown. A third continuum has now been reported for all rare gases. They have been observed in both gas and condensed phases and recently in the excitation of cluster beams [16]. They are mainly characterised by their exceptional broadness, in the range from 10 to 100 nm (FWHM) and, when considering the different Rg: Xe, Kr, Ar, Ne and He, in this order, they almost entirely cover the UV–VUV domain from 400 nm down to 60 nm. In contrast to what has been observed on the Rg second continuum, the so-called third continuum usually has a complex spectral structure that depends on gas pressure. The observed emissions have been interpreted following two main hypotheses: the first one, as mentioned above, is based on the participation of doubly ionized excited molecular ions ($Rg_2^{+\,**}$) and the other one is based on the participation of singly ionized excited molecular ions (Rg_2^{+*}) [17–19]. Ab initio potential curves calculations in the case of Ar_2^{+*} states [5] and $Ar_2^{+\,**}$ states [4,6] have shown that, unfortunately, both systems could be involved in the fluorescence of the third continuum of argon. Different authors [3,9,11] also suggested the possible intervention of larger ionic species, specially $Rg_3^{+\,**}$, at high pressure. The exact assignment of the states responsible for the third continuum fluorescence will not be discussed here since this paper concentrates on aspects of the fluorescence production and characterization.

The production of significant levels of fluorescence in the third continua from inert gas plasmas generally requires the use of extremely expensive means of excitation in high pressure media. For example, significant fluorescence has been obtained with excitation from synchrotrons [16] and powerful beams of charged particles [9,11]. At lower levels of intensity, laboratory-scale devices suffice for excitation but under rather restrictive conditions. The use of silent discharges [12] and small electron beam systems is limited to pressures of a few atmospheres, and α-particle excitation of high pressure plasma [17] produce only very weak fluorescence often requiring complex photon counting apparatus for detection. All this reinforces the difficulty in identifying the origin of the third continuum, but the relevant states undoubtedly lie at very high potential energies above the ground state of the neutral molecule at large internuclear distances which may explain why the continuum has not been detected in conventional discharges.

In this work we report on the intense fluorescence radiated in the third continuum by high pressure rare gas samples excited by an energetic laboratory-scale flash X-ray source. Flash X-ray excitation has already been shown very well suited for this type of study [10] and provides the possibility of investigation over a very wide range of pressures which was generally not the case with other excitation sources. For this work, a new type of powerful X-ray device has been specially developed [20]. With this excitation source, intense fluorescence of the third continuum was obtained and appears to be the second dominant feature, after the second continuum emission, from the VUV to the near infrared spectral domain. Due to the strong X-ray doses involved, the levels of fluorescence obtained allowed time-resolved measurements by conventional means. Time-resolved spectroscopy of photoexcited pure gases over a wide pressure range reveals new features in the third continuum emission spectra. The use of flash X-ray excitation has provided an extended database on the third continua of rare gases which was the first aim of this work. The availability of time-resolved spectra over a wide pressure range produced and recorded with a single experimental device might be very useful in the identification of the third continuum fluorescence and allowed us to explain the apparently contradictory results previously reported.

2. Experimental set-up

The experimental set-up, schematically drawn in Fig. 1, includes three main parts: an excitation source, a high pressure gas cell with a gas handling system and different investigation tools.

Gas samples were excited using a linear flash X-ray source [20]. Briefly, this table-top device has been shown to deliver high X-ray doses from a filamentary source in nanosecond pulses. Both X-ray dose and pulse duration were tunable parameters. Two major improvements have been realized on the previous device described in reference [20]. First, the electrode separation is now adjustable from the outside of the diode and second, the use of a rotating anode

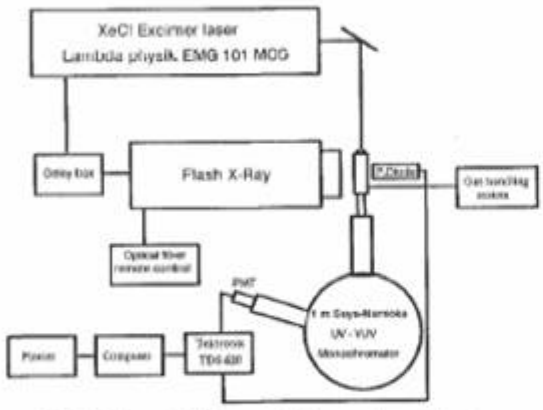

Fig. 1. Schematic diagram of the experimental set-up.

has lengthened the system lifetime at constant output power. As a result, our device can now emit doses between a few millirads up to 2 rad per shot at the output window in a 3 to 50 ns pulse from either a plasma spot in point-rod configuration or from a plasma filament 10 cm in length and 1 mm in diameter with a 10 cm graphite blade as a cathode (this last configuration was used for fluorescence studies in this work). This corresponds to a maximum energy deposition of about 150 μJ in the rare gas cell. Repetition rates can be varied from single shot up to 50 Hz.

Typical working conditions correspond to the emission of 0.4 rad per shot, at the output window, at 25 kV charging voltage during several hours at 15 Hz. X-rays of 5 to 40 keV, with the major part of the photons being radiated in the characteristic lines of the anode material, are produced under these conditions. In these experiments, tungsten was used as the anode and thus the emitted X-ray energy was mainly centered around 10 keV (L lines). The energy deposition occurs by inner shell photoexcitation followed by electronic cascade. One can estimate that each X-ray photon could produce about 500 electrons when taking into account the energy, w, necessary to produce an electron–ion pair. For example, the quantity w has been recently measured around 24 eV in pure xenon at 1030 mbar with 5.9 keV X-rays [21]. As the energy deposited at each shot in the rare gas cell was estimated to be around 30 μJ for typical working conditions (25 kV charging voltage), the number of 10 keV X-ray photons should be of the order of 2×10^{10}. Depending on the Rg pressure and so on the X-ray penetration depth, such a photon flux lead to an electron density around 10^{12}–10^{13} cm^{-3}. Both spatial homogeneity and temporal stability were available with this device. This enables an homogeneous irradiation in the rare gas cell, all over its length, for periods of hours. The typical time required to record one spectrum (200 nm scanned with a 0.5 nm step) was one hour with a signal averaged over 50 shots at each wavelength.

High purity gases, supplied by l'Air Liquide, were excited in a 10 cm^3 high pressure aluminum cell at pressures ranging between 0.1 and 30 bar. Gases were flowed through the cell, previously pumped down to 5×10^{-5} mbar, at flow rates between 0.01 and 2 l/min. X-ray photons entered the cell through a 60 μm thick, 10 cm^2 surface kapton window supported by a stainless steel mesh. Plasma observation was possible through three MgF_2 windows (see Fig. 2), one of which was connected to the monochromator entrance arm through a 10 cm long transfer tube which was 1 cm in diameter. The opposite side window was used for light absorption measurements. Finally the last window allowed a transverse view of the plasma in the UV-visible spectral domain. For spectra recording, the plasma was viewed along its main axis (plasma length: 10 cm).

In this experiment two monochromators and three different photomultiplier tubes were used. A first set-up allowed recording of spectra between 150 and 800 nm. In this case, the fluorescence from the plasma was spectrally dispersed with a high resolution Sopra 1 m Seya-Namioka monochromator pumped by a secondary pumping system. For analysis below 150 nm and down to MgF_2 cut-off (110 nm), light was dispersed with a small Jobin Yvon 0.2 m grating monochromator maintained under a high purity ni-

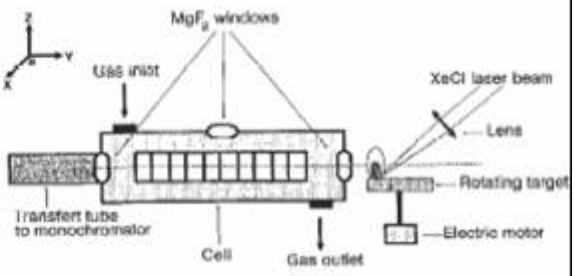

Fig. 2. Schematic diagram showing the high pressure cell and plasma laser probe source. The flash X-ray device is directed along the Ox axis.

trogen flow. Light was detected with either R 955 (160–900 nm) or solar blind R 1080 (115–320 nm) and R 1220 (115–320 nm) Hamamatsu photomultiplier tubes. The transient intensity was recorded with a Tektronix TDS 620 transient digitizer connected to a computer. X-ray signals were monitored behind the pressure cell with a 1-ns rise time Hamamatsu S1722-03 PIN diode which also served as a trigger signal for data acquisition. It should be noted that all the data presented in this paper were not corrected for the spectral response of the systems.

An intense probe source emitting around 200 nm was used to check if there was any transient absorption in argon plasmas. This source has been obtained by focusing an XeCl excimer laser (Lambda Physik EMG 101 MSC) delivering 150 mJ in a 10 ns pulse at 308 nm on a rotating disk. A graphite disk was used as a target to emit a very bright laser-produced plasma. In this way, a strong UV continuum of about 170 ns (FWHM) was emitted with a few target material emission lines superimposed. The plasma emission was very reproducible. Variation in intensity was less than 5%. As shown in Fig. 2, the laser-produced plasma was created in front of the cell window, in order to pass the probe light through the 10 cm long rare gas plasma created by X-ray photoexcitation. The synchronization between the flash X-ray source and the XeCl laser was achieved by the use of a tunable delay box triggered by the flash X-ray high voltage power supply. During the experiment, the delay between the emissions from the laser-produced plasma and the X-ray produced plasma was monitored on the digitizer. The jitter between the two signals was measured to be around 5 ns.

3. Results

3.1. Third continuum production

In this work, pure rare gases have been photoexcited at pressures between 0.1 and 30 bar. We were able to produce the so-called third continuum in argon, krypton and xenon by X-ray radiation but for lighter gases, helium and neon, no fluorescence corresponding to the third continuum above 110 nm was observed. For helium this could be understood because the gas was almost completely transparent to 10 keV centered X-rays even at the highest pressure supported by the rare gas cell. In the case of neon, up to 80% of X-ray photons were stopped in the gas but no emission was recorded from 110 to 800 nm.

Short wavelength parts of helium and neon emission spectra have been reported by Griegel et al. [11] with dc ion beam excitation and by Krötz et al. [22] in the case of neon with pulsed sulfur ion beam excitation. With these same gases, third continuum fluorescence has been obtained with dielectric controlled discharge excitation [12,14] and with an electron beam for neon [23]. In the case of neon, the long wavelength part of the third continuum was observed from 160 up to 400 nm with a maximum of intensity around 250 nm while the short wavelength part was reported between 85 and 110 nm centered at 99 nm. All this underlines the differences between the different exciting systems in the production of third continua. Heavier Rg (Ar, Kr and Xe) fluorescence exhibits the same peculiar behaviour. Depending on the excitation means and pressure range, authors reported either one spectral component centered at various wavelengths or two more-or-less well separated spectral components.

The third continua which are exceptionally broad are presented in Fig. 3 in the case of Ar, Kr and Xe. In argon, it extended from 150 nm up to 300 nm at one bar. In the case of krypton, for a pressure of 1.2 bar, it extended from 170 nm up to 500 nm with a maximum around 255 nm. Finally, for xenon at a pressure of 1.1 bar, it extended from 170 nm up to 500 nm with a maximum around 290 nm.

Fig. 4 shows a comparison of temporal evolutions of the second continuum emission at 126 nm arising from the lowest excited dimer state, namely Ar_2^* ($^1\Sigma_u^+$), and the third continuum at 220 nm at a pressure of 5 bar. The temporal evolution of the second continuum exhibits the well known fast and slow components [24]. The temporal evolution of the third continuum appears as the fastest event and the fluorescence decays on a ns time scale following the termination of the excitation pulse. The maximum of intensity in the third continuum occurs in the rising part of the second continuum which represents the final step in the relaxation of a Rg plasma at high pressure. Such behaviour strongly confirms the high energy level origin of the third continuum. The third continuum is the dominant feature of the whole spec-

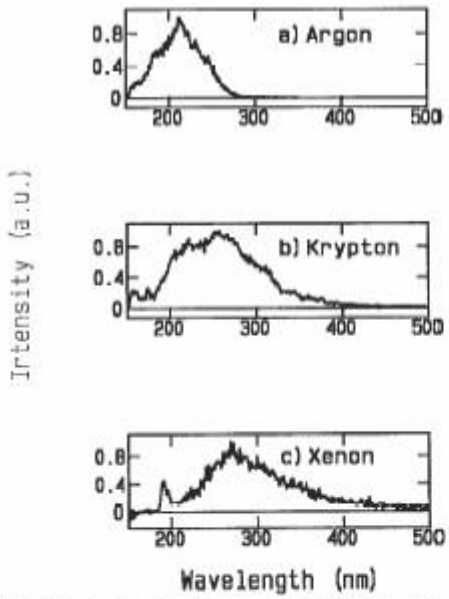

Fig. 3. (a) Time-integrated spectrum of the third continuum of argon at 1 bar. (b) Time-integrated spectrum of the third continuum of krypton at 1.2 bar. (c) Time-integrated spectrum of the third continuum of xenon at 1.1 bar. The red wing of the second continuum of xenon (peaking at 173 nm) is observable below 200 nm.

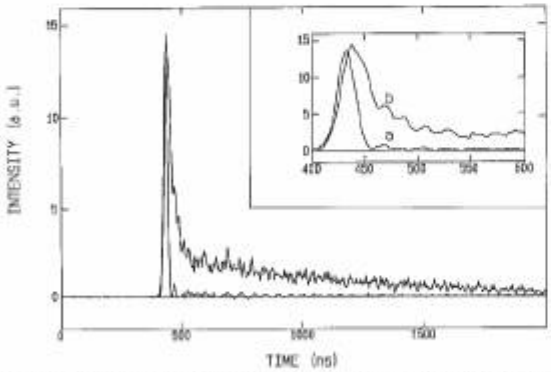

Fig. 4. Comparison of the temporal evolution of the third continuum ((a) $\lambda = 220$ nm) and of the second continuum ((b) $\lambda = 126$ nm) of argon at 5 bar excited by X-ray pulses of 20 ns (FWHM). Inset is an enlarged view of temporal evolutions at early time.

trum at the very early stage of the plasma evolution whatever the Rg considered. Another point has to be noted; even though spectral responses of gratings can only be estimated, integrated fluorescence of the third continuum is roughly of the same order as the second continuum one. This is a very promising result in connection with the possibility of developing efficient ns duration sources, based on the third continua emission, in the UV–VUV wavelength range.

For all Rg, the fluorescence at longer wavelengths than the third continuum up to the near infrared domain was extremely weak. In the case of argon, the few weak lines observed at moderate pressure come from atomic excited states produced through molecular ion dissociative recombination. They are due to transitions from $Ar^*(4p)$ to the $Ar^*(4s)$ levels. The most intense line was recorded at 696.5 nm and corresponds to the $2p_2$–$1s_5$ transition in Paschen notation. The $2p_2$ level of argon is known to be selectively populated by dissociative recombination of Ar_2^+ [25,26].

As already mentioned, both pressure and time dependence of the third continuum emission are of special interest and are presented in the next two sections.

3.2. Pressure dependence of the third continuum

In contrast to most previous experiments, flash X-ray excitation provides the possibility to study the third continuum over a very large range of pressures. In this work, this has been done for pressures between 0.1 and 30 bar.

Time-integrated spectra of argon at 0.5, 1, 8 and 17 bar are shown in Fig. 5. Large differences in the spectral shape are evident. For this gas, the spectrum evolves from one component, centered at 200 nm at 0.5 bar and around 215 nm at 1 bar to a spectrum with a maximum at 185 nm and a plateau between 210 and 250 nm at 8 bar. Higher pressure spectra, see for example Fig. 5d, exhibit three maxima at 185, 220 and 245 nm with two troughs at 200 and 240 nm. One can also notice the increasing importance of the 185 nm centered component with rising pressure in comparison with other long wavelength features.

Time-integrated spectra of Kr and Xe have also revealed an evolution in the shape of third continuum emission as a function of pressure. For krypton the spectrum exhibits three maxima at 170, 225 and 245 nm at 0.5 bar. With rising pressure the relative intensity of the maxima at 170 nm decreases. At 1.2 bar (see Fig. 3b) the spectrum still exhibits the three maxima but the longer wavelength one is much more intense and slightly shifted to 255 nm. A new spectral feature appears around 300 nm, revealed by a shoul-

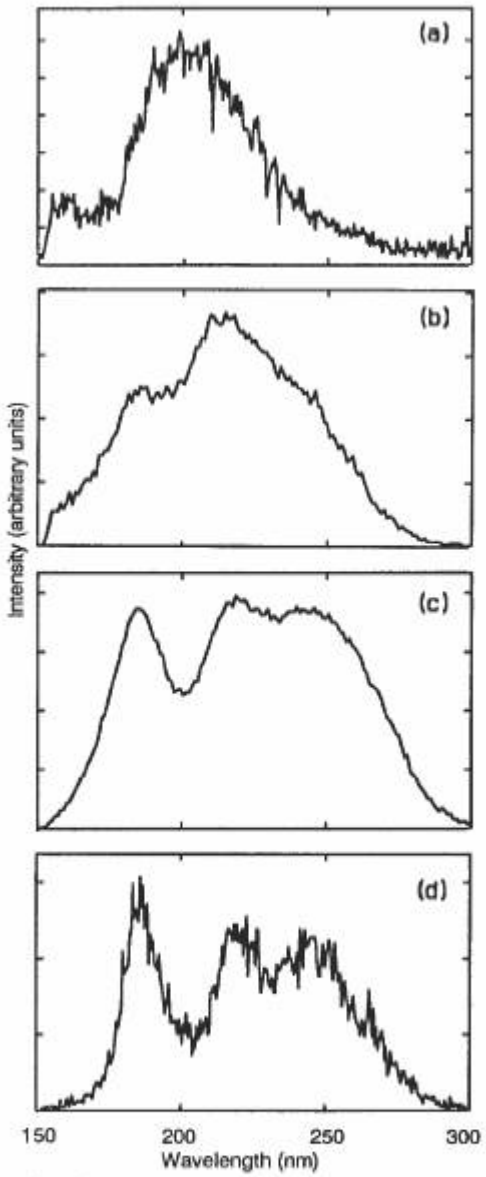

Fig. 5. Time-integrated spectra of the third continuum of argon at (a) 0.5, (b) 1, (c) 8 and (d) 17 bar.

der on the fluorescence spectrum in this wavelength region. This evolution is confirmed by the recorded spectrum at 2 bar. At this pressure, the 170 nm structure has disappeared. The rise of the 300 nm component is confirmed and the maximum is then located around 270 nm. Xenon spectrum evolution cannot be described in a simple way. Different overlapped spectral components were observed leading to a broad fluorescence from 170 nm up to 500 nm with a maximum around 290 nm at 1.1 bar (see Fig. 3c). No clear component around 390 nm, as reported by Amirov et al. [8] and Asselman et al. [27], was detected over the pressure range studied (1–10 bar).

3.3. Time-resolved spectroscopy

Fig. 6 shows time-framed spectra of the third continuum of Kr at 0.5 bar. Attention must be drawn to the fact that the changes in the spectrum shape during the plasma relaxation closely follow the evolution of the integrated spectrum as a function of pressure described in the preceding paragraph. The spectrum first exhibits (Fig. 6a) a single spectral component centered at 230 nm. Then (Fig. 6b), it presents two maxima at 225 nm and 245 nm and a narrow spectral component at 170 nm. Later (Fig. 6c), the narrow component at 170 nm has almost disappeared and the long wavelength component, slightly shifted to 255 nm, has become greater than the one at 225 nm. One can also discern the beginning of the rise of another component around 300 nm. Finally (Fig. 6d), in the last stage of the third continuum temporal evolution, the maximum is located around 265 nm and the long wavelength structure around 300 nm remained. Between 150 nm (cut-off of the photomultiplier tube) and 180 nm, the red wing of the second continuum (peaking at 146 nm) is observable and is the only remaining feature later in the plasma relaxation.

In the case of argon, the continuum begins as a spectral component extending from 150 nm to 280 nm and centered around 210 nm with a bump between 150 and 170 nm. Then a hole appears in the continuum around 200 nm to rapidly disappear at later times. The relative intensity of the long wavelength part of the spectrum (above 230 nm) in comparison with the emitted fluorescence below 230 nm has increased. In the latter stages of the argon third continuum emission, the spectrum again exhibits a single spectral component centered around 220 nm. This behaviour, unambiguously shown in Fig. 7 at one bar, is also relevant up to 5 bar of argon even if at this pressure the evolution between different shapes is shortened down to the overall time resolution of the data acquisition system (~ 2 ns). At pressures above

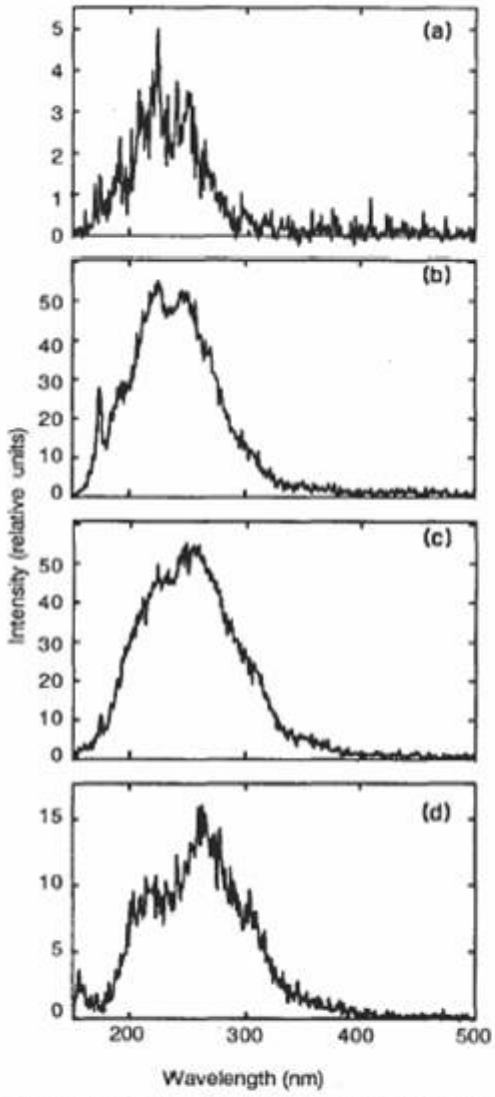

Fig. 6. Time-resolved spectra of the third continuum of krypton at 0.5 bar. Time windows: (a) 0–5 ns, (b) 15–20 ns, (c) 30–35 ns and (d) 45–50 ns.

5 bar, the limitation of our data acquisition system does not allow measurement of spectral modification at the very early times.

In summary, for Ar and Kr, a broad single spectral component was observed at the beginning of the fluorescence. Then several components appear at different wavelengths and times. In both cases, the spectrum is broadening with time.

The time evolutions described, together with spectral behaviour as a function of pressure might be relevant to the controversial origin of the third continuum deduced from experiments performed under very different experimental conditions, especially over pressure ranges that in most cases did not overlap. As already mentioned, previous experiments led to contradictory results especially on the determination of the wavelength of the intensity maxima. It must be pointed out that most previous results concerning the spectral shapes can be obtained with our experimental set-up because of both the large pressure range that can be explored and the availability of time-resolved spectroscopy. These results clearly indicate that care must be taken when analyzing data related to this study. Beside the possible intervention of Rg_3^{+*} excimers at high pressure [3,9,11], data have usually been analyzed considering only one possible species at the origin of the fluorescence. At the light of the present results, this analysis does not appear the most appropriate and it is clear that several species must be taken into account to explain the third continuum fluorescence.

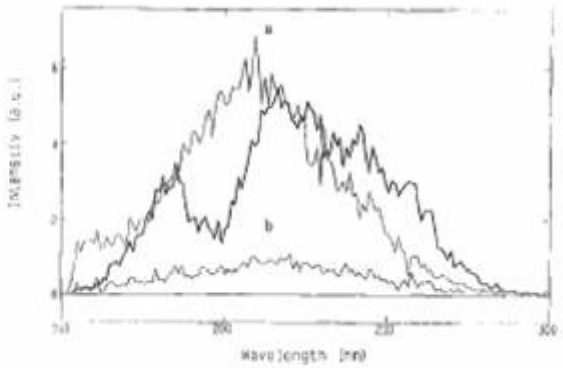

Fig. 7. Time-resolved spectra of the third continuum of argon at 1.3 bar. Time windows: (a) 10–20 ns, bold line 40–50 ns, (b) 70–150 ns.

3.4. Comparison with the literature

Results obtained in this work can be compared with those previously reported in the literature especially in the case of Ar and Kr.

α-particle bombardment appears to produce a similar Rg excited states population as flash X-ray excitation when making a comparison between fluorescence spectra. One can for example consider the

work of Strickler and Arakawa [28] for low pressure argon plasma or the work of Klein and Carvalho [17] at higher pressure together with our spectra in Figs. 5a and 5c to note the good agreement between the results obtained with both excitation means. Similarly, the xenon experimental spectrum obtained in this work exhibits a shape close to the one reported by Millet et al. [29]. We must underline that energetic flash X-ray excitation provides a much higher level of fluorescence and homogeneous excitation over a large volume.

Ar and Kr fluorescences obtained with beams of charged-particles with energy in the range 0.5–3.9 MeV (He^+, Ne^+, Ar^+) [11] or with heavy ion beam (100 MeV, $^{32}S^{9+}$) [9] can be also compared to the one reported in this study. In the paper of Griegel et al. [11], a far UV component, both in static and jet configurations, around 190 nm in Ar and 220 nm in Kr were reported, as in our case. In their work, long wavelength spectral emission increased with rising pressure. With 100 MeV ions, the third continuum of argon extended from 175 to 250 nm and Krötz et al. interpreted the emission by considering two components at 190 and 210 nm, the second being delayed in time with respect to the first one. We did report those two maxima at 185 and 220 nm, but also showed evidence of a third one at 245 nm.

For electron beam excitation, one can consider the work of Amirov et al. [13]. Argon continuum at 1.5 bar is presented in this paper and depicted as "*a plateau between 205 and 250 nm with two reproducible peaks at 215 and 230 nm*". This corresponds quite closely to our argon spectra in Figs. 5b and 5c above 200 nm up to 300 nm. Weak continuum depicted between 300 and 360 nm has not been recorded in our work. For the case of krypton, the same paper was also of interest. At low pressure (0.05 bar) the spectrum exhibited two peaks at 220 and 250 nm. With increasing pressure, the second maximum at 250 nm was still reported. In the common range of pressure studied, flash X-ray and e-beam excitation of krypton fluorescence has revealed similar features.

3.5. Light absorption measurements in argon plasmas

Both Ar and Kr third continuum time evolution can be understood following two different hypotheses: either transient absorption occurs at 200 nm and 240 nm for Ar and around 230 nm for Kr or alternatively several components rise and disappear on different time scales as the plasma grows and relaxes. According to the first hypothesis, only one ionic state could be at the origin of the observed spectrum, while the second one imposes that different states must be involved in the production of the third continua fluorescence. Absorption measurements performed in argon plasmas are reported below in order to check the first hypothesis.

Absorption measurements in electron beam excited argon at high pressure (0.5–8 bar) have been performed by Sauerbrey et al. [30]. According to these authors, the broad absorption band extending from 230 nm to 350 nm was caused by photoionisation from $Ar_2^*(1_u, 0_u^-)$. The three absorption bands centered at 512, 423 and 428 nm were ascribed to bound-bound transitions from $Ar_2^*(1_u, 0_u^-)$ to higher Ar_2^* excited levels. They also observed a "background" absorption between 350 and 600 nm which was identified to be caused mainly by photoionisation of Ar*(4p) and photodissociation of vibrationally excited Ar_2^+ levels. In all these cases, cross sections were determined to be around 10^{-17} cm^2. Finally, Sauerbrey et al. also reported several other strong absorption lines between 418.3 nm and 565.2 nm. These absorptions were assigned to atomic transitions from Ar*(4p) towards Ar*(5p, 5d, 6d) levels, and cross sections were estimated to be around 10^{-15} cm^2. They did not observe the narrow absorption continuum around 310 nm due to the photoexcitation of Ar_2^+ observed or calculated by different authors (see references in Ref. [30]). To our knowledge, no absorption measurements in the presence of strong third continuum fluorescence has been performed to date.

In our experiment, the transient trough around 200 nm in the argon third continuum spectrum could be the result of a transient absorption in the plasma. In this case, at least 50% of the plasma emission around 200 nm would be trapped, so this absorption, if it exists, could be clearly measured using an external probe source.

The spectral shape conservation at different positions across the cell was checked before the light absorption experiment. This was performed by introducing a 1 mm width slit in the transfer tube between

the pressure cell and monochromator to select a plasma slab. The spectrum recorded in this configuration has exactly the same shape as without the slit. Absorption measurements were performed with the slit in place in the transfer tube. In this way, with the presence in the probed slab of a trough in the spectrum around 200 nm, no transient absorption in the argon plasma at the origin of the third continuum was proven. This result has been checked using a second method based on the length of the excited plasma. Spectra were recorded by irradiating different cell lengths (0.5 to 10 cm). In this case, the obtained spectral shapes were identical to the one recorded with full length excitation. This would not have been so in the case of strong absorption. This has also been confirmed by the transverse observation of the plasma through the top MgF_2 window of the cell. Temporal evolution in this configuration was identical to the one recorded along the axis.

4. Summary

The broad emission of the so-called third continuum of rare gases (Ar, Kr and Xe) appears to be formed by several spectral components whose relative intensities depend upon pressure and time.

Using energetic flash X-ray excitation, argon "third continuum" fluorescence has been shown to be, in fact, composed of five different continua:

– a very broad one extending from 150 nm to 280 nm whose maximum, centered around 200 nm at low pressure (0.5 bar), rapidly shifts with increasing pressure, stabilizing around 210 nm above atmospheric pressure;

– one appears like a bump between 150 and 170 nm,

– three of roughly the same spectral width, ≈ 15 nm, centered around 185, 220 and 245 nm.

As for argon, the krypton "third continuum" fluorescence has been found to be composed of five continua:

– a very broad one extended from 160 nm to 300 nm whose maximum is located around 230 nm at 0.5 bar,

– a narrow one around 170 nm,

– two centered around 225 and 300 nm,

– one with a clearly defined maximum which shifts from 245 nm at 0.5 bar to 270 nm at 2 bar.

The xenon "third continuum" has been less studied at the moment. It appears that different overlapped spectral components can be at the origin of the fluorescence between 170 nm and 500 nm (with a maximum around 290 nm at 1.1 bar). More work is needed to specify their exact peak wavelengths.

The multi-component aspect of the "third continuum" of Ar, Kr and Xe strongly support that the "third continuum" must be analyzed taking into account different upper levels for the transition and not only one, contrary to what has been usually done. This, a priori, could explain the disagreement between the different interpretations of previous works. Authors are struggling around different features that up to now received the same designation. In the future, the name "third continuum", may have to be reformulated taking into account all the new results obtained in the last few years for all Rg and their mixtures.

5. Conclusion

An extended database on "third continua" of rare gases (Ar, Kr and Xe) excited by an energetic flash X-ray source over a very large pressure range has been obtained. Time-resolved measurements obtained in this work over a very wide pressure range enabled us to understand the great variety of previously contradictory experimental results reported in the literature and produced with various excitation means. Flash X-ray excitation has proven very efficient and powerful and appears to be a unique excitation means of high pressure plasmas, given the accessible pressure range and high levels of fluorescence. Light absorption measurements performed in argon plasmas have not proven any transient absorption in the plasma emitting the "third continuum" confirming that the "third continuum" spectral structure is composed by several continua as suggested by time and pressure dependence of the fluorescence spectrum. This multi-component aspect has also been confirmed by quenching studies performed in binary mixtures of gases which will be discussed in a forthcoming paper. The name of "third continuum" must be reformulated taking into account the different spectral components whose apparition depends on

pressure, time in the plasma relaxation in the case of pulsed excitation and excitation source. Each of these spectral components must be clearly defined in term of spectral position and width and named, at least for Ar and Kr, third, fourth, fifth, sixth and seventh continuum following the procedure used for the first and second continua.

Acknowledgments

The authors gratefully acknowledge Dr. C.B. Collins and Dr. F. Davanloo, from the Center for Quantum Electronics at the University of Texas at Dallas, for their invaluable contribution in the study and development of the flash X-ray device. They also wish to express their sincere appreciation to A. Bonnet, M. Dudemaine, B. Dumax, J. Mathias and R. Viladrosa for their technical assistance. This work was supported in part by CNRS and in part by the Conseil Régional du Centre.

References

[1] Y. Tanaka, J. Opt. Soc. Am. 45 (1955) 170.
[2] W.M. Hughes, J. Shannon and R. Hunter, Appl. Phys. Lett. 24 (1974) 488.
[3] H. Langhoff, Optics Comm. 68 (1988) 31.
[4] C. Cachoncinlle, J.M. Pouvesle, G. Durand and F. Spiegelmann, J. Chem. Phys. 96 (1992) 6085.
[5] C. Cachoncinlle, J.M. Pouvesle, G. Durand and F. Spiegelmann, J. Chem. Phys. 96 (1992) 6093.
[6] M. Daskalopoulou and S. Peyerimhoff, Molec. Phys. 79 (1993) 985.
[7] J. Ackermann and H. Hogreve, Chem. Phys. Lett. 202 (1992) 23.
[8] A.Kh. Amirov, O.V. Korshunov and V.F. Chinnov, High. Temp. 29 (1991) 856.
[9] W. Krötz, A. Ulrich, B. Bush, G. Ribitzki and J. Wieser, Phys. Rev. A 43 (1991) 6089.
[10] C. Cachoncinlle, J.M. Pouvesle, F. Davanloo, J.J. Coogan and C.B. Collins, J. Phys. D: Appl. Phys. 23 (1990) 984.
[11] T. Griegel, H.W. Drotleff, J.W. Hammer and K. Petkau, J. Chem. Phys. 93 (1990) 4581.
[12] C. Cachoncinlle, J.M. Pouvesle, F. Davanloo, J.J. Coogan and C.B. Collins, Optics Comm. 79 (1990) 41.
[13] A.Kh. Amirov, O.V. Korshunov and V.F. Chinnov, High. Temp. 29 (1991) 661.
[14] J.M. Pouvesle and C. Cachoncinlle, XIth ESCAMPIG 16F (1991) 366.
[15] A.Kh. Amirov, O.V. Korshunov and V.F. Chinnov, J. Phys. B: At. Mol. Phys. 27 (1994) 1753.
[16] E. Rühl, C. Heinzel and H.W. Jochims, Chem. Phys. Lett. 211 (1993) 403.
[17] G. Klein and M.J. Carvalho, J. Phys. B: At. Mol. Phys. 14 (1981) 1283.
[18] A.Kh. Amirov, V.M. Batenin, O.V. Korshunov and V.F. Chinnov, XXth ICPIG 6 (1991) 1386.
[19] C. Cachoncinlle, J.M. Pouvesle, F. Spiegelmann, G. Durand, F. Davanloo and C.B. Collins, XXth ICPIG 6 (1991) 1398.
[20] J.M. Pouvesle, C. Cachoncinlle, E. Robert, R. Viladrosa, C.B. Collins and F. Davanloo, Rev. Sci. Instrum. 64 (1993) 2320.
[21] F.I.G.M. Borges and C.A.N. Conde, IEEE Transactions on Nuclear Science 40 (1993) 661.
[22] W. Krötz, A. Ulrich, B. Busch, G. Ribitzki and J. Wieser, Appl. Phys. Lett. 55 (1989) 2265.
[23] F.V. Bunkin, V.I. Derzhiev, G.A. Mesyats, V.S. Skakun, V.F. Tarasenko, V.G. Shpak and S.I. Yakovlenko, Sov. Phys. Tech. Phys. 31 (1986) 1341.
[24] H.A. Kochler, L.J. Ferderber, D.L. Redhead and P.J. Ebert, Phys. Rev. A 9 (1973) 768.
[25] C.Y. Kuo and J.W. Keto, J. Chem. Phys. 78 (1983) 1851.
[26] J.W. Keto and C.Y. Kuo, J. Chem. Phys. 74 (1981) 6188.
[27] H. Asselman, P. Rives, J. Galy, H. Brunet and J.L. Teyssier, J. Phys. B: At. Mol. Opt. Phys. 26 (1993) 2311.
[28] T.D. Strickler and E.T. Arakawa, J. Chem. Phys. 41 (1964) 1783.
[29] P. Millet, A. Birot, H. Brunet, J. Galy, B. Pons-Germain and J.L. Teyssier, J. Chem. Phys. 69 (1978) 92.
[30] R. Sauerbrey, F. Emmert and H. Langhoff, J. Phys. B: At. Mol. Phys. 17 (1984) 2057.